Dissecting the theories of lanthanide magnetic resonance

ALEXANDER MAX FUNK

Dissecting the theories of lanthanide magnetic resonance

Alexander Max Funk

A thesis submitted for the degree of Doctor of Philosophy

Department of Chemistry

Durham University

2014

Abstract

The NMR relaxation and chemical shift behaviour of isostructural series of macrocyclic lanthanide(III) complexes has been investigated.

The ^{1}H, ^{31}P and ^{19}F longitudinal relaxation rates of multiple series of lanthanide(III) complexes (Tb, Dy, Ho, Er, Tm, Yb) have been measured in solution at five magnetic field strengths in the range 4.7 to 16.5 Tesla. The electronic relaxation time, T_{1e}, is a function of both the lanthanide(III) ion and the local ligand field. Analysis of the field-dependent nuclear relaxation rates, based on Solomon-Bloembergen Morgan theory, describing the paramagnetic enhancement of the nuclear relaxation rates, has allowed reliable estimates of the electronic relaxation times, T_{1e}. It has been shown that in systems of high symmetry, the electronic relaxation times are directly proportional to the ligand field and that in some cases changing the ligand field can have a greater effect on the nuclear relaxation rates than lanthanide selection.

The chemical shift data for the series of lanthanide(III) complexes were analysed. The pseudocontact shift of lanthanide(III) complexes is described by Bleaney's theory of magnetic anisotropy. Most of the assumptions in this theory were shown to be questionable. In particular for systems in low symmetry significant deivations between the experimental chemical shifts and those predicted by theory were found.

The low symmetry systems exhibit crystal field splittings of the same order of magnitude as the spin-orbit coupling. The possibility of a mixing of the electronic energy levels of the lanthanide(III) ion has to be considered. The effect of the coordination environment on the magnetic susceptibility was investigated using a variety of methods. Significant deviation (10 – 20%) from the theoretical values was observed in systems of low symmetry.

These investigations show that paramagnetic relaxation enhancements and magnetic susceptibility are dependent on the ligand field. Applying this knowledge allows the design of more efficient paramagnetic probes, as needed in PARASHIFT magnetic resonance.

Declaration

The work described herein was carried out in the Department of Chemistry, University of Durham between October 2011 and December 2014. All the work is my own, no part has previously been submitted for a degree at this or any other university

Statement of Copyright

Acknowledgments

I would like to thank my supervisors Prof. David Parker and Dr. Alan Kenwright for the continuous support and guidance.

I also would like to thank the solution state NMR service (Dr. Alan Kenwright, Katherine Heffernan, Ian McKeag and Dr. Juan Aguilar) for letting me steal their beloved magnets so frequently.

There are a few people that I have to thank to guided my way towards chemistry and then NMR spectroscopy. Namely, Dr. Derek Craston, Prof. Gareth Morris, Dr. Günter Funk and the rest of Mikromol.

I have to, of course, show my greatest thanks to the busy chemists that were so kind to let me borrow their complexes for this analysis. In no particular order: James, Kanthi, Peter, Emily, Brian and Katie.

Naturally, I would also like to thank the rest of the DP group and further friends for the comradery and friendships. In particular, I like to thank all the chemists, geologists, museum studies people that made my stay in Durham much more pleasant. Special mention goes to Martina, Valentina and Mickaële for the Vic Wednesdays and Sam, Katie, Bryonie and, of course, Colleen for the Sunday walks.

Finally I would like to thank my parents and also Colleen for the love and support.

List of Abbreviations

$12N_4$	1,4,7,10-tetraazacyclododecane
$9N_3$	1,4,7 –triazacyclononane
BM	Bohr magneton
BMS	Bulk magnetic susceptibility shift
BRW	Bloch-Redfield Wansgness
BZ	Benzyl
CEST	Chemical exchange saturation transfer
DFT	Density functional theory
DOMTA	1,4,7,10-tetraazacyclododecane-1,4,7,10-tetraacetamide
DOTA	1,4,7,10-tetraazacyclododecane-1,4,7,10-tetraacetic acid
DOTAM	1,4,7,10-tetrakis(carbamoylmethyl)-1,4,7,10-tetraazacyclododecane
DOTMA	Tetramethyl-1,4,7,10-tetraazacyclododecane-1,4,7,10-tetraacetic acid
DOTP	1,4,7,10-tetraazacyclododecane-1,4,7,10-tetra(methylene phosphonic acid)
dpa	Dipicolinic acid
gDOTA	1,4,7,10-tetraazacyclododecane -1,4,7,10-tetrapentancedioic acid
HSQC	Heteronuclear single quantum coherence spectroscopy
MHz	Megahertz
MRI	Magnetic resonance imaging
nm	nanometer
NMR	Nuclear magnetic resonance
NMRD	Nuclear magnetic resonance dispersion
ns	nanosecond
NSF	Nephrogenic systemic fibrosis
PARACEST	Paramagnetic chemical exchange saturation transfer
ppm	Parts per million
ps	picosecond
py	pyridine
SAP	Square antiprism
SBM	Solomon-Bloembergen Morgan
SQUID	Superconducting quantum interference device
TCF	Time correlation function
tert	tertiary
TSAP	Twisted square antiprism
ZFS	Zero field splitting

Table of Content

1. Introduction

1.1 Lanthanides in magnetic resonance – a historical perspective

Paramagnetic lanthanide ions have unique properties that make them particularly valuable in NMR spectroscopy. In the early days of NMR spectroscopy, when magnets with lower magnetic field strengths were more common, the limited shift dispersion of the NMR spectrum was enhanced by using lanthanide shift reagents. These paramagnetic agents extended the chemical shift of the spectrum.

It was established as early as the 1950's that the influence of unpaired electrons extends the chemical shift range, and also enhances the nuclear relaxation rates by providing additional relaxation pathways.[1–3] The effect of unpaired electron density on shift and relaxation properties was studied extensively and most of the theories postulated in these early days are still in use today. For example, Bleaney's theory of magnetic anisotropy for the pseudocontact shift and the Solomon-Bloembergen Morgan equations that rationalise paramagnetic relaxation enhancements.[1,2,4,5]

Figure 1 : *Examples of images obtained from contrast enhanced MRI images. Arrows highlight arthritis. Taken from [6].*

The interest in lanthanides as shift reagents started to ease with the introduction of multidimensional NMR and the availability of high-field superconducting magnets. The spectral resolution problem seemed to have found a solution.

However, with the introduction of magnetic resonance imaging (MRI) came the rise of contrast agents. Again, the modest sensitivity at lower magnetic field strengths could be enhanced by modifying the rate of relaxation of the observed water signal, leading to enhanced contrast in those regions of interest, where the paramagnetic lanthanide contrast agent was located (Figure 1).[7]

The following introduction will focus on the physical basis of these paramagnetic NMR properties and will cover the basic properties of lanthanide complexes that determine the local magnetic susceptibility and the overall relaxation enhancement. In addition, further detail will be given concerning the modern uses of complexes of lanthanide(III) ions in magnetic resonance.

1.2 Lanthanide properties and their influence in magnetic resonance

The special properties of the 4f orbitals contribute to the overall chemical and physical behaviour of the lanthanides. The seven 4f orbitals have a small radial extension and are normally described as 'core-like'. The gadolinium(III) ion is a special case among the lanthanide series. Its seven unpaired electrons contribute to a half filled shell of electrons, which renders the electron distribution isotropic.[8]

The lanthanide electronic energy levels and the respective emission spectral properties are thought to be well understood. Commonly, the energy levels of lanthanide(III) ions are expressed using the Russell-Saunders coupling scheme of the total angular momentum. Here, the total spin, *S*, and the total orbital angular momentum, *L*, are combined to give the total angular momentum, *J*, and the respective energy levels. In Russel-Saunders coupling, these quantum numbers are combined to create the overall term symbol of the lanthanide(III) ion in the following form:

$$^{(2S+1)}L_J$$

On binding to a complex, the lanthanide electron cloud around the ion is disturbed by the ligand. The symmetry around the ion is destroyed and the energy levels are split.

This crystal field splitting is generally assumed to be smaller than the spin-orbit coupling, as defined by Russell-Saunders coupling scheme (Figure 2).[8]

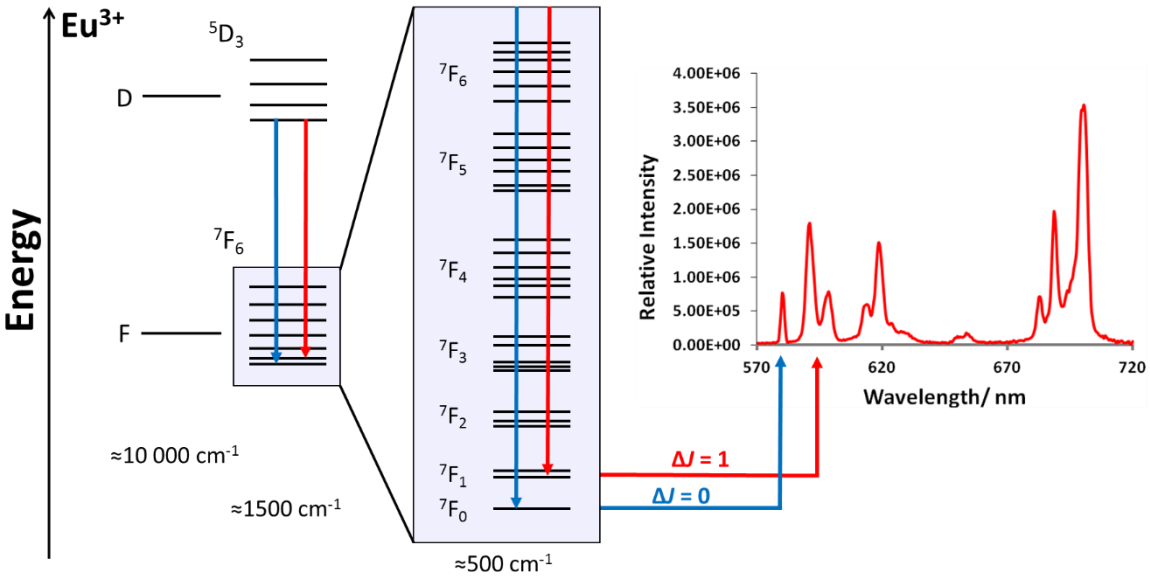

Figure 2 : *Electronic energy levels of a model Eu(III) system and emission spectrum of a model complex (H_2O, 295 K) with the $\Delta J = 0$ and $\Delta J = 1$ transitions highlighted.*

The electronic energy levels of the lanthanide(III) ions are split first by the electron-electron repulsion, and then further divided into *J* energy levels by virtue of spin orbit coupling. Finally, the crystal field splits these *J* states into further 2*J*+1 states. An example for the splitting of the electronic properties of the later lanthanide(III) ions can be found in Table 1. The crystal field splitting is quantified by a series of parameters in the form of B_q^k.

The splitting of energy levels can be directly observed, in certain cases, by examination of the emission spectrum. For example, the $\Delta J = 1$ band in the emission spectrum of Eu(III) complexes is split into two peaks, A_{1g} and E (Figure 2). Binnemans showed that, to a good approximation, the splitting of these two energy levels is directly correlated to the second order crystal field splitting parameter, B_0^2.[9,10]

Table 1 : *Selected electronic properties of lanthanide(III) ions*

Ln^{3+}	J	Crystal field splitting levels ($2J$+1)	μ_{eff} / BM (theo)[a]
Eu	0	1	3.5
Tb	6	13	9.8
Dy	15/2	16	10.3
Ho	8	17	10.4
Er	15/2	16	9.4
Tm	6	13	7.6
Yb	7/2	8	4.5

[a]Taken from [11], quoted at 298 K.

The crystal field interactions arise from electrostatic interactions between the ligands and the lanthanide(III) ions, which come from interactions between the 4f electrons with the lattice of the complex.

The crystal field splitting parameters come in the form of B_q^k, which are derived from the spherical tensor operators, $C_q^{(k)}$. The tensor operators are directly linked to the C_n site symmetry of the complex and depend on the coordinates of the 4f electrons. The second order crystal field splitting parameter, B_0^2, is mentioned above, but for the lanthanides *k* and *q* can vary to provide a large number of splitting parameters. The two parameters *k* and *q* are the rank and component labels of a tensor. They are heavily dependent on the symmetry of the crystal field and its corresponding irreducible representations (Mulliken symbols). In the lanthanide series, they relate directly to the total angular momentum, *J*, (Table 1).

The rank label, *k*, has allowed values from 0 to 7. However, these values can be split into even and odd numbers of *k*. The even numbers are responsible for the crystal field splitting. They are associated with the electrostatic interactions of electrons in specific orbitals. For example, the value *k* = 0 describes the contribution of the s-orbital. The odd

numbers are associated the intensities of induced electric dipole transitions. Therefore, only values of *k* of 2, 4 and 6 are considered here, because the contribution of rank zero is negligible to the overall crystal field splitting.

The component label, *q*, is defined by the point group symmetry (e.g. C_{2h}, C_{2v}, D_{2h}) of the lanthanide complex. The allowed values range from (–*k*) to (*k)*.[10]

The complexity of this parameter set increases with reducing symmetry. So, for example, in a C_4 symmetric complex, the parameters describing the ligand field interactions are only $B_0^2, B_0^4, B_4^4, B_0^6, B_4^6$. However, in complexes of lower symmetry higher order parameters will play a more important role, and their relative value and sign can vary dramatically, with up to 27 possible parameters in use.[12,13]

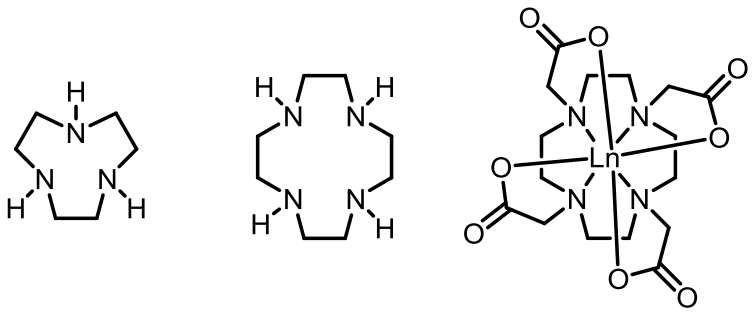

Figure 3 : *Archetypal ligands for many of the lanthanide(III) complexes used: $9N_3$ (left) and $12N_4$ (middle) and $[Ln.DOTA]^-$ (right).*

Due to the core-like nature of the 4f orbitals and the large ionic radii, the lanthanide(III) ions prefer coordination numbers of 8 or 9. In most cases, macrocyclic complexes are used to satisfy the demand for these high coordination numbers.

In this discussion, these complexes are based on $9N_3$ and $12N_4$ systems (Figure 3). In some cases, these ligands cannot saturate the coordination number of the lanthanide(III) ion. In such cases, there are water molecules directly bound to the lanthanide(III) ion. The number of water molecules can be estimated and is labelled the common hydration number, *q*. The lanthanide contraction causes the ionic radius to decrease across the lanthanide series and the hydration number may also decrease, as the coordination demand diminishes. The lanthanide contraction is due to poor shielding of the nuclear charge, which causes the 4f electrons to be closer to the nucleus.[8]

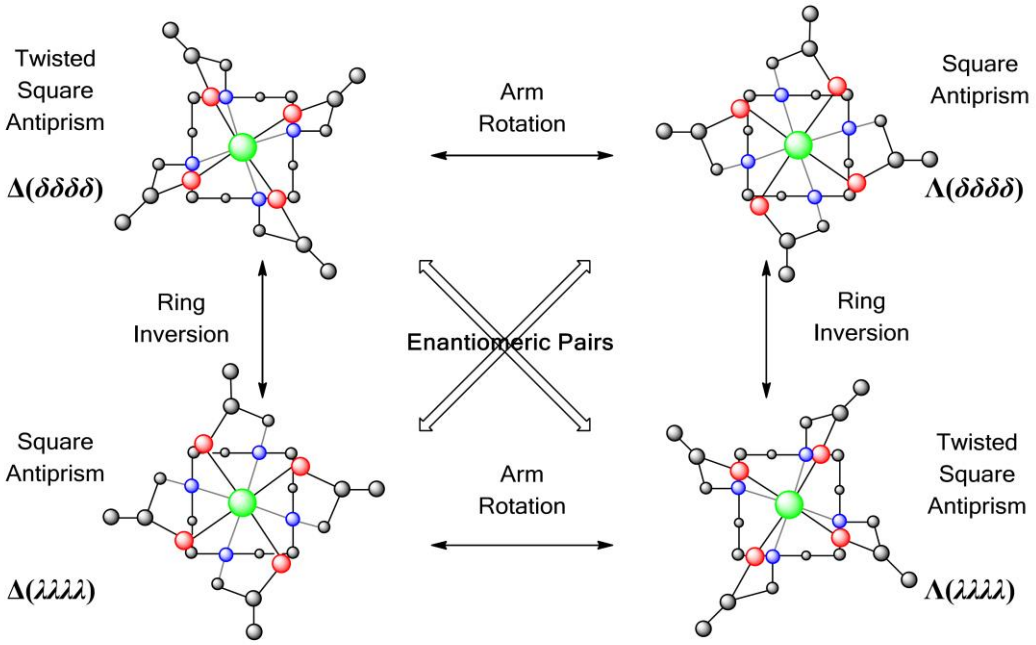

Figure 4 : *Diastereoisomers of the 12N4 based [Ln.DOTA] complexes.*[14]

The archetypal example of a lanthanide(III) complex is $[Ln.DOTA]^-$. There are two main elements of chirality that define this system, relating to the sign of the ring NCCN and the NCCO dihedral angles (Figure 4). There are two different macrocyclic ring conformations possible in C_4 symmetry, giving λλλλ or δδδδ stereoisomers. Additionally, there are two conformations for the acetate arms, Δ and Λ, resulting in four possible stereoisomers, existing as two enantiomeric pairs. These complexes are described as a twisted square antiprismatic (TSAP, Δ / δδδδ) or a monocapped square antiprismatic geometry (SAP, Δ / λλλλ).[15,16]

Generally, both diastereoisomers are observable in the NMR spectrum. The ratio between them can vary from ligand to ligand.

1.2.1 Magnetic susceptibility and the paramagnetic shift

Another important property that affects the paramagnetic NMR spectrum is the magnetic susceptibility. In a magnetic field, the electron spin of the unpaired electrons

is forced to precess along the orientation of the magnetic field. This leads to the Zeeman splitting of the energy levels and the induction of localised magnetic moments. When the contribution of the electron orbital magnetic moment is considered, the magnetic susceptibility behaves in an anisotropic way, at least for non - Gd lanthanide(III) ions.[17,18]

The magnetic susceptibility anisotropy has a direct effect on the chemical shift in an NMR spectrum of lanthanide(III) complexes, with the exception of Gd(III), due to the isotropic nature of its electron density. Overall, three contributions to the observed shift can be considered: a diamagnetic contribution, the contact shift and the pseudocontact shift.

$$\delta_{obs} = \delta_{dia} + \delta_{contact} + \delta_{pseudo}$$

The diamagnetic term is the change of the shift of the ligand resonances that occurs on coordination of the free ligand to the lanthanide(III) ion. This is accompanied by small structural changes that will contribute to the shift difference of the complex to the free ligand (diamagnetic contribution). This term is commonly assessed by examining the diamagnetic analogues of the lanthanide(III) ions. (e.g. the Y(III), La(III) or Lu(III) analogues of a complex).[19]

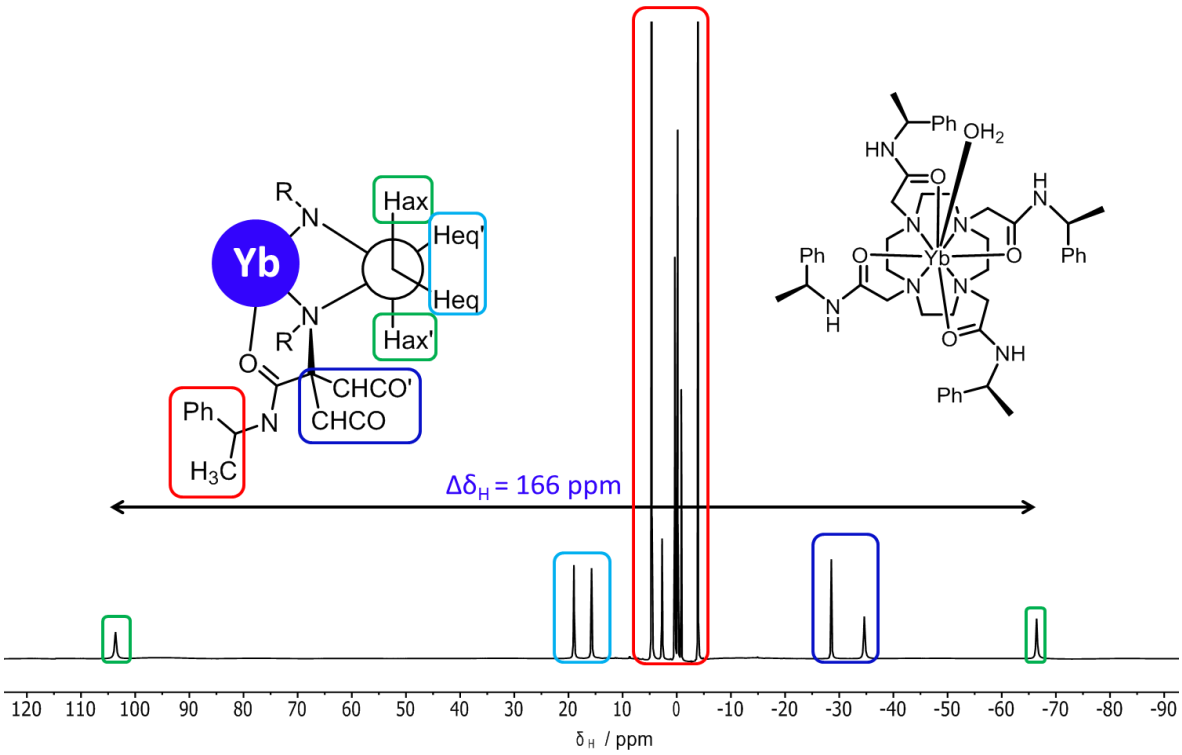

Figure 5 : *Model paramagnetic NMR spectrum of a C_4 symmetric Yb(III) complex, with shifted resonances highlighted (295 K, D_2O, 9.4 T).*[19]

The contact and pseudocontact shifts are based on magnetic susceptibility anisotropy and provide a much bigger contribution to the total observed shift. An example of the large shift contribution is given in Figure 5. The contact shift is only relevant for resonances coordinated to the lanthanide(III) ion and is of diminishing size at distances larger than 4.0 Å from the paramagnetic centre. Its contribution arises from the unpaired electrons sharing electron density through chemical bonds. There are two possible ways that the electron density is shared: either by some degree of covalency in the bond or by spin-polarisation from the core-like 4f orbitals. Experimentally, the strength of the contribution decreases for a given resonance, the more donors there are directly bound to the lanthanide(III) ion.[20]

The final contribution to the overall shift is the pseudocontact shift. Here, the magnetic field induces a dipolar interaction between the nucleus and the unpaired electron. The static magnetic moment is anisotropic and behaves differently depending on its orientation with the average dipolar interactions. This effect is strongly influenced by the shape and distribution of the f-electron cloud of the lanthanide(III) ion.[2] The

pseudocontact shift is, therefore, different for every lanthanide(III) ion. The pseudocontact shift is discussed in more detail in section 1.4.1.1

1.2.2 Paramagnetic relaxation enhancement

The standard NMR experiment and classical relaxation theory will only be covered briefly here, but can be found in any standard NMR textbook.[21,22] In most paramagnetic relaxation studies, the relaxation rates, R_1 and R_2, are analysed instead of relaxation times, T_1 and T_2, which are simply correlated in an inverse relationship. R_1 is the longitudinal and R_2 is the transverse relaxation rate and are commonly quoted in s^{-1}.

The unpaired electrons of the lanthanide(III) ion provide the nuclei with additional relaxation pathaways, leading to much faster nuclear relaxation rates than in a standard diamagnetic system. There a number of paramaters that influence the paramagnetic relaxation enhancements of ligand resonances. The main contributions are associated with the internuclear distance, *r*, of the ligand resonance to the lanthanide(III) ion, the effective magnetic moment of the lanthanide(III) ion, μ_{eff}, the rotational correlation time, τ_R and the electronic relaxation time, T_{1e}.[1,4,23] The effect of the internuclear distance, the magnetic field strength and the rotational correlation time was simulated for Figure 6 and is further discussed in section 1.4.1.2.

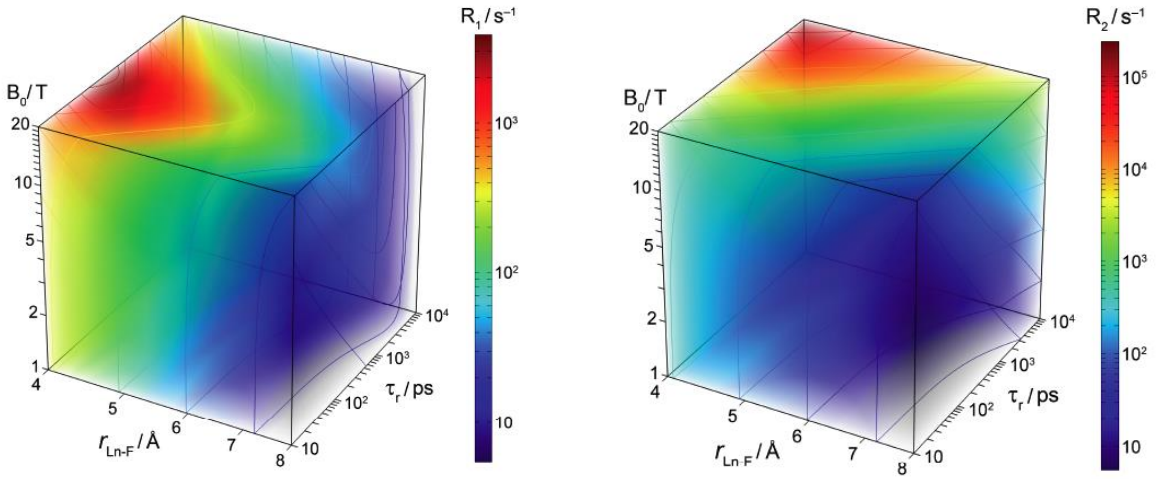

Figure 6 : *3D simulation of the variation of ^{19}F relaxation rates, R_1 and R_2, with magnetic field, B_0, distance of the CF_3 label, r , and rotational correlation time, τ_R, of a model complex (T_{1e} = 0.2, μ_{eff} = 10 BM, 298 K).*[11]

Overall, this leads to much shorter nuclear relaxation times for the observed resonances. In paramagnetic systems, the relaxation rates, R_1 and R_2, are of the order of 10^2 - 10^3 s^{-1}, for a nucleus 4 to 7 Å from the lanthanide(III) ion, and, in some cases, even faster, depending on the resonance and the lanthanide(III) ion involved.[24].

1.3. Applications of lanthanide(III) complexes in magnetic resonance

Lanthanide complexes have found extensive applications in magnetic resonance. There are hundreds of Gd(III) based contrast agents that have been characterised, and nearly a dozen have been clinically approved and are used in hospitals daily. Tens of millions of MRI scans taken each year are assisted by administration of a Gd(III) contrast agent. But not only Gd(III) is used, the lanthanide(III) ions of the second half of the 4f series have also been extensively studied. The Gd(III) complexes provide much faster relaxation enhancements, but lack the large chemical shifts differences that occur with some of the other lanthanide(III) ions [7]

1.3.1 Lanthanide complexes in biomedical imaging

Gd(III) contrast agents in MRI provide the biggest class of lanthanide agents currently in use. The main requirement for these complexes is a hydration number of greater than zero. High kinetic stability of the complexes is critical, whilst lanthanide(III) complexes are inert, but free lanthanide(III) ions are much more dangerous, with an IC_{50} value of around 0.1 mM kg^{-1}.[24,25]

Indeed, the cause of the debilitating disease, nephrogenic systemic fibrosis (NSF) has been directly linked to the premature dissociation of Gd(III) ions from their complexes with DTPA-based ligands, notably in patients where a compromised renal system led to longer retention and slower clearance of the complex, after their MRI scan.[26]

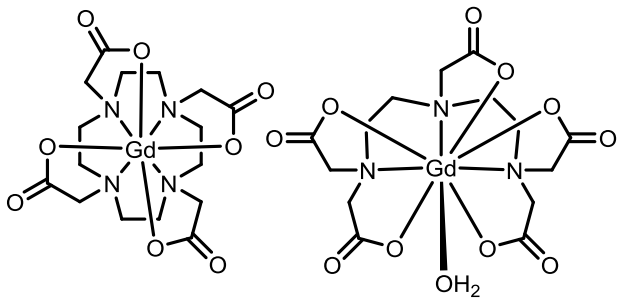

Figure 7 : *Structures of the contrast agents $[Gd.DOTA]^-$ (commercial name: DOTAREM, left) and $[Gd.DTPA]^{2-}$ (commercial name: Magnevist, right)*

Gd(III) complexes are mostly used in these contrast agents due to their superior relaxation enhancements compared to complexes of the other lanthanide(III) ions (Figure 7). Generally, Gd(III) complexes provide much faster relaxation enhancement than the other lanthanide(III) ions, due to the much larger electronic relaxation times, T_{1e} (10^4 ps versus 0.1 -1 ps). The enhanced electronic relaxation times promote nuclear relaxation much more efficiently than for the other lanthanide(III) ions. Indeed, ligand resonances may be observed only at lower magnetic field strengths, due to the severe line broadening that is correlated to very fast transverse relaxation rates, R_2.[7,24,27,28]

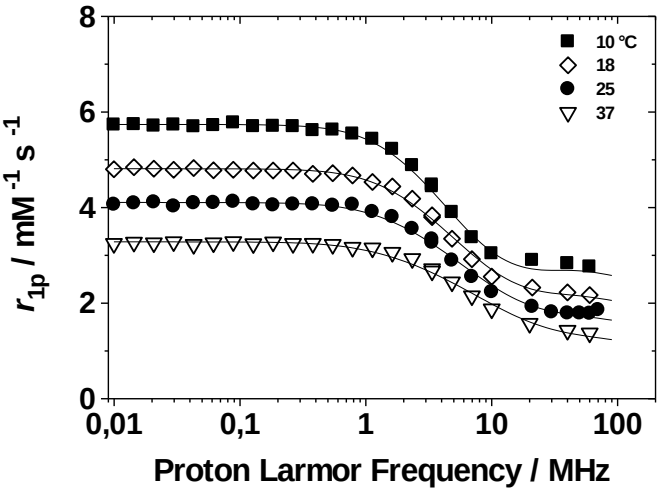

Figure 8 : *A typical ^{1}H NMRD profile showing the behaviour of the relaxivity with magnetic field strength showing the best fit (line) to the data points (283-310 K). Taken from [29].*

In contrast-enhanced MRI, the Gd(III) based contrast agents are used to enhance the relaxation rate of the bound water molecule. A fast water exchange rate ensures that the rate of relaxation of the bulk water around the complex is significantly enhanced. As a consequence of a faster longitudinal relaxation rate, application of a T_1-weighted spin echo pulse sequence leads to enhanced image contrast. The enhancement of the relaxation rate of the water molecules and other molecules around the contrast agent is the relaxivity and is commonly expressed in mM^{-1} sec^{-1} .

The relaxivity of potential contrast agents is often measured by using an NMR dispersion (NMRD) profile, which involves measuring the relaxivity at varying magnetic field strengths (Figure 8). In addition to the inner sphere contribution to the relaxivity described above, the contrast agent can enhance the relaxivity of water molecules through H-bonding (outer sphere relaxivity).[7] The relaxivity is described in equation (1):

$$r_{1p} = \frac{R_{1p}}{[c]} \qquad (1)$$

,where r_{1p} is the relaxivity in mM^{-1} sec^{-1}, R_{1p} is the relaxation rate and [c] is the local concentration of the Gd(III) complex. The relaxation rate can be modified by changing the hydration number, q, varying the overall size of the complex and thereby changing the molecular tumbling time, τ_M, by modifying the electronic relaxation time, T_{1e}, and, of course, it is dependent on the local concentration. Current research focuses on optimising these parameters to modify the relaxivity of Gd(III) complexes.[30–33]

Additionally, the complexes can be modified chemically to permit specific targeting, for example, measure ion concentrations[34], enzyme activity[35], pH[36], temperature[37] and the relative concentration of other chemical species[7,32,33,38]. There is also a variety of bio-activated molecules that only increase the relaxivity under specific conditions.[7,35] Another application is the extension of chemical exchange saturation transfer experiment (CEST) to include paramagnetic species (PARACEST). In CEST the relative intensity of the water signal (or another exchangeable proton) is reduced by selectively applying a pulse and saturating the resonance in exchange with the water.[39]

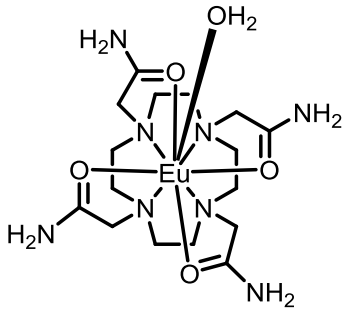

Figure 9 : *Structure of the common PARACEST agent [Ln.DOTAM]$^{3+}$ of which multiple derivatives are in use, in which prototopic exchange occurs for the NH and the OH protons.*[40]

In PARACEST, the normal range of CEST is extended by increasing the shift range of the resonance undergoing exchange, typically with the bulk water signal. This allows an increased sensitivity over the standard CEST experiment. Additionally, shorter acquisition times lead to a shorter experiment time for PARACEST agents. However, the sensitivity of this method is rather limited and local complex concentrations of > 2 mM are required for practical MR imaging experiments, hence the restricted use so far.[39,41,42]

1.3.2 Paramagnetic relaxation and shift probes

Contrast agents are mainly used to enhance the relaxivity of the water signal. However, the enhanced relaxation and shift of the ligand nuclei in a paramagnetic lanthanide(III) complex is another property that can be exploited in biomedical imaging. By shifting the resonances of interest away from the busy diamagnetic range and by enhancing their relaxation rates, the ligand resonances can be observed using short acquisition times and without the interference from the large signals due to water. In other cases, even ^{19}F or ^{31}P probe resonances have been used. In the former case there is a zero background signal.[11,37,43–46]

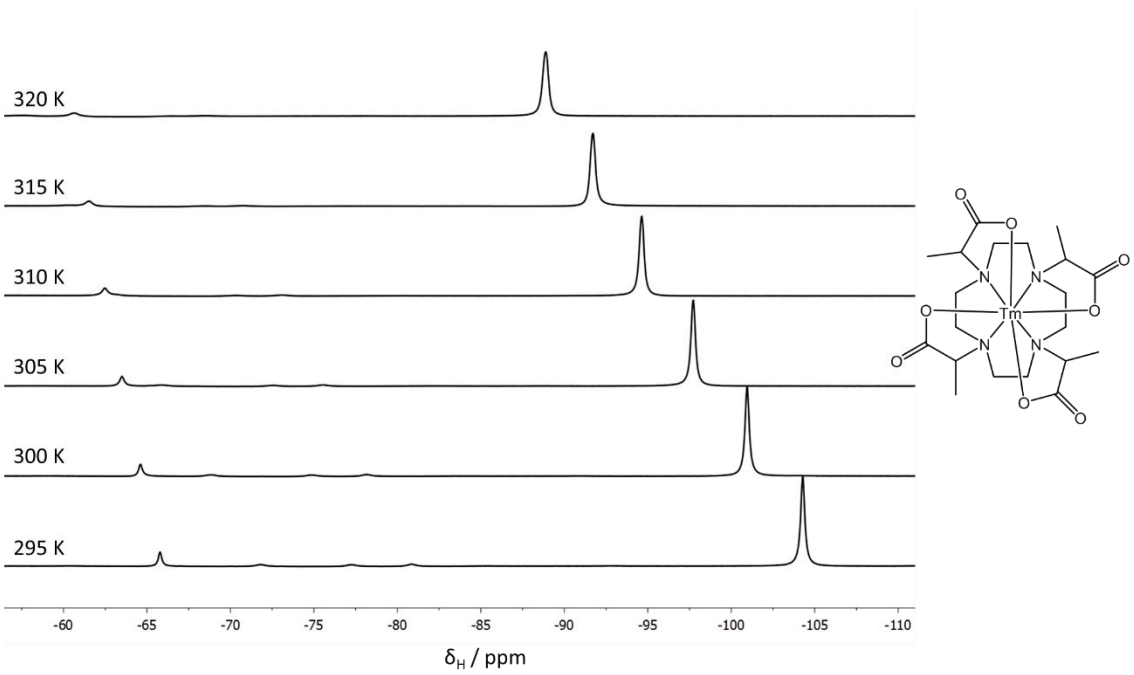

Figure 10 : *Change in the chemical shift of the CH_3 (major and minor) resonance of [Tm.DOTMA]$^-$ at the six stated temperatures. (16.5 T, D_2O).*

Similar to the Gd(III) contrast agents, the complexes have been modified for specific targeting and other applications.[34] The signal intensity is, again, highly dependent on the local concentration of the complexes. This problem is overcome in part by using highly symmetrical complexes, for example $[Ln.DOTP]^{5-}$ or $[Ln.DOTMA]^-$.[47,48]

The pseudocontact shift is temperature-dependent typically varying as 1 / T^2 (K) and can, therefore, be used directly to measure the temperature in vivo. It is desirable to analyse shifted complexes to maximise the shift in frequency per Kelvin (Figure 10). A recent example involves the use of [Tm.DOTMA]$^-$, which has successfully been used to map temperature changes in a human brain.[20,47–50]

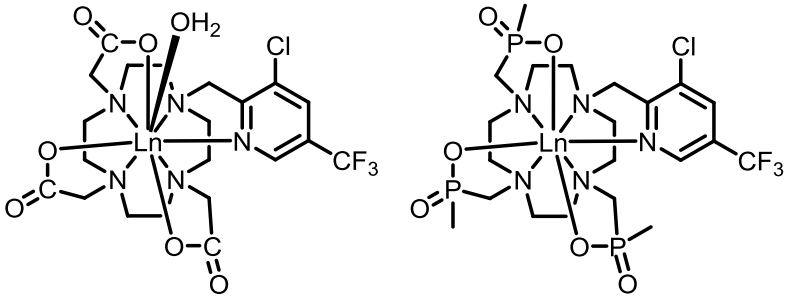

Figure 11 : *Structure of the relaxation agents possessing a ^{19}F receptor group. The two complexes differ in form of their anionic donor group and in their hydration number.*[23]

The paramagnetic relaxation enhancements and the shift range of lanthanide(III) complexes have been exploited to design fast-relaxing complexes containing ^{19}F receptor groups (Figure 11). In MRI, a ^1H / ^{19}F probe can be used to switch from the crowded ^1H spectral range to the ^{19}F spectrum.[43,44,51] However, the ^{19}F nucleus has a limited sensitivity in MRI. Here, the sensitivity issue is overcome by using the enhanced relaxation of the paramagnetic complex. By carefully designing the complexes, the relaxation enhancement and the observable shift can be tuned to maximise the sensitivity increase.[23] The paramagnetic relaxation enhancement and how it can be tuned will be discussed further in section 1.4.1.2.

1.3.3 Paramagnetic protein tags

The relaxation and shift enhancements not only have an advantage in biomedical imaging but also offer assistance in the NMR analysis of protein structures.[52]

Lanthanides have no function in living biological systems, and either need to be substituted into binding sites for endogenous metals (e.g. Ca^{2+}) or need to be introduced

by using complex tags. In recent years, tags using lanthanide(III) ions have gained popularity.[18,52,53] In most cases, the lanthanide(III) tags are covalently linked to the protein. Due to the close proximity of the lanthanide(III) to the protein, the resonances of the protein are perturbed in terms of their shift and relaxation rates.

The large pseudocontact shifts caused by lanthanide(III) ions, e.g. Dy(III), Tm(III), and their associated relaxation enhancements can affect nuclei up to 40 Å away from the lanthanide ion(III). Well known macrocyclic lanthanide(III) complexes have been modified to contain a cysteine- or amide active group, which can be covalently linked to the protein (Figure 12).[18,54]

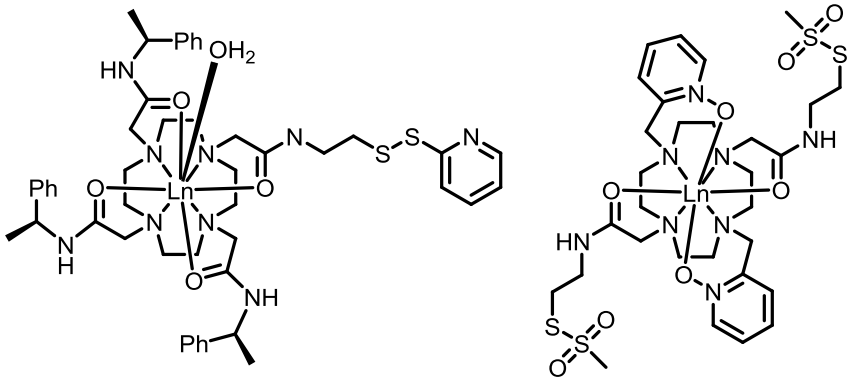

Figure 12 : *Structures of C1 (left) and ClaNP-5 (right), which are currently employed in protein tagging*[55,56]

There are a few methods to investigate the structure of proteins. A common method employed by Otting and also Luchinat, is to make a series of isostructural complexes and examine the differences in the shift induced by different lanthanide(III) ions using ^{15}N HSQC spectra, in comparison to a diamagnetic analogue. The main problem with using lanthanide tags, however, is that it is not known how the paramagnetic tag perturbs the structure of the biomolecules. Additionally, it is not always guaranteed that a given lanthanide(III) complex will form an isostructural series. Therefore, the nature of the complexes has to be considered carefully.[52,53,57–59]

1.4. Designing paramagnetic probes

1.4.1 Theoretical framework

The following sections will examine the theoretical framework that is necessary to understand the theories underpinning the pseudocontact shift and paramagnetic relaxation enhancements. The pseudocontact shift was famously rationalised in Bleaney's theory of magnetic anisotropy (1972).[2] The relaxation enhancements are commonly explained with reference to Solomon-Bloembergen Morgan equations.[4,5]

1.4.1.1 Bleaney's theory of magnetic anisotropy

The magnetic susceptibility anisotropy is responsible for the contact and pseudocontact shift (equation 2 and 3) in a paramagnetic NMR spectrum of a lanthanide(III) complex.[2,3]

$$\delta_{pseudo} = \frac{C_J \mu_B^2}{60\,(kT)^2}\left[\frac{(3cos^2\theta - 1)}{r^3} B_0^2 + \sqrt{6}\,\frac{(sin^2 cos2\varphi)}{r^3} B_2^2\right] \qquad (2)$$

$$C_J = g_J^2 \langle J \| \alpha \| J \rangle J(J+1)(2J-1)(2J+3)\,(1+p) \qquad (3)$$

,where θ and *r* define the polar coordinates and internuclear distance to the lanthanide(III) ion, C_J is the Bleaney constant, μ_B is the Bohr magneton, B_0^2 and B_2^2 are second order crystal field splitting parameters, $\langle J \| \alpha \| J \rangle$ is a numerical coefficient, *J* is the total spin orbit coupling and *g* the electron g-factor. The Bleaney constant varies with the electronic configuration of the lanthanide(III) ions. Table 2 contains some electronic properties, including a normalised value for the Bleaney constant. In this theory, only the second-rank crystal field splitting parameters, B_0^2 and B_2^2 are considered.[2]

By selecting a specific lanthanide(III) ion, it is possible to influence the direction and the magnitude of the pseudocontact shift through the Bleaney constant. However, as can

be seen from equation (2) there are more factors influencing the overall pseudocontact shift. Another major issue is the location of the nucleus of interest with respect to the principal (or easy) axis of the magnetic field, i.e. the internuclear distance and the polar coordinates. It is assumed that the easy axis of magnetisation follows the direction of the symmetry element.

Table 2 : *Overview of Bleaney constants, and the electronic properties of selected lanthanide(III) ions*

Ln^{3+}	*J*	$\langle J\|\alpha\|J\rangle$	C_J	C_J normalised
Tb	6	0.0101	-157.5	-87
Dy	15/2	-0.0076	-181	-100
Ho	8	-0.0022	-71.2	-39
Er	15/2	0.0025	58.8	33
Tm	6	0.0101	95.3	53
Yb	7/2	0.0318	39.2	22

The geometrical term consists of two parts: one describing position and another describing distance. The position of the nucleus with respect to the magnetic principal axis contributes to the sign of the overall term. For example, depending on whether $3cos^2\theta \leq 1$, the resonance may shift in a certain direction while if $3cos^2\theta \geq 1$, it shifts in the other direction. However, the maximum values for the angle term may only vary between (2) and (-2). The distance dependence provides this term with a magnitude. It is based on a dipolar interaction; therefore the dependence of the internuclear distance is r^{-3}. Combining these two effects will provide the term with a sign and magnitude depending on the polar coordinates of the resonance (Figure 13).

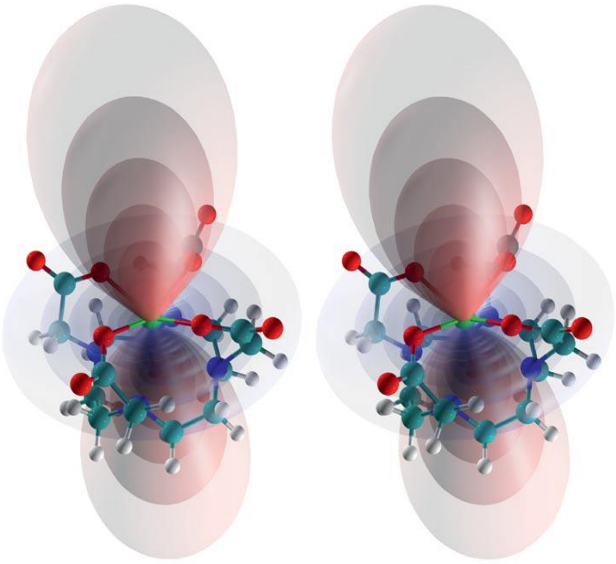

Figure 13 : *Graphical depiction of [Ln.DOTA]$^-$, where the geometrical term in red indicates a negative shift value and purple indicates a positive value. Colour intensities correlate to shift strength. Taken from [23].*

The last term that determines the pseudocontact shift relates to the local ligand field described by various crystal field splitting parameters. In his theory, Bleaney only considered the second order parameters. However, in Bleaney's theory the crystal field splitting is always assumed to be smaller than *kT (*205 cm^{-1} at 298 K). The overall crystal field splitting parameters, however, have been estimated to be up to ± 2000 cm^{-1}.[10,12,60] Again, this term can contribute with a sign and with magnitude to the overall pseudocontact shift. A selection of the crystal field splitting parameters from the literature can be found in Table 3.

Table 3 : *Overview of reported crystal field splitting parameters for Eu(III) complexes of stated ligands.*[19,23,61]

Ligand	Δ*J* = 1 splitting /cm^{-1}			sign	A_0^2 /cm^{-1}	B_0^2 /cm^{-1}
aqua	16920	16880		-	40	133
NTA	16900	16840		+	60	200
NOTA	16930	16790		+	140	467
$(NTA)_2$	16900	16800		+	100	333
DOTA	16990	16920	16800	-	190	633
$(DPA)_3$	16930	16820		-	110	367
HEDTA	16930	16870	16790	+	140	467
CyDTA	16910	16820		+	90	300
EDTA	16950	16870		-	80	267
DTPA	26960	16810		-	150	500
TETA	17020	16840	16790	+	230	767

[a]For the C symmetric systems two isomers are present giving rise to the observed transitions, two of which overlap. Data is given for major isomer. [b]Values of B_0^2 were estimated using the approximation of $B_0^2 = \frac{10}{3}\, x\, \Delta J = 1$ splitting (vide infra: see chapter 3) of the Eu(III) emission spectrum. The associated error of this measurement is ±40 cm^{-1}.[9]

As can be seen, the values of B_0^2 can vary from 133 to 767 cm^{-1}, which might be even further enhanced by higher order parameters that are not considered here. The values for the crystal field splitting parameters were estimated using a method developed by Binnemans[9]. In his later work, Binnemans investigated this splitting further and concluded that the crystal field spitting might be even larger than estimated here. He showed that the splitting of the Δ*J* = 1 level is correlated to the B_0^2 parameter by a factor of 4.05. A few studies have tried to incorporate the higher order crystal field splitting parameters into the theory of magnetic anisotropy, but still reported a significant deviation between experimental and theoretical values.[3,62]

1.4.1.2. Solomon-Bloembergen Morgan theory

The relaxation rate, R_1, of a paramagnetic resonance follows Bloch-Redfield Wangsness theory (BRW) and is commonly described by Solomon-Bloembergen Morgan theory (SBM) (equation 4 and 5). One of the main assumptions is that the coupling between spin and lattice is smaller than the reciprocal of the rotational correlation time, the so-called Redfield limit ($R_1 << 1 / T_{1e}$). The lanthanide(III) complexes used here, should all fall below the Redfield limit.[1,4,5,23]

$$R_1 = \frac{2}{15}\left(\frac{\mu_0}{4\pi}\right)^2 \frac{\gamma_N^2 g_{Ln}^2 \mu_B^2 J\,(J+1)}{r^6}\left[3\frac{T_{1e}}{1+\omega_N^2\,T_{1e}^2}+7\frac{T_{2e}}{1+\omega_e^2\,T_{2e}^2}\right] + \frac{2}{5}\left(\frac{\mu_0}{4\pi}\right)^2 \frac{\omega_N^2 \mu_{eff}^4}{(3k_B T)^2\,r^6}\left[3\frac{\tau_r}{1+\omega_N^2\,\tau_r^2}\right] \quad (4)$$

$$R_2 = \frac{2}{15}\left(\frac{\mu_0}{4\pi}\right)^2 \frac{\gamma_N^2 g_{Ln}^2 \mu_B^2 J\,(J+1)}{r^6}\left[2T_{1e}\frac{3}{2}\frac{T_{1e}}{1+\omega_N^2\,T_{1e}^2}+\frac{13}{2}\frac{T_{2e}}{1+\omega_e^2\,T_{2e}^2}\right] + \frac{2}{5}\left(\frac{\mu_0}{4\pi}\right)^2 \frac{\omega_N^2 \mu_{eff}^4}{(3k_B T)^2\,r^6}\left[2\tau_r\frac{3}{2}\frac{\tau_r}{1+\omega_N^2\,\tau_r^2}\right] \quad (5)$$

where γ_N is the gyromagnetic ratio, g the Landé g-factor, J the total spin orbit coupling, r the internuclear distance to the lanthanide centre, T_{1e} and T_{2e} the longitudinal and transverse electronic relaxation times, ω_N and ω_E the nuclear and electronic Larmor frequency, $\mu_B^2 J(J+1)$ the effective magnetic moment, from now on called μ_{eff}, and τ_R is the rotational correlation time.

There are two main contributions, the dipolar and the Curie term. In the dipolar term, the spin transitions induced by the unpaired electrons are described. The dipolar pathway is described by a dipolar interaction between the unpaired electron and the nucleus. When point-dipoles are considered, there are anisotropic fluctuations around the nucleus of interest, leading to a relaxation pathway based on the rotation of the

molecule. Normally, an overall correlation time of $\frac{1}{\tau_S} = \frac{1}{T_{1e}} + \frac{1}{\tau_R}$ is considered to describe this process. However, in the case of the fast relaxing lanthanides (Tb(III), Dy(III), Ho(III), Er(III), Tm(III) and Yb(III)) the electronic relaxation rate is much faster than the rate of rotation, which means, at least in the dipolar term, that the rotational correlation time can be neglected. The electronic relaxation times, T_{1e} and T_{2e} can be assumed to be of the same order of magnitude and are hereafter considered to be of the same magnitude.[11] The physical mechanisms describing electronic relaxation times are not well understood. However, it is commonly assumed that they are a consequence of magnetic field fluctuations induced by collisions of solvent molecules perturbing the electron cloud of the complex. Such collisional processes typically occur at a rate of 10^{13} s^{-1}.[63,64]

Curie relaxation arises from the rotational variation of the direction in the average induced magnetic dipole moment. It is mainly modulated by the effective magnetic moment and the rotational correlation time.

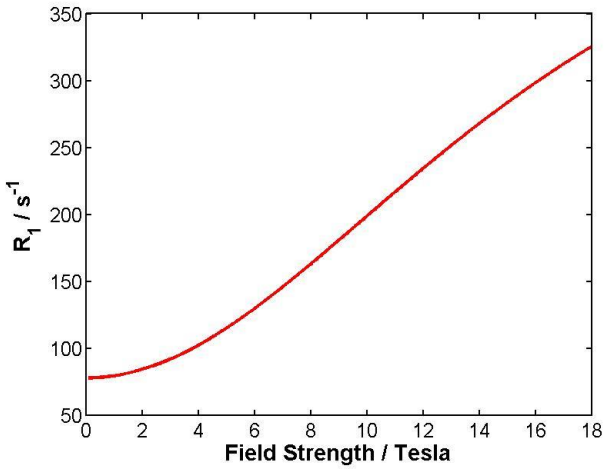

Figure 14 *: Simulation of the variation of the ^{1}H NMR relaxation rate of a nucleus with field in a model complex system (295K, T_{1e} = 0.5 ps, τ_r = 250 ps, μ_{eff} = 10 BM, r= 6 Å).*

The relaxation rates are proportional to the magnetic field strength. At lower field strengths the dipolar term is dominant, but at higher fields the Curie term is dominant, due to the $\omega_N^2 \mu_{eff}^4$ term. As these terms are additive, this leads to a slight slowing of the increase of the relaxation rate at higher field strengths, as shown in Figure 14. Here the variation of R_1 with B_0 is described, in ^{1}H NMR for a resonance 6 Å away from an idealised

lanthanide centre (295 K). In this simulation, it is assumed that T_{1e} = 0.5 ps, μ_{eff} = 10 BM and τ_R = 250 ps.

1.4.2. Practical aspects of designing paramagnetic probes

There are certain practical aspects that facilitate the efficient design of non-Gd(III) based paramagnetic probes. It is highly desirable for the ratio of R_1 /R_2 to be as close to unity as possible. Under these conditions, line broadening is minimised for a given maximal enhancement of R_1. Additionally, for efficient use of the short times the R_1 should be around 100 to 200 s^{-1} at 7 T. Relaxation rates of that magnitude allow signal intensity to be acquired using modified ultrafast gradient spin-echo sequences, which can provide high signal-to-noise ratio increases, of the order of 15 to 25:1 over diamagnetic analogues.[11,23,43,51]

1.4.2.1 Lanthanide(III) ion selection

The selection of the lanthanide(III) ion has a significant impact on the relaxation and shift behaviour. The Bleaney constant, C_J, gives a good indication about the magnitude and sign of the pseudocontact shift. It is highly desirable to have the resonance as far away as possible from the diamagnetic range and Dy(III), Tb(III) and Tm(III) systems commonly provide the best shift range of all lanthanide(III) ions, as they possess the highest magnetic susceptibility. The Bleaney constant for Tm(III) is only +55 compared to the normalised values of -100 and -89 of Dy(III) and Tb(III). However, it has been reported that the Tm(III) resonances in certain complexes shift much more than the Bleaney constant would suggest.[49,65]

Of course, the relaxation rate enhancement has to be considered too. Due to its lower magnetic moment, Tm(III) systems give rise to smaller relaxation rate enhancements and in normal circumstances, it is a less attractive candidate.

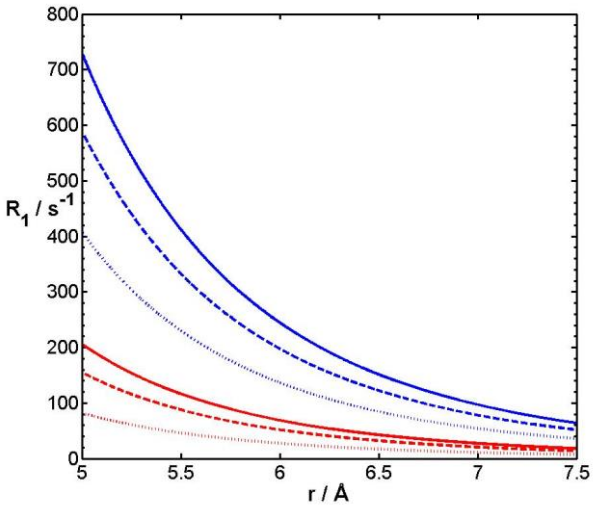

Figure 15 : *Simulation of the nuclear relaxation rate R_1 (s^{-1}), with internuclear distance (Å) of a hypothetical ^1H resonance in idealised systems with Dy(III) (blue) and Tm(III) (red) at three different magnetic field strengths (4.7, 7 and 9.4 T) (295 K, T_{1e} = 0.5 and 0.3 ps, τ_R =250 ps).*

The dependence of R_1 and R_2 on the magnetic susceptibility is particularly significant at higher magnetic field strengths. This renders Dy(III) an ideal candidate for use as a paramagnetic probe (Figure 15). At a distance of 6 – 7 Å, the relaxation rate is enhanced to values in the range of 100 – 200 s^{-1}. At closer distances, the broadening of the signals caused by enhanced R_2 values makes data acquisition in imaging and spectroscopy more difficult. At larger distances from the paramagnetic centre, the resonance of interest may not be at a fixed distance, because of local conformational mobility, making the 'effective' distance shorter than may be surmised in a 'static' structural analysis (e.g. X-ray data). Furthermore, dynamic conformational exchange may lead to uncertainty broadening. Figure 15 shows not only the effect of lanthanide selection, but also the effect of variation of the internuclear distance on the nuclear relaxation rates. The r^{-6} dependence leads to a significant increase in R_1 at smaller distances.

The electronic relaxation time, T_{1e}, also varies amongst the lanthanide(III) ions. While T_{1e} has a diminishing effect at higher magnetic field strengths, due to the dominance of the Curie term, it has a major influence in the field range of 0.1 to 7 Tesla. This range

includes the clinical imaging instruments. At lower fields, T_{1e} significantly perturbs the nuclear relaxation rates, R_1, by almost an order of magnitude as seen in Figure 16.

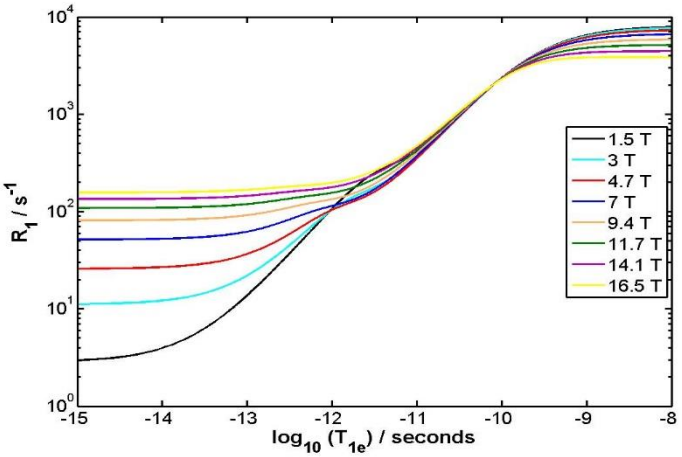

Figure 16 : *Simulation of the dependence of R_1 on T_{1e} at a variety of fields (295 K, μ_{eff} = 10 BM, r = 6.5 Å, τ_R = 250 ps).*

The expected T_{1e} values range from 0.1 to around 1 ps for the fast relaxing lanthanide(III) ions.[20,28,66–68] At field strengths between 1.5 and 7 Tesla, the nuclear relaxation rate can be enhanced by almost an order of magnitude over the expected range of the electronic relaxation time. Such an analysis highlights the importance of the electronic relaxation time, especially at the field strengths relevant for biomedical MRI. However, the physiochemical mechanistic basis of electronic relaxation is largely unknown and it is not yet possible to predict a T_{1e} value from ligand design.

1.4.2.2 Impact of ligand design on MR properties

The main factor that needs to be considered in ligand design is the dependence of shift and relaxation, of a given resonance, on the internuclear distance, *r*, from the lanthanide(III) centre. The immediate impact of the internuclear distance on R_1 was shown above (Figure 15). An additional factor that has to be considered is the rotational correlation time, τ_r. It is directly linked to the overall size of the complex and is often estimated using Stokes-Einstein theory for an idealised spherical object.[69] However, as

most biomedical probes are based on $12N_4$ macrocyclic systems, the rotational correlation time will usually lie in the range of 120 to 300 ps. The correlation times that are estimated by NMRD fitting experiments are always much smaller than the true volumes. This discrepancy occurs, because the measurement of the water relaxation relates to the Gd-OH_2 vector, whose motion is not normally efficiently coupled to that of the whole molecule. Indeed, Szabo et al, showed that there are localised rotational correlation times in molecules.[70,71]

In terms of the correlation time experienced by the resonances and its effect on relaxation, the resonances closest to the paramagnetic centre should experience a rotational correlation time that is closest to the true value of the complex. In this situation, these atoms (e.g. ^{31}P centres in a phosphinate complex) are rigidly linked to the lanthanide(III) centre and must lie close to the barycentre of the molecule. Resonances further away from the paramagnetic centre will experience more degrees of freedom, which will lead to more localised and shorter apparent rotational correlation times.[70]

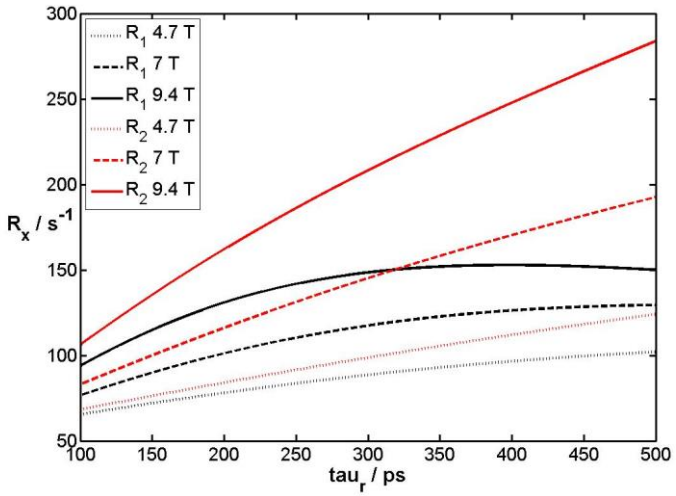

Figure 17 : *Simulation of the dependence of the ^1H NMR R_1 and R_2 values in an idealised complex on the rotational correlation time, τ_R, at different field strengths (295 K, μ_{eff} = 10 BM, T_{1e} = 0.5 ps, r = 6.5 Å)*

The effect of the variation of the rotational correlation time on R_1 and R_2, is shown in Figure 17. In particular, an increasing effect on R_2 is visible. It can be seen that depending on the size of the molecule, the R_1 / R_2 ratio changes significantly. Rotational correlation

times of the order of 200 - 300 ps should give the best results in terms of the balance between relaxation enhancements and the maximisation of R_1 / R_2.

1.5. Aims & Objectives

1.5.1 Investigating the electronic relaxation times

The electronic relaxation times can have a significant impact on the nuclear relaxation rates of lanthanide(III) complexes. Understanding the principles and mechanism underpinning electronic relaxation will benefit our understanding of the use of lanthanide(III) ions in magnetic resonance. Paramagnetic probes for biomedical imaging and even paramagnetic protein tags will also benefit from this knowledge. In each case, the nuclear relaxation rates play an important role, and by predicting electronic relaxation times, a more efficient design of probes may be possible. To an extent, this thinking also applies to the series of Gd(III)-based contrast agents, notably when used at low magnetic field strengths.

1.5.1.1 Electronic relaxation rate studies

Lanthanide(III) electronic relaxation times have been investigated only a few times using NMR spectroscopy. The earliest reports by Alsaadi, Rossotti and Williams[66,67] focused on measuring the relaxivity of the water resonances at low magnetic field strengths. By estimating the magnetic moment and the internuclear distance, they estimated the electronic correlation time for a variety of aqua-cations and ligand complexes of varying speciation. No clear correlation was found in the four systems investigated, but a general order of T_{1e} values for the lanthanides was established, Tb(III) > Dy(III) > Ho(III). They concluded that the electronic correlation times are much shorter than the Gd(III) analogues. Additionally, it was stipulated that the changes in the correlation time arose from perturbation of the crystal field due to vibrations of the water molecule.

A similar approach was used by Bertini and Luchinat in 1993.[28] In their study, the range of magnetic fields in a standard NMRD experiment was extended from 50 MHz to 600 MHz. As a large range of magnetic fields strengths were used, it was possible to analyse the dipolar and the Curie term independently. However, while a lot of data points were analysed in the lower field range, there were only three fields measured between 100 and 600 MHz (Figure 18). This limited the quality of the data analysis and the fitting of curves at higher fields was not rigorously undertaken. The values calculated follow similar trends to those observed by Alsaadi et al. Luchinat and Bertini concluded that the ground state splitting of the energy levels due to the crystal field is the main determinant of the electronic relaxation times.

Aime et al. used a different method to estimate electronic relaxation times by measuring the longitudinal relaxation rates at a single field strength, but the transverse relaxation rates at three different field strengths. The differences between the values were used to calculate the internuclear distance and the electronic relaxation times. The electronic relaxation times for $[Ln.DOTA]^-$ complexes of Tb(III), Dy(III) and Ho(III), were estimated with values for Ho(III) being the lowest.[68]

Such a study was extended to the $[Ln.DOTP]^{5-}$ series by Ren and Sherry. However, their study was limited to higher field strengths to examine the effect of the Curie term and how the ligand field influences the overall dipolar shift. The T_{1e} values they observed mostly fell in the range of 0.4 – 0.8 ps, much higher than values found in earlier studies, especially for $[Tm.DOTP]^{5-}$ (1.34 ps).[20]

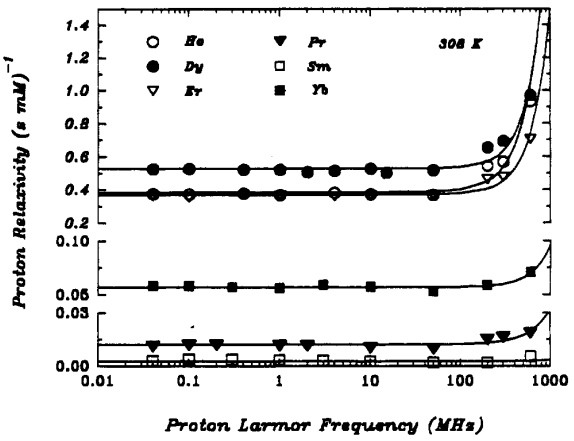

Figure 18 : *Field independence of the relaxation rate of the lanthanide aqua ions at lower fields, as examined by Bertini and Luchinat. Taken from [28].*

Finally, the most recent study on the electronic relaxation times of lanthanides was reported by Fries et al during the first few months of this PhD project. Here, they calculated the electronic relaxation times using an analytical Redfield theory and a numerical Monte-Carlo simulation. In their calculations using Redfield theory, they assumed the zero-field splitting (ZFS) due to the ligand field to be the main cause of electronic relaxation.[72,73] The authors used time correlation functions of the electronic spin, as they reflect fluctuations caused by the ZFS. In their approach using Monte-Carlo methods, the authors also investigated the impact of the static and transient ligand field of lanthanide(III) complexes, which are disturbed by solvent collisions.

They directly correlated the fluctuations in the transient ligand field to the crystal field splitting parameters. However, they neglected the influence of any of the higher order terms. In addition the ligand field splitting used in their simulations is around 200 cm^{-1} in each case, which is comparatively small in size. Overall, an inverse proportionality between T_{1e} and B_0^2 was concluded. Additionally, it was suggested that the difference between lanthanides is due to the splitting of their *J* energy levels. These hypotheses do not follow the trends observed in earlier studies

Table 4 : *Calculated values for the electronic relaxation times in the literature.*[20,28,66–68,72]

	T_{1e} /ps				
Ln^{3+}	Alsaadi $[Ln.(dpa)_3]^{3-}$	Bertini $[Ln.(H_2O)_9]^{3+}$	Aime $[Ln.DOTA]^-$	Sherry $[Ln.DOTP]^{5-}$	Fries[a]
Eu	-	-	0.30	-	-
Tb	0.29	-	0.25	0.69	0.21
Dy	0.45	0.39	0.27	0.82	-
Ho	0.17	0.27	-.	0.54	-
Er	0.32	0.31	-	0.85	0.35
Tm	0.16	n.d.	-	1.54	0.11
Yb	0.10	0.22	-	0.28	-

[a]The values of Fries are computed for a model complex with a ligand field splitting of 200 cm^{-1}; other values are estimated based on experimental measurement

An overview of all the available data sets in the literature is provided in Table 4 and the underlying trends reported by the groups can be seen.

1.5.1.2 Electronic relaxation times estimation through nuclear relaxation

In 2009 Kuprov and Parker reported calculations and simulations that allow estimation of the internuclear distances by measuring the nuclear relaxation rates of ligand resonances at different magnetic field strengths and fitting the data to the Solomon-Bloembergen Morgan equations.[11] Due to the dependence of the nuclear relaxation rates on the nuclear Larmor frequency, it is possible to create a data set that allows fitting of parameters using standard minimisation techniques. This technique can be slightly modified to calculate the electronic relaxation times. With the help of X-ray structural analysis and DFT calculations to assess molecular volume, estimates can be made for the internuclear distance and the rotational correlation times (Figure 19). The effective magnetic moment is believed to be a well understood quantity in the lanthanide(III) ions and, therefore, estimates from the literature values can be used. This only leaves the electronic relaxation times as an unknown in the Solomon-Bloembergen Morgan equations.[11,23]

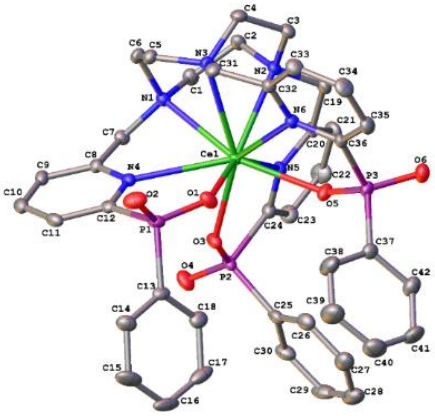

Figure 19 : *Crystal structure of RRR-Λ- [Ce.L^2] (120K).*[29]

Based on the work, a Matlab™ algorithm was written with the help of Dr. Ilya Kuprov. A Levenberg-Marquardt minimisation of the least squares function is used to fit nuclear relaxation rate data for sets of ligand resonances of paramagnetic lanthanide(III) complexes, measured at the five different magnetic fields strengths: 4.7, 9.4, 11.7, 14.1 and 16.5 Tesla available at Durham Unversity.

To extend the data sets, isostructural series of lanthanide(III) complexes are used, so that the rotational correlation time and the internuclear distance can be taken as global variables and are assumed to be the same across a complex series of lanthanides. Even though the lanthanide contraction is present across the 4f series, the effect can be neglected when looking at internuclear distances, as the change in ionic radius is of the order of 0.05 Å from Tb(III) to Yb(III) and this is a relatively small change compared to other errors.[15]

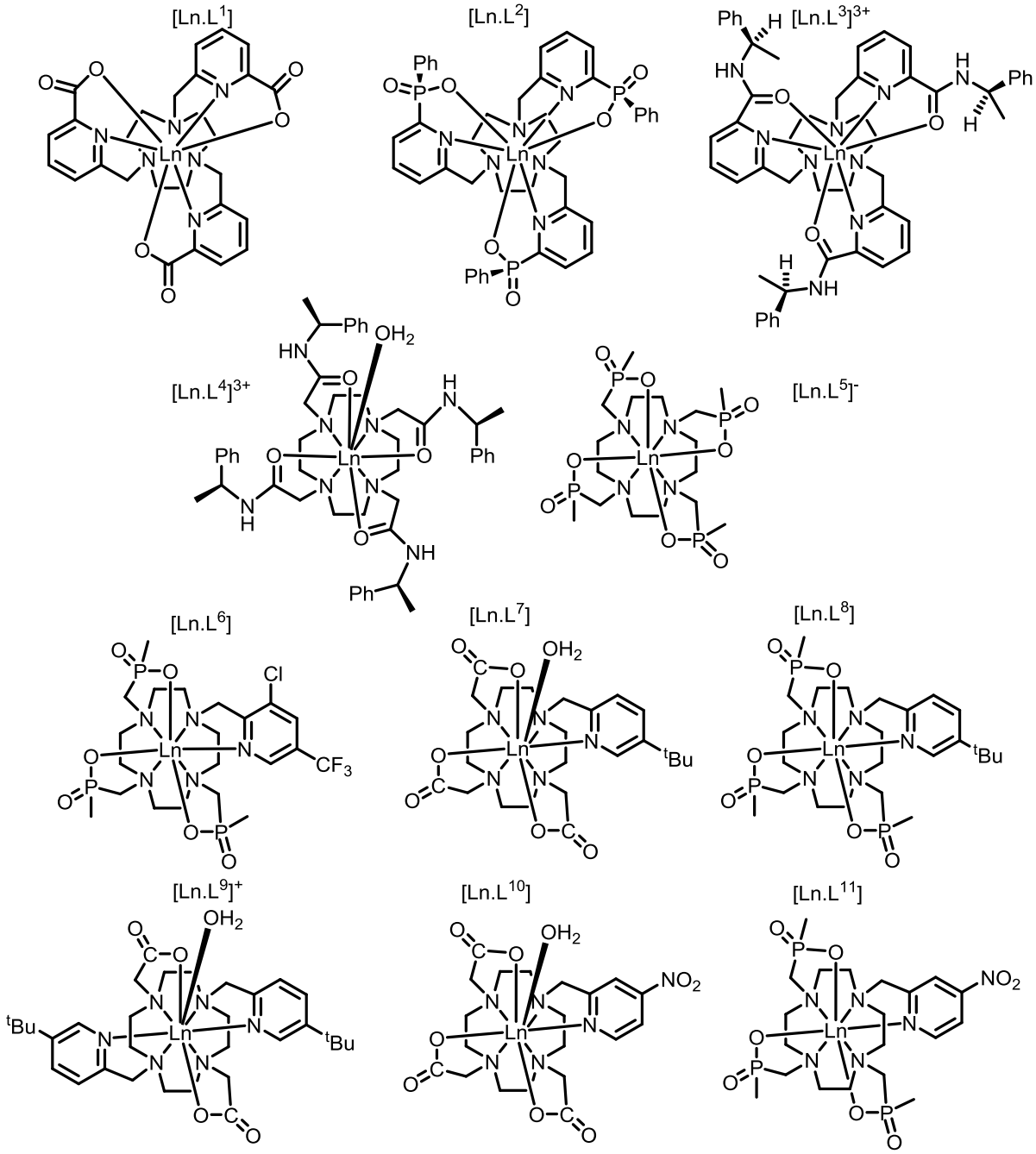

Scheme 1 : *Structures of the isostructural series of lanthanide(III) complexes studied in this thesis.*

A wide range of complex series was used to gain insight into the factors that influence the rate of electronic relaxation (Scheme 1). The complexes [Ln.L^{1-3}] are C_3 symmetric and adopt a tricapped trigonal prismatic coordination geometry with no bound water. They only differ in the anionic donor group (carboxylate, phosphinate and amide respectively), creating a different ligand field at the metal centre.[74]

The cationic complex [Ln.$L^4(OH_2)$]$^{3+}$ (from here on labelled as [Ln.L^4]$^{3+}$) has a hydration number of one and adopts a C_4 symmetric monocapped SAP coordination geometry.[15] The phosphinate complex [Ln.L^5]$^-$ also has a C_4 symmetric coordination geometry. However, it has no bound water molecule and forms a TSAP complex.[75] The remaining complexes lack C_n time-average symmetry and form a SAP coordination environment, with the exception of [Ln.L^9]$^+$, which forms C_2 symmetric SAP complexes. Again, the main differences between these complexes are the differences between the anionic donor groups. The series of complexes [Ln.L^7], [Ln.L^8] and [Ln.L^{10}], [Ln.L^{11}] are direct analogues of each other and should behave similarly as only their anionic donor groups change.[46,61] The main difference between the carboxylate and the phosphinate complex series, apart from donor atom polarizability and size, is the common hydration number of one and zero.

Some of the complexes possess heteroatoms (^{19}F, ^{31}P), allowing multinuclear NMR analysis. Therefore, wherever possible, multiple resonances were analysed. The analysis was limited to resonances at an intermediate distance to the paramagnetic lanthanide(III) ions. Too short a distance will lead to severe line broadening and too long a distance introduces more degrees of freedom to the resonance of interest.[11]

Overall, this selection of isostructural series of lanthanide complexes permits a wide overview of electronic relaxation times, in different environments, from the symmetrical C_3 and C_4 systems to the low symmetry complex series.

A few more individual complexes (e.g. [Ln.gDOTA]$^{5-}$, [Tm.DOTMA]$^-$) were analysed and will be shown and described as appropriate.

1.5.2 Investigating the pseudocontact shift

The magnetic anisotropy of lanthanide(III) complexes is another quantity that, when modified correctly, can enhance a paramagnetic probe or contrast agent significantly. For example, in PARACEST the sensitivity of the technique is directly linked to the shift difference of the resonance in exchange. Investigations in the true behaviour of magnetic susceptibility would not only benefit our understanding and design of PARACEST agents, but also benefit in the design of paramagnetic probes for biomedical imaging and protein tagging, as larger pseudocontact shifts are desirable in these systems.

1.5.2.1 The limitations of Bleaney's theory of magnetic anisotropy

Bleaney's theory of magnetic anisotropy is widely accepted and is normally used to estimate the pseudocontact shift of paramagnetic lanthanide(III) complexes. However, there are a few assumptions that do not allow accurate determination of the pseudocontact shift. First of all, a point dipole approximation is used, which is known to be an inaccurate depiction. Binnemans et al. have carried out extensive studies on magnetic anisotropy, and highlighted the many discrepancies of Bleaney's theory.[76] They showed that Dy(III) is not always the lanthanide(III) ion that exhibits the highest magnetic anisotropy, as the Bleaney coefficient would indicate, but depending on the coordination environment, Tb(III) and even Tm(III) can surpass Dy(III) in the magnitude of magnetic anisotropy. This would indicate a much higher dependence on the ligand field than suggested by Bleaney.[77] Another of Bleaney's initial assumptions is the temperature independence of certain parameters. Several studies investigated the variation of shift with *T* in detail, seeking to explain the deviation from the proposed $1 / T^2$, but no conclusive results were reached.[62,76,77]

Bleaney had also underestimated the ligand field contribution to the overall dipolar shift. In his original proposal[2], Bleaney assumed that the overall ligand field was of the order of 100 cm^{-1} (vs 205 cm^{-1} for *kT* at 298 K) and that it would tend to be cancelled out

by the (*kT*) term. Such a situation arises for systems with small ligand field splitting. However, much bigger ligand fields have been observed of up to 2000 cm^{-1}, which is of the same order of magnitude as the splitting of the electronic energy levels due to spin-orbit coupling. Additionally, Bleaney only considered the second rank crystal field splitting parameters, B_0^2 and B_2^2 and ignored higher order parameters. Again, the higher order parameters associated with multiple electrostatic interactions, may contain a significant part of the overall crystal field. In particular, this is the case for the low symmetry systems as the higher order parameters are likely to play an even more important role. While the sign of the magnetic anisotropy is correctly predicted by Bleaney's theory, the magnitude and differences are difficult to quantify, due to the approximations made.[9,12,77]

1.5.2.2 Shift behaviour in isostructural series of lanthanide(III) complexes

In some cases it is not possible to explain the difference in the dipolar shift, by simply looking at the relative B_0^2 values postulated by Bleaney's theory. An extensive study reported by Sherry and Ren et al. showed that the experimental values of the dipolar shift may deviate significantly from theoretical predictions.[78]

The isostructural series of lanthanide(III) complexes presented in Scheme 1 create the perfect opportunity to investigate pseudocontact shift behaviour in a large series of related systems. For resonances that are further than 4.5 Å away from the paramagnetic centre, there is a vanishing small contact contribution that can be neglected. Comparing a resonance to a diamagnetic analogue (e.g. Y(III)), allows the pseudocontact shift to be estimated, independent of the contact and diamagnetic contributions.

Of course, the ionic radius of the lanthanide ions decreases across a lanthanide series due to lanthanide contraction. This contraction will slightly change the internuclear distance and the angle with respect to the magnetic principal axis. However, the

resonances under investigation each possess big pseudocontact shifts and the differences due to these changes will be small.

A numerical method can be employed to predict the shift by Bleaney's theory, by comparing the shift values for every complex in a series to the value of the Yb(III) analogue. The Yb(III) ion possess the smallest magnetic susceptibility among all the lanthanides in the second half of the 4f series and it is generally regarded as the lanthanide(III) ion which is best characterised by Bleaney's theory.[10,76] Additionally, a linear correlation should be observed between the values of the Bleaney constant and the true pseudocontact shift.

The complexes in Scheme 1 also present a variety of different types of symmetry. In C_n symmetry, the crystal field splitting is dominated by B_0^2, which can be estimated for every complex using the method developed by Binnemans et al.[10] However, the crystal field splitting is expected to be much more complicated for the low symmetry systems, due to the influence of the higher order parameters. These higher order terms are not considered by Bleaney's theory. Consequently, these low symmetry systems should show interesting behaviour in terms of the pseudocontact shift.

2. Electronic relaxation times estimated through analysis of nuclear relaxation rates

By measuring nuclear relaxation rates of ligand resonances as a function of the magnetic field, it is possible to estimate the electronic relaxation times of lanthanide(III) complexes. The nuclear relaxation data is fitted to the Solomon-Bloembergen Morgan equations, obtaining estimates of, not only the electronic relaxation times, but also the internuclear distances, the effective magnetic moments and the rotational correlation times.

2.1 Parameters influencing the nuclear relaxation rates

The method of fitting the nuclear relaxation rates at different fields was developed by Kuprov and Parker in 2009.[23] The measured nuclear relaxation rates were measured at 4.7, 9.4, 11.7, 14.1 and 16.5 Tesla and can be fitted to the Solomon-Bloembergen Morgan equations for the longitudinal relaxation rate, R_1 (equation 4) or the transverse relaxation rate, R_2 (equation 5):

$$R_1 = \frac{2}{15}\left(\frac{\mu_0}{4\pi}\right)^2 \frac{\gamma_N^2 g_{Ln}^2 \mu_B^2 J\,(J+1)}{r^6}\left[3\frac{T_{1e}}{1+\omega_N^2\,T_{1e}^2}+7\frac{T_{2e}}{1+\omega_e^2\,T_{2e}^2}\right] + \frac{2}{5}\left(\frac{\mu_0}{4\pi}\right)^2 \frac{\omega_N^2 \mu_{eff}^4}{(3k_B T)^2\,r^6}\left[3\frac{\tau_r}{1+\omega_N^2\,\tau_r^2}\right] \quad (4)$$

$$R_2 = \frac{2}{15}\left(\frac{\mu_0}{4\pi}\right)^2 \frac{\gamma_N^2 g_{Ln}^2 \mu_B^2 J\,(J+1)}{r^6}\left[2T_{1e}\frac{3}{2}\frac{T_{1e}}{1+\omega_N^2\,T_{1e}^2}+\frac{13}{2}\frac{T_{2e}}{1+\omega_e^2\,T_{2e}^2}\right] + \frac{2}{5}\left(\frac{\mu_0}{4\pi}\right)^2 \frac{\omega_N^2 \mu_{eff}^4}{(3k_B T)^2\,r^6}\left[2\tau_r\frac{3}{2}\frac{\tau_r}{1+\omega_N^2\,\tau_r^2}\right] \quad (5)$$

There are a few underlying assumptions in SBM theory. Similar to Bleaney's theory of magnetic anisotropy, a point-dipole approximation is assumed. Additionally, the zero-field splitting (ZFS) of the energy levels is neglected in the dipolar term. However, Bertini and Luchinat[28] proposed a variant of the SBM equations that incorporated the static

ZFS. Inclusion of this modified term led to electronic relaxation times 2 -3 times faster than those calculated previously.

As can been seen in equation 4 and 5, the two terms (dipolar and Curie) are additive and independent of each other. Therefore, no cross-relaxation is allowed.

Lastly, the rotational correlation time is treated as isotropic and is assumed to be the same for each resonance. However, Szabo et al.[70,71] introduced the effect of localised rotational correlation times, which might also have an effect here and will be discussed later (chapter 2.2.1.2).

The sets of measured relaxation rates were fitted using a Levenberg-Marquardt minimisation technique, which allows 'fixing' of individual parameters to specific values, thereby taking the parameter out of the estimation process. By fixing a parameter the minimisation procedure is greatly simplified. Of course, it is necessary to know a reasonable value for the fixed parameter with confidence. For example, the temperature during the measurement is a fixed quantity, as it can easily be controlled and was measured accurately during each measurement in this work (see below, section 2.1.2).

The Levenberg-Marquardt minimisation technique cannot distinguish between global and local minima. Therefore, the quality of the initial estimates of the parameters involved in the fitting is important, to avoid being trapped in a false, local minimum. The parameters that need to be estimated for the fitting are: the internuclear distance, r, the rotational correlation time, τ_R, the effective magnetic moment, μ_{eff}, and the electronic relaxation time, T_{1e}.

The experimental relaxation data can either be fitted on a peak by peak basis (single resonance fitting) or a common resonance across the isostructural series can be fitted on a global level (global fitting). The method is applicable for analysis of R_1 and R_2 data sets, but in this discussion the focus will be on the analysis of the longitudinal relaxation rates, R_1. The nuclear relaxation rates of the ligand resonances of eleven isostructural series of lanthanide(III) complexes and a few more connected complexes were

measured for the Tb(III), Dy(III), Ho(III), Er(III), Tm(III) and Yb(III) analogues. In some cases data for the Eu(III) analogues were also analysed (Scheme 2).

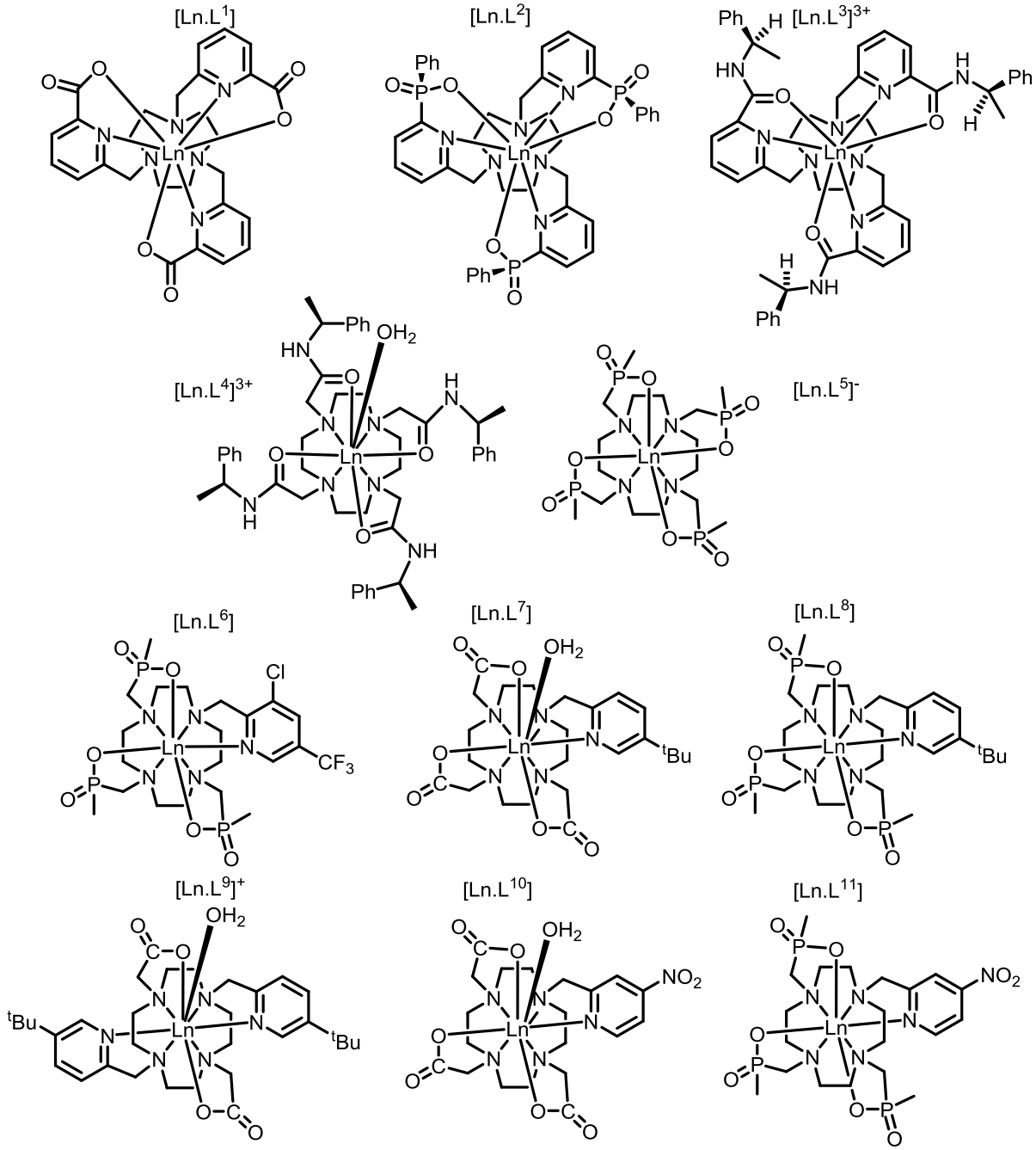

Scheme 2 : *Structures of the isostructural series of lanthanide(III) complexes studied in this thesis.*

Various techniques were used to estimate the parameters involved in the fitting of the nuclear relaxation rates. The electronic relaxation times of these complexes are, of course, unknown, but can be roughly estimated from prior literature studies. The observed range of the electronic relaxation times is thought to be between 0.1 and

1 ps. It is expected that the electronic relaxation times will vary according to the nature of the lanthanide(III) ion. From the reported literature, initial estimates can be obtained and it was noted that Tb(III) and Dy(III) complexes gave higher electronic relaxation times than the remaining lanthanide(III) ions.[28,66–68,72]

The effective magnetic moment, μ_{eff}, is commonly regarded as being independent of the coordination environment of the lanthanide(III) ions and, therefore, can be estimated easily from literature studies.[23,79] These values are most commonly measured from magnetic susceptibilities of solid-state samples.[12]

The global fitting procedure analyses common ligand resonances within an isostructural series of lanthanide(III) complexes, but requires a few assumptions to be made. First of all, the internuclear distances across a series are assumed not to change within their respective errors. It is appreciated that the lanthanide contraction means that the ionic radius of the lanthanide(III) ion decreases, but the expected decrease is contained within the estimated errors. A similar concept applies to the molecular volume of a complex and, therefore, its rotational correlation time. The internuclear distances, *r*, can be estimated from solid-state X-ray diffraction structures. There is often a slight difference between the solid and solution state structures, due to the greater conformational mobility in solution, but the distances obtained from the crystal structures provide the best initial estimates. The origin of differences between solid and solution-state estimates is discussed further in section 2.1.2.

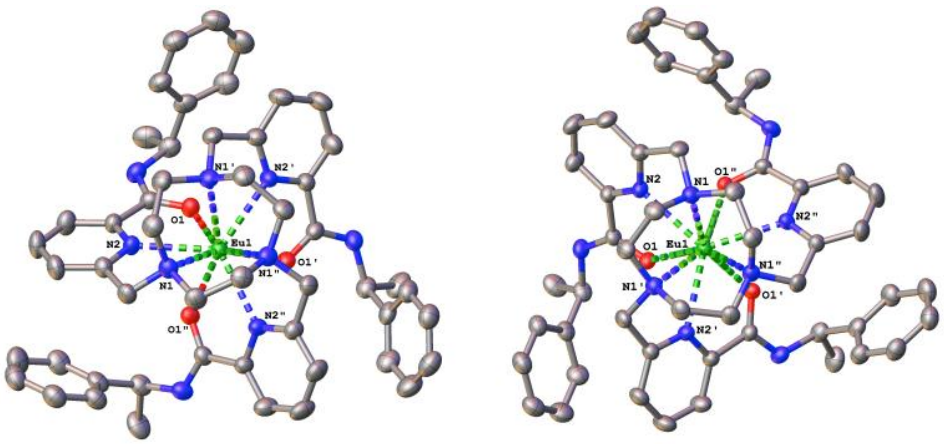

Figure 20: *Views of the X-ray structures of the two diasteroisomers of $[Eu.L^3]^{3+}$: S-Δ-(λλλ) (left) and R-Λ-(δδδ) right (120 K).*[74]

Most of the complexes presented here have published X-ray crystallographic structures available. Structures of $[Ln.L^1]$[80], $[Ln.L^2]$[29] and $[Ln.L^5]^-$[75] have been reported previously. The series of $[Ln.L^3]^{3+}$ complexes were published[74] during the course of the work presented here (Figure 20). Additionally, X-ray structures are available for almost the whole series of lanthanide(III) complexes of $[Ln.L^4]^{3+}$.[15]

An isostructural series of complexes based on crystallographic analyses provides an excellent opportunity to investigate the effect of the lanthanide contraction. Due to the monotonic decrease in ionic radius, it is expected that the internuclear distances will decrease across the series. The whole 4f series was investigated, but only the second half, from Tb(III) to Yb(III), is of interest in this study (Table 5).

Table 5: *Variation of the internuclear distance, r, in X-ray structures across the series of lanthanide(III) complexes of $[Ln.L^4]^{3+}$ (120 K).*[19]

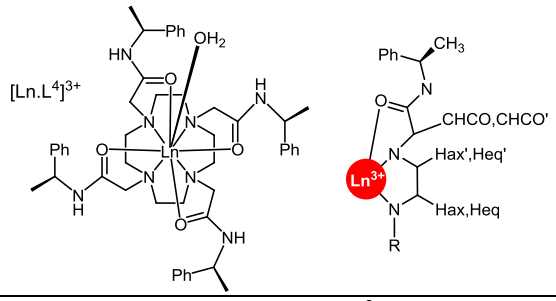

Ln^{3+}	r / Å					
	H_{ax}	H_{eq}	H_{ax}'	H_{eq}'	CHCO'	CHCO
Pr	3.79	4.43	3.75	4.44	3.71	4.36
Nd	3.77	4.41	3.73	4.42	3.70	4.33
Sm	3.74	4.38	3.71	4.40	3.69	4.31
Eu	3.75	4.38	3.71	4.40	3.66	4.31
Gd	3.74	4.38	3.70	4.39	3.67	4.28
Dy	3.73	4.37	3.69	4.37	3.67	4.26
Yb	3.68	4.35	3.65	4.33	3.55	4.24

While the internuclear distances across a whole series (La(III) to Yb(III)) can decrease by up to 0.1 Å, the distances within the latter half of the 4f series decrease by less than 0.05 Å.[81] The limited decrease of the internuclear distance, *r*, allows it to be used as a global fitting variable across a series from Tb(III) to Yb(III).

This type of analysis can be extended to the estimates of the rotational correlation time, τ_R, as it is dependent on the overall size of the complex. According to the Stokes-Einstein

Law (equation 6), the main factor determining τ_R is the hydrodynamic radius, r_H, (Figure 21).[69]

$$\tau_R = \frac{1}{6D} = \frac{4\pi r_H^3 \eta}{3kT} \quad (6)$$

where D is the rotational diffusion constant and η is the viscosity of the solvent.

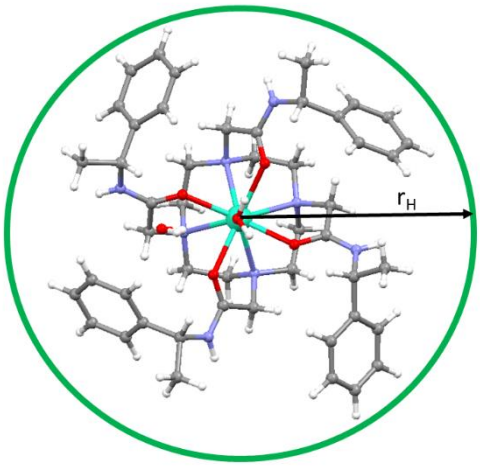

Figure 21: *Illustration of the X-ray structure of [Gd.L^4]$^{3+}$ with the estimation of the hydrodynamic radius highlighted (120 K).*[19]

Assuming a spherical model, it is possible to estimate the rotational correlation time, τ_R, of a complex series by measuring the distance of the nucleus furthest away from the paramagnetic centre and calculating the volume of the model sphere. The measured difference in the hydrodynamic radius from [Gd.L^4]$^{3+}$ (7.15 Å) to [Yb.L^4]$^{3+}$ (7.04 Å) was in a similar range to the decrease in the internuclear distance and contributes to an overall variation of the rotational correlation time of less than 5%. The limited decrease of the hydrodynamic radius associated with the lanthanide contraction permits the use of a common τ_R parameter, across the latter half of the series.

2.1.1 Relaxation behaviour in isostructural series of lanthanide(III) complexes

A variety of parameters influence the nuclear relaxation rates of a paramagnetic lanthanide(III) complex. In an isostructural series, however, the majority of parameters do not change across the series. As discussed above, the internuclear distance and the rotational correlation times can safely be assumed to be constant. The two main parameters that change between the lanthanide(III) ions are the effective magnetic moment, μ_{eff}, and the electronic relaxation time, T_{1e}. Each of these parameters is important in the Solomon-Bloembergen Morgan equations via the Curie and the dipolar term respectively.

In the relaxation experiment undertaken here, the nuclear relaxation rates are measured as a function of the magnetic field, ranging from relatively low magnetic field strengths (4.7 – 9.4 T) to the high field range (9.4 – 16.5 T). Due to the dependence of the Curie term on $\mu_{eff}^4 \omega_N^2$, the Curie terms becomes increasingly important at higher magnetic field strengths. Therefore, at higher field strengths it can be expected that the nuclear relaxation rates follow the order of μ_{eff}. At lower magnetic field strengths, it is expected for T_{1e} to have a dominant influence on the nuclear relaxation rates, which might alter the order of nuclear relaxation rates from the one observed at the higher field strengths.

Table 6 : *Overview of the measured ^{1}H relaxation rate, R_1, of and the observed shift of the CH_3 resonances (9.4 T) of $[Ln.L^4]^{3+}$ (295 K, D_2O).*

Ln^{3+}	δ_H / ppm	R_1[a] / s^{-1}				
		4.7 T	9.4 T	11.7 T	14.1 T	16.5 T
Tb	20.8	66	101	114	125	131
Dy	24.4	76	126	144	160	171
Ho	12.9	52	97	115	130	137
Er	-4.5	30	56	69	78	85
Tm	-13.1	18	28	33	36	38
Yb	-3.9	7.6	6.8	7.1	7.2	7.2

[a]The experimental error estimated for the measurement of R_1 values is less than 5%.

The differences in the nuclear relaxation rates between the lanthanide(III) ions in an isostructural series are due to the variation of values for T_{1e} and μ_{eff} of the different lanthanide(III) ions. Table 6 shows an overview of the relaxation and shift behaviour for the CH_3 resonance of $[Ln.L^4]^{3+}$. At high magnetic field strengths, the order of the nuclear relaxation rates follows the order of magnetic moments ([Dy, Ho] > Tb > Er > Tm >> Yb). The only exceptions are the values of Tb(III) and Ho(III), which are close despite the differences of more than 1 BM in μ_{eff}. At lower magnetic field strengths, the order dictated by the effective magnetic moment can change since the nuclear relaxation rates are influenced more strongly by the electronic relaxation times. Measuring the electronic relaxation times will provide a better understating of the nuclear relaxation behaviour at lower magnetic field strengths. The issue is of particular relevance to selecting probes in biomedical imaging, where fields of 1.5 and 3 T are commonly used. Figure 22 highlights the R_1 vs T_{1e} behaviour from the simulation shown earlier (Figure 16), clearly showing the key role played by T_{1e} variation at 1.5 to 3 T in the modulation of R_1.

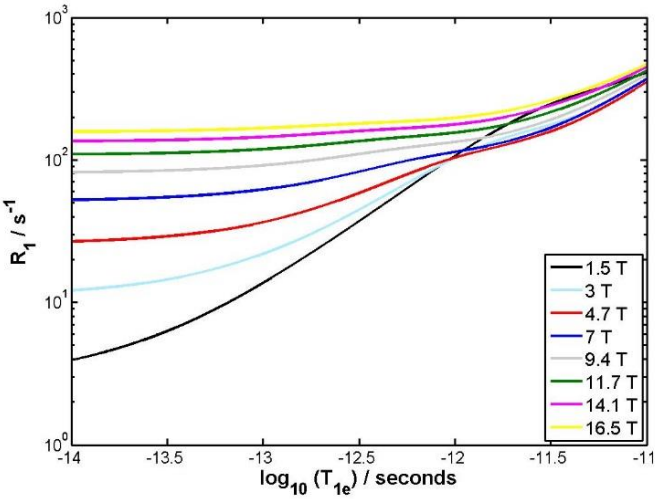

Figure 22 : *Simulation of the dependence of R_1 on T_{1e} at a variety of fields for an idealised lanthanide(III) probe (295 K, μ_{eff} = 10 BM, r = 6.5 Å, τ_R = 250 ps).*

2.1.1.1 Characterisation by relaxation and shift behaviour

In an isostructural series, it is important to confidently assign the ^{1}H NMR resonances to allow the use of the global fitting procedure. Due to the distance dependence of the longitudinal (R_1) and transverse (R_2) relaxation rates, it is easy to map the structure of a

lanthanide(III) complex by considering their relative relaxation enhancements and by reference to published X-ray structures (Figure 15).

The effect of the internuclear distance on the nuclear relaxation rates is still constrained by the lanthanide(III) ion, its associated effective magnetic moment and the individual electronic relaxation times. Therefore, the steepness of the measured distance dependence varies according to the nature of the lanthanide(III) ion. However, in a comparative analysis of the relaxation rates across different lanthanide(III) ions, it is possible to differentiate between different resonances, by virtue of their shift and relative relaxation rates.

The Yb(III) ion has a small effective magnetic moment (4.5 BM) and, coupled with low estimated electronic relaxation times, low nuclear relaxation rates are observed. The slow transverse relaxation rates, together with a smaller observed shift range than for the other lanthanide(III) ions, make a full characterisation of the ^{1}H NMR spectrum of a Yb(III) complex relatively straightforward, which is normally not possible for the other lanthanide(III) ions.

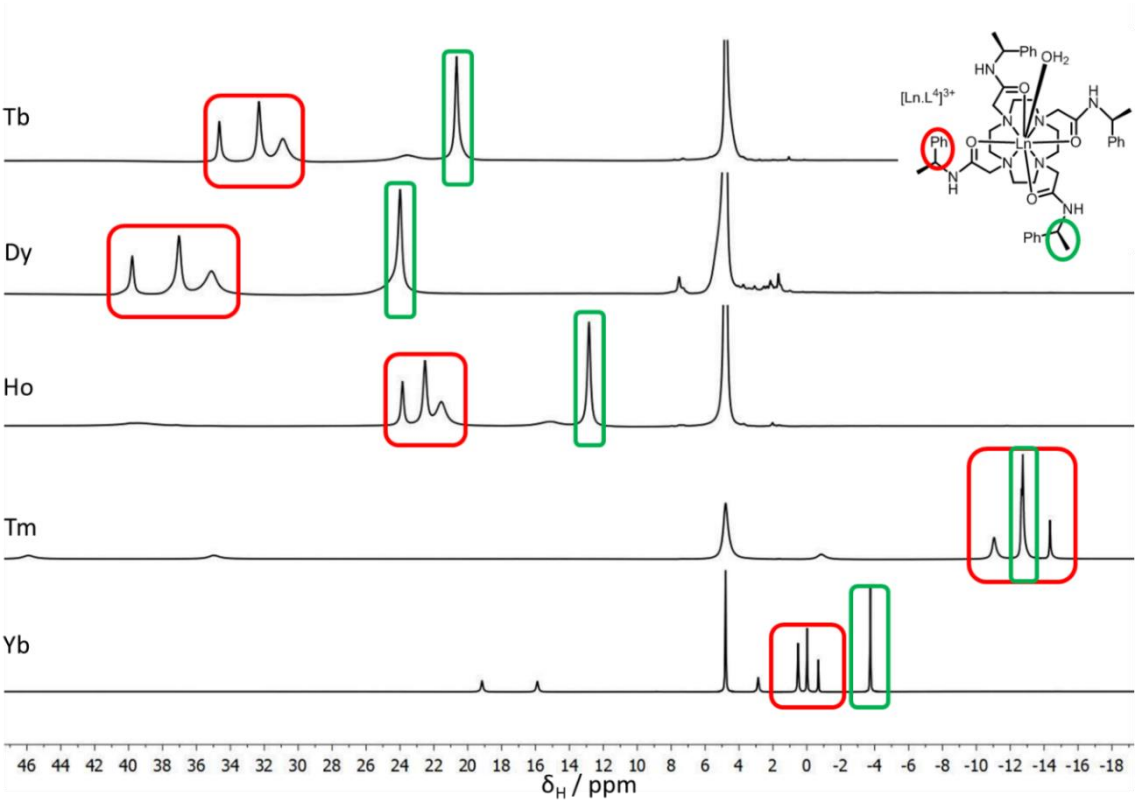

Figure 23 : *Part of the ^{1}H spectrum of some selected $[Ln.L^{4}]^{3+}$ complexes in which the phenyl and methyl resonances are highlighted. The different shift dispersion and line widths of the lanthanide(III) ions are apparent (D_2O, 11.7 T, 295 K).*

Due to increased R_2 values, the resonances of complexes of Tb(III), Dy(III) and Ho(III) suffer from excessive line broadening, which complicates spectral analysis significantly. For these complexes difficulties in the analysis of the most shifted resonances often occur. Owing to the different sign of the magnetic anisotropy from Tb(III), Dy(III) and Ho(III), to Er(III), Tm(IIII) and Yb(III) the ^{1}H NMR spectrum of these two groups are mirrored around the diamagnetic area of the ^{1}H NMR spectrum (Figure 23).

2.1.2 Control experiments

In preliminary control experiments with selected model complexes, the parameters estimated in the iterative fitting procedure were tested for internal consistency and, where possible, were compared to available literature studies. The series of control

experiments include investigations into the estimated values of the effective magnetic moment, the rotational correlation time and the internuclear distance.

2.1.2.1 Effect of the temperature

In the standard experiment, the nuclear relaxation rates were measured at constant temperature across all five different fields (295 K). This is important as in the Solomon-Bloembergen Morgan equations (4 and 5) there are a few parameters that are influenced by the temperature. There is a direct dependence of the nuclear relaxation rates to temperature in the Curie term ($1 / T^2$), but the rotational correlation time is also influenced by the temperature ($1 / T$).

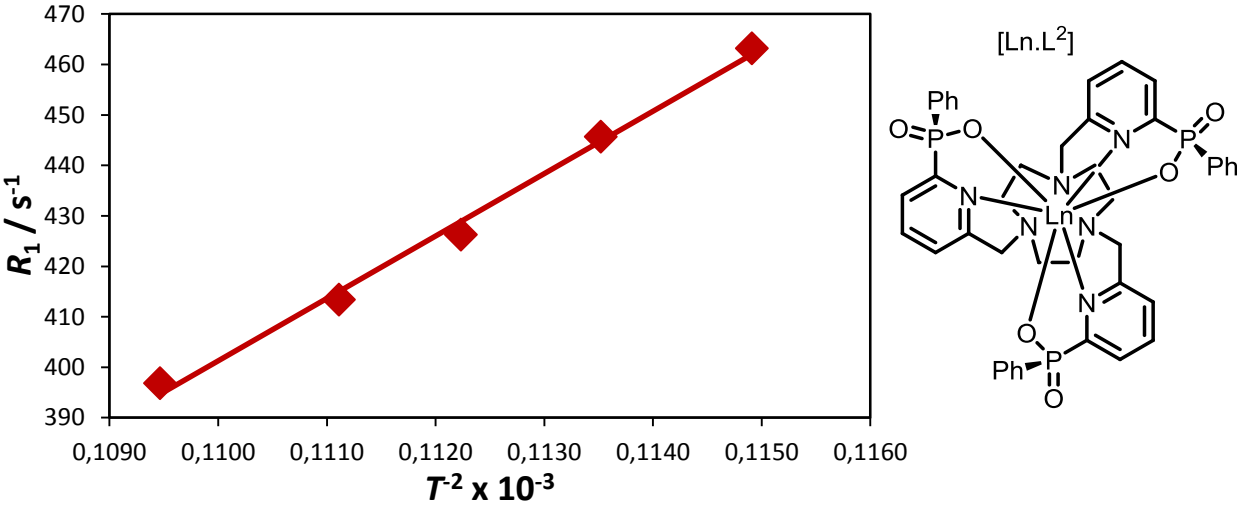

Figure 24: *Variation of the nuclear relaxation rate, R_1, of the ^{31}P resonance of [Tm.L^2] with the temperature(16.5 T, CD_3OD).*

The nuclear relaxation rate of the ^{31}P resonance of [Tm.L^2] was measured at different temperatures. A linear variation was found at 16.5 Tesla between R_1 and $1 / T^2$ (Figure 24). However, the magnetic field strength needs to be considered carefully in this study, due to the increasing influence of the Curie term at higher magnetic field strengths.

2.1.2.2 Effect of the internuclear distance

The fitting algorithm can be modified to allow fixing of individual parameters. The possibilities of fixing the effective magnetic moment, the rotational correlation and the internuclear distance were investigated in order to minimise the errors of the fitting procedure. Fixing the effective magnetic moment allows calculation of the electronic relaxation times, the internuclear distances and the rotational correlation times. To show the validity and accuracy of the estimated values, the internuclear distances can be compared to values found in the X-ray crystallographic structures. Confidence in these values will also establish confidence in the estimated values of the electronic relaxation times.

For the C_3 symmetric isostructural series of complexes based on triazacyclononane ([Ln.$L^{1\text{-}3}$]), the relaxation rate data for each separate common resonance were minimised, holding the relevant μ_{eff} to their literature values and varying T_{1e}, τ_R and r.

A very good agreement was found between the internuclear distances estimated through single resonance fitting and the X-ray data (Table 7).

Table 7: *Calculated average internuclear distances, r, across the C_3 complex series using single fitting with a fixed μ_{eff} (295 K, CD_3OD, [Ln.L^1] in D_2O) compared with the X-ray data (120 K).*

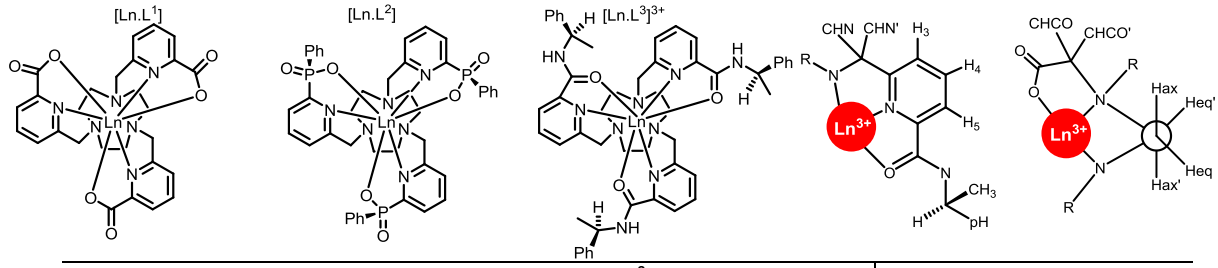

	Calculated *r* / Å			X-ray data[a]	
	[Ln.L^1]	[Ln.L^2]	[Ln.L^3]$^{3+}$	[Ln.L^2]	[Ln.L^3]$^{3+}$
H_{ax}	4.33 ±0.14	4.34 ±0.10	4.45 ±0.02	4.12	4.06
H_{ax}'	3.78 ±0.10	3.97 ±0.01	3.87 ±0.01	3.45	3.42
H_{eq}	4.49 ±0.03	4.54 ±0.01	4.55 ±0.02	4.30	4.28
H_{eq}'	4.40 ±0.03	4.55 ±0.01	4.53 ±0.02	4.30	4.23
pyCHN	4.45 ±0.10	4.45 ±0.10	4.71 ±0.01	4.30	4.31
pyCHN'	3.92 ±0.10	3.48 ±0.04	3.50 ±0.01	3.50	3.50
pyH^3	5.56 ±0.01	6.00 ±0.20	5.50 ±0.03	5.53	5.45
pyH^4	6.33 ±0.02	7.33 ±0.40	6.43 ±0.01	6.36	6.26
pyH^5	5.40 ±0.20	5.99 ±0.20	5.72 ±0.01	5.59	5.48

[a]Obtained from [29,74,80].

Table 7 shows the average values of the internuclear distance over the isostructural series of [Ln.L^1], [Ln.L^2] and [Ln.L^3]$^{3+}$. A slight deviation was expected due to the differences between solid and solution state structures. The only resonances that seem to deviate from the expected value are the pyH^4 resonance of [Ln.L^2] and the pyCHN' value of [Ln.L^1], which can only be attributed to an error in the R_1 measurements. Overall, the difference between the estimation through the fitting procedure and the X-ray structures gives considerable confidence in the single resonance fitting method with a fixed value for μ_{eff}.

Table 8: *Calculated average internuclear distances, r, across the $[Ln.L^4]^{3+}$ series, using a single fitting method with a fixed μ_{eff} (295 K, D_2O) compared to the X-ray crystallographic data (120 K).*

	r / Å[a]	X-ray[a]
H_{ax}	3.90 ±0.01	3.73
$H_{ax'}$	3.57 ±0.01	3.69
H_{eq}	4.48 ±0.11	4.37
$H_{eq'}$	4.48 ±0.10	4.37
CHCO	4.40 ±0.19	4.26
CHCO'	3.75 ±0.01	3.67

[a]Obtained from [19]

A similar comparative analysis was undertaken for the $[Ln.L^4]^{3+}$ systems. Again, the estimated distances are in very good agreement with the solid-state data. The estimated distances for the ring protons do not change significantly for the remaining $12N_4$ based complexes ($[Ln.L^5]^-$ to $[Ln.L^{11}]$, see Appendix 2).

2.1.2.3 Confirmation of the variation of R_1 with r

To check the internal consistency of the estimated distances, the nuclear relaxation rates of sets of individual resonances in a given complex were compared to the X-ray crystallographic distances. Over multiple resonances, the direct dependence of the nuclear relaxation rates on $1 / r^6$ should be visible for all resonances analysed in a given lanthanide(III) complex. The relaxation rates for five different $[Ln.L^2]$ complexes were measured (295 K, 4.7 T) and the variation of R_1 with the internuclear distance, r taken from the X-ray structures was analysed (Figure 25). The intercept of each graph should go through 1 s^{-1}, which is the theoretical diamagnetic contribution.

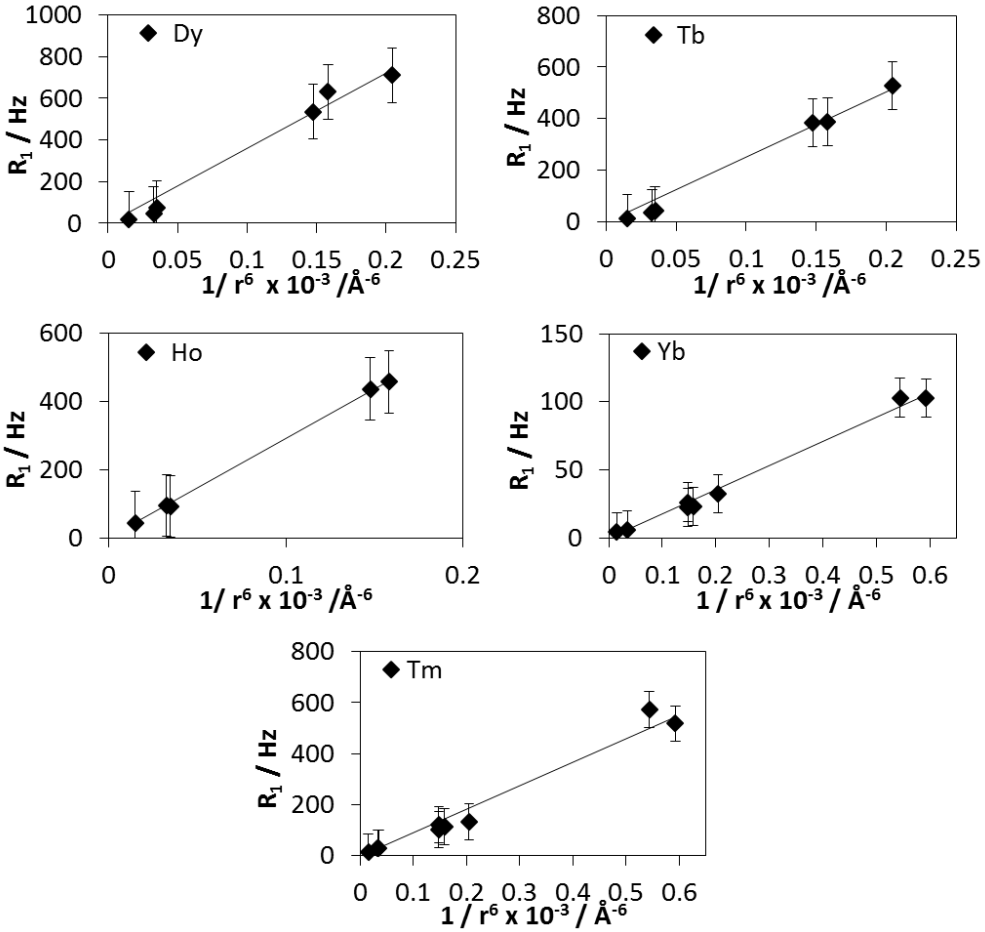

Figure 25 : *Dependence of the relaxation rate, R_1, on the lanthanide to ^{1}H internuclear distance, r, taken from X-ray structures for the [Ln.L^2] series (295 K, CD_3OD).*[82]

Figure 25 shows that the nuclear relaxation rates and the estimated internuclear distances faithfully follow the expected dependence of $1/r^6$, for a variety of lanthanide(III) ions.

2.1.2.4 Variation of τ_R and solvent viscosity

The second parameter that is calculated in any single resonance fitting procedure with a fixed μ_{eff}, is the rotational correlation time, τ_R. The solubility of $[Ln.L^4]^{3+}$ allows the analysis of the nuclear relaxation rates in different solvents. The different viscosities of solvents will give rise to different rotational correlation times and, consequently, lead to modulation of the nuclear relaxation rates. The ^{1}H NMR relaxation rates for ligand

resonances were measured in deuterated water, methanol and acetonitrile (Table 9, and Appendix 2, SI-Table 30 -31).

Table 9 : *Variation of calculated T_{1e} and τ_R values with different solvents for $[Ln.L^4]^{3+}$, at 295 K using a single fitting procedure with a fixed value of μ_{eff}.*

Ln^{3+}	D_2O τ_R / ps	CD_3OD τ_R / ps	MeCN τ_R / ps
Tb[a]	340.0	257.0	184.0
Dy	329.0	248.8	x
Ho	359.0	257.0	x
Tm	381.0	265.0	x
Yb	343.1	237.9	139.0
Total τ_R	350 ±28	253.1 ±17	161.5 ±12
η_{rel}	1.00	0.60	0.36

[a]The τ_R values are an average of at least 6 measured resonance per lanthanide(III) ion., with a standard deviation of 10 ps in each case.

The estimated internuclear distances were within their respective errors and the fitted electronic relaxation times were also independent of the nature of the solvents. The rotational correlation time is the only parameter that changes between the three measurements and it followed the trends of the viscosity relatively well.

In the global fitting procedure a fixed value for the internuclear distance is used to minimise the error of the calculations. The agreement between the solid and solution state structures was shown above, which allows for the internuclear distances to be fixed to the values from the X-ray crystallographic studies. The effective magnetic moments are calculated using this method, and the estimated values are close to the literature values. An extensive analysis of the calculated effective magnetic moments will be given in chapter 4 and in the individual analyses of the complexes below (section 3.3.1 to 3.3.3).

These control experiments substantiate the validity of this experimental technique. The two computational methods used here: single resonance fitting using a fixed μ_{eff} value and global fitting using a fixed value of *r* were each shown to give reasonably accurate values for each parameter.

2.1.2.5 Error Analysis in R_1 and determination of fitting errors

Each R_1 relaxation measurement was repeated at least three times and the mean value recorded. The number of transients used in the measurements was determined by the signal-to-noise ratio and therefore primarily by the concentration of the complex solution and the linewidth of the resonance of interest. This concentration was kept constant across the different experiments and was typically in the range of 0.2 to 1 mM. In each case, the signal analysed was fully recovered during the inversion-recovery sequence.

An experiment was performed to calculate the error associated with the temperature variation between the spectrometers. The relaxation rate of [Tm.L^2] was measured at five different temperatures (295 – 303 K in 2 K steps). For each measurement, the temperature was also determined using the temperature calibration sample (ethylene glycol). According to the Solomon-Bloembergen Morgan equations, the temperature dependence of the relaxation rate, R_1, is 1 / T^2. At a variation of 0.5 K the error was found to be less than 1.3 %. This was assumed to be similar for each complex studied (calculated from Figure 24).

An error analysis was undertaken to determine the fitting errors. The experimental errors of the measured relaxation rates were combined and used to perturb the relaxation rates for each complex at each field. These perturbed rates, together with the unperturbed relaxation rates were used in a statistical error analysis to obtain the error values for the individual parameters (μ_{eff}, r, τ_r and T_{1e}) estimated in the fitting process.

Table 10 : *Variation of the fitting results when perturbing the experimental nuclear relaxation data within their respective errors for the global fitting of the Heq' resonance of $[Ln.L^4]^{3+}$ (295 K, D_2O).*

μ_{eff} / BM						τ_R / ps	T_{1e} / ps					
Eu	Tb	Dy	Ho	Tm	Yb		Eu	Tb	Dy	Ho	Tm	Yb
2.990	8.909	10.325	9.951	7.578	4.344	335.3	0.141	0.564	0.382	0.281	0.262	0.200
2.836	8.898	10.320	9.946	7.568	4.311	334.9	0.101	0.567	0.380	0.278	0.256	0.183
2.979	8.917	10.330	9.956	7.587	4.379	335.6	0.176	0.568	0.386	0.285	0.267	0.216
2.865	8.903	10.323	9.949	7.574	4.328	335.3	0.122	0.568	0.381	0.280	0.259	0.192
2.937	8.911	10.327	9.953	7.592	4.361	335.4	0.159	0.569	0.384	0.283	0.265	0.208

An example for the perturbations and the resulting estimated parameters is given in Table 10.

2.2 Estimated electronic relaxation time, T_{1e} data

The nuclear relaxation rates of selected ligand resonances, in each series of lanthanide(III) complexes, were measured at five different field strengths. Using the fitting methods described previously (section 2.1), up to four parameters were estimated (μ_{eff}, τ_R, r and T_{1e}) for the lanthanide(III) ions of eleven different complexes. However, in most cases, some parameters were 'fixed' to a set value and were, therefore, taken out of the minimisation process. The main procedure for estimating the parameters of the Solomon-Bloembergen Morgan equation involved the global fitting of one or more common resonances across the isostructural series of lanthanide(III) complexes. The analysis has been limited to the very fast relaxing lanthanide(III) ions: Tb(III), Dy(III), Ho(III), Er(III), Tm(III) and Yb(III). The main motivation for this analysis is the estimation of the electronic relaxation times, T_{1e}, of individual lanthanide(III) complexes in a given isostructural series.

Details of the physical basis of electronic relaxation are uncertain. In previous studies, it was postulated that the zero field splitting (ZFS) of the electronic energy levels due to the J energy levels and the ligand field were in some way responsible for the

modulation.[28,66,68,82] In addition, it was proposed by Bertini et al.[28] that the modulation of the nuclear relaxation rates by the electronic relaxation arises from solvent collisions that disturb the ligand field of the complex. Such a process is limited by vibrational motion and therefore sets the lower limit for the electronic relaxation times to 0.1 ps. The expected range of electronic relaxation times can be estimated, from prior literature studies, is in the range of 0.1 ps to 1 ps.

An overview for all estimated parameters using the global fitting procedure with a fixed value of the internuclear distance, *r*, from X-ray crystallographic data can be found in Table 11 and 12. A brief summary of how the estimated values were obtained in section 2.1. Hereafter, the data for each series is divided into different categories, for more specific comment and analysis.

Table 11 : *Calculated electronic relaxation times, T_{1e},[a] effective magnetic moments, μ_{eff} and rotational correlation times, τ_r derived using global fitting with a fixed internuclear distance, r (295K, [Ln.L^1], [Ln.L^4]$^{3+}$, [Ln.L^5]$^-$ in D_2O, [Ln.L^{2,3}] in CD_3OD.*

Ln^{3+}	[Ln.L^1]		[Ln.L^2]				[Ln.L^3]$^{3+}$		[Ln.L^4]$^{3+}$		[Ln.L^5]$^-$	
	^{1}H		^{1}H		^{31}P		^{1}H		^{1}H		^{1}H	
	μ_{eff}/ BM	T_{1e} / ps	μ_{eff}/ BM	T_{1e} / ps	μ_{eff}/ BM	T_{1e} / ps	μ_{eff}/ BM	T_{1e} / ps	μ_{eff}/ BM	T_{1e} / ps	μ_{eff}/ BM	T_{1e} / ps
Tb	9.65 ±0.02	0.26 ±0.03	8.76±0.03	0.21 ±0.04	8.75 ±0.04	0.28 ±0.01	9.81 ±0.03	0.29 ±0.03	9.23 ±0.01	0.57 ±0.01	9.64 ±0.01	0.31 ±0.01
Dy	10.47 ±0.01	0.28 ±0.02	9.50 ±0.03	0.32 ±0.03	9.72 ±0.05	0.26 ±0.01	9.92 ±0.03	0.25 ±0.03	10.30 ±0.01	0.42 ±0.01	10.56 ±0.01	0.41 ±0.01
Ho	10.44 ±0.01	0.17 ±0.02	10.48 ±0.01	0.11 ±0.02	9.39 ±0.04	0.13 ±0.01	10.32 ±0.02	0.23 ±0.03	9.91 ±0.01	0.31 ±0.01	10.29 ±0.01	0.31 ±0.01
Er	9.23 ±0.02	0.23 ±0.03	9.55 ±0.02	0.26 ±0.03	8.50 ±0.04	0.31 ±0.01	8.88 ±0.03	0.26 ±0.04	X	X	9.48 ±0.01	0.57 ±0.01
Tm	7.43 ±0.01	0.08 ±0.02	8.21 ±0.03	0.09 ±0.04	6.76 ±0.03	0.06 ±0.02	7.77 ±0.02	0.13 ±0.03	7.57 ±0.01	0.28 ±0.01	9.07 ±0.01	0.83 ±0.01
Yb	4.27 ±0.02	0.09 ±0.04	4.72 ±0.03	0.12 ±0.06	3.84 ±0.03	0.07 ±0.01	4.55 ±0.04	0.14 ±0.04	4.34 ±0.03	0.21 ±0.02	4.27 ±0.05	0.24 ±0.02
τ_R / ps		132 ±1		186 ±6		328 ±15		184 ±1		293 ±1		230 ±1

[a]The estimates of the following resonances were analysed : [Ln.L^1] = pyH^{3,4}, [Ln.L^2] =H_{ax}, H_{ax}',, pyH^{3,5}, [Ln.L^3]$^{3+}$ = pyH^{3,4}, [Ln.L^4]$^{3+}$ = H_{eq}, H_{eq}', [Ln.L^5]$^-$ = H_{eq}, H_{eq}', Me.

Table 12: *Calculated electronic relaxation times, T_{1e},[a] effective magnetic moments, μ_{eff} and rotational correlation times, τ_r using global fitting with a fixed internuclear distance, r, for the lower symmetry complexes[Ln.L$^{6\text{-}11}$] (295 K, D_2O).*

	[Ln.L^6]		[Ln.L^7]		[Ln.L^8]		[Ln.L^9]$^+$		[Ln.L^{10}]		[Ln.L^{11}]	
Ln^3+	^{1}H+^{19}F		^{1}H		^{1}H		^{1}H		^{1}H		^{1}H	
	μ_{eff}/ BM	T_{1e} / ps	μ_{eff}/ BM	T_{1e} / ps	μ_{eff}/ BM	T_{1e} / ps	μ_{eff}/ BM	T_{1e} / ps	μ_{eff}/ BM	T_{1e} / ps	μ_{eff}/ BM	T_{1e} / ps
Tb	9.23 ±0.04	0.44 ±0.03	9.89 ±0.03	0.71 ±0.05	8.74 ±0.06	0.57 ±0.04	10.23 ±0.03	0.91 ±0.04	9.47 ±0.02	0.55 ±0.02	9.63 ±0.01	0.69 ±0.01
Dy	9.88 ±0.03	0.40 ±0.02	10.44 ±0.03	0.55 ±0.03	9.44 ±0.05	0.45 ±0.03	10.78 ±0.03	0.88 ±0.04	10.00 ±0.01	0.43 ±0.01	9.80 ±0.01	0.47 ±0.03
Ho	9.74 ±0.03	0.33 ±0.02	10.02 ±0.02	0.26 ±0.03	9.73 ±0.04	0.39 ±0.04	9.97 ±0.03	0.24 ±0.02	9.97 ±0.01	0.19 ±0.01	10.67 ±0.01	0.48 ±0.03
Er	9.58 ±0.03	0.63 ±0.03	9.18 ±0.02	0.17 ±0.04	9.62 ±0.04	0.97 ±0.06	X	X	9.30 ±0.01	0.12 ±0.01	9.45 ±0.01	0.62 ±0.02
Tm	8.21 ±0.03	0.30 ±0.03	8.21 ±0.06	0.40 ±0.03	9.36 ±0.05	0.48 ±0.03	7.80 ±0.04	0.15 ±0.05	8.02 ±0.01	0.26 ±0.02	7.50 ±0.01	0.32 ±0.02
Yb	4.55 ±0.12	0.36 ±0.04	4.56 ±0.07	0.28 ±0.03	4.57 ±0.07	0.51 ±0.03	4.67 ±0.23	0.14 ±0.04	4.65 ±0.03	0.15 ±0.03	X	X
τ_R / ps		260 ±2		196 ±4		263 ±4		288 ±4		182 ±1		227 ±1

[a]The following resonances were analysed : [Ln.L^6] = CF_3, Me, [Ln.L^{7,8,9}] = ^{t}Bu, [Ln.L^{10}] = pyH^6, H_{eq}, H_{eq}', [Ln.L^{11}] = Me

The large amount of data presented in Table 11 and 12 is difficult to digest. However, a few general observations can be made first.

Interestingly, the range of T_{1e} values experienced by a lanthanide(III) ion across all the isostructural series is larger than the range of T_{1e} values seen within a particular isostructural series. In other words, the coordination environment of the lanthanide(III) ion seems to have an bigger effect on T_{1e} than the nature of the individual lanthanide(III) ion. These differences can be attributed to the change in the ligand field between the isostructural series. Therefore, in some cases, ligand design has a bigger impact on the electronic relaxation times than lanthanide(III) ion selection.

The assumption of a correlation between the ligand field and the electronic relaxation times provides a starting point for this discussion. The lanthanide series [Ln.L^1] to [Ln.L^{11}] were categorised by their dependence on the crystal field splitting parameters, B_q^k. These were estimated using the emission spectra of the Eu(III) analogue of each analysed series. The method proposed by Binnemans et al.[9] allows the analysis of the splitting of the $\Delta J = 1$ band to estimate the second order crystal field splitting parameter B_0^2. There are other parameters influencing the crystal field (e.g. B_0^4 and B_0^6), but only the second rank parameter can be estimated easily.[9,10] It has been found that $B_0^2 > B_2^2$ for these systems reported to date.[83]

In the axially symmetric systems ([Ln.L$^{1\text{-}5}$]), the second order crystal field splitting parameters will be the dominant term in the observed crystal field splitting of a complex.[10] Comparing the differences between B_0^2 and the estimated value of the electronic relaxation times of the lanthanide(III) in isostructural series of [Ln.L$^{1\text{-}5}$] should indicate how well the parameters correlate. In the other systems ([Ln.L$^{6\text{-}11}$]), the higher order parameters are more influential due to the reduced symmetry, which makes a direct comparison of B_0^2 difficult, but does allow for an assessment of the possible role of the higher order parameters in more detail overall.

$$\delta_{pseudo} = \frac{C_J \mu_B^2}{60\ (kT)^2}\left[\frac{(3cos^2\theta - 1)}{r^3}B_0^2 + \sqrt{6}\frac{(sin^2 cos2\varphi)}{r^3}B_2^2\right] \quad (2)$$

Additionally, the overall crystal field splitting can be estimated by comparing the NMR observed shift range, e.g. in the ^{1}H NMR spectrum of each complex. According to Bleaney's theory of magnetic anisotropy (equation 2), the pseudocontact shift is directly proportional to the second order crystal field splitting parameters, B_0^2 and B_2^2. The influence is highlighted in Figure 26, which shows how the ligand field variation leads to an increase in the shift range of the Yb(III) analogue of [Ln.L$^{1\text{-}3}$].

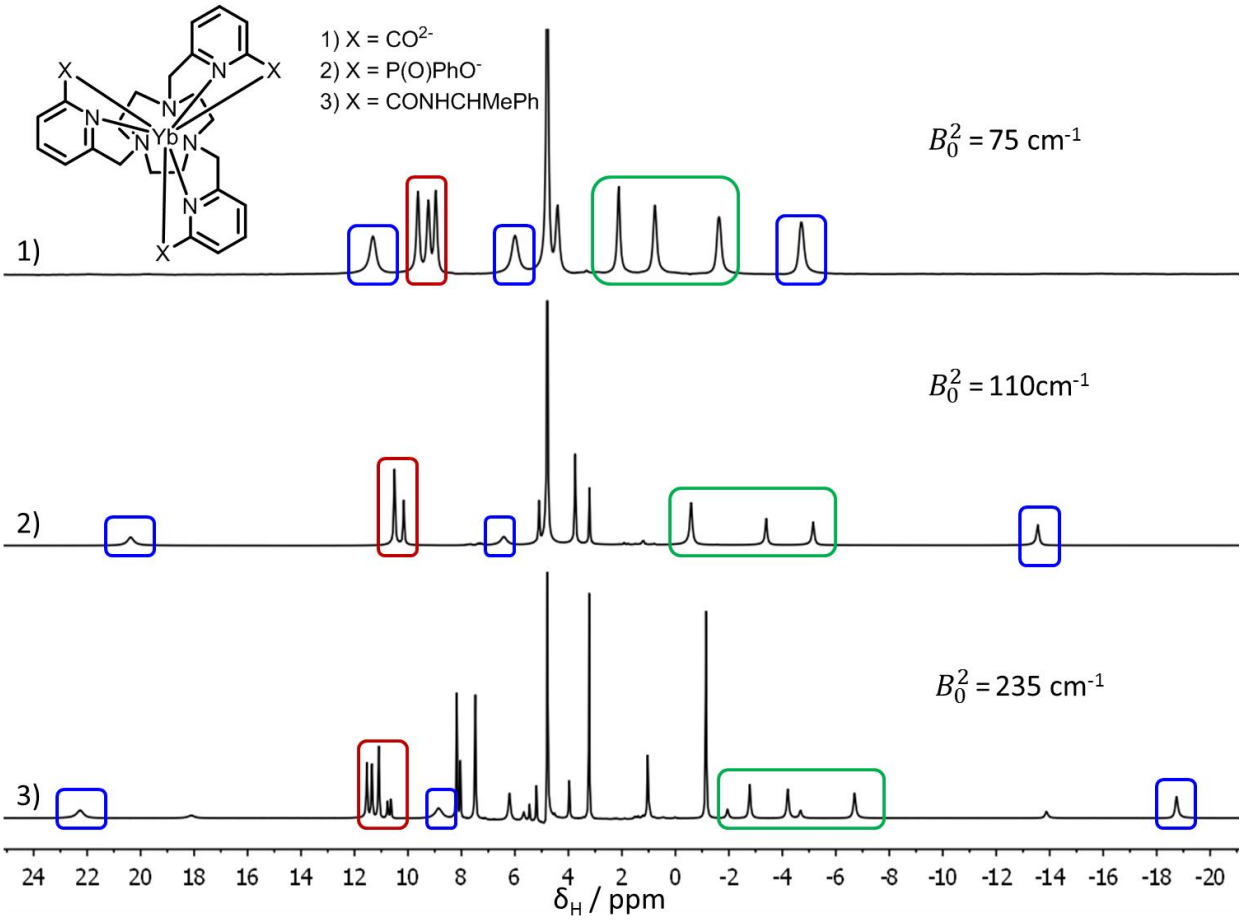

Figure 26 : *^{1}H NMR spectrum of [Yb.L^1] (upper), [Yb.L^2] and [Yb.L^3]$^{3+}$ (lower) showing the variation of shift dispersion with B_0^2 (295K, 9.4 T, CD_3OD, [Ln.L^1] in D_2O).*[74]

The 9N$_3$ based systems ([Ln.L$^{1\text{-}3}$]) were analysed first (section 2.2.1) due to their low crystal field splitting, followed by the cyclen-based complexes of [Ln.L^4]$^{3+}$ and [Ln.L^5]$^-$, which possess time average C$_4$ symmetry (section 2.2.2). The remaining six low symmetry complexes were analysed, but were further sub-divided into carboxylate (section 2.2.3.1) and phosphinate (section 2.2.3.3) series, because of the major

differences between them. The latter are 8-coordinate systems, usually in a TSAP geometry whereas the former adopt a 9 coordinate (q=1) SAP coordination geometry.

2.2.1 The C_3 symmetric series

The first three isostructural lanthanide complex series form a small series by themselves. [Ln.L^1], [Ln.L^2] and [Ln.L^3]$^{3+}$ are all based on a C_3 symmetric $9N_3$ system with pyridine side-arms. The difference between the three systems is the nature of the oxygen donor. In [Ln.L^1] the anionic donor is carboxylate group, whilst in [Ln.L^2] there are phosphinate groups. In [Ln.L^3]$^{3+}$ there is a neutral amide carbonyl donor with a chiral substituent. These different donor groups alter the ligand field experienced by the metal ions and the crystal field splitting increases from [Ln.L^1] to [Ln.L^3]$^{3+}$. The variation in crystal field splitting can be tentatively attributed to the differing polarizability of the donor oxygen atoms.

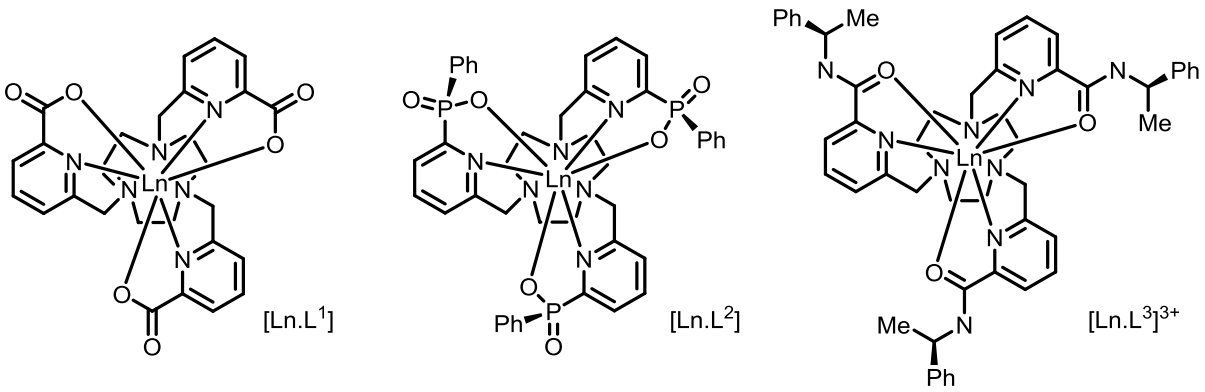

Scheme 3 : *Structures and ^{1}H labels for the C_3 symmetric complexes [Ln.L^1], [Ln.L^2] and [Ln.L^3]$^{3+}$.*

The crystal field splitting parameters have different signs depending on the coordination environment. The three $9N_3$ systems analysed here each possess a positive sign of the second rank crystal field splitting parameter, B_0^2. In contrast, the sign of the B_0^2 parameter for every complex in the $12N_4$ systems was found to be negative, as analysed through the Eu(III) emission spectrum.[74,82]

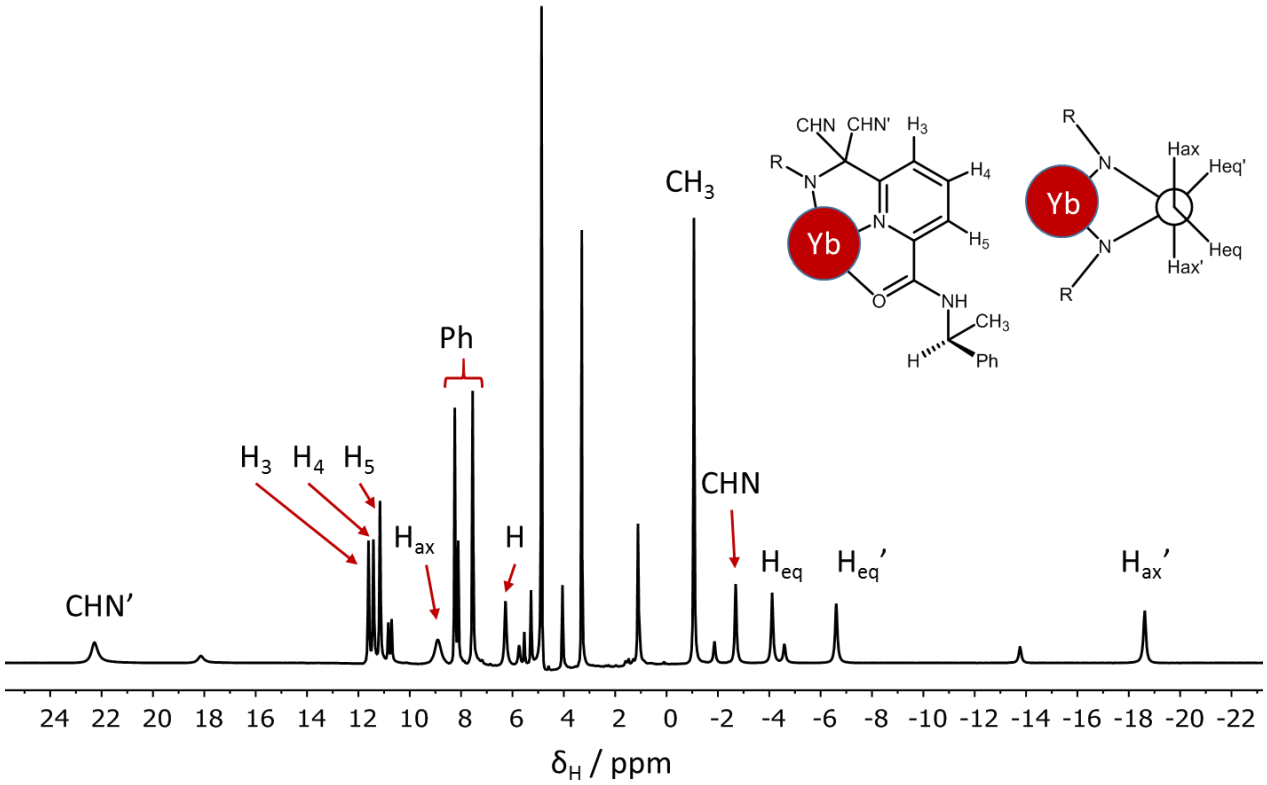

Figure 27 : *Annotated ^{1}H NMR spectrum of (S)-[Yb.L^{3}]$^{3+}$ in CD_3OD, (295 K, 9.4 T). Unassigned resonances relate to the minor isomer.*

For the three $9N_3$ systems, the entire ^{1}H NMR spectrum was analysed and assigned using relaxation and shift data. An example is given for [Yb.L^{3}]$^{3+}$ (Figure 27); the same assignment method was used for the lanthanide(III) complexes of [Ln.L^{1}] and [Ln.L^{2}].

2.2.1.1 Global fitting analysis of [Ln.L$^{1\text{-}3}$]

The pyridyl resonances are analysed in this section and were compared across each series. More common resonances were also analysed and the full data is available in Appendix 2 (SI-Table 1 -23). Each set gave consistent trends in the range and order of values for μ_{eff} and T_{1e}.

The experimental nuclear relaxation rate values, R_1, and the simulated fitting curves from the iterative minimisation process are shown in Figure 28 and are comparable across all three series.

The differences in the measured R_1 values can be directly attributed to the variation in the estimated T_{1e} values. The increase of R_1 with the nuclear Larmor frequency reveals itself in the steady increase of R_1 with increasing magnetic field strength (equation 4).

$$R_1 = \frac{2}{15}\left(\frac{\mu_0}{4\pi}\right)^2 \frac{\gamma_N^2 g_{Ln}^2 \mu_B^2 J\,(J+1)}{r^6}\left[3\frac{T_{1e}}{1+\omega_N^2\,T_{1e}^2} + 7\frac{T_{2e}}{1+\omega_e^2\,T_{2e}^2}\right] + \frac{2}{5}\left(\frac{\mu_0}{4\pi}\right)^2 \frac{\omega_N^2 \mu_{eff}^4}{(3k_B T)^2\, r^6}\left[3\frac{\tau_r}{1+\omega_N^2\,\tau_r^2}\right] \quad (4)$$

Generally, the R_1 data and the fitting curves tend to level off slightly at high magnetic field strengths as the contribution of the Curie term diminishes when $\frac{\tau_R}{1+\omega_N^2\tau_R^2}$ tends to dispersion, i.e.as $\omega_N^2\tau_R^2$ becomes much larger than 1. This effect is most evident for [Ln.L^2] (Figure 28, top right).

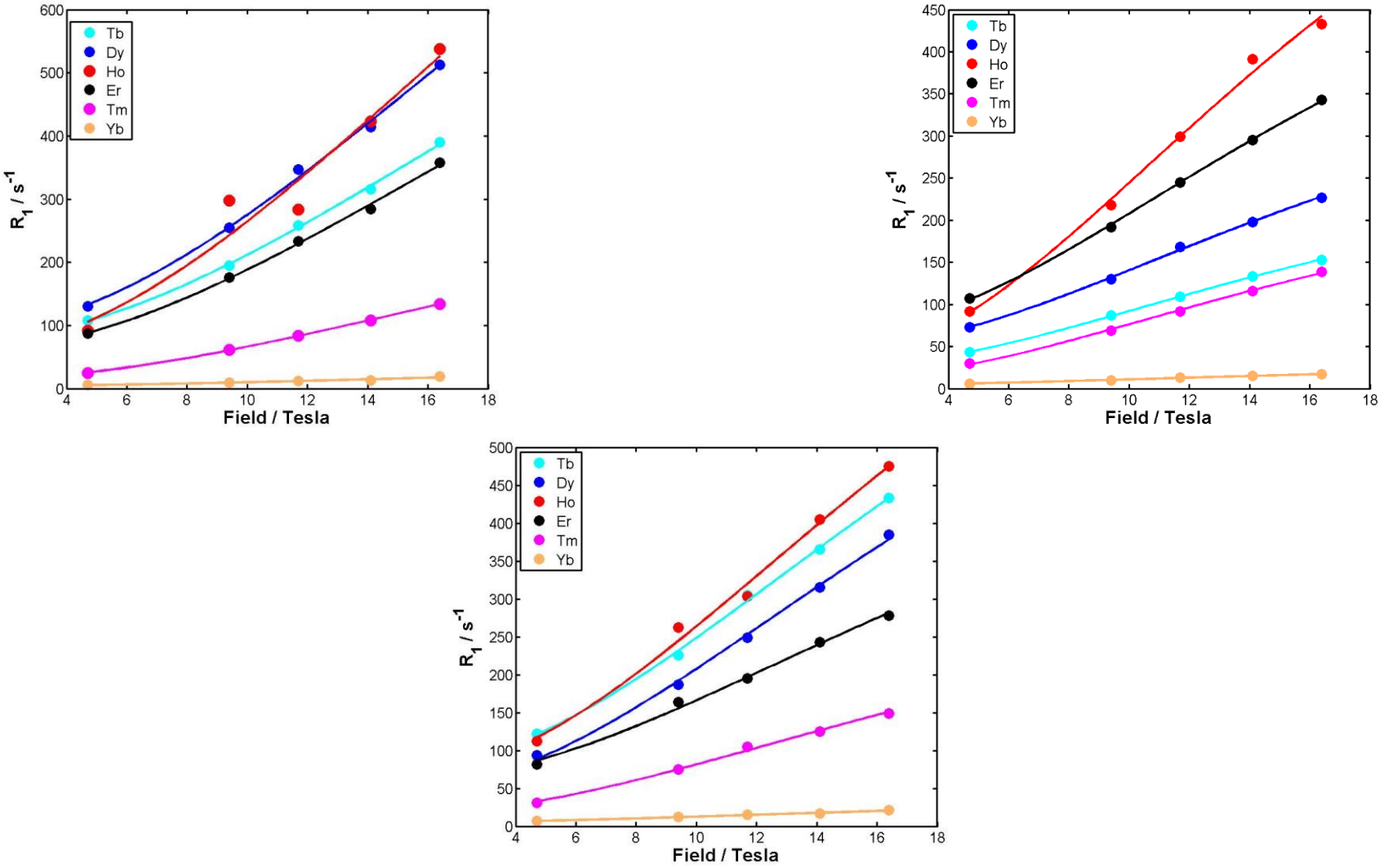

Figure 28 : *Relaxation data (data points) and best global fit (lines) for the pyH^3 resonance for [Ln.L^1] (left), [Ln.L^2] (right) and [Ln.L^3]$^{3+}$ (bottom) with a fixed internuclear distance, r, of 5.6 Å (295 K, CD_3OD, [Ln.L^1] in D_2O).*

As expected, at higher magnetic field strengths, the Curie term is dominant and therefore, the relative size of the effective magnetic moment, μ_{eff}, is the main driving force behind the rise in the nuclear relaxation rates. However, the influence of the electronic relaxation times is directly apparent in the fitting curves of the lanthanide(III) ions at lower magnetic field strengths.

Seemingly small changes in the electronic relaxation times have a significant impact on the behaviour of the nuclear relaxation rates. For example, the T_{1e} values of the Tb(III) analogues range from 0.21 ([Tb.L^2]) to 0.29 ps ([Tb.L^3]$^{3+}$). Figure 28 shows how these changes affect the nuclear relaxation rates for these complexes. In [Tb.L^2] the relaxation rates are as low as the rates of [Tm.L^2] despite the theoretical difference in effective magnetic moments of almost 2 BM. This is due to the low electronic relaxation time (T_{1e} = 0.21 ps). Interestingly, the nuclear relaxation rates of [Tb.L^3]$^{3+}$ are among the fastest (T_{1e} = 0.29 ps), even competing with [Ho.L^3]$^{3+}$, which possesses a larger effective magnetic moment. The nuclear relaxation rates of [Ln.L^1] cannot be compared directly to the other two series, due to the different solvents used.

Table 13 : *Calculated electronic relaxation times, T_{1e}, effective magnetic moments, μ_{eff} and rotational correlation times, τ_r using global fitting with a fixed internuclear distance, r, (295K, [Ln.L^1] in D_2O, [Ln.L^{2,3}] in CD_3OD).*

Ln^{3+}	[Ln.L^1] ^{1}H		[Ln.L^2] ^{1}H		[Ln.L^3]$^{3+b}$ ^{1}H	
	μ_{eff}/ BM	T_{1e} / ps	μ_{eff}/ BM	T_{1e} / ps	μ_{eff}/ BM	T_{1e} / ps
Tb	9.65 ±0.02	0.26 ±0.03	8.76 ±0.03	0.21 ±0.04	9.81±0.03	0.29 ±0.03
Dy	10.47 ±0.01	0.28 ±0.02	9.50 ±0.03	0.28 ±0.03	9.92 ±0.03	0.25 ±0.03
Ho	10.44 ±0.01	0.17 ±0.02	10.48 ±0.01	0.14 ±0.02	10.32 ±0.02	0.23 ±0.03
Er	9.23 ±0.02	0.23 ±0.03	9.55 ±0.02	0.32 ±0.03	8.88 ±0.03	0.26 ±0.04
Tm	7.43 ±0.01	0.08 ±0.02	8.21 ±0.03	0.12 ±0.04	7.77 ±0.02	0.13 ±0.03
Yb	4.27 ±0.02	0.09 ±0.04	4.72 ±0.03	0.12 ±0.06	4.55 ±0.04	0.14 ±0.04
τ_R / ps		132 ±1		186 ±6.		184 ±1
B_0^2/ cm^{-1} [a]		75		110		235

[a]The estimated error of the B_0^2 measurement is ±40 cm^{-1}.[b]pyH^4 resonance data shown here, as irregularities were found in Dy(III) analogue when analysing pyH^3.

Another complex that stands out is [Er.L^2]. The high electronic relaxation times estimated for [Er.L^2] are quite surprising. The nuclear relaxation rates are as high as the values of the Ho(III) analogue, even though there is a difference of 1 BM in μ_{eff}. However, similar behaviour was observed in every phosphinate based lanthanide(III) complex series. This phenomenon will be discussed in more detail in section 2.2.3.2.

Generally, the electronic relaxation times increase from [Ln.L^1] to [Ln.L^3]$^{3+}$ and seem to follow a specific trend ([**Tb, Dy] > Er > Ho > [Tm, Yb]**). This sequence closely follows the order of T_{1e} values in literature studies.[28,66,68] The only exception is the case of [Er.L^2] The steady increase in T_{1e} values also follows the small increase in their B_0^2 parameters. However, the changes in crystal field splitting and the electronic relaxation times are comparatively small in each of these three complex systems (Table 15). Therefore, more complexes showing a wider range of values for both parameters need to be analysed in order to establish this correlation.

2.2.1.2 Comparison of ^{31}P and ^{1}H resonance analysis for [Ln.L^2]

In the [Ln.L^2] series multiple nuclei were analysed. In addition to the ^{1}H NMR resonances analysed, the relaxation rates of the ^{31}P resonances were also measured. The values for the electronic relaxation times and the effective magnetic moment were in a similar range and within two standard deviations of the values analysed when the ^{1}H resonances measured (Figure 29).

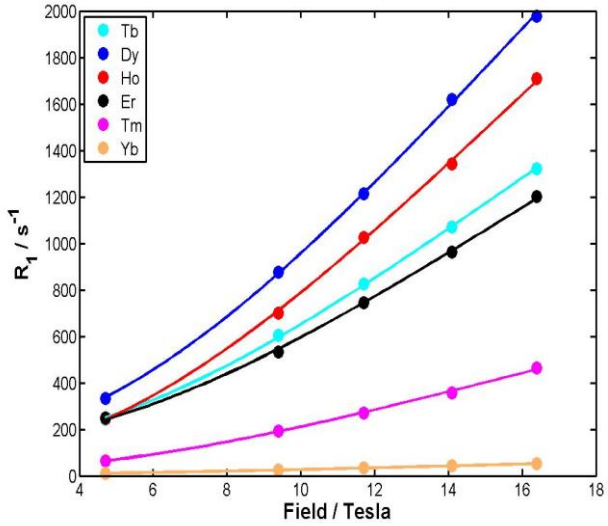

Figure 29 : *Relaxation rate data (data points) and best global fit (lines) for the ^{31}P resonance of [Ln.L^2] (295 K, CD_3OD).*

The main differences between the estimated values from ^1H and ^{31}P analysis arise from differences in the rotational correlation times (204 and 329 ps respectively). The ^{31}P atom is much closer to the paramagnetic lanthanide(III) ion than the pyridyl ^1H resonances analysed here. The ^{31}P resonance is closely anchored in the centre of the complex and has limited degrees of freedom. It can be assumed that the ^{31}P resonance lies close to the barycentre of the complex and its motion is, therefore, coupled more strongly to the overall molecular rotational motion. The pyridyl ^1H resonances have an increased distance from the paramagnetic centre. These resonances being in a less rigid local environment are, therefore, subject to localised rotational correlation times, and give rise to smaller apparent values for τ_R.[70,71] Overall, the nature of the nucleus does not seem to affect the estimated values of T_{1e} significantly (Table 11), and the estimated values are within two standard deviations of each other.

Generally, the values of the rotational correlation time follow the increased molecular volume of lanthanide(III) complexes increasing from 132 ±1 ps for [Ln.L^1] to 185 ±2 ps for [Ln.L$^{2\text{-}3}$].

The last remaining parameter that can be estimated by iterative fitting is the effective magnetic moment. The estimated values of μ_{eff} agree very well with the literature values (Table 14). In fact, they deviate by less than 5% of the theoretical value, with the

exception of $[Er.L^3]^{3+}$. A full discussion of the issues in calculating effective magnetic moments is given in chapter 4.

Table 14 : *Overview of estimated values of the effective magnetic moments, μ_{eff}, for $[Ln.L^1]$, $[Ln.L^2]$ and $[Ln.L^3]^{3+}$ and the theoretical values taken from the literature (295K, $[Ln.L^{2,3}]$ in CD_3OD, $[Ln.L^1]$ in D_2O).*

Ln^{3+}	μ_{eff} / BM[a]			
	$[Ln.L^1]$	$[Ln.L^2]$	$[Ln.L^3]^{3+}$	theo[11]
Tb	9.65 ±0.02	8.76 ±0.03	9.59 ±0.03	9.8
Dy	10.47 ±0.01	9.50 ±0.03	10.09 ±0.03	10.3
Ho	10.44 ±0.01	10.48 ±0.01	10.31 ±0.02	10.4
Er	9.23 ±0.02	9.55 ±0.02	8.80 ±0.03	9.4
Tm	7.43 ±0.01	8.21 ±0.03	7.77 ±0.02	7.6
Yb	4.27 ±0.02	4.72 ±0.03	4.56 ±0.04	4.5

Being able to calculate the effective magnetic moments in such good agreement with the literature, gives further confidence in the use of the single resonance fitting analysis method. Using a fixed value of the effective magnetic moment, the validity of this method has already been discussed above, by comparing the internuclear distances estimated through single resonance fitting to the X-ray crystallographic studies.

2.2.1.3 Single resonance fitting analysis of [Ln.L$^{1\text{-}3}$]

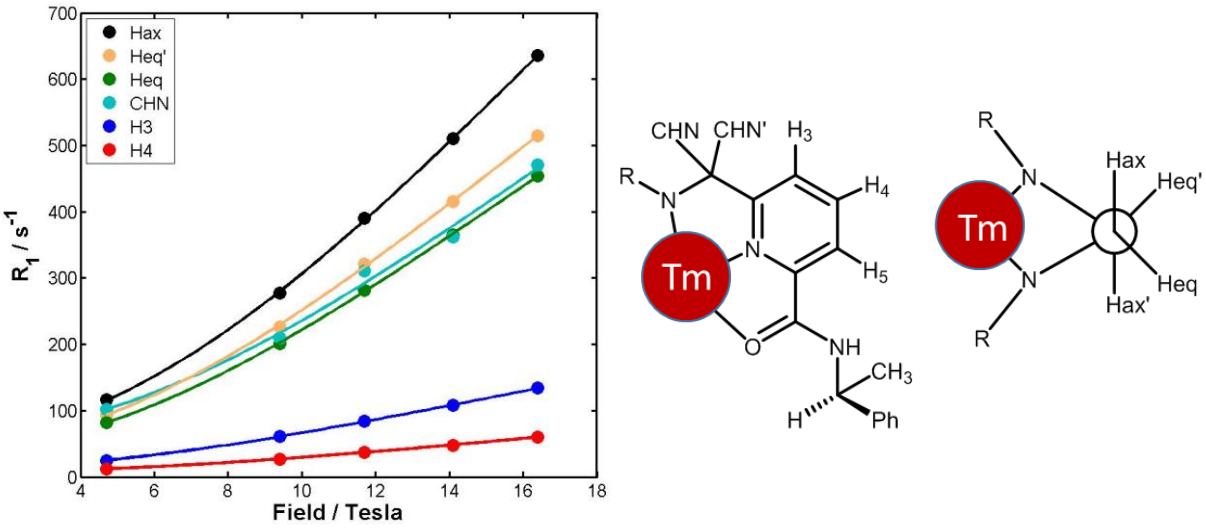

Figure 30 : *Relaxation data (points) and best single fit (lines) for [Tm.L^{1}] using a fixed value of μ_{eff} of 7.6 BM (295 K, D_2O).*

The global fitting procedure requires a common resonance to be analysed across the whole isostructural series. This procedure sometimes proved to be difficult due to severe line broadening and overlap of signals.

The dependence of R_1 on the internuclear distance, r, is evident in single resonance fitting. Figure 30 shows clearly the enhanced R_1 values of the ring protons (H_{ax}, H_{eq}), over the more distant pyridyl resonances. In single resonance fitting, the nuclear relaxation rates of multiple resonances were measured as a function of the magnetic field strength, and the estimated parameters were combined to obtain averaged values of the electronic relaxation time, the rotational correlation time and the internuclear distance across the isostructural series (Table 15).

The order of the electronic relaxation times is consistent with the global fitting procedure. There is only a small variation in the T_{1e} values between the two procedures, but, overall, the values agree within their respective errors.

The fitting curves and relaxation data for the main ^{1}H resonances of [Tm.L^1] also behave similarly (Figure 30). The estimated rotational correlation times also agree with the values estimated using the global fitting method.

Table 15 : *Overview of the single fitted electronic relaxation times following analysis of the pyH^3 resonance of the C$_3$ symmetric systems, ([Ln.L^1] in D$_2$O, [Ln.L^{2,3}] in CD$_3$OD, 295 K).*

Ln^{3+}	T_{1e} / ps[a]		
	[Ln.L^1]	[Ln.L^2]	[Ln.L^3]$^{3+}$
Tb	0.24 ±0.03	0.27 ±0.02	0.32 ±0.02
Dy	0.24 ±0.02	0.30 ±0.04	0.35 ±0.03
Ho	0.15 ±0.02	0.18 ±0.07	0.21 ±0.03
Er	0.23 ±0.03	0.31 ±0.06	0.35 ±0.04
Tm	0.08 ±0.02	0.09 ±0.02	0.10 ±0.02
Yb	0.07 ±0.03	0.11 ±0.03	0.12 ±0.03
τ_R / ps	135 ±8	190 ±17	188 ±9
B_0^2 /cm^{-1}	75	110	228

[a]The shown values are an average of at least 6 resonances (Appendix 2, SI-Table 1 - 23).

Inspection of the data in Table 15 reveals a direct proportionality between the electronic relaxation times and the second order crystal field splitting parameters. However, the increases in both T_{1e} and B_0^2 are rather small. To fully establish the correlation between these two parameters, the remaining axially symmetric systems were taken into consideration. Their ligand field is much bigger than those reported for the 9N$_3$ systems, and should, theoretically, give rise to larger electronic relaxation times.

2.2.2 High symmetry cyclen based complex systems

The remaining two highly symmetrical systems, [Ln.L^4]$^{3+}$ and [Ln.L^5]$^-$, were analysed together with selected related complexes currently of interest in the literature: [Ln.gDOTA]$^{5-}$ [19] and [Tm.DOTMA]$^-$.[49] The sign of their second order crystal field splitting parameters is inverted compared to the 9N$_3$ systems, which leads to an inverted ^{1}H NMR spectrum seen, for example, in the relative shift of the equatorial ring protons

(Figure 27 and Figure 31). Of course, there are structural differences between the C_3 and C_4 symmetric series and thus, resonances cannot be compared directly across every isostructural series.

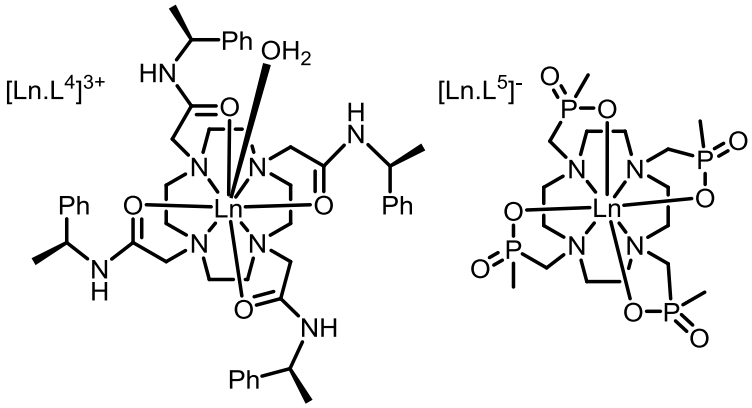

Scheme 4 : *Structures of the C_4 symmetric tetra-amide complex $[Ln.L^4]^{3+}$ and tetra-methyl phosphinate complex $[Ln.L^5]^-$.*

The ^{1}H NMR spectra of the $[Ln.L^5]^-$ complexes are similar in form (Figure 31) to the $[Ln.L^4]^{3+}$ spectra shown earlier (Figure 23).

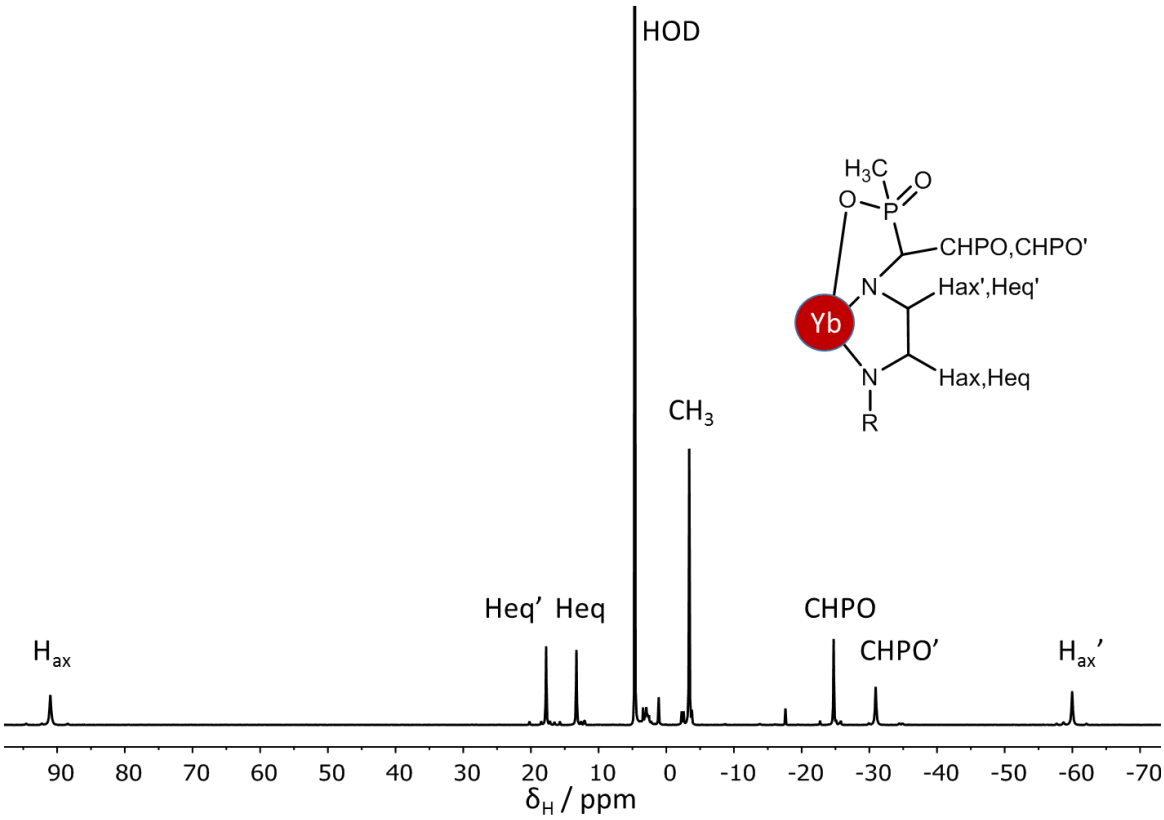

Figure 31 : *Annotated ^{1}H NMR spectrum of $[Yb.L^5]^-$ (D_2O, 295 K, 9.4 T). Not assigned resonances relate to a minor isomer.*

The two C_4-symmetric systems possess higher crystal field splitting values (-470 and -700 cm^{-1} for $[Ln.L^4]^{3+}$ and $[Ln.L^5]^-$ respectively) than the $9N_3$ systems. Bearing this in mind, a different behaviour of the T_{1e} values would be predicted. The curves for the best global fit and the experimental relaxation data is shown in Figure 32.

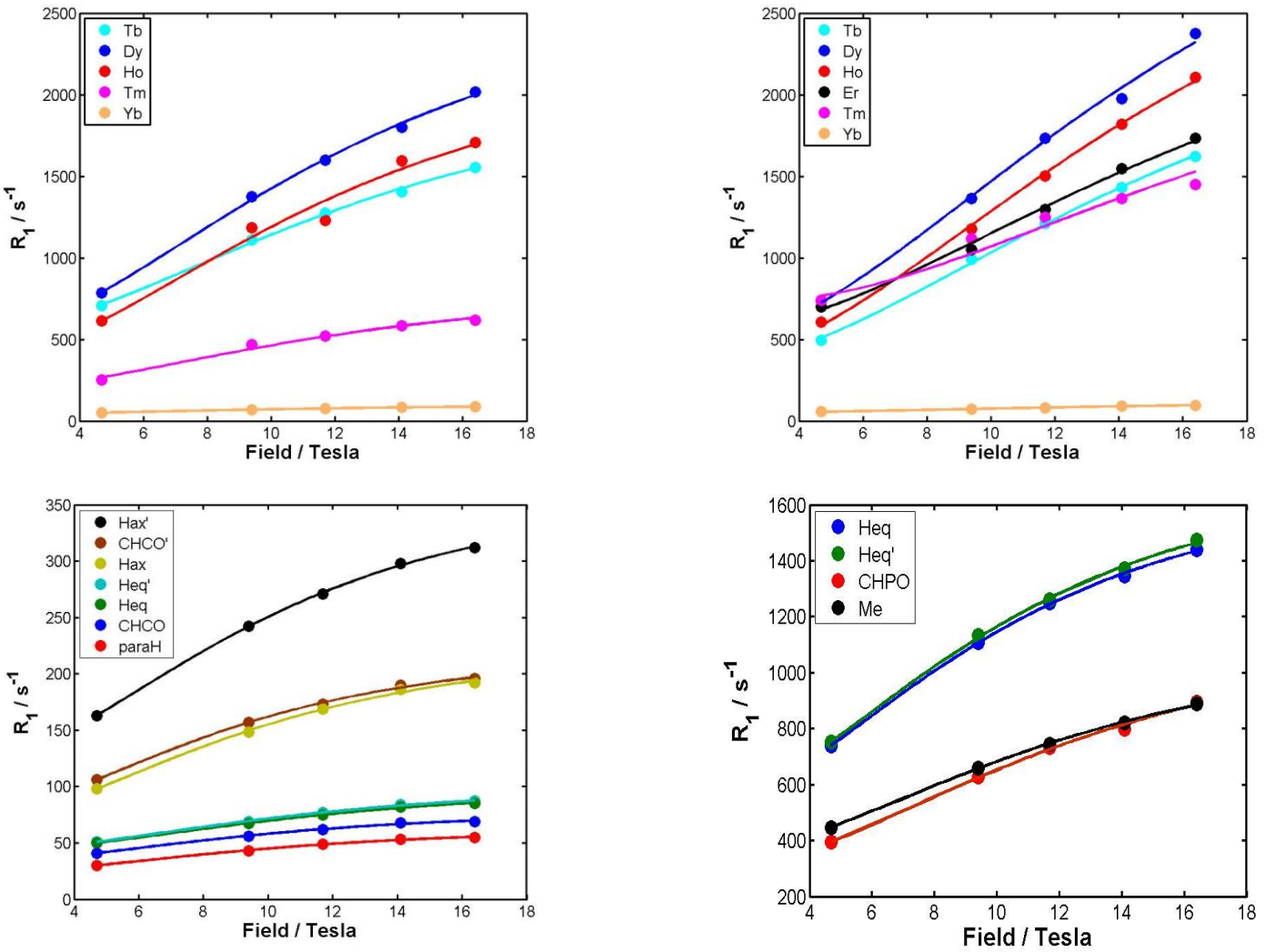

Figure 32 : *Relaxation data (data points) and best global fit (top, lines) and single fit (bottom, lines) for $[Ln.L^4]^{3+}$ (left) and $[Ln.L^5]^-$ (right) (295 K, in D_2O) Single fitting for $[Tm.L^4]^{3+}$ and $[Tm.L^5]^-$ shown.*

At lower magnetic field strengths, the rate of nuclear relaxation mirrors the order of the electronic relaxation times, while at higher fields, the values follow the order of the effective magnetic moment. It was not possible to include the $[Er.L^4]^{3+}$ resonance into the analysis using the global fitting method, as the common resonance was not measurable. However, it was possible to include other $[Er.L^4]^{3+}$ resonances in the single fitting procedure. Table 16 gives an overview over the estimated parameters using the global fitting procedure.

Table 16 : *Overview of the estimated values of the electronic relaxation times, T_{1e} and the effective magnetic moments of $[Ln.L^4]^{3+}$ and $[Ln.L^5]^-$ in comparison to literature, (295 K, D_2O).*

Ln^{3+}	$[Ln.L^4]^{3+}$		$[Ln.L^5]^-$		theo[11]
	μ_{eff} / BM	T_{1e} / ps	μ_{eff} / BM	T_{1e} / ps	μ_{eff} / BM
Tb	9.23 ±0.01	0.57 ±0.01	9.64 ±0.01	0.31 ±0.01	9.8
Dy	10.30 ±0.01	0.42 ±0.01	10.56 ±0.01	0.41 ±0.01	10.3
Ho	9.91 ±0.01	0.31 ±0.01	10.29 ±0.01	0.31 ±0.01	10.4
Er	x	x	9.48 ±0.01	0.57 ±0.01	9.4
Tm	7.57 ±0.01	0.28 ±0.01	9.07 ±0.01	0.83 ±0.01	7.6
Yb	4.34 ±0.03	0.21 ±0.02	4.27 ±0.05	0.24 ±0.02	4.5
τ_R / ps	293 ±1		230 ±1		
B_0^2 / cm^{-1}	-470		-700		

The values of the electronic relaxation times between these two systems behave significantly differently. In fact, the estimated values of T_{1e} for $[Ln.L^5]^-$ behave similar to $[Ln.L^2]$, where the Er(III) analogue had shown an increased value of T_{1e} and an enhanced nuclear relaxation rate compared to the other lanthanide(III) ions. Here, the Tb(III), Dy(III) and Ho(III) values of T_{1e} do not follow the changes observed to $[Ln.L^4]^{3+}$, and not showing the increase of T_{1e} with B_0^2, observed in the previous systems. However, the remaining $[Ln.L^5]^-$ complexes follow the increase reported for the $[Ln.L^{1-3}]$ series. These anomalies with Dy(III) and Ho(III) are, in fact, observed in all phosphinate based systems, and are tentatively ascribed to a greater influence of the higher order crystal field splitting parameters (B_0^4 and B_0^6) (see section 2.2.3.2).

The electronic relaxation times for $[Tm.L^5]^-$ are amongst the highest values estimated across all series. Additionally, the estimated effective magnetic moment, μ_{eff}, shows the

biggest deviation from the expected literature value. The overall fitting curve of $[Tm.L^5]^-$ does not correspond well to the measured data. Its shape is significantly different than observed in the other complexes.

Generally, the effective magnetic moments of $[Ln.L^4]^{3+}$ and $[Ln.L^5]^-$ follow the literature values closely (Figure 31), with the exception of the aforementioned $[Tm.L^5]^-$ complex. In light of the good agreement, a single resonance fitting procedure was employed to estimate the electronic relaxation times, the internuclear distances and the rotational correlation times. Indeed a good agreement was found comparing the two procedures (Figure 32 (bottom) and Table 17), even for $[Tm.L^5]^-$. Additionally, estimated parameters for $[Er.L^4]^{3+}$ were obtained. The estimated T_{1e} value for $[Er.L^4]^{3+}$ is in a similar range (0.31 ps) than for the Er(III) analogues obtained earlier, but are much smaller than those observed in the phosphinate series.

Table 17*:* *Single fitting values for C_4 symmetric complexes $[Ln.L^4]^{3+}$ and $[Ln.L^5]^-$ using a fixed effective magnetic moment, μ_{eff}, (295 K, D_2O).*

Ln^{3+}	T_{1e} /ps[a]	
	$[Ln.L^4]^{3+}$	$[Ln.L^5]^-$
Tb	0.54 ±0.06	0.30 ±0.01
Dy	0.43 ±0.03	0.41 ±0.01
Ho	0.34 ±0.01	0.35 ±0.01
Er	0.31 ±0.09	0.56 ±0.02
Tm	0.21 ±0.02	0.39 ±0.01
Yb	0.17 ±0.03	0.23 ±0.02
τ_R / ps	353 ±30	234 ±2
B_0^2 /cm^{-1}	-470	-700

[a]The shown values represent an average of at least 6 resonances (Appendix 2, SI-Table 24 -39)

The estimates for the rotational correlation time are larger than for the $9N_3$ counterparts. The larger size of the $12N_4$ system creates a larger hydrodynamic radii and, thus, bigger rotational correlation times. The $[Ln.L^4]^{3+}$ series is one of the biggest complex series analysed (353 ps). The $[Ln.L^5]^-$ complex is more compact and is only marginally bigger (234 ps) than the $9N_3$ based complexes (< 200 ps).

In the $[Ln.L^5]^-$ complexes an increase in the electronic relaxation times was noted with increasing crystal field splitting only for the last three complexes (Table 17). Moreover,

a different behaviour was observed in the behaviour of the electronic relaxation times of the phosphinate system, where the order of the electronic relaxation times was particularly different compared to [Ln.L$^{1\text{-}4}$].

2.2.2.1 Analysis of [Ln.gDOTA]$^{5-}$ and [Tm.DOTMA]$^{-}$

To complement the study of the highly symmetrical systems, two well-known complexes were investigated ([Ln.gDOTA]$^{5-}$ and [Tm.DOTMA]$^{-}$).[49] These two systems experience high crystal field splitting parameters (≈ 700 cm^{-1}).[19] By comparing the data with the previous five systems, it should be possible to further the link between the crystal field splitting and the electronic relaxation times.

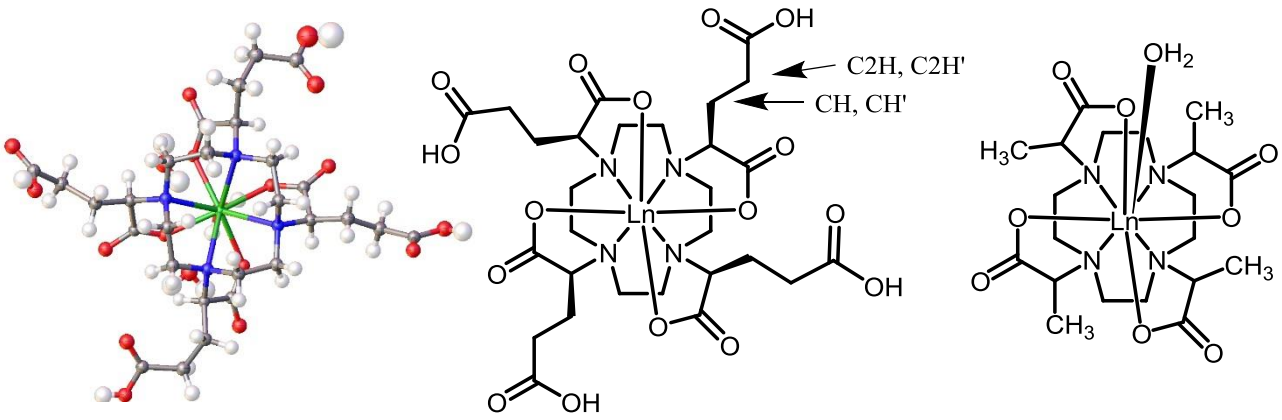

Scheme 5 : *Structures of (S)-[Ln.gDOTA]$^{5-}$ (left, middle) and [Ln.DOTMA]$^{-}$ (right) and unpublished X-ray structure of [Tm.gDOTA]$^{5-}$ (left).*

For [Ln.gDOTA]$^{5-}$, the Er(III), Tm(III) and Yb(III) complexes were examined and for [Ln.DOTMA]$^{-}$ only the Tm(III) analogue was analysed. An isostructural series does not occur with these two systems.[19] The analysis of these complexes is limited to the single resonance fitting procedure, examining the most distant CH_3 group resonance in [Tm.DOTMA]$^{-}$ and the diastereotopic CH_2 resonances in the carboxylate side chain in [Ln.gDOTA]$^{5-}$ (Figure 33).

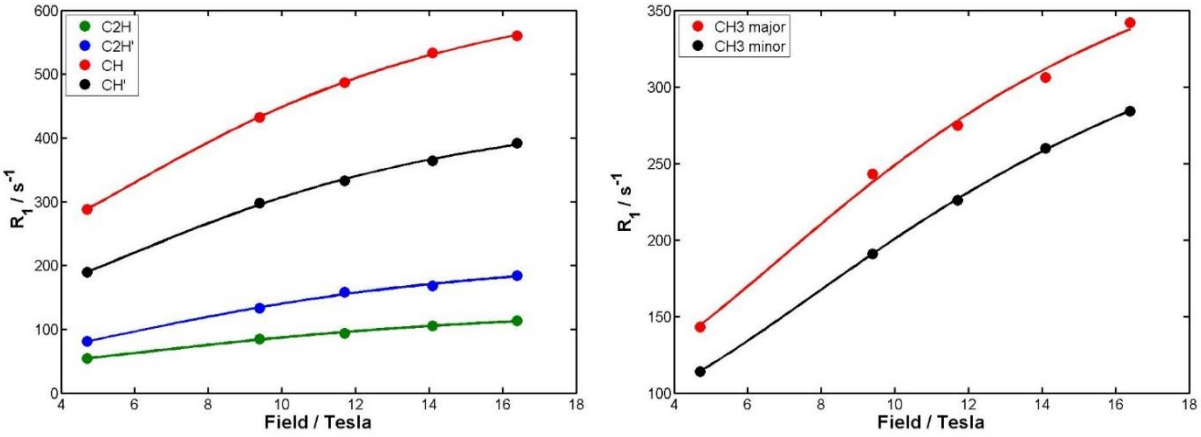

Figure 33 : *Relaxation data (data points) and best single resonance fit (lines) of [Tm.gDOTA]$^{5-}$ (left) and [Tm.DOTMA]$^{-}$ (right), (295 K, in D_2O). In [TmDOTMA]$^{-}$ the major species is TSAP, q=0, minor is SAP q=1.*

Each complex possesses a large crystal field splitting, with the highest values of B_0^2 among all series analysed (comparable to [Ln.L^5]$^-$). However, the T_{1e} values are not as high as those values observed for some of the phosphinate complex series ([Ln.L^5]$^-$). This further suggests that the phosphinate systems behave anomalously (Table 18).

Table 18 : *Estimated values of the electronic relaxation time of [Ln.gDOTA]$^{5-}$, [Ln.DOTMA]$^{-}$, [Ln.L^4]$^{3+}$ and [Ln.L^5]$^{-}$ using single resonance fitting with a fixed μ_{eff}, (295 K, D_2O).*

Ln^{3+}	[Ln.L^4]$^{3+}$	[Ln.gDOTA]$^{5-}$	[Ln.DOTMA]$^{-}$	[Ln.L^5]$^{-}$
		T_{1e} / ps		
Er	0.31 ±0.09	0.46 ±0.02	x	0.56 ±0.02
Tm	0.21 ±0.02	0.34 ±0.02	0.30 ±0.02	0.39 ±0.01
Yb	0.17 ±0.03	0.36 ±0.01	x	0.23 ±0.02
τ_R / ps	353 ±30	290 ±5	272 ±4	234 ±2
B_0^2[a] / cm^{-1}	-470	-700	-700	-700

[a]The values of the ΔJ = 1 transition of the Eu(III) emission spectrum were taken from [19].

The electronic relaxation times estimated for these two complex series follow the increase observed in T_{1e} with increasing size of the B_0^2 parameter observed in the other highly symmetrical systems. The order of T_{1e} observed across the lanthanide(III) ions observed in [Ln.L$^{1-4}$] was maintained.

The rotational correlation times correspond well to the different sizes of the two complex series, with [Ln.gDOTA]$^{5-}$ having the slightly larger hydrodynamic radius and therefore rotational correlation time than [Ln.DOTMA]$^{-}$, as revealed in Table 18. The internuclear distances estimated in this fitting procedure were compared to those available from X-ray structures and good agreement was found (Appendix 2, SI-Table 67). For example, the CH_3 group in [Tm.DOTMA]$^{-}$ is 5.2 Å from the Tm(III) ion in the minor species as analysed from the X-ray structure, and the estimated distance from the single fitting procedure was 5.1 ±0.02 Å.[49] The two isomers of [Tm.DOTMA]$^{-}$ were analysed from the mixture that was present. The electronic relaxation time (0.23 ps) of the minor 9-coordinate isomer (SAP) was found to be slightly smaller than the value of the major 8-coordinate isomer (0.30 ps, TSAP). These two values also follow the variation in B_0^2, as the shift of the CH_3 group in the minor isomer is smaller (-67 ppm) compared to the shift in the major species (-104 ppm) and therefore it can be assumed to possess a smaller crystal field splitting.

2.2.2.2 Assessment of the direct proportionality of T_{1e} to B_0^2

In their original proposal, Fries and Belorizky[72] proposed an inverse proportionality between the electronic relaxation times, T_{1e}, and the second order crystal field splitting parameter, B_0^2. In his study, however, the authors neglected to consider the different sizes and signs of the higher order parameters, which could lead to additional complications.

Indeed, a direct proportionality of T_{1e} with B_0^2 can be proposed on the basis of this thesis in complexes of high symmetry. The isostructural series in Table 19 are ordered by the size of the second order crystal field splitting parameter. A correlation between the second order crystal field splitting parameters and the electronic relaxation times can be postulated.

Table 19 : *Overview of all electronic relaxation times, T_{1e}, estimated for the highly symmetrical complex series using single resonance fitting with a fixed μ_{eff} (295 K, D_2O, [Ln.L^{2,3}] in CD_3OD).*[b]

Ln^{3+}	T_{1e} / ps[b]						
	[Ln.L^1]	[Ln.L^2]	[Ln.L^3]$^{3+}$	[Ln.L^4]$^{3+}$	[Ln.DOTMA]$^-$	[Ln.gDOTA]$^{5-}$	[Ln.L^5]$^{-a}$
Tb	0.24	0.27	0.32	0.54			0.30
Dy	0.24	0.30	0.35	0.43			0.41
Ho	0.15	0.18	0.21	0.34			0.35
Er	0.23	0.31	0.35	0.31		0.46	0.56
Tm	0.08	0.09	0.10	0.21	0.30	0.34	0.39
Yb	0.07	0.11	0.12	0.17		0.36	0.23
B_0^2 / cm^{-1}	75	110	228	-470	-700	-700	-700

[a]The phosphinate complex [Ln.L^5]$^-$ shows the greatest deviations, compared to other systems. [b]Errors are omitted, but were shown previously.

The T_{1e} values of the Tb(III), Dy(III) and Yb(III) analogues of [Ln.L^5]$^-$ show the only exception to this trend. The remaining values of the electronic relaxation time increase with an increasing crystal field splitting parameter. The relatively low values of T_{1e} for [Tb.L^5]$^-$ and [Dy.L^5]$^-$ are common among all phosphinate systems and will be discussed in section 2.2.3. It is proposed that higher order crystal field splitting parameters (B_0^4 and B_0^6) may have a bigger contribution to the overall crystal field in the phosphinate systems, thereby leading to variation in T_{1e} values for individual lanthanide(III) ions compared to [Ln.gDOTA]$^{5-}$ and [Tm.DOTMA]$^-$, even though they share a similar size of B_0^2.

The order of the estimated electronic relaxation times, first observed in the C_3 symmetric complex series is maintained for most of the high symmetry systems (**[Tb,Dy] > Er > Ho >[Tm.Yb]**).

Overall, a direct proportionality was shown in these high symmetrical systems. However, the influence of the higher order crystal field splitting parameters may lead to some deviation in strong ligand fields. The influence of these higher order parameters were investigated further using low symmetry systems. Crystal field theory dictates a greater influence of the higher order parameters in complexes of low symmetry. Accordingly, the study was extended to systems in lower symmetry.[76]

2.2.3 Low symmetry cyclen-based systems

The remaining complex series studied are in low symmetry, with the exception of $[Ln.L^9]^+$, which possesses C_2 symmetry, but was included due to the structural similarities to $[Ln.L^7]$ and $[Ln.L^8]$. The six complex series analysed here are based on the $12N_4$ system with a pyridine side arm that contains different substituents. For example, $[Ln.L^6]$ contains a meta-CF_3 reporter group and an electron withdrawing chlorine atom in the 5 position of the pyridine ring. The complexes $[Ln.L^{7\text{-}9}]$ each have a tert-butyl group in the meta position and differ in the nature of the anionic oxygen donor group: (carboxylate ($[Ln.L^7]$) and phosphinate ($[Ln.L^8]$)) and in their symmetry ($[Ln.L^9]^+$). The complexes $[Ln.L^{10}]$ and $[Ln.L^{11}]$ are the carboxylate and phosphinate analogues of a ligand containing an electron-withdrawing nitro group in the para position.

Depending on the point group of the complexes, more parameters are involved in the overall crystal field splitting of a complex. In these systems, the second order crystal field parameter, B_0^2, is no longer expected to be the dominant contribution to the crystal field splitting anymore. Indeed, an increased influence of the higher order crystal field splitting parameters (e.g. B_0^4 and B_0^6) can be expected.[10]

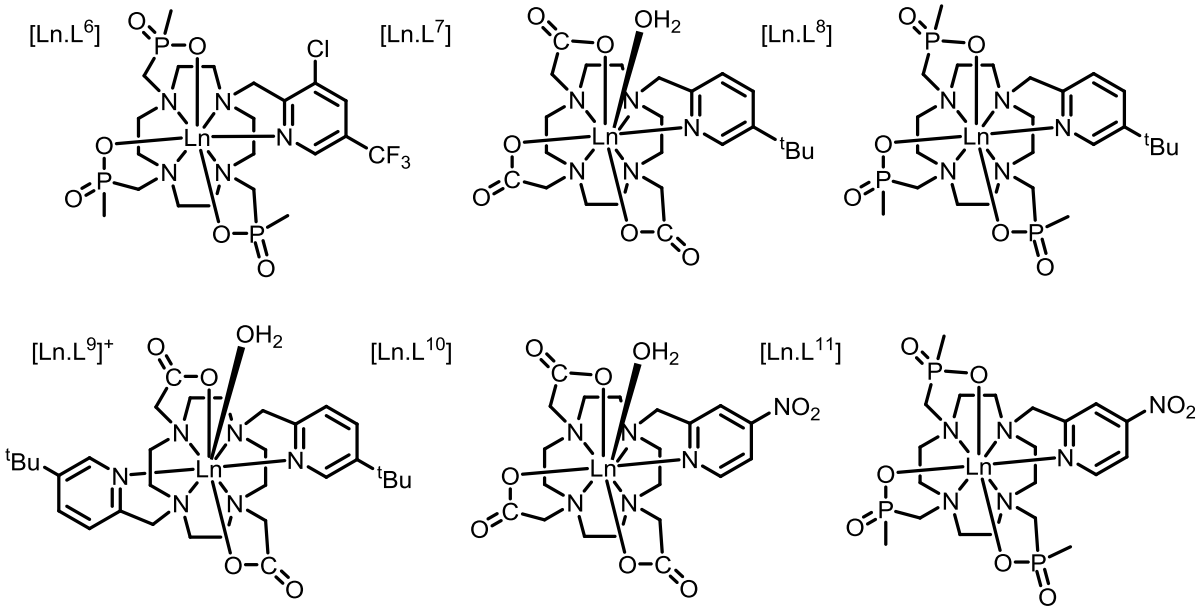

Scheme 6: *Structures of the low symmetry complex series [Ln.L[6]] to [Ln.L[11]].*

For each series, an overview of the estimated electronic relaxation times, rotational correlation times and effective magnetic moments derived from relaxation analysis using the global fixing procedure is given in Table 20. The second order crystal field splitting parameters are also quoted in each case. It is clear that the size of the estimated values of T_{1e} do not follow the estimated B_0^2 values as closely as was observed in the high symmetry systems. The order of the estimated T_{1e} values between lanthanide(III) ions was not retained from that seen in the high symmetry systems. In addition, it seems to differ from series to series.

Table 20: *Calculated electronic relaxation times, T_{1e}, effective magnetic moments, μ_{eff} and rotational correlation times, τ_r using global fitting with a fixed internuclear distance, r, at 295K of the low symmetry systems of [Ln.L^6] to [Ln.L^{11}] (D_2O, 295 K).*[a]

Ln^{3+}	[Ln.L^6]		[Ln.L^7]		[Ln.L^8]		[Ln.L^9]$^+$		[Ln.L^{10}]		[Ln.L^{11}]	
	^{19}F+ ^{1}H		^{1}H		^{1}H		^{1}H		^{1}H		^{1}H	
	μ_{eff}/ BM	T_{1e} / ps	μ_{eff}/ BM	T_{1e} / ps	μ_{eff}/ BM	T_{1e} / ps	μ_{eff}/ BM	T_{1e} / ps	μ_{eff}/ BM	T_{1e} / ps	μ_{eff}/ BM	T_{1e} / ps
Tb	9.23 ±0.04	0.44 ±0.03	9.89 ±0.03	0.71 ±0.05	8.74 ±0.06	0.57 ±0.04	10.23 ±0.03	0.91 ±0.04	9.55 ±0.02	0.55 ±0.02	9.63 ±0.01	0.69 ±0.01
Dy	9.88 ±0.03	0.40 ±0.02	10.44 ±0.03	0.55 ±0.03	9.44 ±0.05	0.45 ±0.03	10.78 ±0.03	0.88 ±0.04	10.01 ±0.01	0.44 ±0.01	9.80 ±0.01	0.47 ±0.03
Ho	9.74 ±0.03	0.33 ±0.02	10.02 ±0.02	0.26 ±0.03	9.73 ±0.04	0.39 ±0.04	9.97 ±0.03	0.24 ±0.02	9.99 ±0.01	0.19 ±0.01	10.67 ±0.01	0.48 ±0.03
Er	9.58 ±0.03	0.63 ±0.03	9.18 ±0.02	0.17 ±0.04	9.62 ±0.04	0.97 ±0.06	X	X	9.32 ±0.01	0.12 ±0.01	9.45 ±0.01	0.62 ±0.02
Tm	8.46 ±0.03	0.30 ±0.03	8.21 ±0.06	0.40 ±0.03	9.36 ±0.05	0.48 ±0.03	7.80 ±0.04	0.15 ±0.05	8.03 ±0.01	0.26 ±0.02	7.50 ±0.01	0.32 ±0.02
Yb	4.55 ±0.12	0.36 ±0.04	4.56 ±0.07	0.28 ±0.03	4.57 ±0.07	0.51 ±0.03	4.67 ±0.23	0.14 ±0.04	4.66 ±0.03	0.15 ±0.03	X	X
τ_R / ps	260 ±2		196 ±4		263 ±4		288 ±4		182 ±1		227 ±1	
B_0^2 / cm^{-1}	-550		-455		-570		-355		x		x	

[a]The common resonances used in the analysis are : [Ln.L^6] CF_3 and PCH_3 , [Ln.L$^{7\text{-}9}$] = ^{t}Bu, [Ln.L^{10}] = pyH^6, [Ln.L^{11}] = PCH_3

The higher order crystal field splitting parameters cannot be estimated easily by interpretation of the emission spectrum of the Eu(III) analogue. However, the overall ^{1}H NMR chemical shift range of a complex can give an indication about the crystal field splitting experienced by a lanthanide(III) complex. While Bleaney's theory of magnetic anisotropy only considers the second order crystal field splitting parameters B_0^2 and B_2^2, it is clear from the literature and the discussion presented here that it is reasonable to hypothesise that the higher order parameters may play an important role in the pseudocontact shift (section 2.3 and chapter 3).

Over the next few pages, the six remaining series will be analysed in groups as no clear trends can be observed from looking at the very large amount of data. First, the carboxylate complexes will be assessed ([Ln.L^{7,9,10}]), then, the focus will shift to the phosphinate complexes ([Ln.L^{6,8,11}]), before finishing with a comparison of the systems that are structurally closely related, e.g. ([Ln.L^{6,6C}],[Ln.L^{7,8}] and [Ln.L^{10,11}]).

2.2.3.1 Carboxylate pyridyl complexes

The three carboxylate systems are structurally closely related. In particular [Ln.L$^{7\text{-}9}$] (Scheme 7).

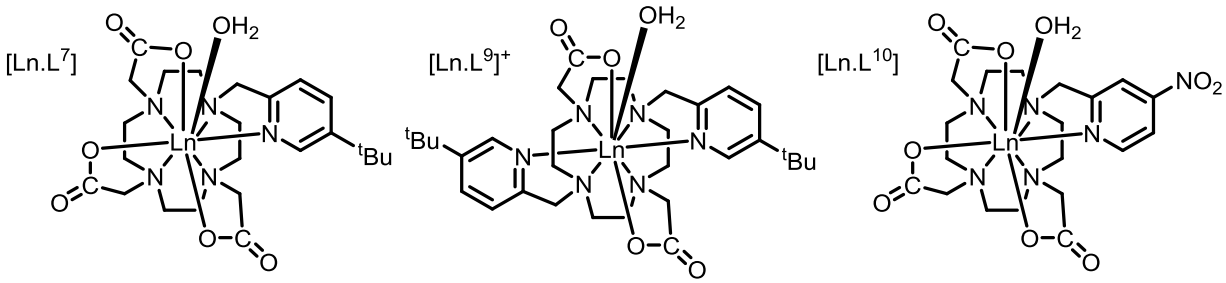

Scheme 7 : *Structures of the low symmetry, carboxylate based systems [Ln.L^7], [Ln.L^9]$^+$ and [Ln.L^{10}].*

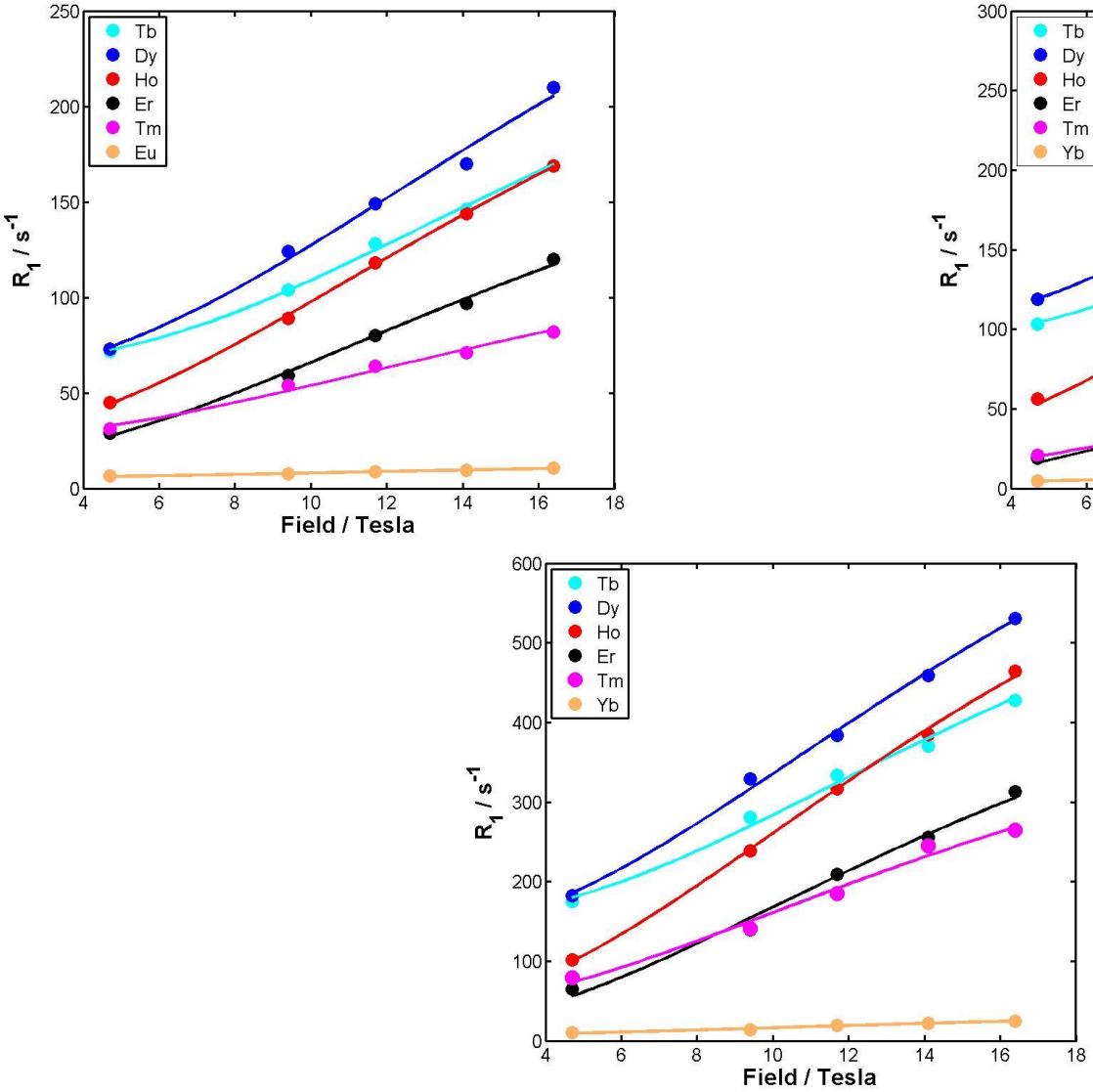

Figure 34 : *Relaxation data (data points) and best global fit (lines) for the carboxylate complex series [Ln.L[7]] (upper left), [Ln.L[9]]⁺ (upper right, ^{t}Bu resonance) and [Ln.L[10]] (bottom, pyH[6]) using a fixed r (6.5 and 5.6 Å respectively),(295 K, D_2O).*

Consideration of the data in Table 21 shows that in the carboxylate series, the order of the electronic relaxation times of the lanthanide(III) ions is mostly retained compared to the systems in high symmetry.

Table 21 : *Calculated electronic relaxation times, T_{1e}, effective magnetic moments, μ_{eff} and rotational correlation times, τ_r using global fitting with a fixed internuclear distance, r, at 295K of the low symmetry systems of [Ln.L^7], [Ln.L^9]$^+$ and [Ln.L^{10}] (D_2O, 295 K).*

Ln^{3+}	[Ln.L^7]		[Ln.L^9]$^+$		[Ln.L^{10}]	
	μ_{eff}/ BM	T_{1e} / ps	μ_{eff}/ BM	T_{1e} / ps	μ_{eff}/ BM	T_{1e} / ps
Tb	9.89 ±0.03	0.71 ±0.05	10.23 ±0.03	0.91 ±0.04	9.47 ±0.02	0.55 ±0.02
Dy	10.44 ±0.03	0.55 ±0.03	10.78 ±0.03	0.88 ±0.04	10.00 ±0.01	0.43 ±0.01
Ho	10.02 ±0.02	0.26 ±0.03	9.97 ±0.03	0.24 ±0.02	9.97 ±0.01	0.19 ±0.01
Er	9.18 ±0.02	0.17 ±0.04	x[a]	x	9.30 ±0.01	0.12 ±0.01
Tm	8.21 ±0.06	0.40 ±0.03	7.80 ±0.04	0.15 ±0.05	8.01 ±0.01	0.26 ±0.02
Yb	4.56 ±0.07	0.28 ±0.03	4.67 ±0.23	0.14 ±0.04	4.65 ±0.03	0.15 ±0.03
τ_R / ps	196 ±4		288 ±4		182 ±1	
B_0^2 / cm^{-1}	-455		-355		x	

[a]It was not possible to use the data of [Er.L^9]$^+$ in global fitting procedure, but it was analysed using single resonance fitting (0.20 ps ±0.05)

Tb(III) and Dy(III) complexes provided the highest values of the electronic relaxation times. Through the combination of these large estimated T_{1e} values and the large values of μ_{eff} of these two lanthanide(III) ions, these complexes possess the highest nuclear relaxation rates amongst the carboxylate based systems. The Tm(III) and Yb(III) complexes also show increased values in each series relative to the other lanthanide(III) ions and the systems studied previously. The estimated T_{1e} values of Er(III) and Ho(III) are in the range of the C_4 symmetric tetra-amide complex [Ln.L^4]$^{3+}$.

Generally, the T_{1e} values of the lanthanide(III) ions follow the order : [**Tb, Dy,] > Tm > [Ho, Yb] > Er** in these low symmetry carboxylate based systems. It seems that the introduction of low symmetry influences every lanthanide(III) ion differently. In particular Ho(III) and Er(III) seem to be affected to a different degree than the remaining lanthanide(III) ions, which alters the order of estimated T_{1e} values significantly from the complex series analysed previously.

Normally, Ho(III) complexes are among the fastest relaxing systems due to the high effective magnetic moment of the Ho(III) ion (10.4 BM). But here, even its high value of

μ_{eff} does not compensate for the low electronic relaxation times (Figure 34). A similar effect is observed with the Er(III) analogues. The nuclear relaxation rates were as low as those observed for the Tm(III) complexes, despite the difference of almost 2 BM in the theoretical values of the effective magnetic moments.

The values of B_0^2 derived from the Eu(III) complex analysis decrease from [Ln.L^7] to [Ln.L^9]$^+$, while the estimated T_{1e} values of Tb(III) and Dy(III) show a significant increase. In particular, the estimated T_{1e} values for Tb(III) and Dy(III) are among the highest values encountered for these two lanthanide(III) ions. The values for Ho(III) experience a slight increase. It was not possible to fit the nuclear relaxation rates of [Er.L^9]$^+$. However, single resonance fitting allowed a value of 0.20 ±0.05 ps to be estimated, which is the same as the value for [Er.L^7]. In addition, both [Tm.L^9]$^+$ and [Yb.L^9]$^+$ also experience a small decrease in their estimated T_{1e} values. The order of the estimated electronic relaxation times of the high symmetry complex series is mostly maintained for this series (**[Tb, Dy] > [Er, Ho] >[Tm, Yb]**), with only [Er.L^9]$^+$ having a slightly deviated value, but this could be presumably attributed to the larger estimated error.

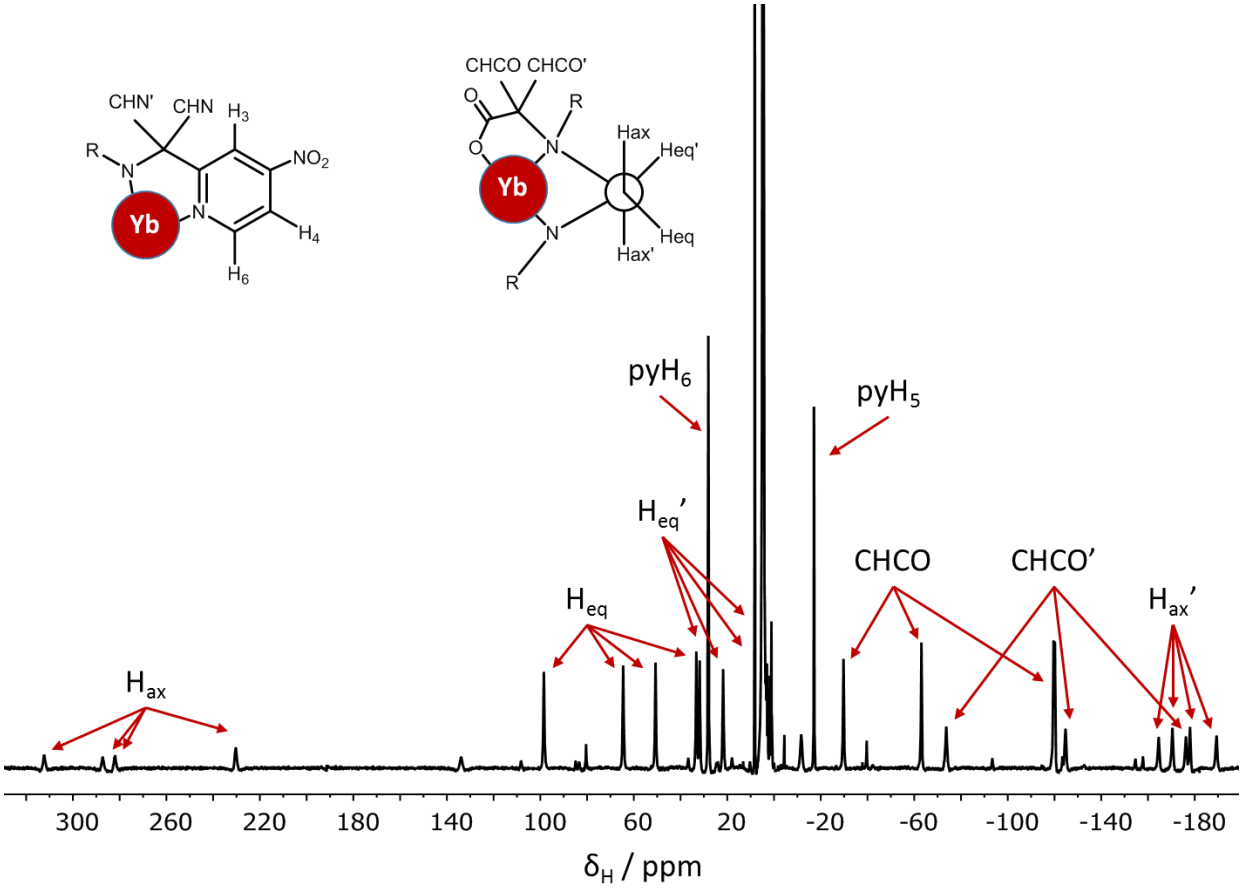

Figure 35 : *Annotated ^{1}H NMR spectrum of [Yb.L^{10}]. Unassigned resonances are due to the minor isomer (D_2O, 295 K, 16.5 T).*

Generally, the second half (Er(III), Tm(III) and Yb(III)) of the fast relaxing lanthanide(III) ions shows a decreasing T_{1e} value with decreasing B_0^2, while the others (Tb(III), Dy(III) and Ho(III)) show an increase in values. Intriguingly, this trend follows the sign of the magnetic anisotropy of these lanthanide(III) ions. Overall, this is another indication that different lanthanide(III) ions are affected differently by reducing the symmetry of the point group of the complex.

The other carboxylate system, [Ln.L^{10}] (example in Figure 35) behaved in a very similar way. The estimated T_{1e} values for [Ho.L^{10}] and [Er.L^{10}] were of comparable size to the previous carboxylates.

It is tempting to hypothesise that the higher order ligand field parameters may be exerting a big influence in these low symmetry systems. There is no clear correlation between the crystal field splitting and the electronic relaxation times from these three

systems. However, it can be hypothesised that the higher order terms can affect each lanthanide(III) ion differently. The phosphinate complexes studied earlier ([Ln.L^3]$^{3+}$ and [Ln.L^5]), had already shown some anomalous behaviour in, for example, the Er(III) analogues. By extending the study to additional phosphinate complexes, further information on this aspect can be gained.

2.2.3.2 Phosphinate pyridyl complexes

For [Ln.L^6], the ^{19}F resonances of the CF_3 group and the proton P-Me resonances were analysed. Similar to the observation made in [Ln.L^2], no significant deviation in estimated parameters was found, whether analysing the ^{19}F or the ^{1}H resonances of the complex (Appendix 2, SI-Table 39 -47)

[Ln.L^6] [Ln.L^8] [Ln.L^{11}]

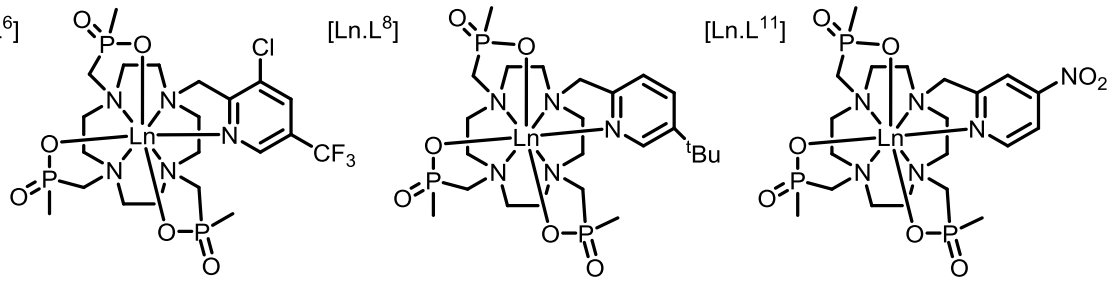

Scheme 8 : *Structures of the low symmetry phosphinate complexes [Ln.$L^{6,8,11}$].*

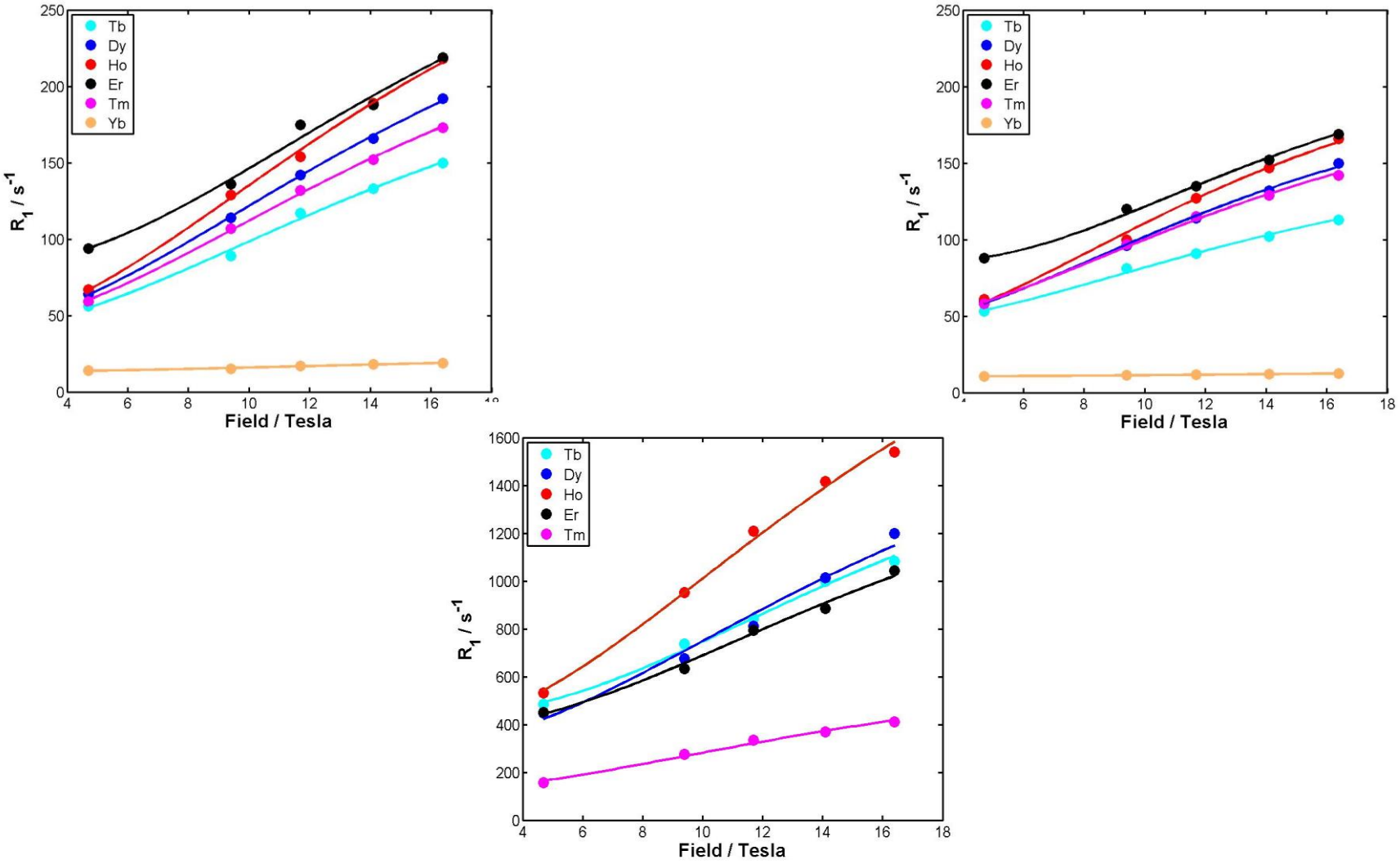

Figure 36 : *Relaxation data (points) and best global fit (lines) of [Ln.L^{6}] (top left), [Ln.L^{8}] (top right) and [Ln.L^{11}] (bottom centre) using a fixed r of 6.1 Å (CF_3), 6.5 Å (^{t}Bu) and 4.8 Å (CH_3) respectively (D_2O, 295 K)*

For these sets of phosphinate complexes, the calculated T_{1e}, μ_{eff} and τ_R values are given in Table 22, based on the experimental data presented in Figure 36. The Ho(III), Er(III), Tm(III) and Yb(III) analogues seem to have enhanced electronic relaxation times, similar to the values of $[Ln.L^5]^-$, while, the values for the Tb(III) and Dy(III) complexes fall within the range of estimated T_{1e} values.

Table 22 : *Calculated electronic relaxation times, T_{1e}, effective magnetic moments, μ_{eff} and rotational correlation times, τ_r using global fitting with a fixed internuclear distance, r, at 295K of the low symmetry systems of [Ln.L^6], [Ln.L^8] and [Ln.L^{11}] (D_2O, 295 K).*

Ln^{3+}	[Ln.L^6]		[Ln.L^8]		[Ln.L^{11}]	
	μ_{eff}/ BM	T_{1e} / ps	μ_{eff}/ BM	T_{1e} / ps	μ_{eff}/ BM	T_{1e} / ps
Tb	9.23 ±0.04	0.44 ±0.03	8.74 ±0.06	0.57 ±0.04	9.63 ±0.01	0.69 ±0.01
Dy	9.88 ±0.03	0.40 ±0.02	9.44 ±0.05	0.45 ±0.03	9.80 ±0.01	0.47 ±0.03
Ho	9.74 ±0.03	0.33 ±0.02	9.73 ±0.04	0.39 ±0.04	10.67 ±0.01	0.48 ±0.03
Er	9.58 ±0.03	0.63 ±0.03	9.62 ±0.04	0.97 ±0.06	9.45 ±0.01	0.62 ±0.02
Tm	8.46 ±0.03	0.30 ±0.03	9.36 ±0.05	0.48 ±0.03	7.50 ±0.01	0.32 ±0.02
Yb	4.55 ±0.12	0.36 ±0.04	4.57 ±0.07	0.51 ±0.03	x	x
τ_R / ps	260 ±2		263 ±4		227 ±1	
B_0^2/ cm^{-1}	-550		-570		x	

Complexes of lanthanide(III) ions with comparatively low effective magnetic moments, notably Er(III) and Tm(III)), possess higher electronic relaxation times. Thus, at lower magnetic field strengths, these systems possess very similar nuclear relaxation rates to the lanthanide(III) ions with the highest values of μ_{eff} (Dy(III), Ho(III)).

In these systems, the Er(III) complex stands out. It is the fastest relaxing example in [Ln.L^6] and [Ln.L^8] and this is directly attributable to high T_{1e} values (0.63 and 0.97 ps respectively). A similar trend can be seen with [Ln.L^{11}], abeit it is not as pronounced as in the other two systems. The electronic relaxation time of [Er.L^{11}] is also large, but is slightly smaller than for [Dy.L^{11}].

This high electronic relaxation time seems to counterbalance the differences in the effective magnetic moments, especially for [Ln.L^6] and [Ln.L^8]. Therefore, the nuclear relaxation rates at low field are very similar range for most of the lanthanide(III) ions. The Er(III) analogues differ, by showing a further enhancement in [Ln.L^{6,8}].

The order of electronic relaxation times of lanthanide(III) ions calculated in the phosphinate series of complexes is : **Er > Tb > [Dy, Ho, Tm, Yb]**.

The values of the estimated effective magnetic moments will be discussed in more detail in chapter 4. However, it should be noted that the estimated value for [Tm.L^8] is exceptional. Similar to [Tm.L^5]$^-$ the value is significantly higher than would be expected. With a value of 9.36 BM, it shows the highest deviation from the literature value (7.6 BM) encountered across all series. Its relaxation data fitting curve, however, does not show anomalous behaviour. Indeed, the nuclear relaxation rates seem comparatively slow (Figure 36).

Overall, the trends observed with these phosphinate based complexes are similar to those observed in the high symmetry phosphinate complex series ([Ln.L^2] and [Ln.L^5]$^-$).

2.2.3.3 Direct comparison of carboxylates and phosphinates

Owing to structural similarities of [Ln.L^{6-11}], a direct comparison of common resonances across different series was made.

The ^{t}Bu receptor group is a common resonance in [Ln.L^{7-9}] and their rate data were analysed. There will be small structural differences between each series that might alter the Ln(III)-^{t}Bu internuclear distances, *r*. For example, the phosphinate anionic donor groups of [Ln.L^8] are bulkier than the carboxylate groups of [Ln.L^7]. Additionally, [Ln.L^9]$^+$ is the C_2 symmetric analogue of [Ln.L^7], which will increase the overall bulk of the complex.

The ^{19}F resonance of the CF_3 receptor group of [Ln.L^6] was compared to two complexes of a carboxylate analogue [Ln.L^{6C}].

2.2.3.3.1 Comparison using single resonance fitting

The single resonance fitting procedure was used to allow a direct comparison of the common resonances.

The values of the electronic relaxation times using the single resonance fitting agree well with the global fitting data. The average internuclear distances calculated for the ^{t}Bu receptor group using the single resonance fitting procedure are in very good agreement, across each isostructural series (6.7 ±0.1, 6.6 ±0.5 and 6.6 ±0.1 Å for [Ln.L^{7}], [Ln.L^{8}] and [Ln.L^{9}]$^{+}$ respectively).

Table 23 : *The electronic relaxation times calculated using single resonance fitting with a fixed μ_{eff} (295 K, D_2O).*

Ln^{3+}	T_{1e} / ps[a]					
	[Ln.L^{6}]	[Ln.L^{7}]	[Ln.L^{8}]	[Ln.L^{9}]$^{+}$	[Ln.L^{10}]	[Ln.L^{11}]
Tb	0.49 ±0.04	0.68 ±0.03	0.64 ±0.04	0.70 ±0.03	0.55 ±0.02	0.59 ±0.01
Dy	0.41 ±0.03	0.54 ±0.03	0.59 ±0.04	0.68 ±0.02	0.45 ±0.02	0.50 ±0.02
Ho	0.41 ±0.03	0.29 ±0.03	0.52 ±0.03	0.34 ±0.03	0.20 ±0.02	0.33 ±0.03
Er	0.58 ±0.02	0.22 ±0.04	0.85 ±0.02	0.20 ±0.05	0.14 ±0.02	0.66 ±0.03
Tm	0.25 ±0.02	0.29 ±0.04	0.31 ±0.02	0.20 ±0.05	0.23 ±0.03	0.25 ±0.01
Yb	0.37 ±0.04	0.22 ±0.05	0.46 ±0.01	0.15 ±0.03	0.13 ±0.04	x
τ_R / ps[b]	241 ±13	197 ±7	271 ±12	242 ±6	186 ±9	229 ±2
B_0^2 / cm^{-1}	-550	-455	-570	-355	x	x

[a]The common resonances used are : [Ln.L^{6}] = CF_3, PCH_3, [Ln.L$^{7\text{-}9}$] = ^{t}Bu, [Ln.L^{10}] = average of at least 6 resonances, [Ln.L^{11}] = CH_3.

Naturally, a big deviation in the estimated internuclear distance across a series in the global fitting procedure, leads to a deviation in the estimated parameters in the single resonance fitting procedure, as the estimated internuclear distance is a globally fixed parameter. For example, the [Tm.L^{8}] and, even the [Tb.L^{8}] complex showed a large variation in the internuclear distance from the expected value of 6.6 Å. The estimated values were 5.8 and 7.1 Å respectively, representing the biggest deviations experienced in this work in estimating internuclear distances. As was found with the tetra-phosphinate complexes, [Ln.L^{5}]$^{-}$ these values do not seem to be estimated accurately with the methods used. Such behaviour might be due to the considerable variation of the effective magnetic moment with the ligand field. This concept will be discussed in

chapter 4. Generally, the fitting procedure showed greater deviation for [Ln.L^{8}] than for any other series (even compared to [Ln.L^{5}]$^{-}$), creating doubt about the applicability of the Solomon- Bloembergen Morgan theory for these systems.

The estimated rotational correlation times follow predictable trends between the carboxylate and phosphinate groups. The phosphinate complexes have an increased rotational correlation times (196 and 263 ps for [Ln.L^{7}] and [Ln.L^{8}] respectively) attributed to the greater bulk of the phosphinate groups. Introducing two coordinate pyridyl moieties increases the bulk of the complexes, and, therefore the rotational correlation times (288 ps).

2.2.3.3.2 Comparison of [Ln.L^{7}] and [Ln.L^{8}]

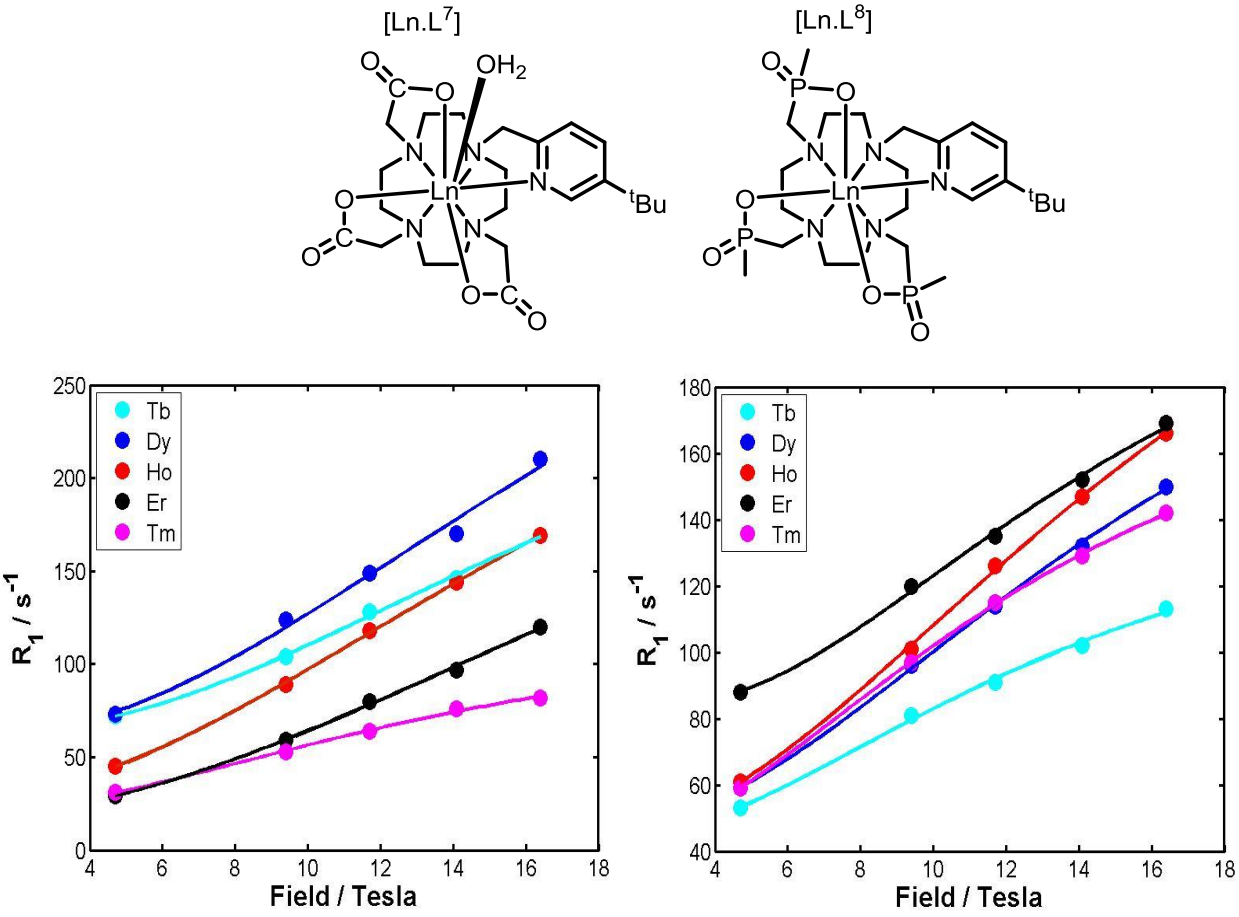

Figure 37 : *Relaxation data (points) and best single fit (lines) for the ^{t}Bu resonance of [Ln.L^{7}] (left) and [Ln.L^{8}] (right), with a fixed μ_{eff}, (295 K in D_2O).*

In [Ln.L^7] and [Ln.L^8] the nuclear relaxation rates at lower field behave very differently to each other. In the phosphinate analogues, the R_1 values at lower fields are much closer to each other, with [Dy.L^8] and [Tb.L^8] possessing lower nuclear relaxation rates compared to the carboxylate analogues. The remaining lanthanide(III) complexes have an increased rate of relaxation, in particular, the aforementioned rates of [Er.L^8] increase significantly. This complex is the fastest relaxing example in this series (Figure 37).

Table 24: *The electronic relaxation times calculated for [Ln.L^{7,8}], using single resonance fitting with a fixed μ_{eff}, (295 K, D_2O)*

Ln^{3+}	T_{1e} / ps	
	[Ln.L^7]	[Ln.L^8]
Tb	0.68 ±0.03	0.64 ±0.04
Dy	0.54 ±0.03	0.59 ±0.04
Ho	0.29 ±0.03	0.52 ±0.03
Er	0.22 ±0.04	0.85 ±0.02
Tm	0.29 ±0.04	0.31 ±0.02
Yb	0.22 ±0.05	0.46 ±0.01
τ_R / ps	197 ±7	271 ±12
B_0^2 / cm^{-1}	-455	-570

The estimated T_{1e} values of Dy(III) (change of +0.05 ps) and Tb(III) (-0.04 ps) and Tm(III) do not change significantly, while Ho(III) (+0.23 ps), Er(III) (+0.63 ps) and Yb(III) (+0.24 ps) values increase dramatically. As observed with [Ln.L^5]$^-$, the effect on nuclear relaxation rates is dramatic even in the high field regime, where it can have as big an influence as the effective magnetic moment in determining nuclear relaxation rates.

Overall, the effect of the different anionic donor groups on the electronic relaxation times cannot be neglected, even though their effect on the second order crystal field splitting parameters is apparently relatively small.

2.2.3.3.3 Comparison of [Ln.L^{6C}] and [Ln.L^{6}]

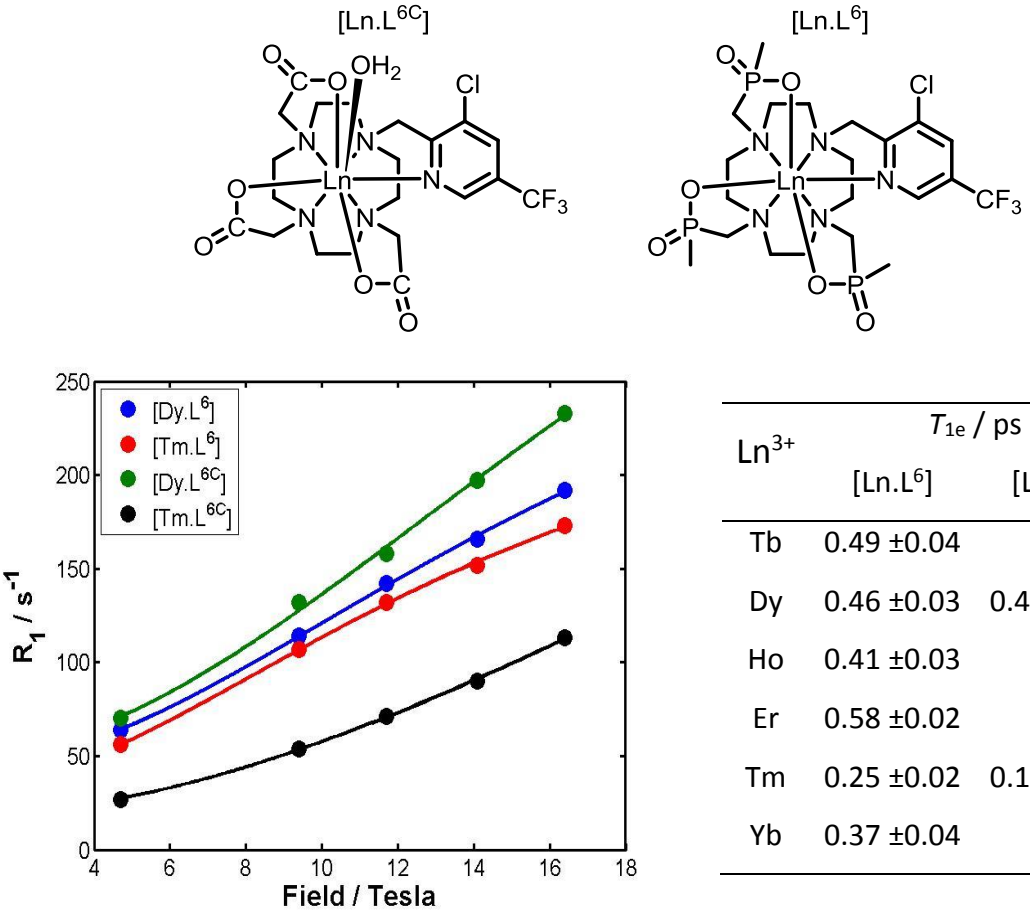

Ln^{3+}	T_{1e} / ps	
	[Ln.L^{6}]	[Ln.L^{6C}]
Tb	0.49 ±0.04	
Dy	0.46 ±0.03	0.42 ±0.02
Ho	0.41 ±0.03	
Er	0.58 ±0.02	
Tm	0.25 ±0.02	0.14 ±0.02
Yb	0.37 ±0.04	

Figure 38 : *Structures, comparison of nuclear relaxation rates (points) and best single fit (lines) for the CF_3 resonance of [Ln.L^{6}] and [Ln.L^{6C}] (295 K, D_2O) and estimated electronic relaxation times using the mentioned fitting procedure.*

With [Ln.L^{6}], the Er(III) analogue has the highest nuclear relaxation rates at low magnetic field strengths amongst all lanthanide(III) ions (shown in Figure 36). However, only the Dy(III) and Tm(III) analogues were compared here. The estimated T_{1e} values for [Dy.L^{6}] do not vary (+0.04 ps), while the phosphinate [Tm.L^{6}] has slightly enhanced values compared to the carboxylate analogue (+0.11 ps). The underlying trends observed in [Ln.L^{7,8}] are also observable in these two complex systems.

2.2.3.3.4 Comparison of [Ln.L^{10}] and [Ln.L^{11}]

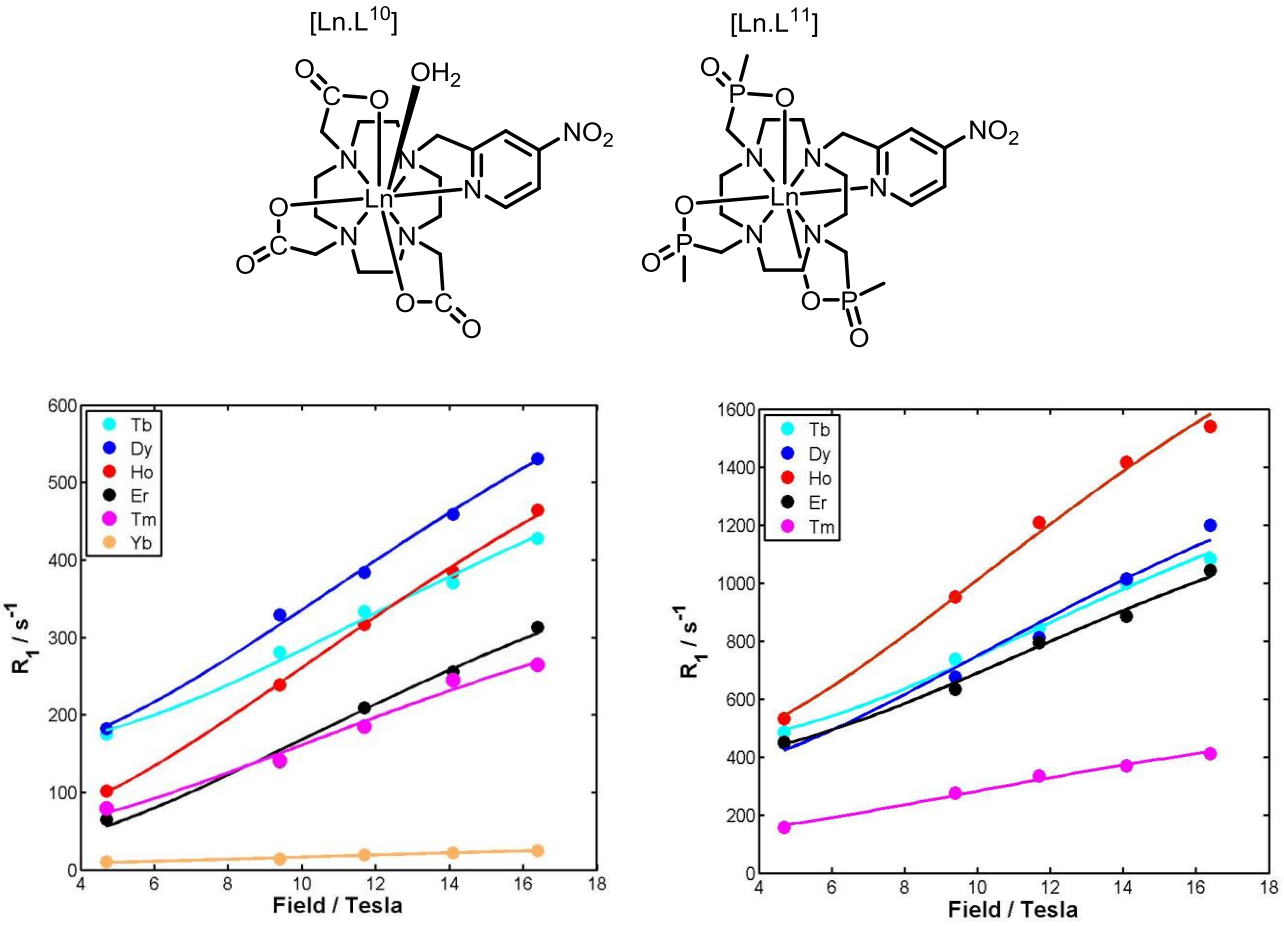

Figure 39: *Relaxation data (points) and best global fitting (lines) for the pyH^6 resonance of [Ln.L^{10}] (left) and the CH$_3$ resonance of [Ln.L^{11}] (right) (D$_2$O, 295K)*

A common resonance could not be analysed between these two systems, so a direct comparison of the fitting curves is not possible. The T_{1e} values of the Dy(III) analogues increase slightly between [Ln.L^{10}] and [Ln.L^{11}] (+0.14 ps), but the Tb(III) values do not change significantly (+0.03 ps). In addition, the estimated T_{1e} values of the Tm(III) complexes (+0.06 ps) only show a slight increase. However, both Ho(III) (+ 0.29 ps) and Er(III) (+0.5 ps) again show a remarkable increase in the relaxation rates in the phosphinate systems.

2.2.3.3.5 Overview of the changes between carboxylate and phosphinate based complexes

The differences in T_{1e} values between carboxylate and phosphinate analogues are tabulated below (Table 25). For a given lanthanide(III) ion, changes in T_{1e} are broadly similar in every case. The changes in the estimated electronic relaxation times are, in parts, remarkably similar across all six series.

Table 25 : *Overview of the changes in electronic relaxation times, T_{1e} between carboxylate and phosphinate analogues, using single resonance fitting data with a fixed μ_{eff}, (295 K, D_2O).*

Ln^{3+}	ΔT_{1e} / ps		
	[Ln.L^6] - [Ln.L^{6c}]	[Ln.L^8] - [Ln.L^7]	[Ln.L^{11}] - [Ln.L^{10}]
Tb	x	-0.04 ±0.05	+0.04 ±0.02
Dy	+0.04 ±0.04	+0.05 ±0.05	+0.05 ±0.03
Ho	x	+0.23 ±0.04	+0.13 ±0.04
Er	x	+0.63 ±0.05	+0.52 ±0.04
Tm	+0.11 ±0.03	+0.02 ±0.05	+0.02 ±0.03
Yb	x	+0.24 ±0.05	x

The most dramatic variation is shown by the Er(III) complexes. Here, the faster nuclear relaxation rates of the phosphinate systems are directly attributable to the large increase in T_{1e}. It is apparent that each lanthanide(III) ion is affected to a different degree.

The [Tb.$L^{7,8}$] example is the only one with a decrease in estimated electronic relaxation times. However, with the exception of the values where a significant change can be observed, the differences are within their respective errors.

The behaviour of the Yb(III) complexes has been rarely mentioned in this discussion. Due to the combination of a low effective magnetic moment (4.3 BM) and its low electronic relaxation times, the nuclear relaxation rates hardly increase as a function of the magnetic field strength.

The main difference between the carboxylate and phosphinate series is that the former are 9-coordinate complexes with a capping axial water in a SAP coordination geometry. The phosphinate complexes, on the other hand, are 8-coordinate (q=0) complexes in a TSAP coordination environment.

The complex series $[Ln.L^{9}]^{+}$ should, in theory, be treated differently due to its C_2 symmetry, but was analysed here due to the structural similarities. The para 4-nitro group in $[Ln.L^{10}]$ and $[Ln.L^{11}]$ slightly alters the electron density distribution in the pyridine ring and makes the pyN a weaker, thereby altering the ligand field experienced by the lanthanide(III) ions.

Comparing the estimated data of the low symmetrical systems with the second order crystal field splitting parameters led to inconclusive results. However, it is hypothesised that the electronic relaxation times show a different dependence on changes in the coordination environment according to the nature of the lanthanide(III) ion.

2.3 The influence of the higher order crystal field parameters

The direct proportionality of the second order crystal field splitting parameter with T_{1e} in high symmetrical systems was noted in section 2.2.2.2.

The NMR pseudocontact shift is linked to the second order crystal field splitting parameters by Bleaney's theory of magnetic anisotropy. However, Binnemans in particular[9,10,76,77] has shown that the influence of higher order parameters in the pseudocontact shift cannot be neglected. The most shifted resonances analysed are the ring protons, normally 3.6 to 4.5 Å away from the paramagnetic centre. At this distance, the contact shift contribution is likely to be very small and these nuclei are not directly coordinated to the lanthanide(III) ion. Measuring the overall shift range can give a rough estimate of the overall crystal field splitting, assuming an additive nature of the higher order parameters to the pseudocontact shift.

The analysis of the shift range cannot be performed for all lanthanide(III) ions. Given the large enhancements of R_2 to the ring protons, in, for example the lanthanide(III) ions that possess a high magnetic moment (Tb(III), Dy(III) Ho(III) and Er(III)), it is often not possible to observe the resonances of every ring proton, especially at high field. Therefore, this analysis is confined to the Tm(III) and Yb(III) analogues of the complexes.

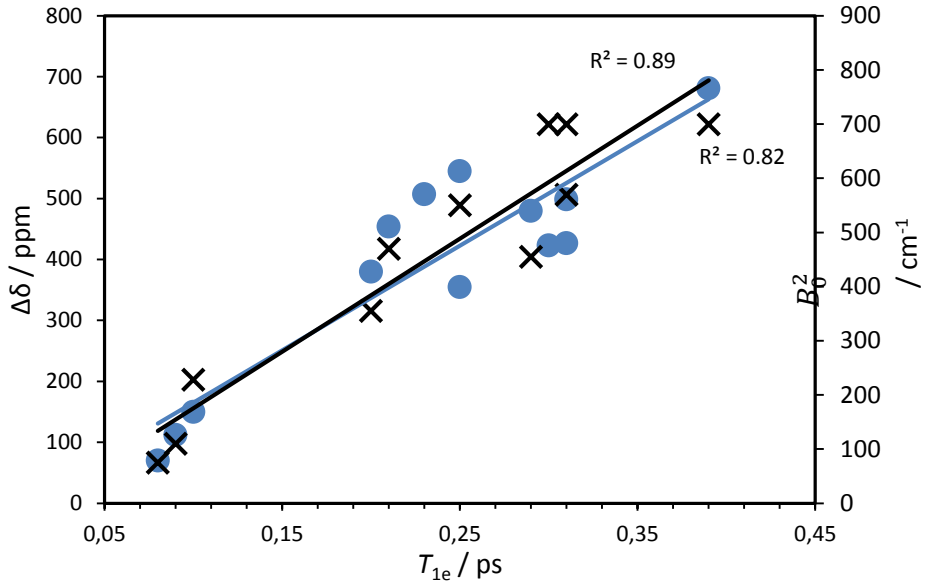

Figure 40 : *The correlation between the estimated T_{1e} values with the overall shift range (●) and the second order crystal field splitting parameter (**x**) for the Tm(III) complexes, with the highly symmetrical systems highlighted (Appendix 2, SI-Table 68).*

The estimated electronic relaxation times and crystal field splitting parameters were plotted with the observable shift range for Tm(III) (Figure 40). In the highly symmetrical complex series, it is possible to see an increase in the crystal field splitting parameter, the overall shift range and the electronic relaxation time in [Ln.L^1] to [Ln.L^5]$^-$, [Ln.gDOTA]$^{5-}$, [Ln.DOTMA]$^-$ and even [Ln.L^9]$^+$. The correlation over all complexes shows an R^2 values of 0.82 for the correlation between the electronic relaxation time and the crystal field splitting parameters, and 0.89 for the overall shift range.

The values of the Yb(III) complexes are less well correlated with R^2 values consisting of 0.47 and 0.60 for crystal field splitting and shift range respectively (Appendix 2, SI-Figure 2 and SI-Table 69). In a few cases, a linear trend is observable in the shift range of selected complexes ([e.g. [Ln.L$^{1-3}$]).

2.3.1 Using time correlation functions to simulate T_{1e}

In an attempt to rationalise the influence of the higher order parameters, a collaboration with Pascal Fries (Grenoble) was initiated with the intention of revisiting his previous simulations (Chapter 1, Section 1.4.3.1).[63,72] It was reasoned that with the extensive available data for [Ln.L^{1,2}] and [Ln.L^{4,6}] and the knowledge of the likely influence of the higher order parameters, neglected in the original study, more reliable results should emerge.

The electronic energy levels of the lanthanide(III) ions are split by the spin-orbit coupling and then sub-divided by the crystal field splitting into (2*J*+1) levels (Figure 41) causing the overall zero-field splitting (ZFS) of the energy levels.

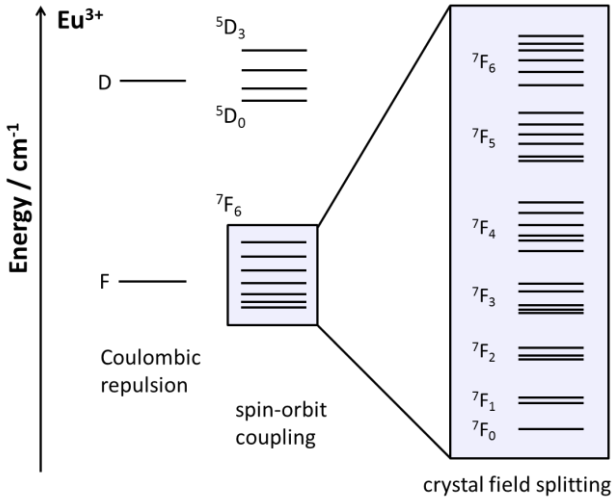

Figure 41 : *Electronic energy levels of a model Eu(III) system.*

This zero-field splitting splitting is considered to influence the electronic relaxation times,[28,72] which requires consideration of various crystal field splitting parameters and the total angular momentum. While an inverse correlation between the crystal field splitting and the electronic relaxation times was proposed by Fries, a connection to the total angular momentum cannot be made here and indeed is not noted in the literature either.[66–68,78]

Fries revisited his original calculations with data obtained in this work. The simulations were repeated using varying higher order crystal field splitting parameters to ensure an fuller description of the influence of the ligand field and the spin-orbit coupling on the electronic relaxation times.

The details of the computation at work are discussed in the 2013 paper, but a brief description will be given here.[63]

In this work the main causes of electronic relaxation are described to arise from random, time-dependent fluctuations acting on the ground state energy levels. These fluctuations consist of the sum of a time average static ligand field and of the residual fluctuating transient ligand field. The static ligand field is due to the Brownian movement and rotation of the complexes and consequently modulated by the rotational correlation time. The transient ligand field is due to distortions and vibrations caused by solvent collisions, which leads to a modulation due to the electronic relaxation time.

By including the effect of *J* degeneracy and the impact of the crystal field splitting parameters it was possible to estimate weighting factors within the Redfield limit ($R_1 << 1 / T_{1e}$) that almost follow the experimental sequence of the estimated T_{1e} values of the lanthanide(III) ions (Table 26).

Table 26: *Weighting relaxation factors showing the effect of different order of the crystal field parameters on the different lanthanide(III) ions.*

	Tb	Dy	Ho	Er	Tm	Yb
$W_2^{Redfield}$	2.16	1.30	0.18	0.21	2.16	7.75
$W_4^{Redfield}$	0.28	0.98	0.45	0.55	2.01	8.85
$W_6^{Redfield}$	0.19	1.57	4.7	6.28	4.69	7.31
$\sum_{k=2,4,6} W_k^{Redfield}$	2.63	3.85	5.33	7.04	8.86	23.91
$\frac{g_{Ln}^2 J(J+1)}{\sum_{k=2,4,6} W_k^{Redfield}}$	0.36	0.29	0.21	0.13	0.06	0.01

The combined weighting factor $\frac{g_{Ln}^2 J(J+1)}{\sum_{k=2,4,6} W_k^{Redfield}}$ is hypothesised to be directly proportional to the electronic relaxation time.

The values for Er(III) are underestimated and those for Ho(III) are overestimated, leading to slight change in the order of the estimated T_{1e} values. These two lanthanide(III) ions were highlighted earlier to be those that are most affected by the change of coordination environment, and therefore are likely difficult to rationalise.

In this first theoretical approach, the order of the electronic relaxation times was calculated using a simplified Redfield theory. A full computational method was used to simulate actual values of the electronic relaxation times by computing the static and transient fluctuations to validate the experimental values. These Monte-Carlo simulations were based on the numerical solution of the Schrödinger equation to obtain the evolution operator of the electronic states of the *J* ground multiplet as a function of the random rotational (Curie relaxation) and vibrational modes (electronic relaxation) of the complex.

$$T_{1e}^{eff} = \int_0^{\infty} G_{\parallel}^{nor}(t)\, dt$$

,where $G_{\parallel}^{nor}$ is the normalised longitudinal time correlation function (TCF), which is estimated through the size of the transient ligand field and can therefore be used to simulate T_{1e} values.

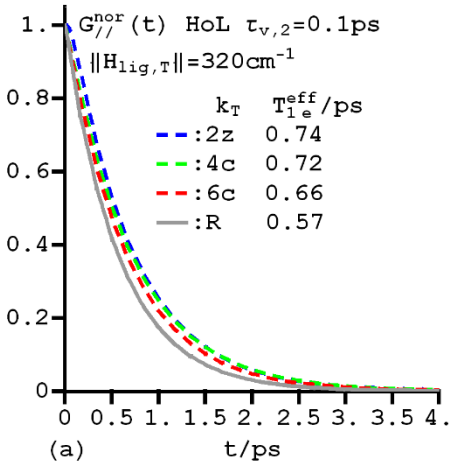

Figure 42 : *Time evolution of $G_{\parallel}^{norm}$ of a model Ho(III) complex induced by various transient ligand field terms, $H_{lig,T}$ of fixed magnitude (320 cm^{-1}) and a lower limit of the vibrational correlation time $\tau_{v,2}$ = 0.1 ps 2z,4z,6z are axial Hamiltonians of pure order, R is the result of Redfield theory.*

The time evolution operator was used to simulate the electronic relaxation times of model complexes, as a function of the higher order crystal field splitting parameters (Figure 42). It was found that the T_{1e} values decrease with increasing influence of the fourth and sixth order terms (Table 27), giving a first indication of the effect that these higher order parameters potentially have on the T_{1e} values.

Table 27 : *Simulated relaxation times, T_{1e}, due to various transient term, $H_{lig,T}$ of fixed magnitude (320 cm^{-1}) and vibrational correlation time τ_v = 0.1 ps.*

$H_{lig,T}$[a]	T_{1e} / ps					
	Tb	Dy	Ho	Er	Tm	Yb
2z	0.416	0.646	0.744	0.646	0.416	0.192
4c	0.363	0.619	0.722	0.619	0.363	0.085
6c	0.298	0.559	0.671	0.559	0.298	0.079

[a]2z is an axial Hamiltonian of pure order 2, 4c,6c are cubic Hamiltonians of pure order 4 and 6.

The simulated values of the electronic relaxation times are of similar sizes as the experimental data shown previously (only data for [Ln.$L^{1\text{-}2}$] and [Ln.$L^{4,6}$] were available at the time of this study).

Overall, the adjustment of this theoretical computational approach allowed the sequence of the electronic relaxation times across an isostructural series of lanthanide(III) ions to be reproduced. It was shown that the electronic relaxation times do vary as a function of the higher order terms, in particular the rank 6 parameters. The simulation technique managed to reproduce the experimental data using the extended influence of the higher order parameters. However, in some cases, the agreement between theoretical and experimental values remains poor, notably for Ho(III).

2.4 Summary & Conclusions

The estimated electronic relaxation times of the lanthanide(III) ions, generally, follow the trends first observed by Alsaadi in 1980.[66,67] It was found that a change in the symmetry of the complexes and the different anionic donor groups affect the electronic relaxation times of the lanthanide(III) ions to different degrees, depending on the lanthanide(III) ion itself. Especially, complexes Ho(III) and Er(III) were affected by the changes in the coordination environment.

2.4.1 The impact on ligand design and lanthanide(III) selection

Prior to this thesis, there were only a few literature values available for the electronic relaxation time of lanthanide(III) ions in solution.[20,28,66–68]

In the systems presented here, the electronic relaxation time not only has a dominant effect at low magnetic field strengths, as suggested by simulations and consistent with the Solomon-Bloembergen Morgan equations (Figure 43), but an effect on the R_1 values at higher magnetic field strengths is also visible. Therefore, even the lanthanide(III) ions with comparatively low magnetic moments (e.g. Er(III), Tb(III)) possess nuclear relaxation rates as high as those with higher effective magnetic moments (Tb(III), Dy(III) and Ho(III)).

Consequently, the consideration of the electronic relaxation times is not only important for paramagnetic probes to be used at low magnetic field strengths (e.g. contrast and shift agents for MRI), but, potentially, in probes that are designed to be used at higher magnetic field strengths (e.g. in protein tagging).[53,55,61,84]

The extensive datasets presented here enhance our capability to estimate electronic relaxation times, and also to predict nuclear relaxation times by considering the coordination environment, its symmetry and their combined impact on the local ligand field.

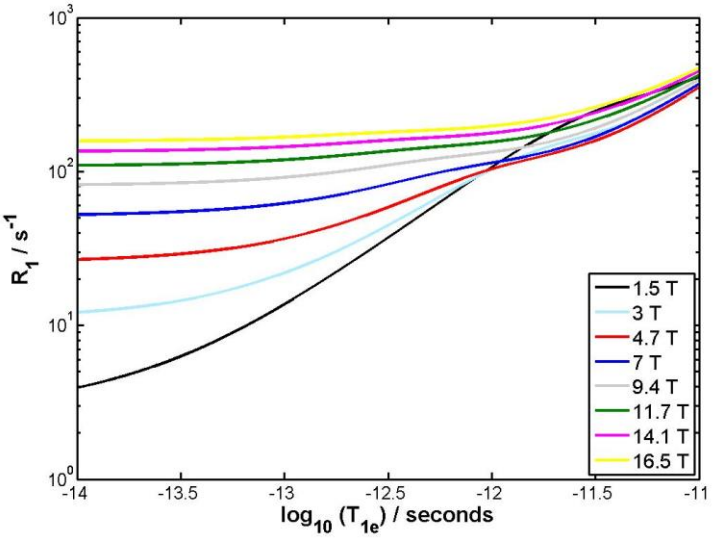

Figure 43 : *Simulation of the dependence of R_1 on T_{1e} at a variety of fields (295 K, μ_{eff} = 10 BM, r = 6.5 Å, τ_R = 250 ps).*

The selection of lanthanide(III) ions has to be considered more carefully in paramagnetic probe design. Normally, Dy(III) is considered to provide the ideal relaxation and shift properties among the non-Gd(III) based agents.[23] Depending on the coordination environment, this thinking has to be revised. By introducing a high symmetry element, e.g. [Ln.L^7] to [Ln.L^9]$^+$, the nuclear and electronic relaxation times of Tb(III) and Dy(III) were significantly increased, while the values for the other lanthanide(III) ions decreased. However, by changing the anionic donor groups from carboxylate to phosphinate based systems, the nuclear and electronic relaxation times of Er(III) were increased the most, while Tb(III) and Dy(III) relaxation times did not vary.

2.4.2 The impact of large crystal field splitting parameters on the total angular momentum, *J*

In the axially symmetric lanthanide(III) complexes, the estimated electronic relaxation times increase as a function of the second order crystal field splitting parameters. It is proposed herein that the electronic relaxation time is directly influenced by the crystal field splitting parameters. In highly symmetrical systems, the estimated values of the

electronic relaxation times of the lanthanide(III) ions follow the order: [Tb, Dy, Er] > Ho > [Tm, Yb].

However, in low symmetry systems the order is different, presumably due to the greater influence of the higher order crystal field splitting parameters. Here, electronic relaxation times and the nuclear relaxation rates of, for example, the Er(III) and Ho(III) complexes are influenced more than for the other lanthanide(III) ions. This behaviour was attributed to the crystal field splitting influencing the individual lanthanide(III) ions differently. It was not possible to quantify the influence of the higher order parameters, but the effects of different anionic donor groups was used to show how different ligand field strengths can influence the electronic relaxation times.

The crystal field in the cyclen-based complexes assessed here, measured in the form of the B_0^2 parameters, is relatively large (700 cm^{-1}). It can be assumed that for the low symmetry system, the higher order parameters contribute significantly more to the overall crystal field splitting. In addition, the B_0^2 value estimated here was calculated via the method developed originally by Binnemans[9]. However, Binnemans himself revised his method, proposing that the method underestimates the size of the parameter.[10] In the original proposal, the ΔJ=1 splitting of the Eu(III) emission spectrum was multiplied by a factor of 3.33. This calculation was later revised with a factor of 4.05, which will increase all the B_0^2 by a common factor of 1.2. Therefore, the actual size of the second order crystal field splitting parameters is not easy to estimate and, therefore, could lie in between these two factors.

Considering the low symmetry systems, where the higher order parameters can contribute significantly to the overall crystal field splitting, the size of the ligand field is of similar magnitude (500 – 1000 cm^{-1}) to the spin orbit coupling. This correspondence leads to *J*-mixing of states associated with less well defined electronic energy levels of the lanthanide(III) ions. It can be safely assumed that the zero field splitting due to the total angular momentum and the crystal field splitting parameters lead to a complicated splitting of the energy levels and that this splitting modulates the electronic relaxation times. *J*-mixing can also affect the magnetic properties of the lanthanide(III) ions in terms of the magnetic susceptibility of a given complex. This phenomenon might explain

the behaviour of the nuclear relaxation rates at the high field regime. This aspect will be further discussed in chapter 3 and 4.

3. The discrepancies in Bleaney's theory of magnetic anisotropy

Bleaney's theory of magnetic anisotropy was first postulated in 1972[2] and is still widely accepted as the most useful description of the theory of magnetic susceptibility anisotropy for lanthanide(III) complexes. Over the years, many discrepancies in the original theory have been discussed. Of these, the discussions by Binnemans et al.[10,76,77] are most pertinent and relate to the validity of the key assumptions, also to be discussed herein.

The various isostructural series of lanthanide(III) complexes studied for their relaxation behaviour in chapter 2 provide a good starting point for an experimental investigation into the theory of magnetic anisotropy and its effects on the pseudocontact shift in solution-state NMR spectroscopy.

3.1 Bleaney's theory of anisotropy

The magnetic susceptibility anisotropy arises from the crystal field splitting of the ground state *J* energy levels of the lanthanide(III) ions and the related thermal population of low lying levels. Bleaney's theory of magnetic anisotropy is based on the temperature expansion of the magnetic susceptibility. In axially symmetric systems, the magnetic susceptibility is different along the three quantization axes (x, y and z), leading to anisotropic behaviour described by equation (7):

$$\Delta\chi = -N_A \frac{\mu_B^2}{20(k_B T)^2} B_0^2 (1+p) C_J \quad (7)$$

where Δχ is the change in the magnetic susceptibilities along the directions of Cartesian coordinates (χ_x,χ_y,χ_z), N_A is the Avogadro number, μ_B is the Bohr magneton, k_B is the Boltzmann constant and B_0^2 is the second order crystal field splitting parameter. The term (1+*p*) corresponds to the thermal population of the lanthanide ion and the C_J is the Bleaney constant, which is given by equation (3):

$$C_J = g_J^2 \langle J \| \alpha \| J \rangle J(J+1)(2J-1)(2J+3) \quad (3)$$

where $\langle J \| \alpha \| J \rangle$ is a numerical coefficient, J is the spin-orbit coupling and g_J is the electron g-factor. The magnetic anisotropy was, largely, assumed to be independent of the coordination environment of the lanthanide(III) complex, which would lead to a specific order of the magnetic anisotropy, among any given series of lanthanide(III) complexes (Table 28).

Table 28 : *Overview of Bleaney constants, and the electronic properties of selected lanthanide(III) ions.*[2]

Ln^{3+}	J	$\langle J \| \alpha \| J \rangle$	C_J	C_J normalised[a]
Tb	6	0.0101	-157.5	-87
Dy	15/2	-0.0076	-181.0	-100
Ho	8	-0.0022	-71.2	-49
Er	15/2	0.0025	58.8	33
Tm	6	0.0101	95.3	53
Yb	7/2	0.0318	39.2	22

[a]The normalised values are normally quoted.

3.1.1 Assumptions in Bleaney's theory and its limitations

In his paper B. Bleaney opens his discussion with the following statement,

"We consider first the magnetic moment of a rare earth ion as arising from its ground J manifold, whose $2J+1$ levels are split by the ligand field by varying amounts which overall do not exceed kT in energy[…]"[85]

In wavenumbers, kT corresponds to a size of 205 cm^{-1} at 295 K. The aqua-complexes originally investigated by Bleaney have a smaller crystal field splitting (<100 cm^{-1}), but many lanthanide(III) complexes possess a splitting due to the crystal field of up to 1000 cm^{-1}.[12,19,49,78] Therefore this assumption is hardly valid for such lanthanide(III) complexes.

In addition, it was assumed that the main contribution to the crystal field splitting arises from the second rank parameters B_0^2 and B_2^2, in which B_2^2 is generally found to be much

smaller than B_0^2 (e.g. 110 vs 20 cm^{-1})[10,83]. However, the higher rank crystal field splitting parameters can vary significantly in size from B_0^2 and were completely neglected in Bleaney's theory of magnetic anisotropy. Depending on the symmetry of the lanthanide(III) complex, the higher order parameters (e.g. B_0^4, B_0^6) can provide a major contribution to the overall crystal field splitting. Golding et al. attempted to incorporate higher order parameters into the theory, albeit with limited success.[3]

Implicitly, Bleaney assumed a point electron at the centre of the paramagnetic lanthanide(III) ion. The electron cloud of the 4f electrons of the lanthanide(III) ions can be much better described by a spherical or elliptical model using the spherical distribution of the 4f orbitals, as simulated by Rinehart and Long when assessing the behaviour of single-molecule magnets.[86]

Some of these discrepancies in Bleaney's theory were first highlighted by Binnemans et al.[10,76,77] A theory of magnetic anisotropy should ideally be able to predict the magnetic anisotropy of lanthanide(III) complexes in isostructural series, where *kT* is greater than the crystal field splitting terms, B_0^2 and B_2^2.

3.2 Control experiments

A few control experiments were performed first to assess the extent to which variations in the pseudocontact shift conform to Bleaney's theory. By varying the temperature and measuring the pseudocontact shift, it was possible to investigate first the influence of T on the magnetic anisotropy. If additional terms with higher order parameters were present, the overall temperature dependence should change, as different power terms in temperature would be introduced.

3.2.1 Determining the temperature dependence

The temperature dependence proposed by Bleaney's theory was 1 / T^2 and can easily be investigated by variable temperature NMR spectroscopy.

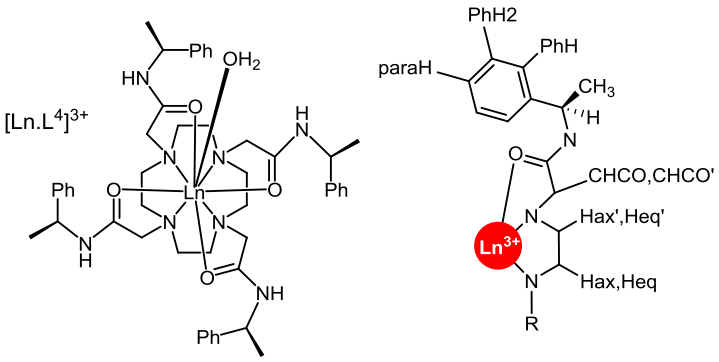

Scheme 9 *:* *Structure of [Ln.L^4]$^{3+}$ and labelling scheme of the ^{1}H resonance.*

A wide range of complexes was analysed for their temperature dependence. Almost all complexes were investigated in the range from 298 to 323 K, but only a few examples are shown (further examples are given in Appendix 3). The behaviour of [Tm.L^4]$^{3+}$ was analysed over a much wider temperature ranging from 241 to 319 K (Figure 44).

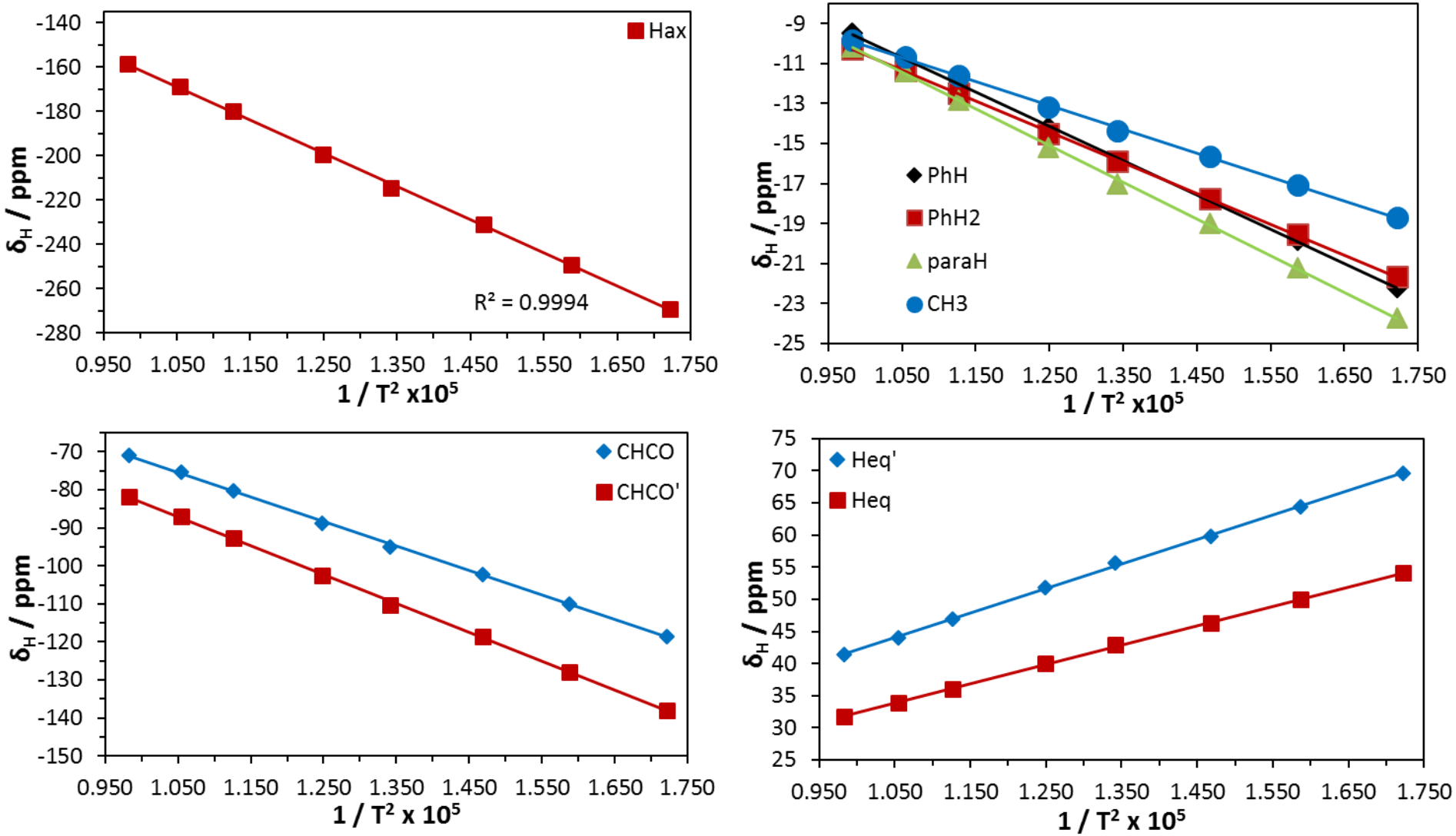

Figure 44 : *Variation of the chemical shift of various resonances of $[Tm.L^4]^{3+}$ with 1 / T^2 from 241 to 319 K, (CD_3OD, 11. 7 T). A steeper gradient indicates a bigger shift in ppm / K (H_{ax} = 1.32, PhH = 0.16, PhH2 = 0.15, paraH = 0.17, CH_3 = 0.11).*

A good correlation between chemical shift data and the inverse temperature squared was found in all cases. Depending on the polar coordinates of a resonance and, consequently, the internuclear distance to the paramagnetic centre and the angle to the principal magnetic axis of the complex, the temperature gradients of the resonances are different. A steeper gradient leads to a bigger shift per unit temperature (ppm / K).

The axial cyclen ring protons normally have the highest temperature gradient compared to the other resonances owing to their proximity to the lanthanide(III) ion and the large ($3\cos^2\theta-1$) term. A steeper temperature gradient is desirable in probes that are designed to measure temperature in vivo. Commonly, the CH_3 resonance of $[Tm.DOTMA]^-$ has been used to map temperature.[47,50] Its temperature gradient of 0.62 ppm / K is not necessarily the highest observed in the ^1H NMR spectrum of $[Tm.DOTMA]^-$, but combined with its high signal intensity over the other resonances, it constitutes a useful probe for measuring temperatures in vivo (Appendix 3, SI-Table 87).

The variation of pseudocontact shift with temperature can be complicated as multiple factors can influence the shifts. The aromatic and the methyl resonances in $[Tm.L^4]^{3+}$ are clustered in the area of (-11) to (-14) ppm at room temperature. With decreasing temperatures, however, the proton resonances show slightly different temperature gradients, which leads to the resonances being in a different order to that observed at room temperature (Figure 45).

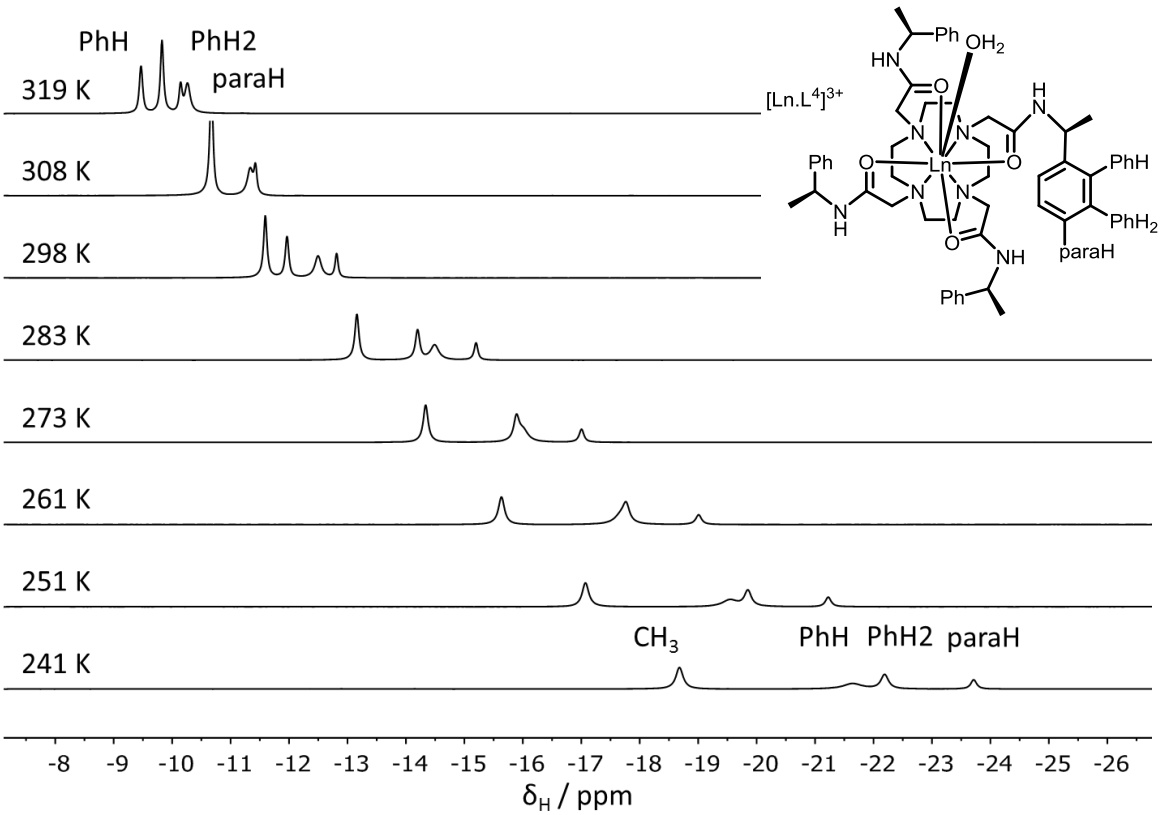

Figure 45 : *Illustration of part of the ^{1}H NMR spectrum of $[Tm.L^{4}]^{3+}$ at varying temperatures, (CD_3OD, 11.7 T). The aromatic and CH_3 resonances are shown.*

The complex $[Ln.L^{4}]^{3+}$ possesses time-averaged C_4 symmetry and has second order crystal field splitting parameter (-450 cm^{-1}) of moderate size. The temperature dependence of the phosphinate systems that were hypothesised to have a significant contribution from higher order crystal field parameters (see chapter 2) were also investigated. As an example, the behaviour of $[Dy.L^{8}]$ is presented in Figure 46.

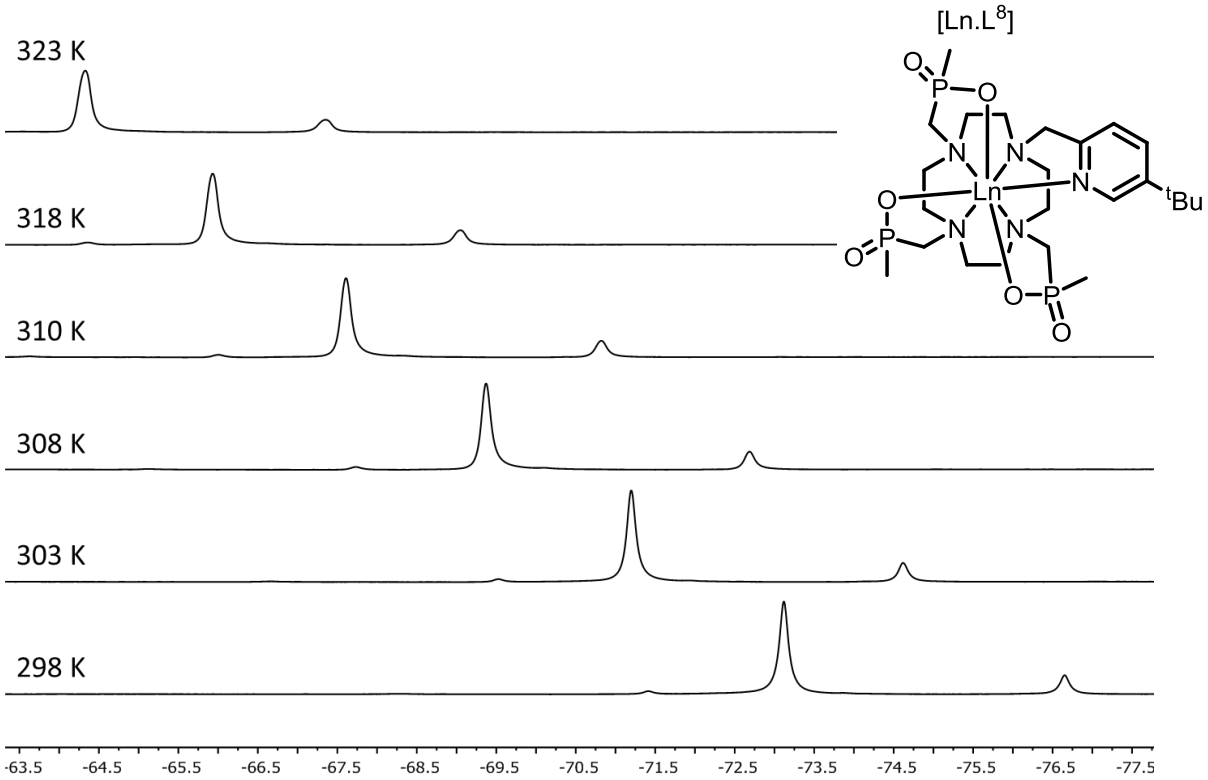

Figure 46 : *Illustration of part of the ^{1}H NMR spectrum showing the ^{t}Bu resonance of [Dy.L[8]] at varying temperatures (D_2O, 16.5 T). Major (SAP, q=0) and minor (TSAP, q=1) isomers are shown, in the ratio of 4:1 that did not change with temperature.*

The higher order parameters should, in theory, provide additional terms with a higher order T dependence, which may alter the temperature dependence from the predicted $1 / T^2$ behaviour proposed in Bleaney's theory. However, no such behaviour was found and a linear trend was still observed for the chemical shift vs $1 / T^2$. Previous literature studies also proved to be inconclusive on this issue.[3,76] In addition, McGarvey concluded for the $1 / T^2$ term to be the dominant one.[62]

3.2.2 The contact shift contribution

The observable shift consists of three different contributions. The contact shift, the diamagnetic shift and the pseudocontact shift.

$$\delta_{obsv} = \delta_{contact} + \delta_{dia} + \delta_{pseudo}$$

Resonances were measured in comparison to a diamagnetic reference complex, namely the Y(III) analogue, to allow examination of the diamagnetic contribution to the observable shift. Additionally, only resonances with an internuclear distance of greater than 4.5 Å from the paramagnetic lanthanide(III) ion were considered in order to exclude any possibility of a contact shift contribution, as it is a diminishing contribution at larger distances.[23] However, for nuclei that are directly linked to the lanthanide(III) ion via a covalent bond, the influence of the contact shift can be quite drastic. The ^{31}P resonances in [Ln.L^2] have an internuclear distance to the lanthanide(III) centre of about 3.7 Å (X-ray, 120 K)[29] and are also directly linked to the lanthanide(III) ion via the oxygen σ-bond. The variation of the observed ^{31}P NMR shift for the [Ln.L^2] series is given in Table 29.

Table 29 : *Overview of the observed chemical shifts of the ^{31}P resonance of [Ln.L^2] (CD_3OD, 11.7 T).*

Ln^{3+}	δ_P / ppm	$\Delta\delta_P$ / ppm[a]	C_J	$\langle S_z \rangle$	$C_J / \langle S_z \rangle$
Ce	27.8	4.0	-6.3	0.98	6.4
Pr	31.3	7.5	-11	2.97	3.7
Nd	21.0	-2.8	-4.2	4.49	0.9
Sm	31.4	7.6	-0.7	-0.06	11.7
Eu	16.6	-7.2	4	-10.68	0.4
Tb	-35.7	-59.5	-87	-31.82	2.7
Dy	-15.9	-39.7	-100	-28.55	3.5
Ho	-24.6	-48.4	-39	-22.63	1.7
Er	-10.5	-34.3	33	-15.37	2.1
Tm	8.4	-15.4	53	-8.21	6.4
Yb	17.7	-6.1	22	-2.54	8.5

[a]The change in the observed shift is compared to the Y(III) analogue (+23.8 ppm).

The expectation value <Sz> gives an indication of the strength of the contact shift for a lanthanide(III). In addition calculating the ratio of the Bleaney constant of the expectation values allows quantification of the effect of the pseudocontact shift over the contact shift. A small value will indicate a big influence of the contact shift , if present. Both Tm(III) and Yb(III) show big values for the ratio indicating a diminishing effect even when the contact shift is present. However, Eu(III) and Nd(III) would show a big influence. The similar ratio for Tb(III) and Dy(III) should be noted.

.

The changes in the shift do not follow the magnitude or even the sign of the Bleaney constant. The importance of analysing resonances with a sufficiently large internuclear distance and no direct coordination to the lanthanide(III) ion is emphasised.

3.3 Pseudocontact shift data

Chemical shift data for resonances that are ≥ 4.5 Å from the paramagnetic centre were analysed to avoid any contact shift contribution, using a wide variety of isostructural lanthanide(III) complexes. The isostructural series were split into groups, similar to the classification used in chapter 2. First, the three C_3-symmetric complex that possess a small crystal field splitting series were analysed ([Ln.L$^{1\text{-}3}$]). The study was then extended to other highly symmetric complex series, e.g. [Ln.L^{4}]$^{3+}$.

Due to the peculiar relaxation behaviour of the phosphinate complexes ([Ln.L^{2,5,6,8,11}]), they were analysed separately. Finally, the complexes containing the ^{t}Bu reporter group ([Ln.L$^{7\text{-}9}$]) and related derivatives will be discussed to allow further insight into perturbations created by varying ligand fields.

In theory, the magnitude of the measured second order crystal field splitting parameter, B_0^2, can give an indication as to how closely these systems may follow the pseudocontact shifts predicted by Bleaney's theory (Table 30), assuming that $B_0^2 > B_2^2$.

Table 30 : *Overview of the isostructural series [Ln.L^x] by the analysis of the estimated second order crystal field splitting parameters, $\boldsymbol{B_0^2}$ (derived from the ΔJ = 1 splitting of Eu(III) emission spectrum), 295 K.*

[Ln.L^x]	B_0^2 / cm^{-1} [a]
[Ln.L^1]	+75
[Ln.L^2]	+110
[Ln.L^3]$^{3+}$	+235
[Ln.L^4]$^{3+}$	-470
[Ln.L^5]$^-$	-700
[Ln.L^6]	-550
[Ln.L^7]	-455
[Ln.L^8]	-570
[Ln.L^9]$^+$	-355

[a]Associated error in the estimation of B_0^2 is ±40 cm^{-1}.

3.3.1 The C_3 symmetric series of complexes

The three complexes ([Ln.L$^{1\text{-}3}$]) differ in the constitution of the oxygen donor. The ligand field in these three 9N$_3$ systems is comparatively small and is less than ([Ln.L$^{1\text{-}2}$]) or of the same order as *kT* ([Ln.L^3]$^{3+}$). Due to the C$_n$ symmetry of these three systems, the second order crystal field splitting parameter, B_0^2, should characterise the overall crystal field splitting of each complex. Bearing this in mind, it was expected that the pseudocontact shifts of these three complexes would follow Bleaney's theory relatively well.

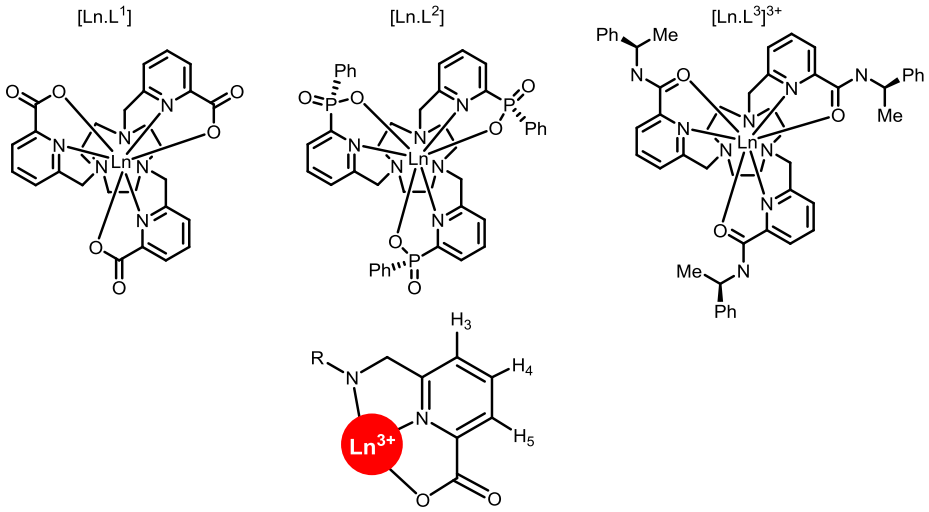

Scheme 10 : *Structures of the three C_3 symmetric, $9N_3$ based complex series [Ln.L$^{1-3}$] with assignment of the pyridyl resonances.*

The imposed distance constraint ($r \geq 4.5$ Å) and the compact nature of the $9N_3$ complexes limits the analysis of the pseudocontact shift to the common pyridyl resonance (labelled pyH^3, pyH^4 pyH^5).

Of course, a correct NMR assignment of the ligand resonances is of utmost importance in this analysis. Due to the discrepancies in the theory, it was not regarded as sufficient to assign the ligand resonances of the complexes based on trends in chemical shift data alone. However, the relaxation rates and their dependence on the internuclear distance, *r*, allow accurate mapping of the lanthanide(III) complexes. In the fitting procedure presented, the estimated internuclear distances together with the availability of the X-ray structures allow a full and self-consistent assignment of the ^{1}H NMR resonances in each complex (Table 31).

Table 31 : *Overview of the chemical shift of the pyridyl resonance (pyH^{3,4,5}) of [Ln.L$^{1-3}$] with estimated average internuclear distances through single fitting analysis (295 K, [Ln.L^1] in D_2O, [Ln.L^{2,3}] in CD_3OD) and X-ray structural analysis (120 K).*

	δ_H / ppm								
^{1}H	pyH^3			pyH^4			pyH^5		
	[Ln.L^1]	[Ln.L^2]	[Ln.L^3]$^{3+}$	[Ln.L^1]	[Ln.L^2]	[Ln.L^3]$^{3+}$	[Ln.L^1]	[Ln.L^2]	[Ln.L^3]$^{3+}$
Tb	0.1	-7.1	-11	4.9	-2.3	-3.2	4.1	-1.3	-4.4
Dy	9.4	-1.4	1.9	10.6	1.4	5.0	11.0	2.7	3.0
Ho	3.9	2.3	-5.5	6.2	4.1	-0.4	6.5	5.5	0.5
Er	8.3	13.6	8.2	7.9	11.9	7.9	6.3	12.6	8.2
Tm	14.2	18.6	23	13.5	16.4	19.6	14.2	17.8	19.2
Yb	9.5	10.7	11.6	9.1	10.3	11.2	8.8	10.7	11.4
Average r /Å[a]	5.56	5.71	5.50	6.28	6.58	6.46	5.72	5.66	5.50
X-ray r / Å[c]	5.40	5.53	5.48	6.22	6.36	6.26	5.50	5.59	5.45
B_0^2 / cm^{-1} [b]		75			110			235	

[a]Average over all 6 lanthanide(III) ions examined. [b]Respective errors of around 40 cm^{-1}. [c]X-ray data taken from [29,74,80]

According to Bleaney's theory the variation of the pseudocontact shift should be proportional to the second order crystal field splitting parameter. The illustration in Figure 47 shows the behaviour of the pyH^3 resonance of each lanthanide(III) complex of the three series with increasing B_0^2.

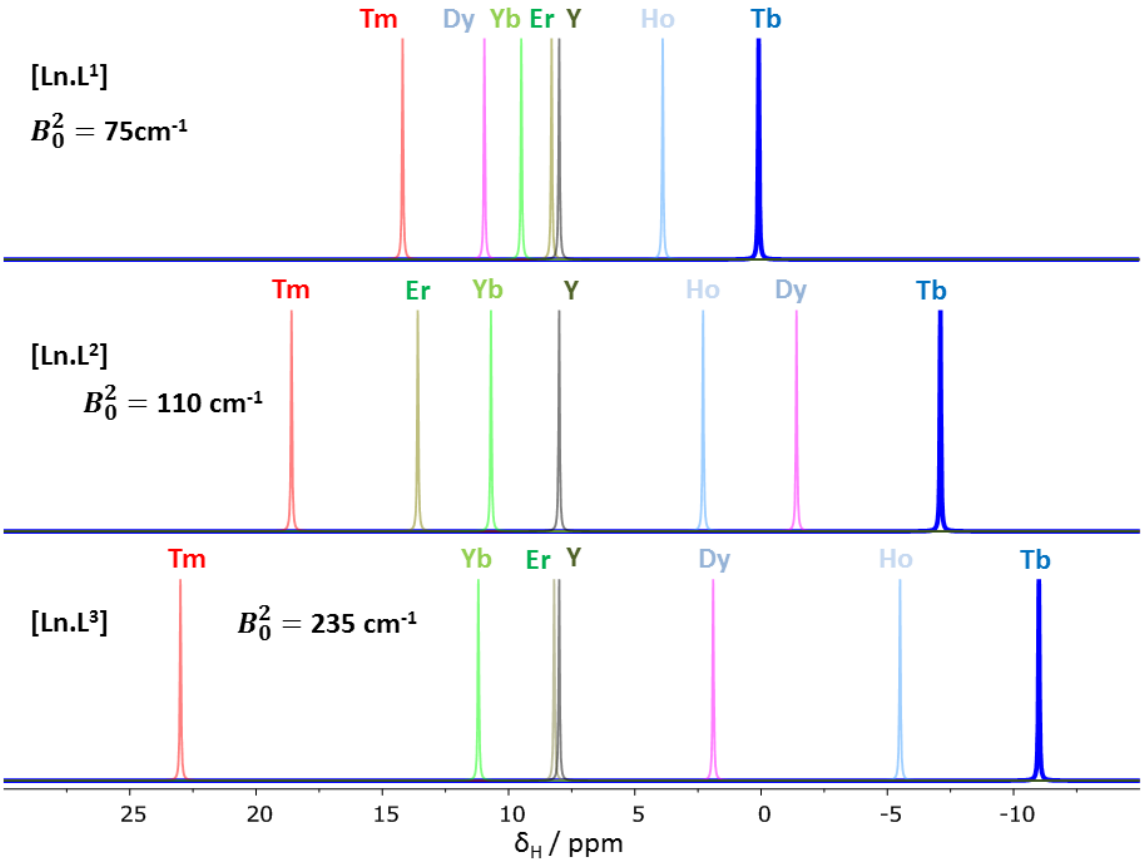

Figure 47 : *Illustration of the pyH³ resonances of the series of [Ln.L¹⁻³], taken from NMR data (295 K, 9.4 T, [Ln.L¹] in D_2O, [Ln.L²,³] in CD_3OD). Sizes of B_0^2 are highlighted. C_J values follow Tb(-89) , Dy(-100), Ho(-49), Er(+33) , Tm(+55), Yb(+22).*

A general increase of the pseudocontact shit is evident from [Ln.L¹] to $[Ln.L^3]^{3+}$ with increasing B_0^2. However, the order and strengths of the magnetic anisotropies of some lanthanide(III) ions show irregularities. In particular, Er(III) stands out due to the almost total absence of a pseudocontact shift in both [Er.L¹] and $[Er.L^3]^{3+}$. The complex [Dy.L¹] also shows unexpected behaviour due to the variable sign of the shift change. This is the only case observed where the sign of a pseudocontact shift value does not follow the trend of the sign of the Bleaney constant.

The chemical shifts of the pyH³ resonance do not follow the predicted values of the magnetic anisotropy. The expected order of Dy(III) > Tb(III) >> Ho(III) is not maintained in each series. The Tb(III) complexes always give rise to the biggest pseudocontact shift and every Dy(III) complex behaves in an anomalous way. It is surprising that even in these systems with a small ligand field, the order of magnetic anisotropy predicted by

Bleaney's theory is not followed. The shift behaviour of pyH^4 and pyH^5 in these complexes behave similarly (selected ^1H NMR and data in Appendix 3).

To investigate the extent to which the pseudocontact shifts differ from the expected strengths of the magnetic anisotropy from the Bleaney constant, C_J, the two parameters were plotted against each other. A linear relationship was added as a visual aid, which assumes ideal behaviour for the Yb(III) analogues and extrapolates the predicted shift from the Yb(III) analogues projects. The Yb(III) analogue was selected because it has the lowest magnetic susceptibility and is generally assumed to be the lanthanide(III) ion whose behaviour can be predicted most accurately in terms of shift and relaxation.[19,87,88]

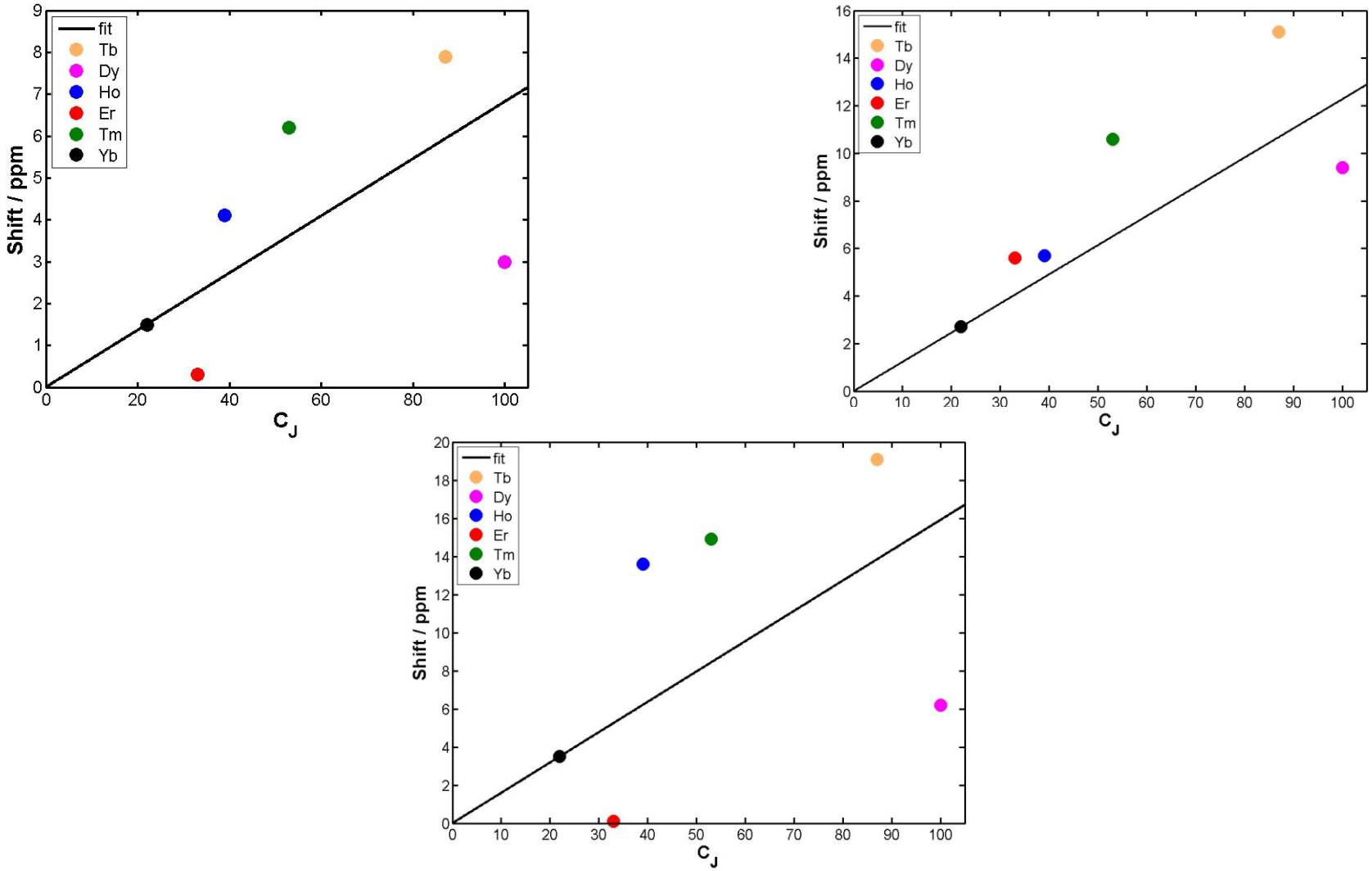

Figure 48 : *Correlation of the pseudocontact shift data of the pyH[3] resonance of [Ln.L[1,2,3]] with the Bleaney constant, C_J (295 K, 9.4 T, [Ln.L[2,3]] in CD_3OD, [Ln.L[1]] in D_2O).*

Figure 48 illustrates the behaviour of the chemical shift anisotropy of each lanthanide(III) ion in the three $9N_3$ systems. Data for the pyH^3 resonances are shown here, but similar analyses were performed for the pyH^4 and pyH^5 resonances (Appendix 3, SI-Figure 3 - 9), and gave rise to the same sort of plot.

As indicated by Figure 47, the sizes of the magnetic anisotropy hardly follow the sizes and sequence for the lanthanide(III) ions predicted by Bleaney's theory. If the theory is followed, a linear trend should be observed between the pseudocontact shift and the Bleaney constant.

Notwithstanding the sign of the Bleaney constant, the sequence for the strength of the magnetic anisotropy and therefore the pseudocontact shift should follow the order: Dy > Tb >> Tm > Ho >> Er > Yb. This sequence is not conserved at all within these three systems. In every cases, the Tb(III) systems possess the largest magnetic anisotropy, while Tm(III) and Dy(III) have a similar size of shift followed by Ho(III) and Yb(III). The behaviour of the Er(III) analogues is curious in both $[Ln.L^1]$ and $[Ln.L^3]^{3+}$, as there is little or no apparent pseudocontact shift.

The pyridine ring is directly coordinated to the lanthanide(III) ion. This could indicate a contribution of the contact shift to the overall observable shift of the pyridyl resonances. However, as it was indicated in Table 29, both Tb(III) and Dy(III) have similar ratios of C_J / <Sz>, which would indicate a similar overall shift behaviour. This is not observed in the data present here.

The discrepancies in Bleaney's theory were highlighted earlier and it was expected that in these low ligand field systems the experimental data should be relatively well behaved with respect to the theory. It was found that even in these systems the theory fails to describe the magnetic anisotropy in terms of magnitude, although, the sign of the shift is correctly predicted in all cases with the exception of $[Dy.L^1]$. However, a general increase of the overall pseudocontact shifts can be observed with increasing B_0^2. A linear variation was not observed, indicating that additional terms are required in order to describe the pseudocontact shift.

3.3.2 The C_4 symmetric complexes

The tetra-amide complex series $[Ln.L^4]^{3+}$ has multiple resonances with an internuclear distance to the paramagnetic centre of ≥ 4.5 Å, allowing consideration of the observable shift without a contact shift contribution.

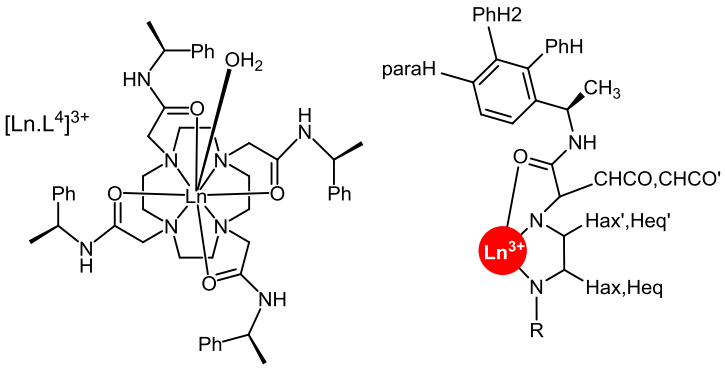

Scheme 11 : *Structure of the tetra-amide complex S-$[Ln.L^4]^{3+}$.*

Among the isostructural series studied here, the $[Ln.L^4]^{3+}$ series possess an average strength crystal field splitting (-470 cm^{-1}). Similar to $[Ln.L^{1-3}]$, it can be assumed that the higher order B_q^k parameters do not play a significant role due to high symmetry. The plots of the pseudocontact shifts of individual resonances against the Bleaney constant of the $[Ln.L^4]^{3+}$ series (Figure 49) show a reasonably good agreement with the theory.

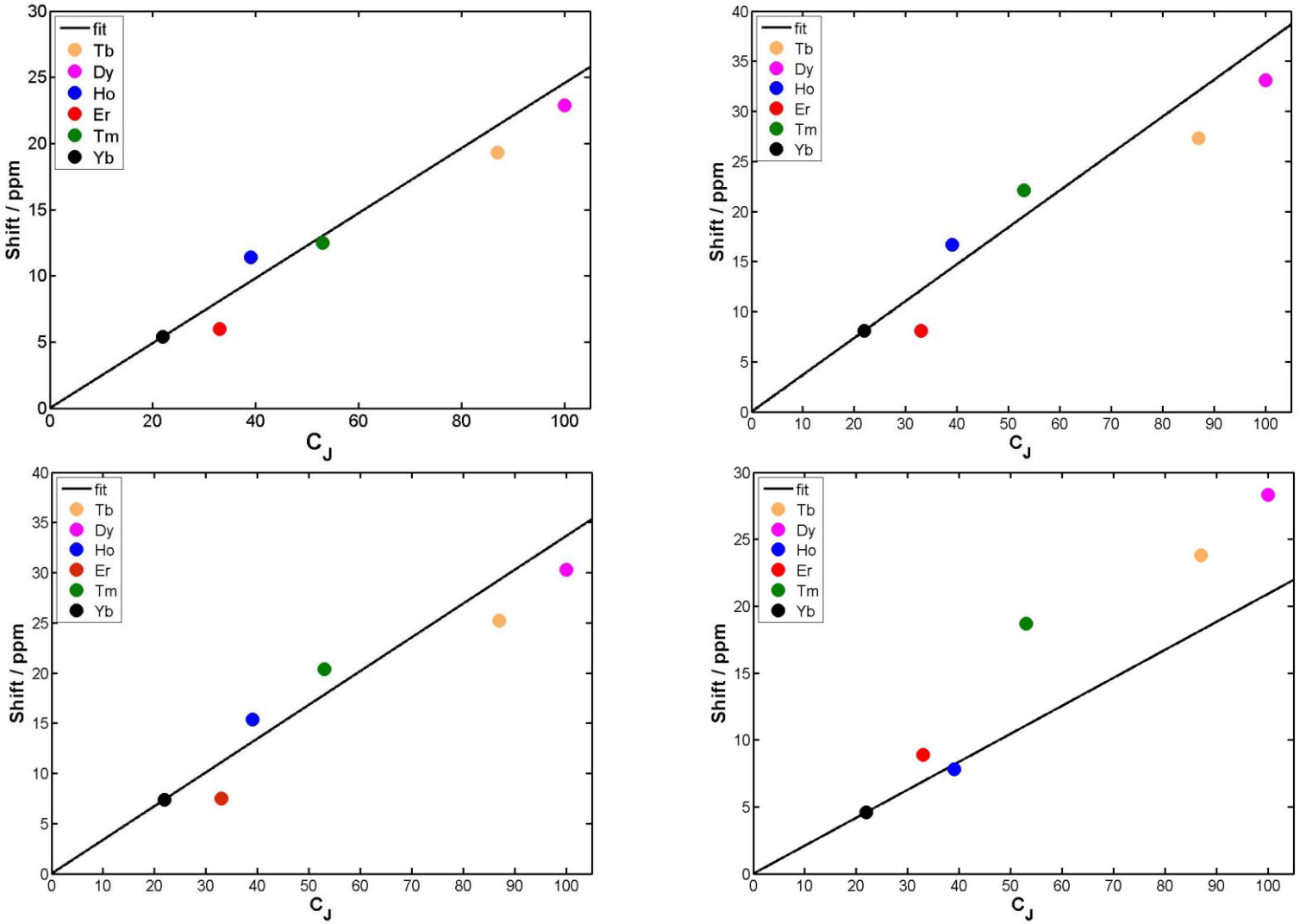

Figure 49 : *Correlation of the pseudocontact shift of the CH_3 (top left), PhH (top right), PhH2 (bottom left) and paraH (bottom right) against the Bleaney constant, C_J (295 K, 9.4 T, D_2O).*

With the exception of the phenyl ring paraH resonance, every pseudocontact shift measured follows the sequence and magnitude predicted by Bleaney's theory relatively closely. The deviation from the fitted line is relatively small compared to the $9N_3$ series of complexes. Overall, the magnetic anisotropy is described relatively well.

The estimated second order crystal field splitting parameter, B_0^2, is roughly twice the size of the value that Bleaney estimated as a maximum in his theory (470 vs 215 cm^{-1}). However, it seems the theory describes the $[Ln.L^4]^{3+}$ series much more accurately than the $9N_3$ systems $[Ln.L^{1-3}]$, notwithstanding the bigger crystal field splitting.

In the $[Ln.DOTMA]^-$ series, there are two major isomers in solution, whose relative proportion and hydration number changes as the size of the lanthanide(III) ion decreases across the lanthanide series. Thus, the Eu(III) and Tb(III) form a 9 coordinate, q = 1 complex in aqueous solution with a monocapped twisted square antiprismatic structure (TSAP) and square-antiprismatic (SAP) isomers. As the size of the lanthanide(III) ion decreases, the major (TSAP) isomer becomes 8-coordinate (q = 0). However, the minor isomer does not change hydration number across the series and was therefore analysed here.[49] The Yb(III) analogue does not form this isomer, but [Eu.DOTMA] was analysed instead.

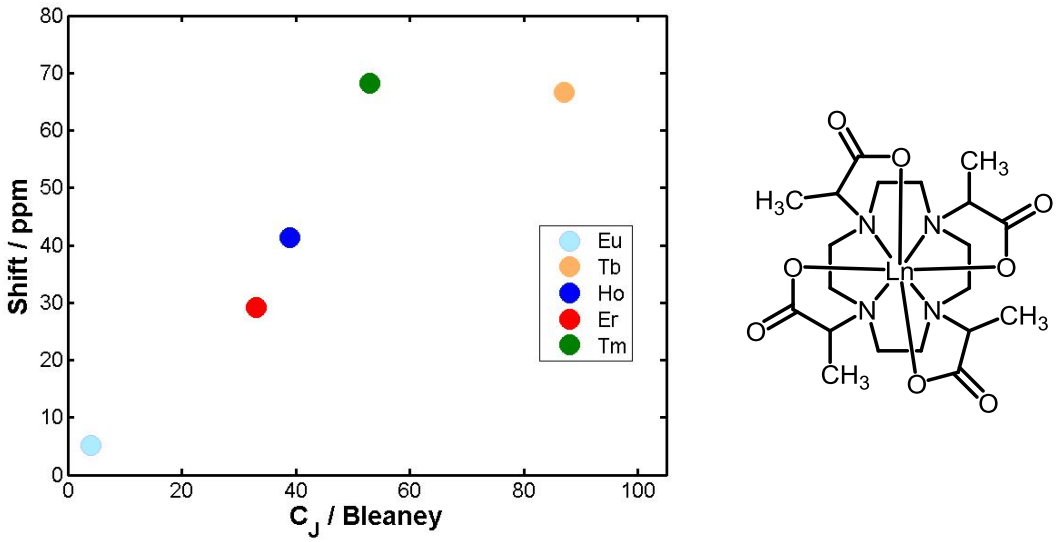

Figure 50 : *Correlation of the pseudocontact shift of the minor isomer (SAP, q=1) of the CH_3 resonance of R,S - $[Ln.DOTMA]^-$ against the Bleaney constant, C_J (295 K, 9.4 T, D_2O).*[89]

The second order crystal field splitting parameter of $[Ln.DOTMA]^-$ is one of the biggest observed (-700 cm^{-1}, major isomer). The pseudocontact shifts of $[Ln.DOTMA]^-$ do not follow the expected trend (Figure 50). A linear correlation could be made between Eu(III), Er(III) and Tb(III), but Ho(III) and especially Tm(III) show much larger pseudocontact shifts.

The Tm(III) and Yb(III) analogues also share a common major isomer (TSAP, q=0). Their respective pseudocontact shifts (102.8 and 13.5) differ by a factor of > 7 (more than 100 ppm). Such a shift variation does not correlate with their normalised C_J values of +53 and +22.

3.3.3 Phosphinate complexes

The tetra-methylphosphinate complex series $[Ln.L^5]^-$ also possess time average C_4 symmetry and normally might be analysed together with the other highly symmetrical complexes. However, as pointed out in the chapter 2, section 2.2.3.2, it is more appropriate to analyse the various phosphinate complex series as a group, as they are each octadentate (q = 0) systems, lacking the axial water found in $[Ln.L^4]^{3+}$, and in the minor isomer of $[Ln.DOTMA]^-$.

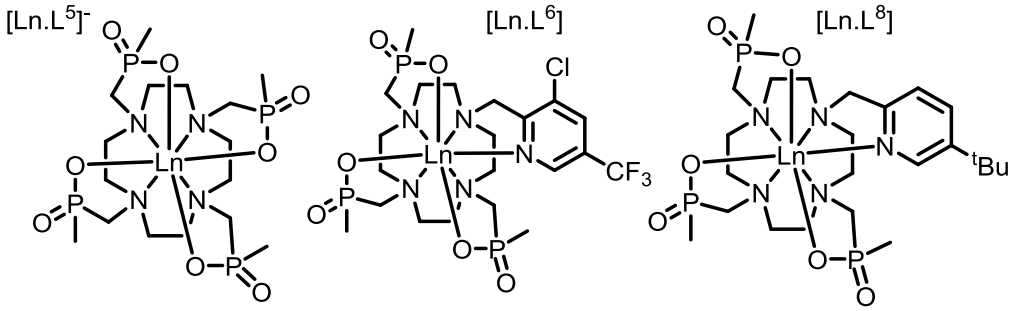

Scheme 12 : *Structures of the 8-coordinate phosphinate based complexes: [Ln.L^{5,6,8}]*

The pseudocontact shift data for these complexes is summarised in Figure 51.

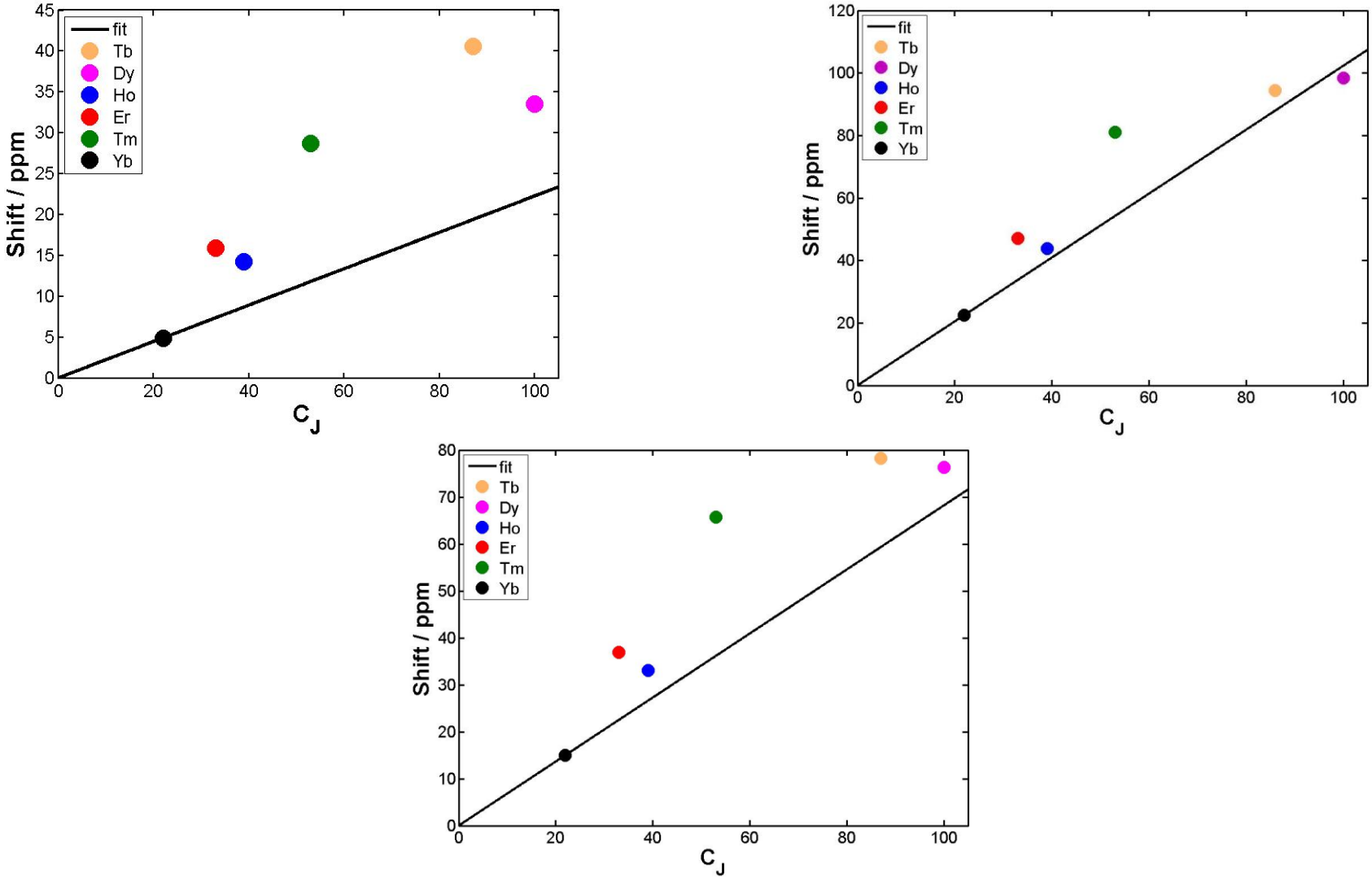

Figure 51 : *Variation of the pseudocontact shift of [Ln.L^5]$^-$ (CH_3), [Ln.L^6] (CF_3) and [Ln.L^8] of the ^{t}Bu resonances against the Bleaney constant, C_J (295 K, 9.4 T, D_2O).*

The pseudocontact shifts for these systems do not correlate well with the Bleaney constant, C_J, in each of the phosphinate complexes, including the [Ln.L^2] resonances shown earlier. In particular, the Tm(III) complexes show larger shifts than predicted. The Tb(III) and Dy(III) complexes possess similar shifts. The expected linear trend is not followed. Additionally, the Ho(III) and Er(III) analogues seem to have switched order in terms of the size of the magnetic anisotropy.

Out of all the phosphinate based systems, the [Ln.L^6] complex series follows the theory most faithfully, exemplified by looking at the P-CH_3 resonance (Figure 52), but the characteristic switch of the order for Ho(III) and Er(III) is still present.

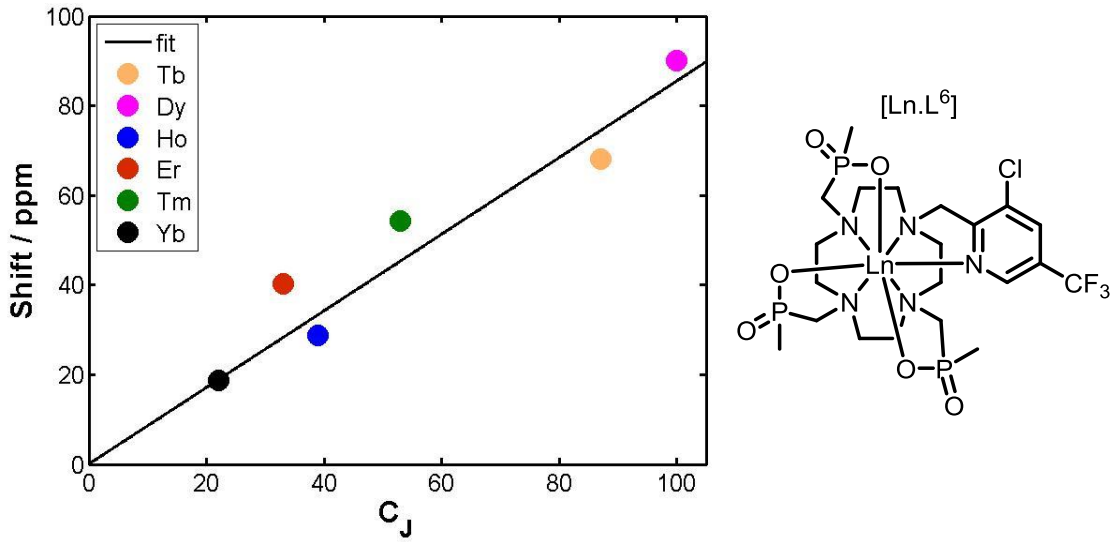

Figure 52 : *Correlation of the pseudocontact shift of the CH_3 resonance for [Ln.L^6] against the Bleaney constant, C_J (295 K, 9.4 T, D_2O).*

The ^{1}H NMR shift of the PCH_3 resonances of [Ln.L^5]$^-$ is less shifted than the mean P-CH_3 resonance shifts in the other low symmetry complexes (e.g. [Tm.L^5]$^-$ = -27.2, [Tm.L^6] = -52.8, [Ln.L^{11}] = -55.4 Appendix 3, SI-Table 78 -85). Even though the [Ln.L^5]$^-$ series possesses one of the highest crystal field splitting parameters (-700 cm^{-1}), it can be assumed that due to the low symmetry in the other complexes, their higher order crystal field splitting parameters may be larger and could contribute more to the overall crystal field splitting, leading to a bigger overall shift than for [Ln.L^5]$^-$.

Overall, these phosphinate systems, do not follow the sequence and magnitudes of the expected pseudocontact shifts according to Bleaney's theory of magnetic anisotropy. Similar observations can be made for [Ln.L[11]] (Appendix 3, SI-Figure 11 and SI-Table 85).

3.3.4 Analysis of ^{t}Bu resonances in related pyridyl complexes

The ^{t}Bu reporter group is useful for ^{1}H NMR studies, as the three methyl groups are homotopic and isochronous.[46] A wide range of derivatives of complexes was available to analyse. In each case, relaxation analysis had established that the ^{t}Bu-Ln(III) distance was 6.6 ±0.2 Å.

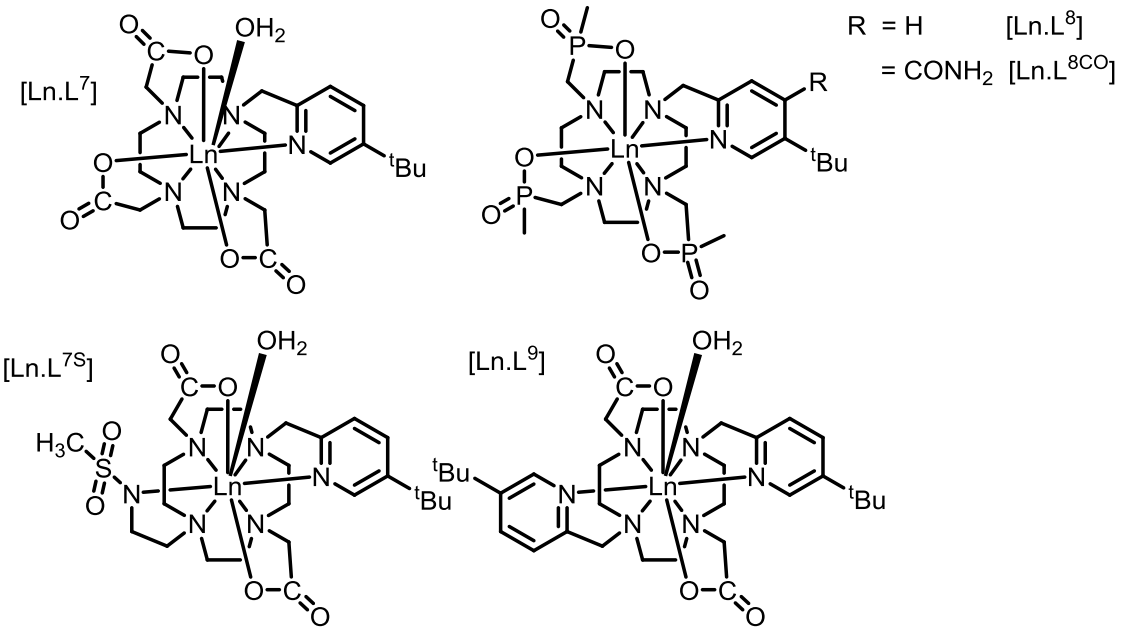

Scheme 13 : *Structures of the complexes [Ln.L[7-9]].*

The structural similarities allow a direct comparison of the shift behaviour of the ^{t}Bu resonance. The second order crystal field splitting parameters of [Ln.L[7-8]] were estimated to be in a similar range (-550 and -570 cm^{-1} respectively), while the estimated parameter for [Ln.L[9]]$^{+}$ is somewhat small (355 cm^{-1}). The splitting of the ΔJ = 1 band of [Eu.L[7S]] is the same as [Eu.L[7]]. An illustration of part of the ^{1}H NMR spectra for selected Dy(III) complexes is given in Figure 53.

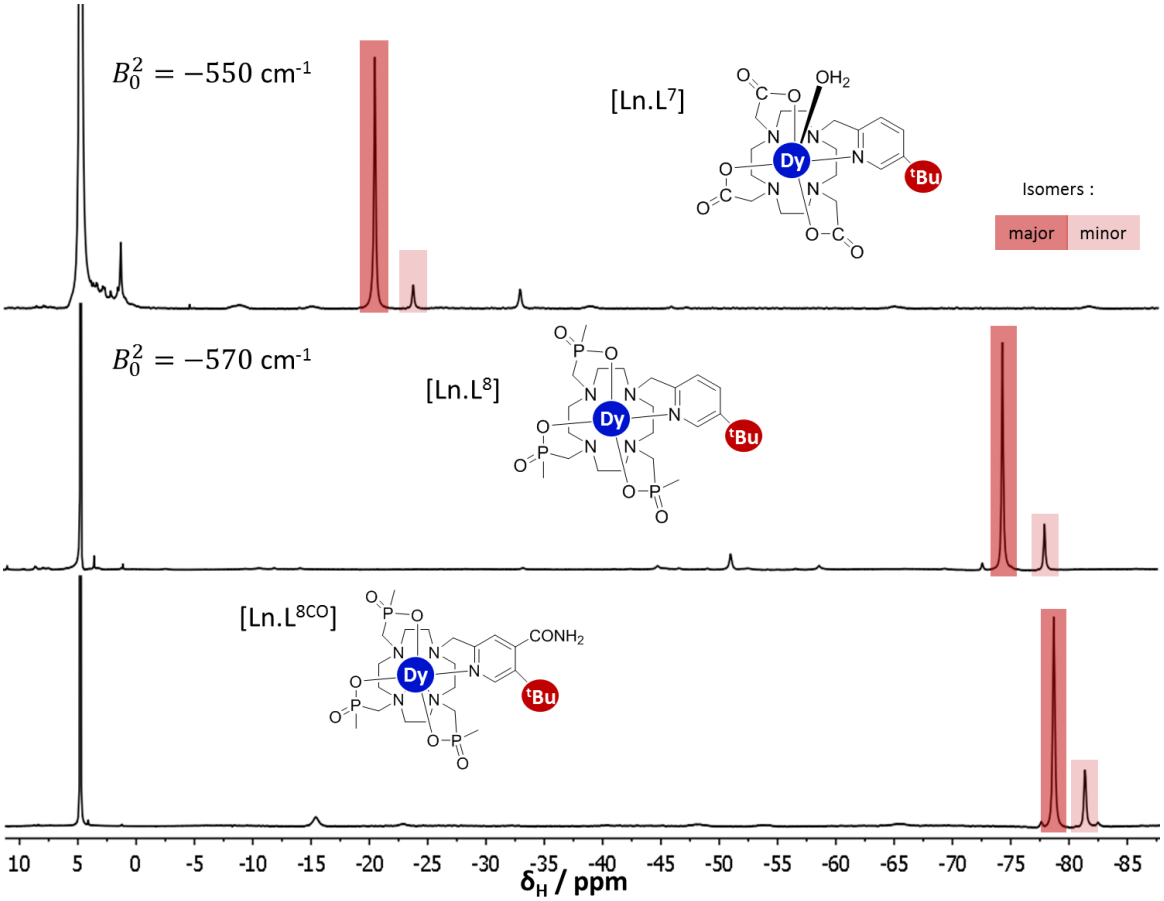

Figure 53 : *Illustration of part of the ^{1}H NMR spectrum of [Ln.L^7], [Ln.L^8] and [Ln.L^{8CO2}], (295 K 9.4 T, D$_2$O). Major (SAP) and minor isomer (TSAP) of the ^{t}Bu resonance highlighted. No values of B_0^2 was estimated for [Ln.L^{8CO2}]. The changes in hydration number should be noted.*

The behaviour of these complexes is exceptional. From [Dy.L^7] to [Dy.L^8] the ^{t}Bu shift changes by almost 60 ppm, even though the splitting of the Eu(III) emission spectrum is roughly the same. The introduction of the 4-carboamide group further enhances the shift of [Dy.L^{8CO}] compared to [Dy.L^8]. This can be attributed to the effect the different distribution of the electron density of the pyridine ring has on the ligand field. The py-Dy(III) interaction is perturbed by the ligand field and changes the observable shift slightly. The large changes in the observable shift of carboxylates and phosphinates are too extreme to be able to correlate them with the changes in the splitting due to B_0^2, derived from the Eu(III) optical spectral analysis.

A full overview of the shift data of the complexes containing the ^{t}Bu reporter group is given in Table 32. The much bigger shift of the 8-coordinate phosphinate complexes can be observed across the whole series.

Table 32 : *Chemical shift data of the ^{t}Bu resonance of [Ln.L^{7,7S,8,9}] and the Bleaney constant, C_J, for comparison (295 K, 9.4 T, D_2O).*

Ln^{3+}	δ_H / ppm[a]				C_J
	[Ln.L^7]	[Ln.L^{7S}][b]	[Ln.L^8]	[Ln.L^9]$^+$	
Tb	-11.6	-55.8	-76.9	-7.2	-89
Dy	-20.5	-58.9	-75.0	-17.8	-100
Ho	-7.4	-26.3	-31.8	-7.0	-49
Er	7.0	x	38.2	3.4	33
Tm	10.8	44.3	67.0	6.2	55
Yb	6.3	x	16.3	9.1	22
ppm / K	0.1	0.3	0.4	0.1	
B_0^2 / cm^{-1}	-550	-550	-570	-350	

[a]Major isomer shown here, minor isomer data available in Appendix 3, SI-Table 82 [b]Measured at pD = 8.

The measured temperature gradient follows the strength of the pseudocontact shift; a larger gradient was observed for the more shifted resonances.

Comparing [Ln.L^7] and [Ln.L^{7S}], the shifts are quite different, even though they possess the same splitting of $\Delta J = 1$ band in the Eu(III) emission spectrum. The pseudocontact shifts for the ^{t}Bu resonance in [Ln.L^9]$^+$ are relatively small, when compared to [Ln.L^7]. Such behaviour is most likely linked to the ligand field changes, as a neutral pyridyl donor replaces a carboxylate oxygen and the B_0^2 values of -550 and -350 cm^{-1} are consistent with this interpretation. The Er(III) analogue is hardly shifted, similar to observation made in [Er.L^{1,3}]. In this complex, the Yb(III) analogue also shows surprising behaviour. Its observed shift is not only larger than the Er(III) and Tm(III) analogues of [Ln.L^9]$^+$, but also [Yb.L^7]. Overall the shift behaviour of [Yb.L^9]$^+$ is highly irregular, and represents the only case where an Yb(III) complex behaves in such a way.

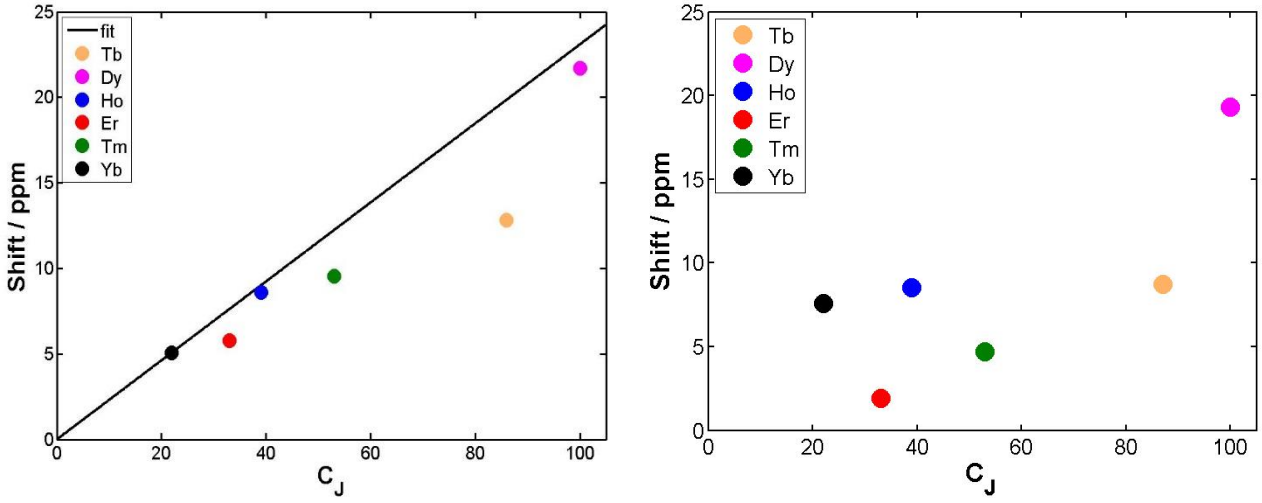

Figure 54 : *Correlation of the pseudocontact shift of the ^{t}Bu resonance for [Ln.L^{7}] (left) and [Ln.L^{9}]$^{+}$ (right) against the Bleaney constant, C_J (295 K, 9.4 T, D_2O).*

In these series, the observed shift of [Ln.L^{7}] follows the trend in C_J values most faithfully, with only a slight underestimation of the shift for the Tb(III), Er(III) and Tm(III) analogues (Figure 54). However, the other complexes show significant deviation from the magnitudes expected on the bias of the Bleaney constant. Due to the irregular behaviour of [Yb.L^{9}]$^{+}$, it was not feasible to use it a reference point for the fitting of the pseudocontact shifts.

3.3.5 Analysis of the CF_3 reporter group

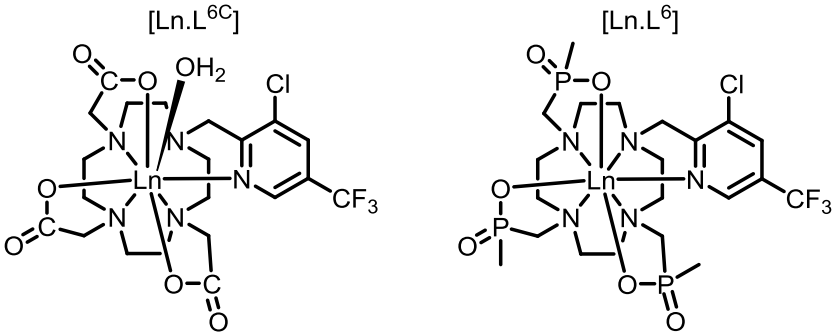

Scheme 14 : *Structures of the carboxylate and phosphinate analogues of [Ln.L^{6}].*

The ^{19}F shift behaviour of the CF_3 resonance in [Ln.L^6] was compared to the carboxylate analogue of the complex ([Ln.L^{6C}]). The large shift differences observed between [Ln.L^7] and [Ln.L^8] were also observed in [Ln.L^6] (δ_F = -162.4 ppm) and [Ln.L^{6C}] (δ_F = -115.1 ppm).

The very large shift difference between analogous carboxylate and phosphinate complexes is evident and cannot be rationalised easily. It can be postulated that differences in oxygen polarizability and the change in coordination number, have a major effect on the overall crystal field splitting. Yet, a more fundamental reconsideration may be required to rationalise the dramatic differences in shift behaviour.

3.5 Summary & Conclusions

There are a number of assumptions in Bleaney's theory of magnetic anisotropy that could easily be held responsible for the significant differences between the experimental and theoretical NMR shift data shown here. The main assumptions involve the crystal field splitting parameters and their influence on the *J* energy levels. The original underestimation of the second order crystal field splitting parameters (B_0^2 << 205 cm^{-1}) and the exclusion of the higher order parameters (e.g. B_0^4, B_0^6) could be one of the causes for the big deviations observed.

The overall correlation between the shift range and the B_0^2 in the axially symmetric systems is given below (Figure 55). But, even here, the linear dependence, as suggested by Bleaney, is not limited ($R^2 \approx 0.85$). Both Tm(III) and Yb(III) analogues behave similarly.

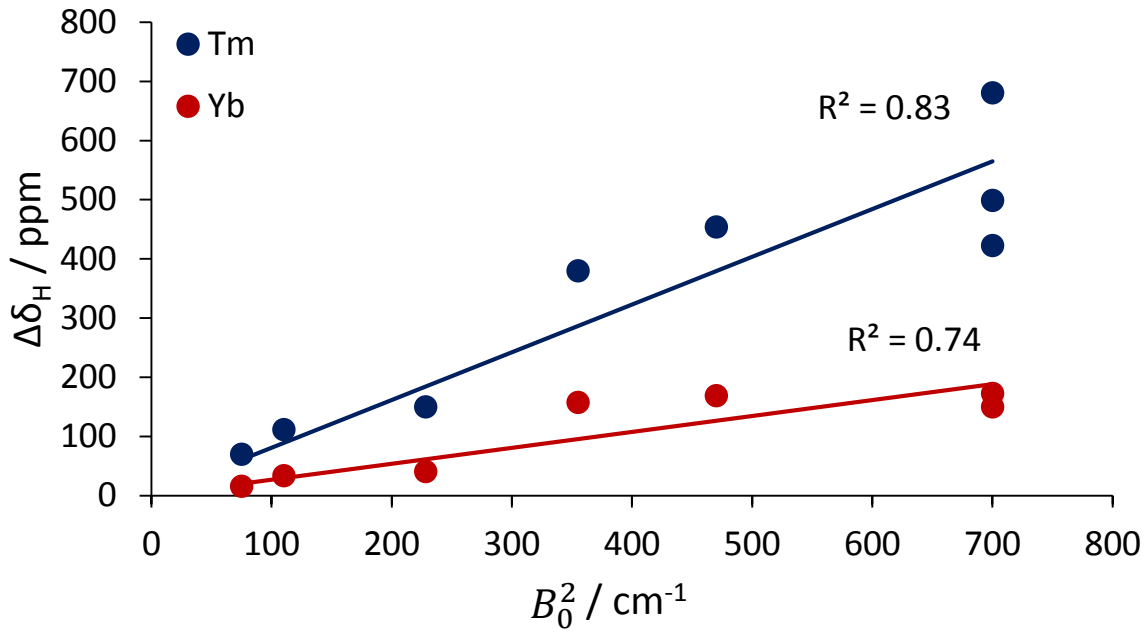

Figure 55 : *Correlation of the total ^{1}H NMR shift range of the Tm(III) and Yb(III) analogues of the axially symmetric systems [Ln.L$^{1\text{-}5,9}$], [Ln.DOTMA]$^-$ and [Ln.gDOTA]$^{5-}$ (295 K, 9.4 T, [Ln.L^{2,3}] in CD_3OD]) with the second order crystal field splitting parameter, B_0^2, measured for the Eu(III) analogue.*

For those complexes possessing a B_0^2 value of 700 cm^{-1} ([Ln.L^5]$^-$, [Ln.DOTMA] and [Ln.gDOTA]$^{5-}$) differences in the spectral behaviour are possibly due to the influence of the higher order parameters. These parameters should not be neglected in any theory that describes the pseudocontact shift. Such a contribution was also suggested earlier by Golding[3].

Binnemans[76,77] also suggested that the local magnetic anisotropy is modulated by the shape and degree of distortion of the coordination polyhedron in a series of lanthanide(III) complexes. An analysis of the twist angle of the mean plane of the $9N_3$ ring with reference to the three oxygen donor atoms in the X-ray structures of the C_3 symmetric complexes ([Ln.L$^{1\text{-}3}$]) was undertaken. There was no correlation between the twist angles (22 ± 2° in all each system) and the measured magnetic anisotropy (Figure 56), showing that polyhedral distortion does not explain the observed shift variation.[74]

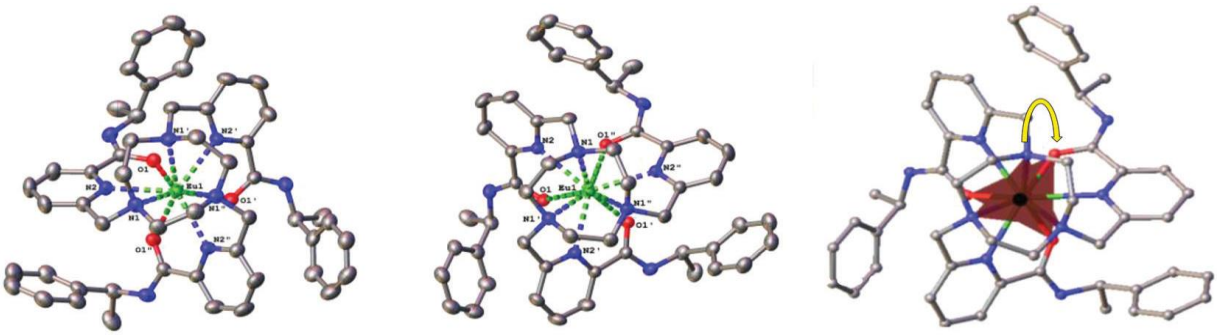

Figure 56: *Views of the X-ray structures of the two diasteroisomers of [Eu.L^3]$^{3+}$: S-Δ-(λλλ) (left) and R-Λ-(δδδ) right (120 K). highlighted the measured twist angles of the O and N planes. No difference in twist angles between Eu(III) and Yb(III) structures was observed. Taken from [74].*

The final assumption made by Bleaney concerns the electron distribution. The point-dipole approximation does not represent the overall electron cloud very well, in particular in these anisotropic lanthanide(III) complexes. Rinehart and Long[86] simulated the quadrupole moment of the 4f electron cloud using the angular dependence of the 4f orbitals whilst investigating the single molecule magnet behaviour of lanthanide(III) ions (Figure 57).

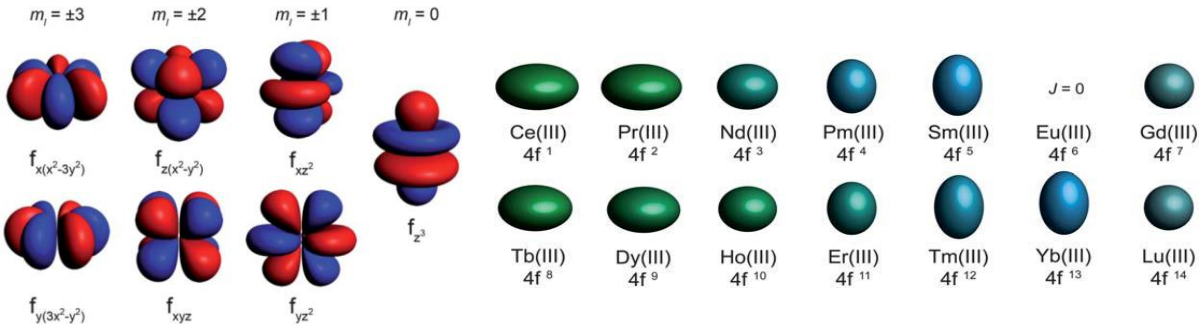

Figure 57 : *Simulations of the shape of the 4f orbitals (left) and quadrupole approximations of the 4f electron cloud for lanthanide(III) ions (right), based on the total angular momentum, J, the Stevens coefficient and the 4f orbital radius. Taken from [86].*

The electron density varies from oblate (in Tb(III), Dy(III), and Ho(III) ions) to prolate (Er(III), Tm(III) and Yb(III)) explaining the signs of the magnetic anisotropy, as predicted by Bleaney. The Er(III) case stands out as rather curious as it almost possesses an isotropic electron distribution, which could explain the lack of pseudocontact shift in many of the Er(III) analogues analysed here.

Sessoli et al.[90] have recently measured and calculated the position of the easy (principal) axis of magnetisation in the C_4 symmetric $[Ln.DOTA]^-$ series. The easy axis of magnetisation is the energetically favoured direction of the spontaneous magnetisations and is considered to be parallel to the direction of the C_4- symmetry axis (along axially bound water) in Bleaney's theory. Their calculations showed that the easy axis of magnetisation changes steadily from the equatorial plane (90° to axial donor, H_2O) to the axial plane (along axial donor group) from Tb(III) to Yb(III) (Figure 58). Such behaviour would indicate that the cone of highest anisotropy is not always along the direction of the axial donor molecule, but will change across the series, according to the electron density of the ligand. However, an irregularity was found for Er(III), as their experimental data deviated significantly from the simulation.

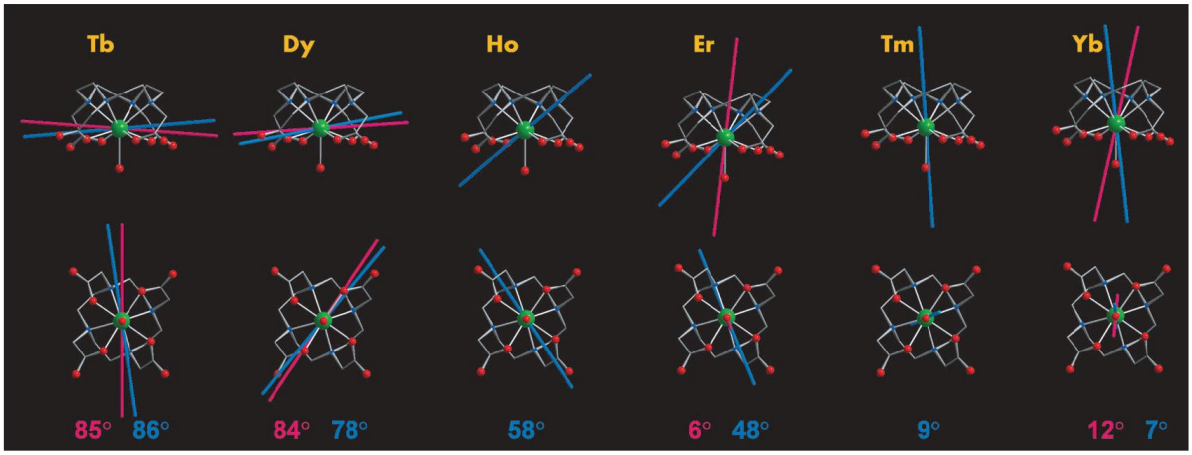

Figure 58 : *Experimental (angle-resolved magnetometry,pink) and calculated (quantum chemistry simulation, blue) easy axis of magnetisation across the series of $[Ln.DOTA]^-$ viewed perpendicular (top) and parallel (bottom) to the four-fold symmetry axis (2 K). Taken from [90].*

Due to the changes in the position of the axis of magnetisation the magnetic anisotropy might be much more complex than anticipated by Bleaney, as the angular reference point in the $(3\cos^2\theta-1)$ term changes from one lanthanide(III) ion to another (Figure 58).[90,91]

Most of the investigations concerning these phenomena originate from studies optimising the single-molecule magnet behaviour of the lanthanide(III) ions, which favours a small energy gap between the electronic energy levels. Sessoli and Long both

concluded that a minimum energy gap (for optimum SMM behaviour) is achieved for oblate ions when the ligand electron density is focused equatorially, while for prolate ions, axial ligand electron density is favoured. This effect could be rationalised to determine the differences in the crystal field splitting across a series of lanthanide(III) ions, as the paramagnetic electron clouds all interact differently with the ligand electron density.[91]

Following this consideration, a maximum energy gap between the *J*-sub levels is observed in systems with high crystal field splitting ([Ln.L$^{4\text{-}11}$)]. Therefore prolate ions (Er, Tm, Yb) may be expected to have the highest magnetic anisotropy in ligand systems possessing equatorial electron density.[86] This is the case for complex systems that have a hydration value of 0, as there is no contribution from the axial donor group. It is, indeed, these q = 0 systems, for which the biggest deviations are found with prolate ions. For example, with Tm(III) systems, where very high pseudocontact shifts were observed in the phosphinate based complexes and also in q = 0 isomer of [Tm.DOTMA]$^{-}$. It is suggested that the magnetic anisotropy in the prolate ions (Er, Tm, Yb) is much more dependent on the ligand field in these cases, compared to their oblate counterparts (Tb, Dy, Ho).

In combination with the change in the easy axis of magnetisation across the lanthanide(III) series, this effect could help to rationalise the pseudocontact shift behaviour of lanthanide(III) complexes.

On a final note, the size of the crystal field splitting parameters can be of similar magnitude to the spin-orbit coupling term, which will lead to an effect called *J*-mixing.[77,92] The uncertainty about the splitting of the energy levels is increased and *J* cannot be assumed to be a "good" quantum number anymore. The magnitude of the Bleaney constant, C_J, is directly connected to these *J* terms and energy levels. If the values differ from the theory, the actual Bleaney constant will deviate significantly. Such behaviour could, at least in part, explain the behaviour of the low symmetry complexes that possess an overall crystal field energy (-700 cm^{-1} in B_0^2, higher in B_0^4 and B_0^6) of similar size to the spin orbit coupling (1000 – 2000 cm^{-1} from Eu(III) to Yb(III)).

In conclusion, it seems that Bleaney theory has outlived its usefulness and the limitations highlighted in this work suggest that a better theory of magnetic anisotropy is required that is more firmly based on the effect of the local ligand, the symmetry and the relative position of the easy axis of magnetisation.

4. The effect of *J*-mixing on the magnetic susceptibility

In lanthanide electronic structure theory, the contribution of the spin-orbit coupling to the splitting of the electronic energy levels has generally been assumed to be much larger than splitting due to the ligand field. The ligand field and its associated crystal field splitting has been assumed to be an order of magnitude smaller than the spin-orbit coupling term and is largely neglected when considering the overall splitting of the electronic energy levels of the lanthanide(III) ions (Figure 2).[2,10]

It was made apparent in the previous chapters that the crystal field spitting parameters can vary significantly for each complex series. Several second order crystal field splitting parameters, B_0^2, have been estimated by analysis of the splitting of the Δ*J* = 1 band in the Eu(III) emission spectrum using the method postulated by Binnemans et al[9]. These values range from 75 – 700 cm^{-1}, but larger values (up to 1000 cm^{-1}) have been reported in the literature.[10] The size of the crystal field splitting changes across a series of lanthanide(III) ions due to their different electron clouds and their differing interactions with the ligand field.[10,86] Only the second-order parameter, B_0^2, is readily obtained by direct analysis of the Eu(III) emission spectrum. However, depending on the symmetry of the complex, more parameters will contribute to the overall crystal field splitting. In particular, for the low symmetry systems, it is presumed that the higher order parameters have a much more significant contribution.[10]

The B_0^2 terms estimated in this thesis were determined using the method developed originally by Binnemans[9]. However, Binnemans has revised his analysis, stating that the method underestimates the size of the parameter.[10] In the original proposal, the splitting of the two transitions in the Δ*J* = 1 manifold in the Eu(III) emission spectrum was multiplied by a factor of 3.33. This was later revised with a factor of 4.05, which will increase all the B_0^2 terms by a common factor of 1.2. Therefore, the actual size of the second order crystal field splitting parameters might be systematically underestimated in all of the estimations given here and could lie in between the two values. A good agreement was found in the solid-state between B_0^2 values derived by iterative spectral analysis and the separation of the main two bands in the Δ*J* = 1 region (585 – 605 nm) (Figure 59).

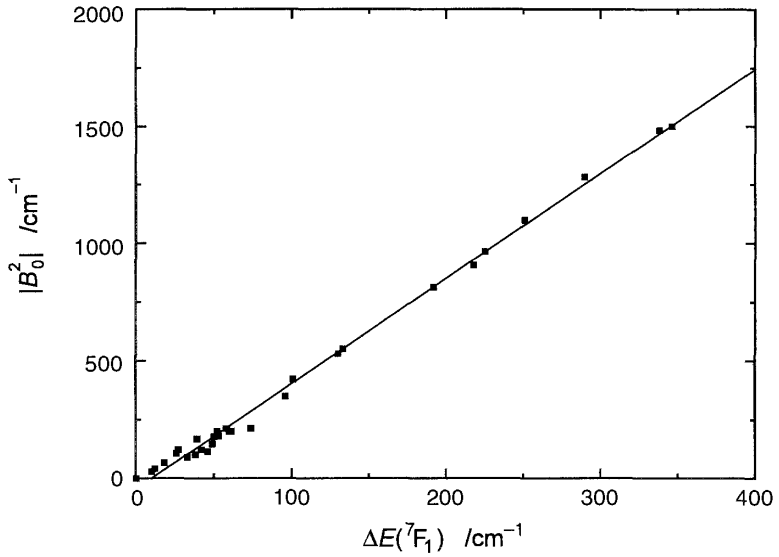

Figure 59 : *Correlation of the splitting of the ΔJ =1 band of the Eu(III) emission spectrum of different lanthanide(III) compounds and complexes in the solid-state with the second order crystal field splitting parameter B_0^2. It was proposed that the splitting corresponds to 4.05 times B_0^2.Taken from [10].*

4.1 The occurrence of *J*-mixing

In the most frequently used theories of lanthanide magnetism, it is assumed that the magnetic susceptibility is independent of the coordination environment of the lanthanide(III) complexes. Such an assumption requires that the size of the crystal field splitting is almost an order of magnitude smaller than the spin orbit coupling.[10,93]

In the systems investigated here, the estimated values of B_0^2 alone are, in some cases, almost of the same order of magnitude as the spin-orbit coupling. A large crystal field splitting results in more overlap between the energy levels split by the total angular momentum, *J*, leading to less defined energy levels for the lanthanide(III) ions. This concept has been reported before.[92] Generally, it is assumed that complexes of low symmetry are more prone to *J*-mixing.[10,92] Experimentally, this effect can lead to changes in the relative intensities of the various Δ*J* = n bands (n = 0 – 4) in , for example, the Eu(III) emission spectrum.[94–96]

For the case of *J*-mixing, the total spin orbit coupling, *J*, is not considered to be a 'good' quantum number anymore. A variety of properties are directly linked to the electronic

energy levels of the lanthanide(III) ions and their respective *J* values. In both chapters 2 and 3 of this thesis, the effect of the crystal field splitting on paramagnetic relaxation and the magnetic susceptibility anisotropy was highlighted.

The magnetic susceptibility anisotropy showed great variation with the crystal field splitting and it can be postulated that the overall magnetic susceptibility could also be affected due to its dependence on *J*. In classical lanthanide magnetism theory, as originally proposed by Landé[97], the effective magnetic moment, μ_{eff} is defined as:

$$\mu_{eff} = g_J \sqrt{J(J+1)} \qquad (8)$$

$$g_J = \frac{J(J+1) + S(S+1) - L(L+1)}{2J(J+1)} \qquad (9)$$

where g_J is the Landé factor (defined in equation 9), *S* is spin-spin coupling, *L* is the orbit-orbit coupling, and *J* is the total angular momentum or spin-orbit coupling. According to these theories the values of the magnetic susceptibility will change on consideration of *J*-mixing and may be expected to deviate from the 'free-ion' values.[92,93,97]

4.2 Ways of estimating the effective magnetic moments of lanthanide(III) ions

Three different methods were used to investigate the influence of the coordination environment on the magnetic susceptibility: firstly, fitting of nuclear relaxation data (section 4.2.1); secondly, NMR investigations using the bulk magnetic susceptibility shift (section 4.2.2), lastly measurements in the solid-state using a SQUID magnetometer (section 4.2.3). The fitted data of the nuclear relaxation rates provides the biggest data set available, while the other two methods were employed for only a few selected complexes.

4.2.1 Fitting of nuclear relaxation data

Measuring the nuclear relaxation rates, R_1, at different magnetic field strengths allows the estimation of the effective magnetic moments of the lanthanide(III) ions, amongst other parameters, through the fitting of the data to equation 4. The method was explained in detail in chapter 2.

$$R_1 = \frac{2}{15}\left(\frac{\mu_0}{4\pi}\right)^2 \frac{\gamma_N^2 g_{Ln}^2 \mu_B^2 J(J+1)}{r^6}\left[3\frac{T_{1e}}{1+\omega_N^2 T_{1e}^2} + 7\frac{T_{2e}}{1+\omega_e^2 T_{2e}^2}\right] + \frac{2}{5}\left(\frac{\mu_0}{4\pi}\right)^2 \frac{\omega_N^2 \mu_{eff}^4}{(3k_B T)^2 r^6}\left[3\frac{\tau_r}{1+\omega_N^2 \tau_r^2}\right] \quad (4)$$

A fixed internuclear distance, *r*, was used to calculate the effective magnetic moments either in a global way or using single resonance fitting of individual complexes in a few selected cases (e.g. $[Ln.DOTMA]^-$, $[Ln.gDOTA]^{5-}$). It was shown that the estimated internuclear distances are in good agreement with values derived from solid state X-ray structures determinations (chapter 2, section 2.1).

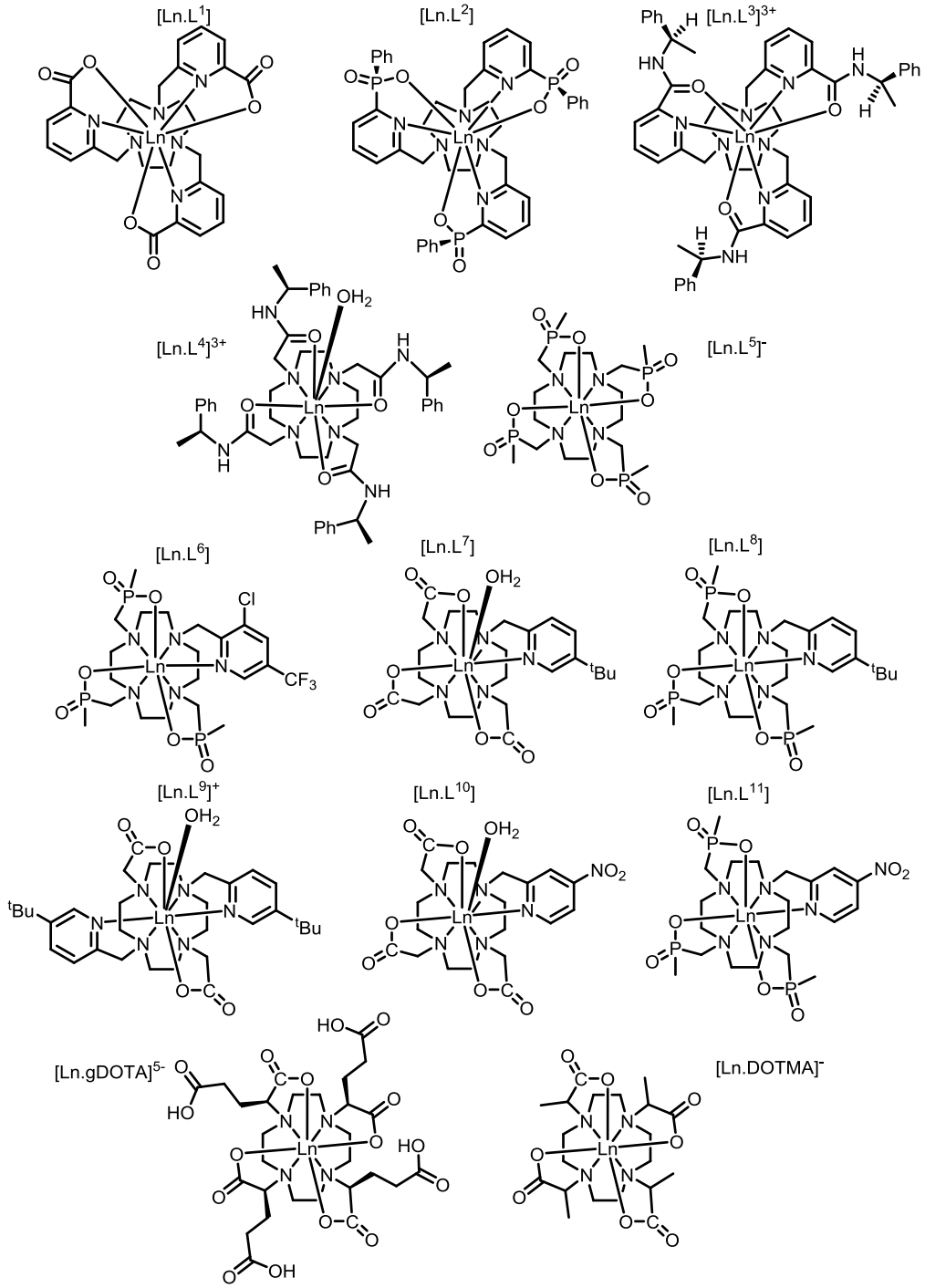

Scheme 15 : *Overview of the structures of [Ln.L$^{1\text{-}11}$], [Ln.DOTMA]$^{-}$ and [Ln.gDOTA]$^{5-}$.*

In addition to the eleven isostructural series of lanthanide(III) complexes studied before, [Tm.DOTMA]$^{-}$ and certain complexes of [Ln.gDOTA]$^{5-}$ were also analysed (Scheme 15). Only a few examples of the latter case could be analysed due to the change in hydration number across the lanthanide(III) series.[19]

4.2.1.1 Estimated values of μ_{eff} though relaxation rate fitting

The eleven isostructural series of lanthanide((III) complexes provide a wide range of different crystal field splittings. An overview of the estimated effective magnetic moments using this method is presented in Table 33. In the procedure, the internuclear distance, *r* , is fixed while the remaining parameters are minimised. However, only the estimated values of μ_{eff} are discussed here, the integrity of the other parameters was discussed in chapter 2, section 2.2.

Table 33 : *Overview of the estimated effective magnetic moments of the lanthanide(III) series [Ln.L[1-11]] using a fixed internuclear distance, r. (295 K, all in D_2O, except [Ln.L[2,3]] in CD_3OD).[b]*

	μ_{eff} / BM[c]												
Ln^{3+}	[Ln.L[1]]	[Ln.L[2]]	[Ln.L[3]]$^{3+}$	[Ln.L[4]]$^{3+a}$	[Ln.L[5]]$^{-}$	[Ln.L[6]]	[Ln.L[7]]	[Ln.L[8]]	[Ln.L[9]]$^{+}$	[Ln.L[10]]	[Ln.L[11]]	[Ln.gDOTA][a]	Lit[11]
Tb	9.65±0.02	9.40±0.03	9.59±0.03	9.23±0.01	9.64±0.01	8.79±0.04	9.87±0.03	8.74±0.06	10.23±0.03	9.55±0.02	9.63±0.01	9.17±0.12	9.8
Dy	10.47±0.01	10.21±0.03	10.09±0.03	10.30±0.01	10.56±0.01	9.44±0.03	10.44±0.03	9.44±0.05	10.78±0.03	10.01±0.01	9.80±0.01	x	10.3
Ho	10.40±0.01	10.22±0.01	10.31±0.02	9.91 ±0.01	10.29±0.01	9.32±0.03	10.02±0.02	9.73±0.04	9.97±0.03	9.99±0.01	10.67±0.01	x	10.4
Er	9.23±0.02	9.05±0.02	8.80±0.03	8.82±0.50	9.48±0.01	9.17±0.02	9.18±0.02	9.62±0.04	8.33±0.03	9.32±0.01	9.45±0.01	9.5 ±0.41	9.4
Tm	7.43±0.01	7.66±0.03	7.77±0.02	7.57±0.01	9.07±0.01	8.13±0.06	8.21±0.06	9.36±0.05	7.80±0.04	8.03±0.01	7.50±0.01	8.95±0.22	7.6
Yb	4.27±0.02	4.36±0.03	4.56±0.03	4.34±0.03	4.27±0.05	4.46±0.07	4.56±0.07	4.57±0.07	4.67±0.10	4.66±0.03	x	4.48±0.31	4.5
B_0^2 / cm^{-1}	75	110	228	-470	-700	-550	-450	-570	-355	x	x	700	

[a]No global fitting was possible for [Ln.gDOTA]$^{5-}$, [Tm.DOTMA]$^{-}$ and [Er.L[4]]$^{3+}$ so an average over multiple resonances using fixed *r* single resonance fitting is shown. [b]The estimated value for [Tm.DOTMA]$^{-}$ is 7.94 ± 0.2 BM from analysis of the R_1 data of the CH_3 resonance. [c]The estimates of the following resonances were analyse for the stated complexes : [Ln.L[1]] = pyH[3,4], [Ln.L[2]] =H_{ax}, H_{eq}, pyH[3,5], H_{eq}, [Ln.L[3]]$^{3+}$ = pyH[4], [Ln.L[4]]$^{3+}$ = H_{eq}, H_{eq}', [Ln.L[5]]$^{-}$ = H_{eq}, H_{eq}', Me, [Ln.L[6]] = CF_3, Me, [Ln.L[7,8,9]] = ^{t}Bu, [Ln.L[10]] = pyH[6], H_{eq}, H_{eq}', [Ln.L[11]] = Me.

A wide range of estimated values was observed in the fitting procedure. Generally, the estimated values show a deviation of around 10 % with respect to their respective theoretical values and in some special cases a deviation of beyond 20 % is observed.

The three C_3 symmetric complex series [Ln.L$^{1\text{-}3}$] show a variation of less than 2 % with respect to the theoretical values, with the exception of [Er.L^3]$^{3+}$, which shows one of the lowest values encountered for an Er(III) analogue (8.83 BM, –6 % deviation). The C_4 symmetric complex series [Ln.L^4]$^{3+}$ follows the theoretical values closely, but shows a slightly bigger deviation in Tb(III), Ho(III) and Er(III) (≥ 5 %). Each of these systems are considered to possess a small ligand field. The values for the highly symmetrical complexes [Tm.DOTMA]$^-$ and [Ln.gDOTA]$^{5-}$ mostly follow the previous systems in good agreement, despite the much bigger crystal field splitting parameter, B_0^2. However, the complex [Tm.gDOTA]$^{5-}$ shows a significant increase in μ_{eff} to 8.95 BM (+18 % deviation from free ion value).

The [Ln.L^5]$^-$ complex series is also one of the highly symmetric systems, but showed some deviation in the electronic relaxation behaviour. This behaviour was postulated to be connected to the impact of significant higher order crystal field splitting parameters in chapter 2, section 2.2.2.2. A bigger deviation can be observed, in particular for [Tm.L^5]$^-$ (9.07 BM, +19 %), which is one of the biggest deviations encountered, together with [Tm.L^8] (+24 %).

The calculated μ_{eff} values of the C_2 symmetric [Ln.L^9]$^+$ complexes show a bigger deviation than observed in the other high symmetry complexes. Indeed, some of the highest values were observed for [Tb.L^9]$^+$ (10.23 BM). This value is still in good agreement (≈5 %) with the theoretical free ion value. Surprisingly, this is one of only a few cases where the value of a Tb(III) analogue is higher than the theoretical value.

Generally, the complexes in low symmetry show a much wider range of estimated values. An overview of the range of μ_{eff} values across every series is given in Table 34.

Table 34 : *Overview of the range of estimates μ_{eff} (BM) using globally fitted nuclear relaxation values and fixed values for the internuclear distances, 295 K.*

	μ_{eff} / BM		
Ln^{3+}	Range	Theoretical	Biggest deviation
Tb	8.74 – 10.23	9.8	11 %
Dy	9.44 – 10.78	10.3	8 %
Ho	9.32 – 10.67	10.4	11 %
Er	8.33 – 9.62	9.4	11 %
Tm	7.43 – 9.36	7.6	24 %
Yb	4.27 – 4.67	4.5	5 %

The complexes of Dy(III), Ho(III) and Er(III) often show a lower than expected estimated effective magnetic moment, especially in the phosphinate based complexes, while the remaining lanthanide(III) ions show larger estimated values. These phosphinate complexes are all 8-coordinate systems that do not possess an axial coordinated water (or solvent) molecule. The overall deviation is around 10 % in most lanthanide(III) ions, but each lanthanide(III) ion shows its biggest deviation in different series.

However, the behaviour of the Tm(III) analogues is particularly interesting, as the estimated μ_{eff} values are almost all higher than the theoretical value. In the high symmetry complexes the μ_{eff} values of the Tm(III) analogues fall in the range 7.43-7.80 BM, while almost all other complexes give an estimated μ_{eff} of > 8 BM, with the highest value (9.36 BM) being observed in $[Ln.L^8]$ (+24 %).

4.2.1.1.1 The special case of $[Ln.L^8]$

The behaviour of $[Ln.L^8]$ is quite remarkable and the estimated effective magnetic moments show the highest deviations in this series. It is, in particular, the complexes $[Tm.L^5]^-$ and $[Tm.L^8]$ that stand out, with values of 9.07 and 9.36 BM respectively. These high values are rather surprising and are consistent with the high the nuclear relaxation rates observed at the high field regime (Figure 60).

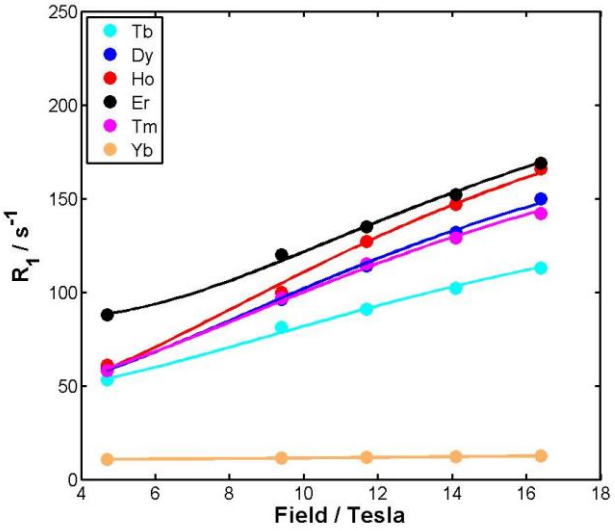

Figure 60 : *Nuclear relaxation rate data (points) and best global fit (lines) of the ^{t}Bu resonance of [Ln.L^{8}], using a fixed internuclear distance, r (6.6 Å) (295K, D_2O).*

At higher field strengths (> 9.4 Tesla), the nuclear relaxation rates are heavily dependent on the Curie term and its dependence on the fourth power of the effective magnetic moments, μ_{eff} (equation 4). Thus, it is highly surprising that the ^{t}Bu resonance of [Tm.L^{8}] relaxes as fast as the Dy(III) analogue and much faster than [Tb.L^{8}], despite the differences of 2 – 3 BM between these lanthanide(III) ions.

$$R_1 = \frac{2}{15}\left(\frac{\mu_0}{4\pi}\right)^2 \frac{\gamma_N^2 g_{Ln}^2 \mu_B^2 J\,(J+1)}{r^6}\left[3\frac{T_{1e}}{1+\omega_N^2\,T_{1e}^2} + 7\frac{T_{2e}}{1+\omega_e^2\,T_{2e}^2}\right] + \frac{2}{5}\left(\frac{\mu_0}{4\pi}\right)^2 \frac{\omega_N^2 \mu_{eff}^4}{(3k_B T)^2\, r^6}\left[3\frac{\tau_r}{1+\omega_N^2\,\tau_r^2}\right] \quad (4)$$

Of course, in chapter 2 the effect of the electronic relaxation times was highlighted in detail. The effect can be observed at low magnetic field strengths (e.g. the high R_1 of [Er.L^{8}] in Figure 60, 4.7 T), but the behaviour observed at high field strengths cannot purely be dominated by the electronic relaxation times.

The [Er.L^{8}] complex also has one the high estimated values for the effective magnetic moment across the whole [Ln.L^{8}] series (9.62 BM) compared to the relatively low values

for Dy(III) (9.44 BM) and Ho(III) (9.73 BM). Therefore, the fast relaxation rates of both Er(III) (9.62 BM) and Tm(III) (9.36 BM) complexes can be rationalised by the high values of μ_{eff} and T_{1e}, in contrast to the lower values for the other lanthanide(III) ions. However, such behaviour cannot be defined as classical behaviour and the high values of μ_{eff} and T_{1e} could be associated with the coordination environment of the [Ln.L^{8}] complexes. The other phosphinate complexes behave in a similar way, albeit not so clearly as with [Ln.L^{8}].

In summary, the estimated effective magnetic moments here show a small range of values for the complexes with low crystal field splittings, e.g. [Ln.L.[1-4,9]], but show significant deviation in the low symmetry, large crystal field splitting systems. In particular, the phosphinate based systems, for which the higher order parameters are assumed to be large, showed greater deviation than the high symmetry complexes, in particular for the Tm(III) examples. Such behaviour could be a first indication that there is significant contribution from *J*-mixing to the electronic energy levels of lanthanide(III) complexes that possess large crystal field splittings.

4.2.2 The bulk magnetic susceptibility shift (BMS) method

Another method based on solution-state NMR was employed to estimate the effective magnetic moment of the lanthanide(III) complexes. The observable shift of the resonances of paramagnetic lanthanide(III) complexes is considered to be made up of the diamagnetic, contact and pseudocontact terms:

$$\delta_{obsv} = \delta_{contact} + \delta_{dia} + \delta_{pseudo}$$

However, there is one more contribution to the shift that has been neglected so far. By addition of a paramagnetic molecule, the magnetic susceptibility of the molecule changes the observed chemical shift, this effect is the bulk magnetic susceptibility shift (BMS).[98,99] In comparison to the other contributions, the BMS in dilute samples in solution is small and was, therefore, not considered so far. The BMS is mainly modulated

by the concentration of the complex solution and the magnetic susceptibility of the lanthanide(III) ion (equation 10). [79,84]

$$\Delta\delta = \frac{1000\ M\ \chi_M^{para}}{3} \quad (10)$$

,where $\Delta\delta$ is the change in shift due to the BMS, M is the concentration of the complex solution and $\chi_M^{para}$is the molar magnetic susceptibility. The difference in the shift is measured through a coaxial insert NMR tube containing tert-butanol as a reference. The effective magnetic moment of the lanthanide(III) complex, μ_{eff}, can be directly associated with χ_M^{para} via equation 11:

$$\mu_{eff}^2 = \frac{\chi_M^{para}\ 3k_BT}{N_A\mu_0} \quad (11)$$

,where μ_0 is the Bohr magneton, N_A is Avogadro's number, k_B is the Boltzmann constant and T the absolute temperature.

In recent years, the BMS method has been used to determine the concentration of the paramagnetic ions in solution[100], and also to estimate the effective magnetic moments of metalloproteins.[84] The concentration of the lanthanide(III) ions in the samples herein was measured accurately using ICP-MS, which allows determination of the effective magnetic moment by equations 10 and 11.

4.2.2.1 Bulk magnetic susceptibility shift (BMS) data

The BMS values were measured in D_2O at three different temperatures and at three different concentrations to allow the creation of a larger dataset. Due to the rather low concentrations of complexes used, the errors in the calculations are rather large. As well as a selection of the complexes analysed before, the benzyl analogue of $[Ln.L^5]^-$ was also examined here (Scheme 16).[75,88]

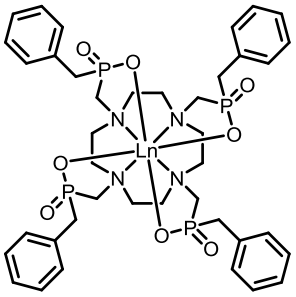

Scheme 16 : *Structure of [Ln.L^{5Bz}]$^-$.*[75,101]

An overview of the calculated effective magnetic moments estimated at 295 K is given in Table 35. The effective magnetic moments were calculated at two more temperatures; only the values at 295 K are shown here (Appendix 4, SI-Table 88-100).

Table 35 : *Overview of the estimated magnetic moments calculated using the BMS (295 K, D_2O, 11.7 T).*

	μ_{eff} / BM						
Ln^{3+}	[Ln.L^2]	[Ln.L^5]$^-$	[Ln.L^{10}]	[Ln.gDOTA]$^{5-}$	[Ln.DOTMA]$^-$	[Ln.L^{5Bz}]$^-$	Lit
Gd	8.36 ±0.53	7.96 ±0.94	x	7.64 ±0.40	x	8.00 ±1.05	8.0
Tb	x	9.33 ±1.06	8.48 ±0.70	x	x	x	9.8
Dy	11.21 ±0.64	10.23 ±1.012	9.40 ±0.57	x	x	x	10.3
Ho	10.93 ±0.73	11.93 ±0.72	9.26 ±0.68	x	x	x	10.4
Er	9.65 ±0.60	9.68 ±0.72	8.23 ±0.83	8.85 ±1.71	x	x	9.4
Tm	7.82 ±0.69	7.66 ±0.70	x	7.13 ±1.58	7.10 ±1.53	x	7.8
Yb	4.02 ±0.53	4.77 ±0.71	4.17 ±0.90	4.72 ±1.70	x	x	4.5
B_0^2 / cm^{-1}	110	-700	x	-700	-700	-700	

The C_3 symmetric tri-phosphinate complex series [Ln.L^2] shows the smallest deviations from the theoretical data, with higher effective magnetic moments in the Dy(III) and Ho(III) analogues, but good agreement with the remaining complexes (overall < 10 % deviation) and relatively small respective errors. The complexes in the phosphinate series [Ln.L^5] behave in a similar way. The estimated value for the Dy(III) analogue is much closer to the literature values for this complex series, but the Ho(III) analogue shows an even larger increase than in [Ln.L^2] (≈ +15 %).

The remaining complex series show significant deviations, but also much higher error values (10 – 20 %). Generally, the values of the Gd(III) analogues are well behaved across each series (< 5 % deviation). The changes across the different series for a specific

lanthanide(III) ion are in a similar range to the ranges observed in the fitting method. However, the values tend to be lower than the theoretical values, which was only observed for the first half of the lanthanide(III) series in the fitting procedure.

Interestingly, both $[Tm.gDOTA]^{5-}$ and $[Tm.DOTMA]^{-}$ have the same crystal field splitting and both posess a similar calculated effective magnetic moment (7.10 vs 7.13 BM, both –10 % with respect to literature value). The high associated experimental error for each of these complexes should be noted (≈ 22 %).

Overall, the calculated effective magnetic moments show a broad range in the complexes presented here. However, the calculated values produced significant associated errors typically in the range of 10 – 20%, which is the about the same size as the observed deviation from the literature values. Even when this method was employed in the literature to estimate the concentration of lanthanide(III) complexes in solution, the estimated errors that were given were of a similar magnitude.[100] It is concluded that this method of analysis is useful for estimating Gd(III) concentrations in solution, but is less generally applicable for the series of Tb(III) to Tm(III).

4.2.3 SQUID measurements

Complementary measurements of the magnetic susceptibility on a solid-state SQUID (superconducting quantum interference device) magnetometer were performed by Dr. Johan Buurma at Durham University.

A SQUID magnetometer contains a coil containing at least two Josephson junctions. Josephson junctions consist of two superconductors separated by a thin non-superconducting layer that allows the transfer of electrons and therefore produces a voltage. These Josephson junctions are heavily modulated by nearby magnetic fields and therefore the observed voltage is a function of the magnetic field and in our case, also of the magnetic susceptibility of the lanthanide(III) sample.[102]

In a standard SQUID experiment, the magnetic susceptibility (in emu) is measured over a wide range of temperatures (1.8 to 300 K) and the Curie-Weiss law is used to fit the data (equation 12):

$$\chi^{-1} = \frac{T - \theta}{C} \quad (12)$$

,where, χ^{-1} is the inverse magnetic susceptibility, *C* is the lanthanide specific Curie constant in emu K / mole, *T* is the absolute temperature and θ is the Weiss constant in Kelvin. The inverse molar magnetic susceptibility is plotted against the temperature to obtain the Curie constant from the fit to the line. The effective magnetic moment can then easily be calculated. An example of such a fitting is given below (Figure 61).

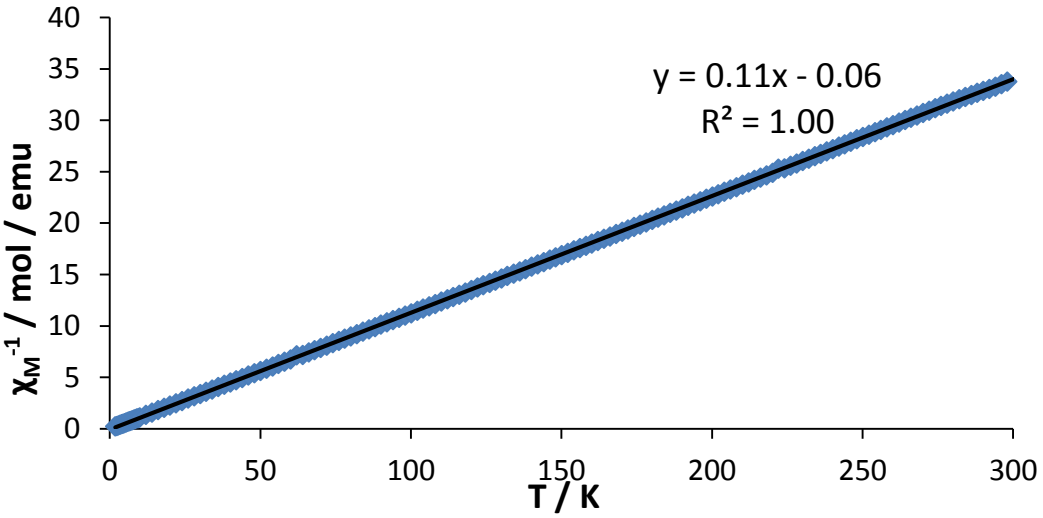

Figure 61 : *Plot of the inverse susceptibility against the temperature range of [Gd.L^{5Bz}]$^{-}$. The gradient of the fitted line is C^{-1} in emu^{-1} K^{-1} mol, which can then be converted by $\mu_{eff} = \sqrt{8C}$ in BM.*

Only a few lanthanide(III) complexes were analysed using the SQUID magnetometer. The complexes and their calculated effective magnetic moments are presented in Table 36.

Table 36 : *Overview of calculated effective magnetic moments, μ_{eff}, calculated from the measured magnetic susceptibility over the range of 1.8 to 300 K.*

Complex	μ_{eff} / BM	
	calc	theo
$[Gd.L^{5Bz}]$	8.4 ±0.1	8.0
$[Gd.L^{4}]^{3+}$	7.5 ±0.1	
$[Tm.DOTMA]^{-}$	6.8 ±0.6	7.8
$[Tm.L^{11}]^{a}$	7.5 ±1.2	

[a]The complex $[Tm.L^{11}]$ showed big deviation from the expected mass in accurate mass measurement. The Tm(III) concentration is scaled using the calculated degree of purity from elemental analysis and ICP-MS data. Actual calculated value in the experiment is 2.8 BM. The error was increased accordingly.

Each of the analysed complexes showed a deviation from the theoretical values. The two Gd(III) effective magnetic moments deviate by around 6 % from the theoretical values. However, the two Tm(III) examples show a much bigger deviation, but with higher associated error. Overall, the few selected complexes shown here show a slight variation of the calculated effective magnetic moments with the coordination environment. The isotropic Gd(III) has no orbital contribution to the total angular momentum, *J*, and should therefore be solely dependent on the spin *S*. It is surprising that the apparent values deviate so significantly. Evidently, many more examples need to be analysed to create a bigger data set.

4.3. Summary & Conclusions

Three independent methods were employed to measure the magnetic susceptibility of selected lanthanide(III) complexes and calculate their effective magnetic moments. A

deviation of 10 – 20 % from the expected literature values was observed, suggesting a dependence of the magnetic susceptibility on the coordination environment of the lanthanide(III) complexes that goes against conventional thinking. This conclusion is consistent with the observations made in chapter 3, considering the magnetic susceptibility anisotropy in NMR.

Few complexes were analysed using multiple methods. Looking at the values calculated over the three methods will give an indication of overall consistency. An overview is given in Table 37.

Table 37 : *Calculated effective magnetic moments, μ_{eff}, using the three methods (R_1 fitting, BMS and SQUID) employed here (295 K).*

Complex	μ_{eff} / BM		
	Fitting	BMS	SQUID
[Gd.L^{5Bz}]	n.d.	8.0 ±1.1	8.4±0.1
[Tm.L^{11}]	7.5 ±0.1	n.d.	7.5 ±1.2
[Tm.DOTMA]$^{-a}$	7.9±0.4	7.1±0.7	6.8±0.6

[a]Fitting value of [Tm.DOTMA]$^-$ was calculated through single resonance fitting.

With the exception of [Tm.DOTMA]$^-$ the values show a reasonable agreement. In particular, the estimates of the fitting and the SQUID measurements of [Tm.L^{11}] show the same value despite the large error associated with the SQUID measurement caused by the inhomogeneity of the sample.

The estimated values of the [Ln.L$^{1\text{-}11}$] series, through the fitting of the nuclear relaxation data, provide the largest data set. The low ligand field, high symmetry systems behave classically in their magnetic susceptibility, while the higher ligand field systems show some variation to the theoretical values, but usually smaller than 10 %. However, it seems that some lanthanide(III) ions are affected more than others. It can be assumed

that the variations are associated with the changes in the coordination environment and the introduction of *J*-mixing in systems of low symmetry and a high ligand field.

The electronic energy levels and also the electron distribution in the clouds are different for each lanthanide(III) ion, suggesting that the magnetic susceptibility is affected differently for each lanthanide(III) ion. The complexity of the electronic energy levels is shown in Figure 62.[93,103]

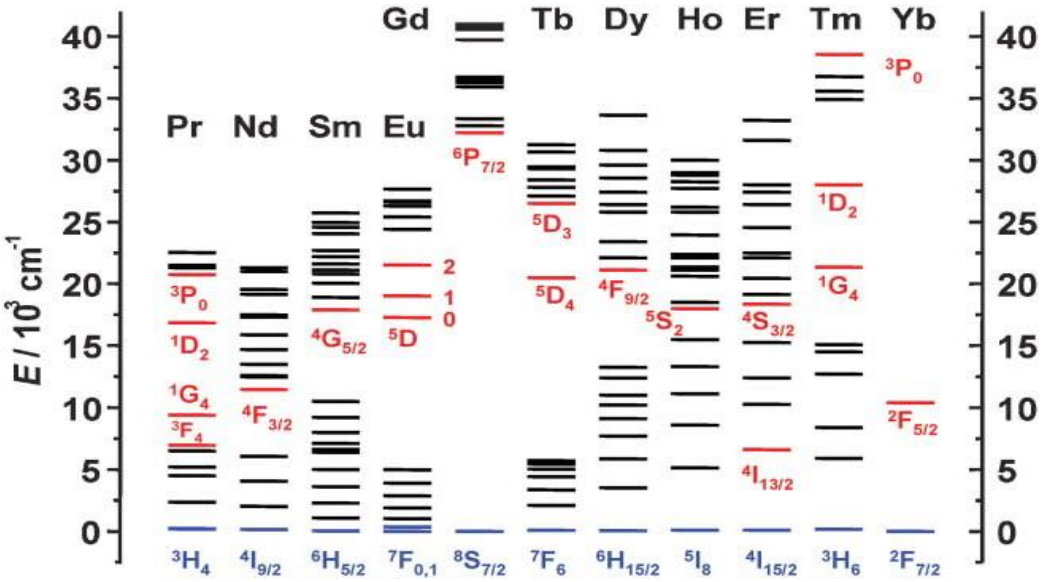

Figure 62 : *Part of the energy level diagram of the lanthanide(III) aqua ions. The levels responsible for the luminescence are highlighted in red and blue. Taken from [103].*

The lanthanide(III) energy levels shown here exclude any splitting derived from the crystal field splitting. A much more complex structure is expected, especially when *J*-mixing of the energy levels is introduced. Full understanding of the splitting behaviour of the lanthanide(III) complexes in low symmetry systems, or generally in systems possessing a large crystal field splitting, should reveal the effect on the magnetic susceptibility, the magnetic anisotropy, but also the behaviour of the nuclear and electronic relaxation rates analysed in chapter 2.

5. Conclusions & Final remarks

A variety of isostructural series of lanthanide(III) complexes was analysed for their solution state NMR relaxation properties and their magnetic behaviour. The nuclear relaxation rates, the pseudocontact shifts and the effective magnetic moments were analysed independently. In all three discussions, it was suggested that the coordination environment and its effect on the electronic energy levels of the lanthanide(III) have an effect on these properties though the crystal field splitting.

5.1 Nuclear relaxation rate phenomena

$$R_1 = \frac{2}{15}\left(\frac{\mu_0}{4\pi}\right)^2 \frac{\gamma_N^2 g_{Ln}^2 \mu_B^2 J\,(J+1)}{r^6}\left[3\frac{T_{1e}}{1+\omega_N^2\,T_{1e}^2} + 7\frac{T_{2e}}{1+\omega_e^2\,T_{2e}^2}\right] + \frac{2}{5}\left(\frac{\mu_0}{4\pi}\right)^2 \frac{\omega_N^2 \mu_{eff}^4}{(3k_B T)^2\, r^6}\left[3\frac{\tau_r}{1+\omega_N^2\,\tau_r^2}\right] \quad (4)$$

Solomon-Bloembergen Morgan theory (equation 4) is commonly used to describe the paramagnetic relaxation enhancements of nuclear relaxation rates for ligand resonances of lanthanide(III) complexes. The nuclear relaxation data measured in this work followed this theory quite closely, using the global and single fitting procedure. The key variable parameters, however, showed significant variation, influencing the nuclear relaxation rates of some complexes to a degree that was highly unexpected. In particular, the behaviour of Er(III) and Tm(III) systems was highlighted. It was concluded that the surprisingly high values in the effective magnetic moments and the electronic relaxation times are associated with the crystal field splitting induced by the ligand field of the complexes.

The fitting procedure assumed that the electronic relaxation times, T_{1e} and T_{2e}, are identical. A detailed investigation to fully see if the two parameters deviate significantly from each other would benefit this discussion.

A connection between the electronic relaxation times and the crystal field splitting was proposed. Especially in systems of high symmetry, a correlation between the electronic

relaxation time, T_{1e} and B_0^2 was apparent. However, in the low symmetry systems there was little evidence that this correlation was not maintained.

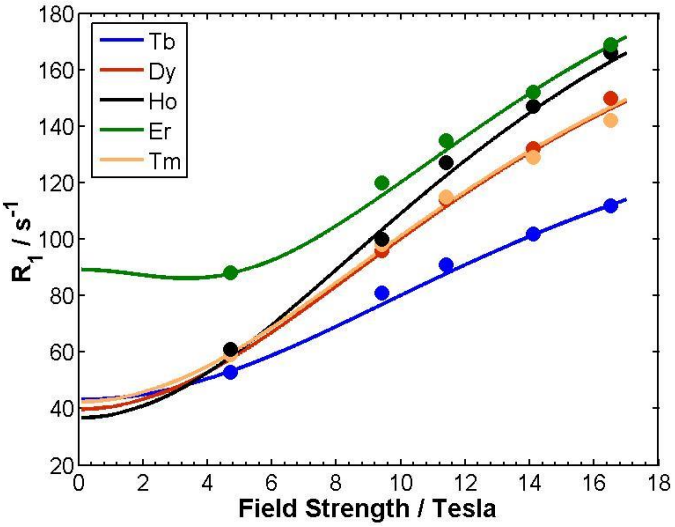

Figure 63 : *Extrapolation of the nuclear relaxation rates, R_1, with the field strength of [Ln.L[8]] using the parameters estimated in the global fitting procedure, but extended to low magnetic field strengths (see Table 12 for data).*

This study was mainly conducted on large magnetic field strength and could be extended to include more field strengths in the low field regime, as indicated by Figure 63.

To fully understand how the crystal field splitting parameters modulate the electronic relaxation times, it is necessary to fully characterise said parameters. There are a very limited number of methods that allow a full analysis of the crystal field splitting parameters. A few methods use the optical emission spectra and relative position and intensity of the transitions of the lanthanide(III) electronic energy levels. However, such a procedure is rarely performed for all lanthanide(III) complexes, due to the great the complexity of the energy levels for some metal ions.[104–107] Gaining insight of the crystal field splitting parameters, especially the higher order parameters and how the crystal field splitting changes across an isostructural series, will provide the means to postulate an accurate theory of the underlying mechanism of electronic relaxation of lanthanide(III) ions and will allow an easier design and application of paramagnetic probes.

5.2 Magnetic susceptibility and anisotropy

A similar observation was made for the magnetic susceptibility and the magnetic anisotropy. The effect of *J*-mixing was introduced and its effect was postulated to have an effect on the electronic energy levels in systems of low symmetry. However, the study is in need of more experimental data. While a big database of values was presented for the fitting of the nuclear relaxation data, the BMS and SQUID studies were limited scope, but could easily be extended. Especially, analysing a full isostructural series of lanthanide(III) complexes using the SQUID method would benefit the discussion of *J*-mixing greatly. The series that already showed the biggest deviations, for example, [Ln.L^5] or [Ln.L^8], would be ideal candidates.

In addition, the modulation of the pseudocontact shift with the coordination environment was shown to highlight the discrepancies in Bleaney's theory of magnetic anisotropy. Insight was gained into the chemical shift behaviour and how to easily modulate the pseudocontact shift. Such observations will be of benefit in designing simple lanthanide(III) tags for protein analysis and for PARASHIFT agents.[46,61] The highest magnetic anisotropy was found to occur in systems possessing no directly bound water. An attempt was made to rationalise the anomalous shift behaviour of the lanthanide(III) ions depending on the shape of the electron clouds and the changing orientation of the easy axis of magnetisation.[86,90,91] Further investigations into the behaviour of the prolate / oblate lanthanide(III) ions with changing hydration number, *q*, and ligand fields would allow to back these postulations with more experimental data.

The theory to describe the magnetic anisotropy is need of complete revision. The original Bleaney theory is not capable of describing the complex prolate / oblate structure of the electron clouds using a point dipole approximation.

Recently, progress has been made by Dr. Ilya Kuprov by eliminating the point dipole approximation and using elliptical electron clouds instead.[108] This is a good first move, but is only a small step towards a descriptive theory of the magnetic anisotropy of the lanthanide(III) ions.

6. Experimental

6.1 General Procedures

Single crystal X-ray data for the $[Tm.gDOTA]^{5-}$ complex were collected at 120 K on Bruker SMART-CCD 6000 diffractometer (ω-scan, 0.3-0.5° / frame) equipped with an Oxford Cryostream open-flow nitrogen cryostat.

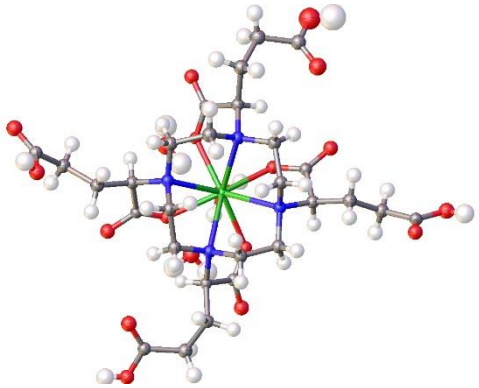

Figure 64 : *Illustration of the X-ray crystallographic structure of the minor isomer (SAP, q=1) of $[Tm.gDOTA]^{5-}$. Unpublished to this date.*

The structures were solved by Patterson method and refined by full matrix least squared on F^2 for all data using SHELXTL and OLEX2 software. All non-disordered atoms were refined with anisotropic displacement parameters. Hydrogen atoms were placed into calculated positions and refined in "riding"-mode. All structures contain a number of disordered solvent molecules. Their contribution to the scattering factor has been taken into account using the MASK procedure of OLEX2 software. When the distance of protons were measured their distances were corrected using the OLEX2 software. The X-ray structures for $[Ln.L^1]$[80], $[Ln.L^2]$[29], $[Ln.L^3]^{3+}$[74], $[Ln.L^4]^{3+}$[109] and $[Ln.L^{5Bz}]$[101] were taken from the quoted literature structures. The $[Tm.DOTMA]^{-}$[49] structure was provided by Dr. Mark Woods of Oregon Health & Science University.

6.1.2 Synthesis & Origin of complexes

The ligands and complexes of $[Ln.L^1]$[80] and $[Ln.L^5]$[75] were synthesised from known synthetic routes, which can be found in the quoted references. The majority of

complexes and their synthetic procedures have been published before or during the course of this PhD: [Ln.L^1] [80] and [Ln.L^5]$^-$ [75] were synthesised from known routes, [Ln.L^2] prepared by Dr. James Walton[29], [Ln.L^3]$^{3+}$ prepared by Emily Neil[74], [Ln.L^4]$^{3+}$ was complexed from the ligand provided by Dr. Kanthi Senanayake[109], [Ln.L^{5Bz}]$^-$ was available from previous synthesis by Dr. Kanthi Senanyake[75] , [Ln.L^6][110], [Ln.L^7], [Ln.L^{7S}] and [Ln.L^9]$^+$ prepared by Dr. Peter Harvey[46], [Ln.L^{10}] prepared by Dr. Brian McMahon[61]. [Tm.DOTMA]$^-$ was provided by Dr. Mauro Botta[49] and [Ln.gDOTA]$^{5-}$ was synthesised from known routes with the help of Dr. Neil Sim[111]. The complex series [Ln.L^8], [Ln.L^{8CO}] and [Ln.L^{11}] are unpublished to this date and were prepared by Dr. Kanthi Senanayake at Durham University. An overview of the structures is given in Scheme 17.

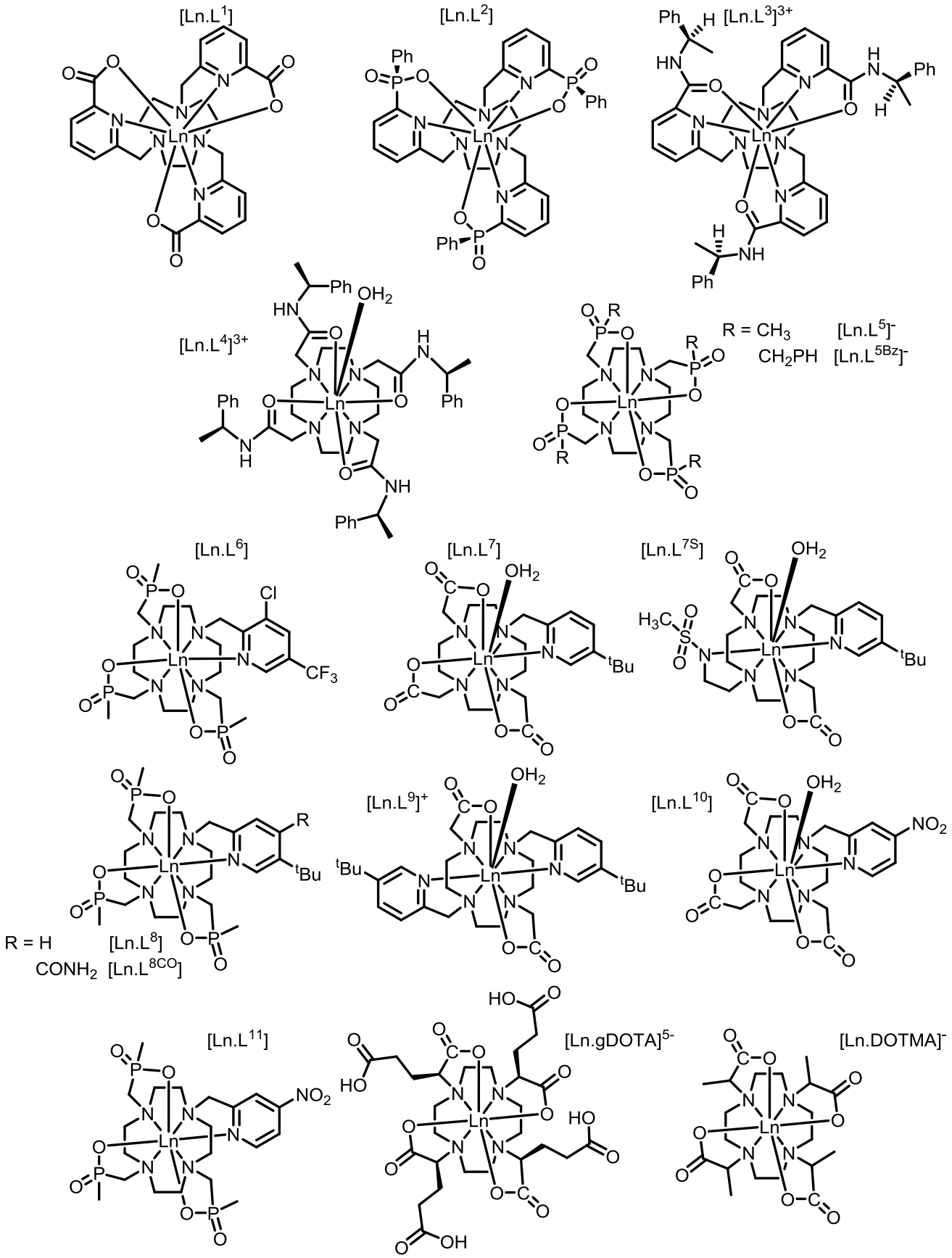

Scheme 17 : *Structures of all complexes analysed in this discussion.*

6.1.3 General NMR procedures

^{1}H, ^{19}F and ^{31}P NMR spectra were obtained at 295 K (unless stated otherwise) on Varian spectrometers operating at 4.7, 9.4, 11.7, 14.1, 16.5 Tesla, specifically on a Mercury 200 spectrometer (^{1}H at 200.057 MHz, ^{19}F at 188.242 MHz, ^{31}P at 80.985 MHz), a Mercury 400 spectrometer (^{1}H at 399.97 MHz, ^{19}F at 376.331 MHz, ^{31}P at 161.910 MHz), a Varian Inova-500 spectrometer (^{1}H at 499.78 MHz, ^{19}F at 470.322 MHz, ^{31}P at 202.340 MHz), a Varian VNMRS-600 spectrometer (^{1}H at 599.944 MHz, ^{19}F at 564.511 MHz, ^{31}P at 242.862 MHz) and a Varian VNMRS-700 spectrometer (^{1}H at 700.000 MHz, ^{19}F at 658.658 MHz, ^{31}P at 283.365 MHz). Commercially available deuterated solvents were used.

The operating temperature of the spectrometers was measured with the aid of an internal calibration sample of neat ethylene glycol for high temperature studies. A calibration sample of neat methanol was used for low temperatures studies. The operating temperature of each spectrometer was measured before each set of measurements of relaxation data.

The ^{19}F and ^{31}P relaxation data were measured without proton decoupling. The ^{31}P chemical shifts are reported relative to 85 % phosphoric acid. The ^{19}F chemical shifts are reported relative to fluorotrichloromethane.

The recorded free induction decays were processed using backward linear prediction, optimal exponential weighting, zero-filling, Fourier transform, phasing and baseline correction (by Whittaker smoothing), if necessary.

6.2 Relaxation data analysis

The nuclear relaxation times of the nuclei of interest were measured at the five different fields mentioned above. The T_1 values were measured using the inversion-recovery technique. At first a crude T_1 value was obtained, which was then used as the initial guess in multiple repeat experiments. The incremented delay time was set to show full

inversion and full recovery to equilibrium of the signal, which is roughly achieved at five times the T_1 value.

The line width and T_2 data were obtained by Lorentzian line fitting. Due to the broad nature of the resonances, the field inhomogeneity is negligible and it can be assumed that in the absence of exchange broadening the T_2* measured from the line width corresponds to the actual T_2 value.[24]

The lanthanide(III) complexes of [Ln.L^2] and [Ln.L^3]$^{3+}$ were analysed in CD_3OD, the remaining complexes series were analysed in D_2O solutions, unless stated otherwise. The concentration of a sample was kept constant throughout a series of measurements, which was in the range of 0.1 to 1 mM. An additional experiment was performed on [Ln.L^4]$^{3+}$ to study the effect of different solvents on R_1 and T_{1e}. The longitudinal nuclear relaxation rates varied as a function of the solvent, as the viscosity affected the rotational correlation time, τ_R. However, the electronic relaxation times did not vary with solvent within their estimated experimental errors (Table 38).

Table 38 : *Estimated values of the electronic relaxation times of [Ln.L^4]$^{3+}$ using single resonance fitting (fixed μ_{eff}) in three different solvents (295 K).*

Ln^{3+}	D_2O	CD_3OD	MeCN
	T_{1e} / ps	T_{1e} / ps	T_{1e} / ps
Tb	0.54 ±0.06	0.50 ±0.05	0.52 ±0.07
Dy	0.43 ±0.03	0.41 ±0.04	
Ho	0.34 ±0.01	0.22 ±0.06	
Tm	0.20 ±0.02	0.19 ±0.04	
Yb	0.17 ±0.03	0.16 ±0.03	0.15 ±0.03
τ_R / ps	350 ±28	253 ±17	162 ±12

For each complex studied, the ^{1}H, ^{19}F and ^{31}P relaxation data measured and used for all complexes can be found in Appendix 2.

The measured nuclear relaxation data was fitted by using a modified Matlab algorithm originally written by Dr. Ilya Kuprov of Southampton University (original code shown in Appendix 2, A24). The algorithm uses the Solomon-Morgan-Bloembergen equations (4) to fit the measured relaxation data using the Matlab internal Levenberg-Marquardt

minimisation of the non-linear squares error function. The results were analysed iteratively. It was assumed that the longitudinal and transverse electronic relaxation times were of a similar magnitude.

$$R_1 = \frac{2}{15}\left(\frac{\mu_0}{4\pi}\right)^2 \frac{\gamma_N^2 g_{Ln}^2 \mu_B^2 J\,(J+1)}{r^6}\left[3\frac{T_{1e}}{1+\omega_N^2\,T_{1e}^2} + 7\frac{T_{2e}}{1+\omega_e^2\,T_{2e}^2}\right] + \frac{2}{5}\left(\frac{\mu_0}{4\pi}\right)^2 \frac{\omega_N^2 \mu_{eff}^4}{(3k_B T)^2\, r^6}\left[3\frac{\tau_r}{1+\omega_N^2\,\tau_r^2}\right] \quad (4)$$

Some parameters were used globally for every lanthanide(III) complex in the series and others were used for each complex individually. The rotational correlation time, τ_r, was considered not to vary across a given series of complexes. An estimate for τ_r was determined by the Stokes-Einstein Law. An estimate of the hydrodynamic radius, *r*, was made by inspecting the X-ray data; in each case a reasonable agreement was found (± 0.2 Å). DFT calculations were performed by Dr. Ilya Kuprov for further analysis of internuclear distances and rotational correlation times.[11] A full discussion is provided in chapter 2, section 2.1.

The magnetic moments estimated for the fitting were taken from literature.[11] The majority of the global fitting curves and the nuclear relaxation data are shown in the main chapters or in the Appendix 2.

6.2.1 Error Analysis

Each relaxation measurement was repeated at least three times and the mean value recorded. The number of transients used in the measurements was determined by the signal-to-noise ratio and also by the linewitdh of the resonance of interest. In each case, the signal was fully recovered during the inversion-recovery sequence.

An experiment was performed to calculate the error associated with the temperature variance of the spectrometers. The relaxation rate of [Tm.L[1]] was measured at five

different temperatures (295 – 303 K in 2 K steps). At each measurement, the temperature was also determined by using the temperature calibration sample (ethylene glycol). According to the Solomon-Morgan-Bloembergen equations, the temperature dependence of the relaxation rate, R_1, is $1 / T^2$. At a variation of 0.5 K the error was found to be less than 1.3 %. This was assumed to be similar for each complex studied (Appendix 2, SI-Table 16).

A statistical error analysis was undertaken to determine the fitting errors. The experimental errors of the measured relaxation rates were combined and used to perturb the relaxation rates for each complex at each field. These perturbed rates together with the unperturbed relaxation rates were used in a statistical error analysis to obtain the error values for the individual parameters (μ_{eff}, r, τ_r and T_{1e}) calculated in the fitting process.[112] An example of the obtained estimates is given inTable 10.

6.3 Pseudocontact shift analysis

The ^{1}H NMR spectra for the complexes [Ln.L$^{1\text{-}5,10}$] were fully characterised and analysed. The full shift data can be found in the data tables in Appendix 3. The complex series [Ln.L$^{6\text{-}9,11}$] were only partially analysed as the attention was given to specific reporter groups (e.g. ^{t}Bu, CF_3), due to varying amounts of available sample material and more difficult analysis in the low symmetry complexes.

The accurate measurement of the chemical shift of a given resonance was performed on the 9.4 Tesla Mercury 400 spectrometer, unless stated otherwise.

The observed shifts were tested for changes due to the bulk magnetic susceptibility shift of the lanthanide(III) complexes. Using a coaxial insert tube containing a tert-butanol reference (1%), it was found that over the concentration range used here (0.1 – 1 mM), the BMS alteration to the observable shift was less than 0.2 ppm. The data is given in Appendix 4. Considering that the observed shift range can vary from +500 ppm to -500ppm in these paramagnetic complexes, this small effect can be largely neglected at the concentrations used here.

6.3.1 Variable temperature NMR studies

The variable temperatures ^{1}H and ^{19}F NMR resonances (D_2O except [Ln.L^2] and [Ln.L^3]$^{3+}$ (CD_3OD)) of most complexes were measured as a function of the temperature on the Varian VNMRS-600 spectrometer, with a few exceptions run on the Varian VNMRS-700 spectrometer, as stated in the discussion. However, the VT experiments on [Tm.L^4] were performed on the Varian Inova-500 spectrometer, due to restrictions for lowering the temperature on the other high field spectrometers. In each measurement, the temperature was measured with the internal calibration standard (ethylene glycol or methanol) to ensure accurate temperature measurements. The error for the shift per unit Kelvin was calculated using linear regression.

6.4 Bulk magnetic susceptibility measurements

The ^{1}H NMR (D_2O, except CD_3OD for [Ln.L^2]) spectra for the bulk magnetic susceptibility (BMS) measurements were recorded at 295, 300 and 305 K using a coaxial insert reference tube. A solution of D_2O and tert-butanol (1%) was placed in the coaxial insert tube, while the solution of the paramagnetic complexes was placed in the outer tube. The sample was shimmed and locked to the D_2O signal.

$$\Delta\delta = \frac{1000\, M\, \chi_M^{para}}{3} \quad (10)$$

$$\mu_{eff}^2 = \frac{\chi_M^{para}\, 3k_B T}{N_A \mu_0} \quad (11)$$

The ^{1}H NMR spectrum revealed the BMS shift between the diamagnetic reference and the paramagnetic sample of the tert-butanol signal. From the BMS shift, the magnetic susceptibility and the effective magnetic moment were calculated, as described in the main text above (chapter 4, section 4.2.2 , and using equation 10 and 11). The concentrations of each complex used in the calculations were obtained from ICP-MS analysis of the complexes. The errors were calculated by performing repeat measurements and the associated error was carried through the calculations. The

temperature error, as shown above, was smaller than the experimental error. An example for the estimation of the errors is given in Table 39, which was then combined with the error of the concentration measurement.

Table 39 : *Example of the error analysis for [Gd.L^{5Bz}]$^-$ (three different temperatures for three different runs) used to estimate the experimental error (11.7 T, D_2O).*

T	$\Delta\delta$ / ppm	χ_M^{para} / m^3 mol^{-1}	μ_{eff} / BM
		Run 1	
295 K	0.15	3.64	8.30
300 K	0.14	3.56	8.29
305 K	0.14	3.49	8.27
		Run 2	
295 K	0.14	3.56	8.22
300 K	0.14	3.49	8.20
305 K	0.14	3.39	8.15
		Run 3	
295 K	0.12	3.54	8.19
300 K	0.14	3.46	8.17
305 K	0.14	3.41	8.18

6.5 SQUID magnetic susceptibility measurements

The SQUID measurements were performed by Dr. Johan Buurma in the Durham University Chemistry department. The instrument used is Quantum Design RC- SQUID magnetometer operating from 1.8 to 300 K. The samples were measured at a magnetic field strength of 0.5 T.

A diamagnetic correction was performed on the structure of the complexes, but was found to be negligible, as the lanthanide(III) ion moment is large (< 2% error).

The Curie constant was determined independently and was found to be in agreement with the calculation derived from the Curie-Weiss fit. The absence of hysteresis was

noted and it was concluded that were no ferromagnetic impurities. Example data for [Gd.L^{5Bz}] is given in Figure 61, similar behaviour was observed in the other samples.

A variety of experiments was performed to establish the consistency of the experiment. For example, the [Gd.L^{5Bz}] sample was prepared with different weights, and the experiment was run at different induced magnetic field strengths. In every case the calculated values were consistent, within the estimated error

$$\chi^{-1} = \frac{T - \theta}{C} \quad (12)$$

The principal error of the measurement comes from the statistical error in the Curie Weiss fit (from equation (12) and was determined using linear regression.

7. References

(1) Bloembergen, N.; Morgan, L. O. *J Chem Phys* **1961**, *34*, 842–850.
(2) Bleaney, B. *J Magn Reson* **1972**, *8*, 91–100.
(3) Golding, R. M.; Pyykkö, P. *Mol. Phys.* **1973**, *26*, 1389–1396.
(4) Solomon, I. *Phys Rev* **1955**, *99*, 559–565.
(5) Bloembergen, N. *J Chem Phys* **1957**, *27*, 572–573.
(6) McQueen, F. M. *Rheumatology* **2000**, *39*, 700–706.
(7) Caravan, P.; Ellison, J. J.; McMurry, T. J.; Lauffer, R. B. *Chem Rev* **1999**, *99*, 2293–2352.
(8) Kaltsoyannis, N.; Scott, P. *The f elements*; Oxford Chemistry Primers; Oxford University Press: New York, 1999.
(9) Binnemans, K.; Görller-Walrand, C. *Chem. Phys. Lett.* **1995**, *245*, 75–78.
(10) Görller-Walrand, C.; Binnemans, K. In *Handbook on the Physics and Chemistry of Rare Earths*; Karl A. Gschneidner, J. and L. E., Ed.; Elsevier, 1996; Vol. Volume 23, pp. 121–283.
(11) Chalmers, K. H.; De Luca, E.; Hogg, N. H. M.; Kenwright, A. M.; Kuprov, I.; Parker, D.; Botta, M.; Wilson, J. I.; Blamire, A. M. *Chem Eur J* **2010**, *16*, 134–148.
(12) Newman, D. J.; Ng, B. *Crystal field handbook /edited by D.J. Newman and Betty Ng*; Cambridge University Press: Cambridge, 2000.
(13) Duan, C.-K.; Tanner, P. A. *J. Phys. Chem. A* **2010**, *114*, 6055–6062.
(14) Carr, R. Lanthanide Complexes as Chiral Probes Exploiting Circularly Polarized Luminescence. Doctoral, Durham University, 2014.
(15) Parker, D.; Puschmann, H.; Batsanov, A. S.; Senanayake, K. *Inorg Chem* **2003**, *42*, 8646–8651.
(16) Walton, J. W.; Bari, L. D.; Parker, D.; Pescitelli, G.; Puschmann, H.; Yufit, D. S. *Chem Commun* **2011**, *47*, 12289–12291.
(17) Bertini, I.; Luchinat, C.; Parigi, G. *Prog. Nucl. Magn. Reson. Spectrosc.* **2002**, *40*, 249–273.
(18) Bertini, I.; Calderone, V.; Cerofolini, L.; Fragai, M.; Geraldes, C. F. G. C.; Hermann, P.; Luchinat, C.; Parigi, G.; Teixeira, J. M. C. *FEBS Lett.* **2012**, *586*, 557–567.
(19) S. Dickins, R.; Parker, D.; I. Bruce, J.; J. Tozer, D. *J Chem Soc Dalton Trans* **2003**, 1264–1271.
(20) Ren J, S. A. *J Magn Reson B* **1996**, *111*, 178–182.
(21) Keeler, J. *Understanding NMR Spectroscopy*; John Wiley & Sons Ltd: Chichester, England, 2005.
(22) Levitt, M. *Spin Dynamics*; John Wiley & Sons Ltd.: Chichester, 2001; Vol. 1.
(23) Harvey, P.; Kuprov, I.; Parker, D. *Eur J Inorg Chem* **2012**, *12*, 2015–2022.
(24) Bertini, I.; Luchinat, C.; Parigi, G. *Solution NMR of Paramagnetic Molecules*; Current Methods in Inorganic Chemistry; Elsevier Science B.V.: Amsterdam, 2001; Vol. 2.
(25) Sigel, A.; Sigel, H. *Metal Ions in biological systems*; The lanthanides and their interrelations with biosystems; Marcel Dekker, Inc.: Netherlands, 2003; Vol. 40.
(26) Thomsen, H. S. *Radiol. Clin. North Am.* **2009**, *47*, 827–831.
(27) Kowalewski, J.; Luchinat, C.; Nilsson, T.; Parigi, G. *J Phys Chem A* **2002**, *106*, 7376–7382.
(28) Bertini, I.; Capozzi, F.; Luchinat, C.; Nicastro, G.; Xia, Z. *J Phys Chem* **1993**, *97*, 6351–6354.
(29) Walton, J. W.; Carr, R.; Evans, N. H.; Funk, A. M.; Kenwright, A. M.; Parker, D.; Yufit, D. S.; Botta, M.; De Pinto, S.; Wong, K.-L. *Inorg. Chem.* **2012**, *51*, 8042–8056.
(30) Aime, S.; Botta, M.; Fasano, M.; Crich, S. G.; Terreno, E. *J. Biol. Inorg. Chem.* **1996**, *1*, 312–319.
(31) Botta, M. *Eur. J. Inorg. Chem.* **2000**, 399–407.
(32) Geraldes, C. F. G. C.; Laurent, S. *Contrast Media Mol. Imaging* **2009**, *4*, 1–23.

(33) Geraldes, C. F. G. C.; Urbano, A. M.; Alpoim, M. C.; Sherry, A. D.; Kuan, K.-T.; Rajagopalan, R.; Maton, F.; Muller, R. N. *Magn. Reson. Imaging* **1995**, *13*, 401–420.
(34) Caravan, P. *Chem. Soc. Rev.* **2006**, *35*, 512–523.
(35) Nivorozhkin, A. L.; Kolodziej, A. F.; Caravan, P.; Greenfield, M. T.; Lauffer, R. B.; McMurry, T. J. *Angew. Chem. Int. Ed.* **2001**, *40*, 2903–2906.
(36) Aime, S.; Barge, A.; Delli Castelli, D.; Fedeli, F.; Mortillaro, A.; Nielsen, F. U.; Terreno, E. *Magn. Reson. Med.* **2002**, *47*, 639–648.
(37) Langereis, S.; Keupp, J.; van Velthoven, J. L. J.; de Roos, I. H. C.; Burdinski, D.; Pikkemaat, J. A.; Grüll, H. *J. Am. Chem. Soc.* **2009**, *131*, 1380–1381.
(38) Heffern, M. C.; Matosziuk, L. M.; Meade, T. J. *Chem. Rev.* **2014**, *114*, 4496–4539.
(39) Liu, G.; Song, X.; Chan, K. W.; McMahon, M. T. *NMR Biomed* **2013**, *26*, 810–828.
(40) Li, A. X.; Wojciechowski, F.; Suchy, M.; Jones, C. K.; Hudson, R. H. E.; Menon, R. S.; Bartha, R. *Magn. Reson. Med.* **2008**, *59*, 374–381.
(41) Vinogradov, E.; Sherry, A. D.; Lenkinski, R. E. *J. Magn. Reson.* **2013**, *229*, 155–172.
(42) Vinogradov, E.; Soesbe, T. C.; Balschi, J. A.; Dean Sherry, A.; Lenkinski, R. E. *J. Magn. Reson.* **2012**, *215*, 64–73.
(43) Chalmers, K. H.; Kenwright, A. M.; Parker, D.; Blamire, A. M. *Magn Reson Med* **2011**, *66*, 931–936.
(44) Chalmers, K. H.; Botta, M.; Parker, D. *J Chem Soc Dalton Trans* **2011**, *40*, 904–913.
(45) Meyerspeer, M.; Robinson, S.; Nabuurs, C. I.; Scheenen, T.; Schoisengeier, A.; Unger, E.; Kemp, G. J.; Moser, E. *Magn Reson Med* **2012**, 1713–1723.
(46) Harvey, P.; Blamire, A. M.; Wilson, J. I.; Finney, K.-L. N. A.; Funk, A. M.; Senanayake, P. K.; Parker, D. *Chem Sci* **2013**, *4*, 4251–4258.
(47) Hekmatyar, S. K.; Hopewell, P.; Pakin, S. K.; Babsky, A.; Bansal, N. *Magn Reson Med* **2005**, *53*, 294–303.
(48) Geraldes, C. F. G. C.; Sherry, A. D.; Kiefer, G. E. *J Magn Reson* **1992**, *97*, 290–304.
(49) Aime, S.; Botta, M.; Garda, Z.; Kucera, B. E.; Tircso, G.; Young, V. G.; Woods, M. *Inorg. Chem.* **2011**, *50*, 7955–7965.
(50) Pakin, S. K.; Hekmatyar, S. K.; Hopewell, P.; Babsky, A.; Bansal, N. *NMR Biomed* **2006**, *19*, 116–124.
(51) Schmid, F.; Höltke, C.; Parker, D.; Faber, C. *Magn. Reson. Med.* **2013**, *69*, 1056–1062.
(52) Keizers, P. H. J.; Ubbink, M. *Prog. Nucl. Magn. Reson. Spectrosc.* **2011**, *58*, 88–96.
(53) Madl, T.; Güttler, T.; Görlich, D.; Sattler, M. *Angew. Chem. Int. Ed.* **2011**, *50*, 3993–3997.
(54) Otting, G. *J. Biomol. NMR* **2008**, *42*, 1–9.
(55) Graham, B.; Loh, C. T.; Swarbrick, J. D.; Ung, P.; Shin, J.; Yagi, H.; Jia, X.; Chhabra, S.; Barlow, N.; Pintacuda, G.; Huber, T.; Otting, G. *Bioconjug. Chem.* **2011**, *22*, 2118–2125.
(56) Keizers, P. H. J.; Saragliadis, A.; Hiruma, Y.; Overhand, M.; Ubbink, M. *J. Am. Chem. Soc.* **2008**, *130*, 14802–14812.
(57) Otting, G. *Annu. Rev. Biophys.* **2010**, *39*, 387–405.
(58) Madl, T.; Bermel, W.; Zangger, K. *Angew. Chem. Int. Ed.* **2009**, *48*, 8259–8262.
(59) Downing, A. K. *Protein Nuclear Magnetic Resonance Techniques*; Springer Science & Business Media, 2004.
(60) Berry, M. T.; Schwieters, C.; Richardson, F. S. *J Chem Phys* **1988**, *122*, 105–124.
(61) Gempf, K. L.; Butler, S. J.; Funk, A. M.; Parker, D. *Chem Commun* **2013**, *49*, 9104–9106.
(62) McGarvey, B. R. *J. Magn. Reson. 1969* **1979**, *33*, 445–455.
(63) Fries, P. H.; Belorizky, E. *J Chem Phys* **2007**, *126*, 204503–204513.
(64) Goldman, M. *J Magn Reson* **2001**, *149*, 160–187.
(65) Zuo, C. S.; Mahmood, A.; Sherry, A. D. *J Magn Reson* **2001**, *151*, 101–106.
(66) Alsaadi, B. M.; Rossotti, F. J. C.; Williams, R. J. P. *J Chem Soc Dalton Trans* **1980**, 2147–2150.

(67) Alsaadi, B. M.; Rossotti, F. J. C.; Williams, R. J. P. *J Chem Soc Dalton Trans* **1980**, 2151–2154.
(68) Aime, S.; Barbero, L.; Botta, M.; Ermondi, G. *J Chem Soc Dalton Trans 2* **1992**, 225–228.
(69) Einstein, A. *Ann. Phys.* **1905**, *322*, 549–560.
(70) Wittebort, R. J.; Szabo, A.; Gurd, F. R. N. *J Am Chem Soc* **1980**, *102*, 5723–5728.
(71) Lipari, G.; Szabo, A. *J Am Chem Soc* **1982**, *104*, 4546–4559.
(72) Fries, P. H.; Belorizky, E. *J Chem Phys* **2012**, *136*, 074513–10.
(73) Fries, P. H.; Belorizky, E. *J Chem Phys* **2005**, *123*, 124510–124515.
(74) Neil, E. R.; Funk, A. M.; Yufit, D. S.; Parker, D. *Dalton Trans* **2014**, 5490–5504.
(75) Broan, C. J.; Cole, E.; Jankowski, K. J.; Parker, D.; Pulukkody, K.; Boyce, B. A.; Beeley, N. R. A.; Millar, K.; Millican, A. T. *Synthesis* **1992**, *1992*, 63–68.
(76) Mironov, V. S.; Galyametdinov, Y. G.; Ceulemans, A.; Görller-Walrand, C.; Binnemans, K. *J Chem Phys* **2002**, *116*, 4673–4685.
(77) Mironov, V. S.; Galyametdinov, Y. G.; Ceulemans, A.; Görller-Walrand, C.; Binnemans, K. *Chem. Phys. Lett.* **2001**, *345*, 132–140.
(78) Ren, J.; Zhang, S.; Dean Sherry, A.; Geraldes, C. F. G. C. *Inorganica Chim. Acta* **2002**, *339*, 273–282.
(79) Evans, D. F. *J. Chem. Soc. Resumed* **1959**, 2003–2005.
(80) Nocton, G.; Nonat, A.; Gateau, C.; Mazzanti, M. *Helv. Chim. Acta* **2009**, *92*, 2257–2273.
(81) Shannon, R. D. *Acta Crystallogr. Sect. A* **1976**, *32*, 751–767.
(82) Funk, A. M.; Fries, P. H.; Harvey, P.; Kenwright, A. M.; Parker, D. *J Phys Chem A* **2013**, *117*, 905–917.
(83) Kang, J.-G.; Kim, Tack-Jin. *Bull Korean Chem Soc* **2005**, *26*, 1057–1064.
(84) Bertini, I.; Luchinat, C.; Turano, P.; Battaini, G.; Casella, L. *Chem. – Eur. J.* **2003**, *9*, 2316–2322.
(85) Bleaney, B. *J Magn Reson* **1972**, *8*, 94.
(86) Rinehart, J. D.; Long, J. R. *Chem. Sci.* **2011**, *2*, 2078–2085.
(87) Aime, S.; Botta, M.; Ermondi, G. *Inorg Chem* **1992**, *31*, 4291–4299.
(88) Aime, S.; Botta, M.; Parker, D.; Williams, J. A. G. *J Chem Soc Dalton Trans* **1995**, 2259–2266.
(89) Di Pietro, S.; Piano, S. L.; Di Bari, L. *Coord. Chem. Rev.* **2011**, *255*, 2810–2820.
(90) Boulon, M.-E.; Cucinotta, G.; Luzon, J.; Degl'Innocenti, C.; Perfetti, M.; Bernot, K.; Calvez, G.; Caneschi, A.; Sessoli, R. *Angew. Chem. Int. Ed.* **2013**, *52*, 350–354.
(91) Cucinotta, G.; Perfetti, M.; Luzon, J.; Etienne, M.; Car, P.-E.; Caneschi, A.; Calvez, G.; Bernot, K.; Sessoli, R. *Angew. Chem. Int. Ed.* **2012**, *51*, 1606–1610.
(92) Souza, A. S.; Couto dos Santos, M. A. *Chem. Phys. Lett.* **2012**, *521*, 138–141.
(93) Jensen, J.; Mackintosh, A. R. *Rare Earth Magnetism*; The international series of mongraphs of physics; Clarendon Press: Oxford, 1991.
(94) Ma, C.-G.; Brik, M. G.; Kiisk, V.; Kangur, T.; Sildos, I. *J. Alloys Compd.* **2011**, *509*, 3441–3451.
(95) Auzel, F.; Malta, O. L. *J. Phys.* **1983**, *44*, 201–206.
(96) Malta, O. L.; Antic-Fidancev, E.; Lemaitre-Blaise, M.; Milicic-Tang, A.; Taibi, M. *J. Alloys Compd.* **1995**, *228*, 41–44.
(97) Ashcroft, N. W.; Mermin, N. D. *Solid state physics*; Saunders College, 1976.
(98) Evans, D. F.; James, T. A. *J. Chem. Soc. Dalton Trans.* **1979**, 723–726.
(99) Sur, S. K. *J. Magn. Reson. 1969* **1989**, *82*, 169–173.
(100) Corsi, D. M.; Platas-Iglesias, C.; Bekkum, H. van; Peters, J. A. *Magn. Reson. Chem.* **2001**, *39*, 723–726.
(101) Aime, S.; Batsanov, A. S.; Botta, M.; Dickins, R. S.; Faulkner, S.; Foster, C. E.; Harrison, A.; Howard, J. A. K.; Moloney, J. M.; Norman, T. J.; Parker, D.; Royle, L.; Williams, J. A. G. *J. Chem. Soc. Dalton Trans.* **1997**, 3623–3636.

(102) Lacheisserie, E. du T. de; Gignoux, D.; Schlenker, M. *Magnetism: Materials and Applications*; Springer Science & Business Media, 2005.
(103) Bünzli, J.-C. G.; Piguet, C. *Chem. Soc. Rev.* **2005**, *34*, 1048–1077.
(104) Kim, J.-G.; Yoon, S.-K.; Sohn, Y.; Kang, J.-G. *J Alloys Compd* **1998**, *274*, 1–9.
(105) Kang, J.-G.; Na, M.-K.; Yoon, S.-K.; Sohn, Y.; Kim, Y.-D.; Suh, I.-H. *Inorg Chim Acta* **2000**, *310*, 56–64.
(106) Gruber, J. B.; Leavitt, R. P.; Morrison, C. A.; Chang, N. C. *J Chem Phys* **1985**, *82*, 5373–5378.
(107) Liusen, H.; Michael, F. R.; Chang-Kui, D.; Shangda, X.; Min, Y. *J. Phys. Condens. Matter* **2011**, *23*, 045501.
(108) Charnock, G. T. P.; Kuprov, I. *Phys. Chem. Chem. Phys.* **2014**, *16*, 20184–20189.
(109) Dickins, R. S.; Howard, J. A. K.; Maupin, C. L.; Moloney, J. M.; Parker, D.; Riehl, J. P.; Siligardi, G.; Williams, J. A. G. *Chem Eur J* **1999**, *5*, 1095–1105.
(110) Harvey, P. Paramagnetic Probes for Magnetic Resonance. Doctoral, Durham University, 2013.
(111) Woods, M.; Aime, S.; Botta, M.; Howard, J. A. K.; Moloney, J. M.; Navet, M.; Parker, D.; Port, M.; Rousseaux, O. *J. Am. Chem. Soc.* **2000**, *122*, 9781–9792.
(112) Motulsky, H.; Christopoulos, A. *Fitting Models to Biological Data Using Linear and Nonlinear Regression: A Practical Guide to Curve Fitting*; Oxford University Press, 2004.

Appendices

The following appendices contain all the relaxation and shift data that lead to the values presented in the main text. The Appendices follow the order of the lanthanide(III) series for each discussion chapter.

Appendix 1 : List of examined complexes

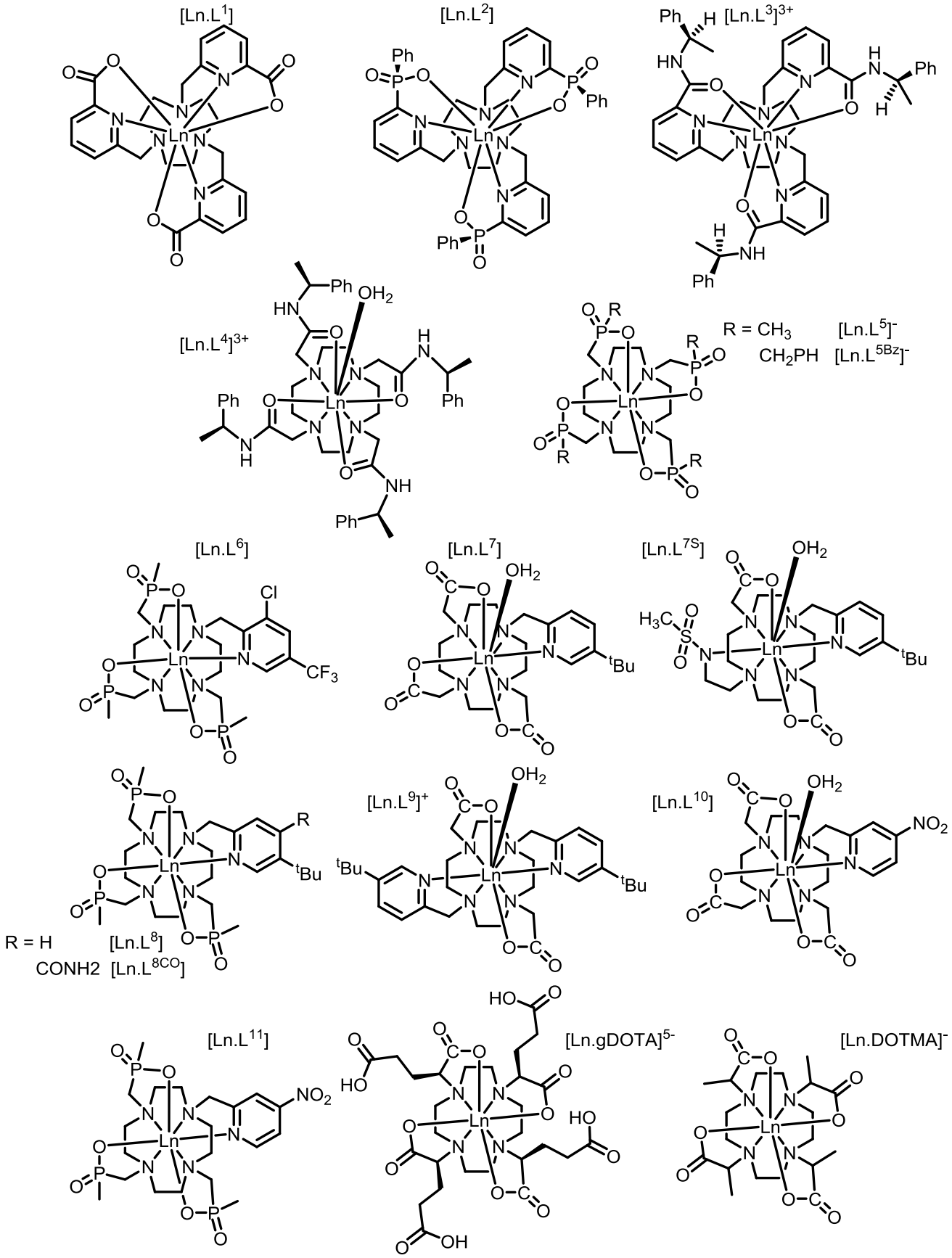

SI-Figure 1 : *Structures of all complexes examined in this discussion*

Appendix 2 : Electronic Relaxation times estimated through analysis of nuclear relaxation rates

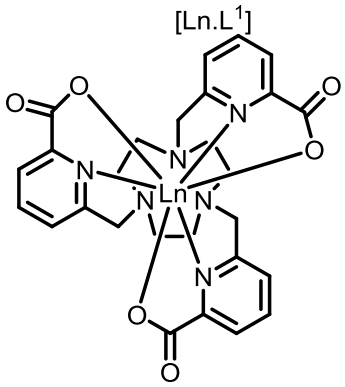

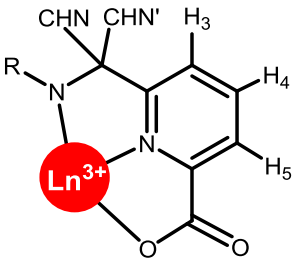

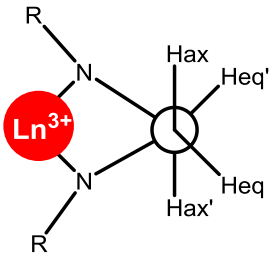

SI-Table 1 : *^{1}H nuclear relaxation rates,R_1, and single fitting values (μ_{eff} = 9.8 BM) for [Tb.L^1] (295 K, D_2O).*

^{1}H	R_1/ s^{-1}					Fitting values		
	4.7 T	9.4 T	11.7 T	14.1 T	16.5 T	*r* / Å	τ_R / ps	T_{1e} / ps
pyH^4	44 ±3	85 ±5	131 ±21	152 ±7	177 ±12	6.48	196.5	0.19
pyH^3	108 ±6	195 ±5	258 ±5	316 ±9	390 ±15	5.58	124.0	0.29
Hax'	499 ±57	1027 ±55	1484 ±86	1639 ±149	1957 ±166	4.36	229.7	0.20
Heq	392 ±25	768 ±25	995 ±41	1268 ±50	1465 ±43	4.55	172.2	0.27
Hax	465 ±28	869 ±45	1155 ±59	1398 ±39	1607 ±50	4.51	195.3	0.30
pyCHN'	403 ±11	714 ±45	1002 ±21	1346 ±30	1575 ±54	4.34	107.5	0.21

SI-Table 2 : *^{1}H nuclear relaxation rates,R_1, and single fitting values (μ_{eff} = 10.3 BM) for [Dy.L^1] (295 K, D_2O).*

^{1}H	R_1/ s^{-1}					Fitting values		
	4.7 T	9.4 T	11.7 T	14.1 T	16.5 T	*r* / Å	τ_R / ps	T_{1e} / ps
pyH^5	125 ±6	238 ±6	314 ±6	395 ±12	503 ±9	5.31	85.4	0.23
pyH^4	64 ±2	126 ±1	164 ±2	211 ±3	258 ±3	6.15	121.6	0.26
pyH^3	130 ±7	255 ±3	347 ±6	414 ±20	513 ±11	5.58	151.5	0.28
Heq	435 ±32	776 ±33	1252 ±37	1576 ±243	1787 ±42	4.50	156.3	0.20

SI-Table 3 : *^{1}H nuclear relaxation rates,R_1, and single fitting values (μ_{eff} = 10.4 BM) for [Ho.L^1] (295 K, D_2O).*

^{1}H	R_1/ s^{-1}					Fitting values		
	4.7 T	9.4 T	11.7 T	14.1 T	16.5 T	*r* / Å	τ_R / ps	T_{1e} / ps
pyH^5	91 ±6	210 ±6	305 ±26	382 ±13	509 ±26	5.21	75.8	0.12
pyH^4	48 ±2	103 ±2	142 ±5	184 ±3	232 ±6	6.16	100.5	0.17
pyH^3	92 ±11	298 ±27	283 ±51	423 ±51	538 ±51	5.47	125.1	0.18
pyCHN	362 ±10	819 ±30	1245 ±32	1556 ±43	1777 ±60	4.55	193.4	0.12

SI-Table 4 : *^{1}H nuclear relaxation rates,R_1, and single fitting values (μ_{eff} = 9.4 BM) for [Er.L^1] (295 K, D_2O).*

^{1}H	R_1/ s^{-1}					Fitting values		
	4.7 T	9.4 T	11.7 T	14.1 T	16.5 T	*r* / Å	τ_R / ps	T_{1e} / ps
pyH^3	87 ±5	176 ±8	233 ±13	284 ±27	358 ±48	5.52	130.3	0.22
pyH^4	39 ±2	68 ±3	88 ±4	119 ±2	140 ±3	6.34	105.5	0.24
pyH^5	84 ±5	181 ±8	223 ±10	272 ±10	325 ±10	5.89	199.4	0.25
Heq	365 ±30	667 ±19	1137 ±47	1352 ±58	1666 ±196	4.40	148.1	0.17
Heq'	389 ±20	657 ±48	1085 ±51	1281 ±67	1597 ±67	4.21	107.7	0.18

SI-Table 5: *^{1}H nuclear relaxation rates,R_1, and single fitting values (μ_{eff} = 7.6 BM) for [Tm.L^1] (295 K, D_2O).*

^{1}H	R_1/ s^{-1}					Fitting values		
	4.7 T	9.4 T	11.7 T	14.1 T	16.5 T	*r* / Å	τ_R / ps	T_{1e} / ps
CHN'	414 ±7	989±44	1431±33	1872±321	2295±108	3.48	132.5	0.07
pyH$^{3/5}$	25 ±1	61 ±0.3	84 ±0.2	108 ±0.3	134 ±0.5	5.63	140.5	0.08
pyH^4	12 ±0.2	27 ±0.2	37 ±0.1	48 ±0.2	60 ±0.3	6.36	116.6	0.09
Hax'	400±19	971±51	1433±52	1745±143	2159±69	3.57	164.2	0.07
CHN	102±85	209 ±8	311 ±8	362 ±19	471 ±21	4.55	122.5	0.11
Heq	82 ±12	201 ±5	282 ±1	365 ±2	454 ±3	4.57	133.5	0.07
Heq'	94 ±1	226 ±4	321 ±2	415 ±3	515 ±3	4.47	132.0	0.07
Hax	116 ±2	277 ±5	390 ±3	510 ±3	636 ±9	4.29	121.5	0.07

SI-Table 6 *^{1}H nuclear relaxation rates,R_1, and single fitting values (μ_{eff} = 4.5 BM) for [Yb.L^1] (295 K, D_2O).*

^{1}H	R_1/ s^{-1}					Fitting values		
	4.7 T	9.4 T	11.7 T	14.1 T	16.5 T	*r* / Å	τ_R / ps	T_{1e} / ps
pyCHN'	89 ±1	159 ±2	210 ±3	257 ±4	311 ±4	3.41	134.7	0.06
pyH^3	5.7 ±0.2	9.5 ±0.5	12.5 ±0.1	12.8 ±0.7	18.6 ±0.2	5.46	112.4	0.07
pyH^4	3.1 ±0.1	4.8 ±0.2	5.8 ±0.1	7.4 ±0.4	8.4 ±0.1	6.29	128.7	0.10
pyH^5	5.4 ±0.1	9.4 ±0.4	12.0 ±0.1	15.4 ±0.7	17.8 ±0.1	5.45	13.5	0.06
CHN	27 ±3	34 ±2	46 ±1	61 ±1	54 ±1	4.42	99.9	0.11
Heq	21 ±1	32 ±1	42 ±1	52 ±1	62 ±1	4.34	92.5	0.07
Heq'	23 ±1	36 ±1	48 ±1	59 ±1	70 ±1	4.33	112.1	0.08
Hax	29 ±1	44 ±1	59 ±1	73 ±1	88 ±1	4.01	79.4	0.06

SI-Table 7 : *Individual estimated values of the effective magnetic moment, μ_{eff}, the electronic relaxation time, T_{1e} and the rotational correlation time, τ_R, using global fitting procedures for the quoted resonances of [Ln.L^1] (295 K, D_2O).*

Ln^{3+}	pyH^3		pyH^4	
	μ_{eff} / BM	T_{1e} / ps	μ_{eff} / BM	T_{1e} / ps
Tb	9.63	0.29	9.67	0.24
Dy	10.38	0.29	10.56	0.28
Ho	10.55	0.18	10.34	0.17
Er	9.46	0.22	9.01	0.23
Tm	7.49	0.08	7.37	0.08
Yb	4.34	0.07	4.20	0.11
τ_R / ps	135.3		129.5	

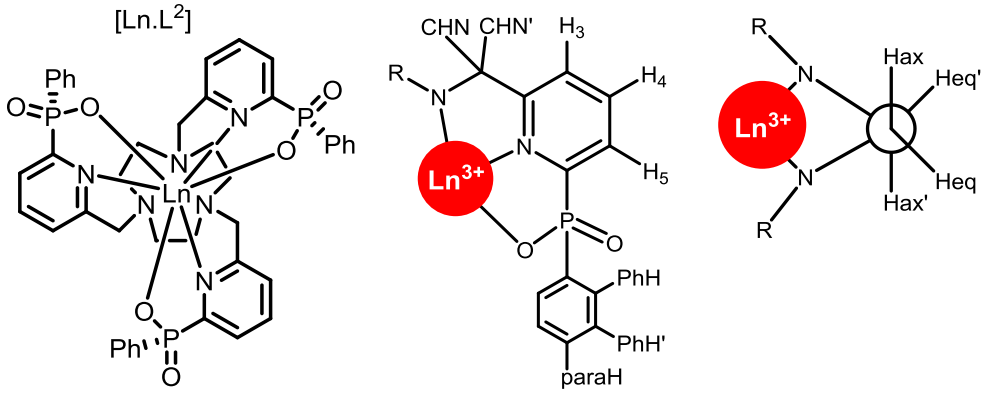

SI-Table 8 : *^{1}H nuclear relaxation rates, R_1, and single fitting values (μ_{eff} = 9.8 BM) for [Tb.L^2] (295 K, CD_3OD).*

^{1}H	R_1/ s^{-1}					Fitting values		
	4.7 T	9.4 T	11.7 T	14.1 T	16.5 T	*r* / Å	τ_R / ps	T_{1e} / ps
Hax'	571 ±18	1178 ±12	1528 ±14	1834 ±22	2208 ±24	4.27	86.7	0.26
Hax	526 ±7	1090 ±11	1357 ±5	1687 ±15	2057 ±26	4.30	160.3	0.27
CHN	384 ±11	809 ±12	1022 ±6	1298 ±26	1550 ±26	4.50	164.8	0.24
PhH'	34 ±1	69 ±1	89 ±1	107 ±1	127 ±1	6.88	194.8	0.27
PhH	14 ±0.1	27 ±1	35 ±1	41 ±1	49 ±1	8.08	196.5	0.31
pyH^5	89 ±1	181 ±1	234 ±1	287 ±3	330 ±6	5.87	206.6	0.25
pyH^4	43 ±1	87 ±1	109 ±1	133 ±1	153 ±1	6.68	214.9	0.28
pyH^3	97 ±2	199 ±2	252 ±2	305 ±3	351 ±6	5.81	220.63	0.26
Heq	388 ±6	806 ±13	1031 ±12	1143 ±31	1471 ±27	4.59	189.6	0.29
CHN'	1877 ±63	3253 ±125	4572 ±82	5848 ±230	6784 ±183	3.52	159.2	0.29

SI-Table 9 : *^{1}H nuclear relaxation rates, R_1, and single fitting values (μ_{eff} = 10.3 BM) for [Dy.L^2] (295 K, CD_3OD).*

^{1}H	R_1/ s^{-1}					Fitting values		
	4.7 T	9.4 T	11.7 T	14.1 T	16.5 T	*r* / Å	τ_R / ps	T_{1e} / ps
Hax'	787 ±25	1608 ±16	2058 ±7	2546 ±20	2895 ±71	4.22	212.8	0.28
Hax	710 ±27	1484 ±9	1848 ±5	2312 ±13	2593 ±45	4.30	225.6	0.27
PhH'	46 ±1	93 ±1	131 ±4	149 ±2	182 ±2	6.69	19.5	0.26
PhH	20 ±1	37 ±1	52 ±1	59 ±1	72 ±1	7.81	181.0	0.32
pyH^5	136 ±2	261 ±5	310 ±16	414 ±13	459 ±12	5.73	187.0	0.36
pyH^3	150 ±2	282 ±5	344 ±7	455 ±7	518 ±11	5.59	213.6	0.35

SI-Table 10 : *^{1}H nuclear relaxation rates, R_1, and single fitting values (μ_{eff} = 10.4 BM) for [Ho.L^2] (295 K, CD_3OD).*

^{1}H	R_1/ s^{-1}					Fitting values		
	4.7 T	9.4 T	11.7 T	14.1 T	16.5 T	*r* / Å	τ_R / ps	T_{1e} / ps
PhH	25 ±3	55 ±1	68 ±1	84 ±2	98 ±2	7.46	206.8	0.26
pyH^5	94 ±4	199 ±10	278 ±19	394 ±25	482 ±25	5.21	72.4	0.12
pyH^4	44 ±2	102 ±4	141 ±5	170 ±4	203 ±4	6.58	199.5	0.17
pyH^3	92 ±4	218 ±13	299 ±8	382 ±8	433 ±16	5.78	207.0	0.14
Heq'	458 ±7	1076 ±26	1367 ±37	1658 ±36	2166 ±38	4.38	135.9	0.23

SI-Table 11 : *^{1}H nuclear relaxation rates, R_1, and single fitting values (μ_{eff} = 9.4 BM) for [Er.L^2] (295 K, CD_3OD).*

^{1}H	R_1/ s^{-1}					Fitting values		
	4.7 T	9.4 T	11.7 T	14.1 T	16.5 T	*r* / Å	τ_R / ps	T_{1e} / ps
CHN'	1893 ±32	3562 ±104	4391 ±44	5408 ±194	6592 ±271	3.43	181.6	0.24
pyH^5	98 ±1	182 ±2	233 ±4	280 ±3	327 ±6	5.73	192.0	0.31
pyH^3	107 ±2	192 ±2	245 ±3	295 ±3	343 ±6	5.69	188.3	0.33
pyH^4	49 ±1	88 ±1	108 ±1	131 ±1	151 ±1	6.53	198.2	0.36
PhH'	33 ±1	58 ±1	74 ±1	90 ±1	104 ±1	6.93	182.8	0.35
Hax	485 ±11	917 ±11	1184 34±	1427 ±39	1662 ±64	4.37	194.1	0.29
Heq	381 ±9	731 ±12	938 ±31	1120 ±33	1319 ±52	4.54	195.3	0.29
CHN	434 ±12	802 ±18	1048 ±30	1252 ±29	1473 ±49	4.45	185.5	0.30
Hax'	553 ±14	1033 ±16	1314 ±31	1586 ±26	1832 ±13	4.30	200.0	0.31

SI-Table 12 : *^{1}H nuclear relaxation rates, R_1, and single fitting values (μ_{eff} = 7.6 BM) for [Tm.L^2] (295 K, CD_3OD).*

^{1}H	R_1/ s^{-1}					Fitting values		
	4.7 T	9.4 T	11.7 T	14.1 T	16.5 T	*r* / Å	τ_R / ps	T_{1e} / ps
CHN'	574±10	1304±35	1700±26	2133±16	2544±88	3.51	182.0	0.11
pyH^3	30±1	69±0.3	92±1	116±1	139±1	5.68	174.1	0.10
pyH^5	28±1	65±0.4	86±1	109±1	130±0.4	5.75	177.2	0.10
pyH^4	13±0.4	31±0.2	40±0.2	50±0.2	56±0.1	6.61	243.9	0.08
Hax'	517±18	1390±53	1550±26	1806±91	2459±25	3.56	178.6	0.14
CHN	120±1	287±3	398±2	495±1	558±13	4.49	227.2	0.06
Heq	104±1	244±2	333±1	415±1	475±12	4.63	215.1	0.08
Heq'	114±1	261±3	360±2	442±1	504±14	4.59	221.6	0.08
Hax	133±2	323±3	430±3	542±1	631±6	4.42	205.0	0.08

SI-Table 13 : *^{1}H nuclear relaxation rates, R_1, and single fitting values (μ_{eff} = 4.5 BM) for [Yb.L^2] (295 K, CD_3OD).*

^{1}H	R_1/ s^{-1}					Fitting values		
	4.7 T	9.4 T	11.7 T	14.1 T	16.5 T	*r* / Å	τ_R / ps	T_{1e} / ps
CHN'	104 ±1	193 ±1	243 ±3	283 ±1	326 ±1	3.45	228.7	0.07
pyH$^{3/5}$	6.2 ±0.1	10.5 ±0.5	12.7 ±0.1	15.0 ±0.1	17.1 ±0.1	5.68	214.3	0.09
pyH^4	4.3 ±0.1	5.7 0.2±	6.5 ±0.1	7.4 ±0.1	8.3 ±0.1	6.58	193.2	0.18
CHN	23 ±2	43 ±1	54 ±1	66 ±1	79 ±1	4.34	161.4	0.07
Heq	23 ±2	37 ±1	46 ±1	55 ±1	63 ±1	4.57	174.1	0.10
Heq'	27 ±1	42 ±1	52 ±1	62 ±1	70 ±1	4.51	178.4	0.11
Hax	33 ±1	51 ±1	64 ±1	75 ±1	87 ±1	4.34	162.2	0.11

SI-Table 14 : *^{31}P nuclear relaxation rates of [Ln.L^2] used for global fitting (295 K, CD$_3$OD).*

Ln^{3+}	δ_H / ppm	R_1/ s^{-1}				
		4.7 T	9.4 T	11.7 T	14.1 T	16.5 T
Eu	16.6	2.5±0.1	7.5±0.2	10.5±0.1	13.9±0.1	18.1±0.1
Tb	-35.7	242±3	603±11	824±4	1071±9	1322±11
Dy	-15.9	332±10	876±15	1213±7	1619±27	1978±18
Ho	-24.6	247±3	701±21	1026±3	1341±18	1709±19
Er	-10.5	248±6	533±10	745±3	963±13	1202±10
Tm	8.4	64±1	194±6	271±2	358±3	463±3
Yb	17.7	11±0.3	24±0.4	34±0.2	42±0.2	54±0.1

SI-Table 15 : *Individual estimated values of the effective magnetic moment, μ_{eff}, the electronic relaxation time, T_{1e} and the rotational correlation time, τ_R, using global fitting procedures for the quoted resonances of [Ln.L^2] (295 K, CD$_3$OD).*

	H_{ax}		H_{eq}		pyH^3		pyH^5		^{31}P	
Ln^{3+}	μ_{eff} / BM	T_{1e} / ps	μ_{eff} / BM	T_{1e} / ps	μ_{eff} / BM	T_{1e} / ps	μ_{eff} / BM	T_{1e} / ps	μ_{eff} / BM	T_{1e} / ps
Tb	9.81	0.22	8.73	0.19	8.31	0.21	8.19	0.21	8.75	0.28
Dy	10.48	0.31	9.39	0.24	9.16	0.33	8.98	0.23	9.72	0.26
Ho	10.27	0.15	8.98	0.11	11.04	0.16	11.64	0.14	9.39	0.13
Er	9.28	0.27	8.29	0.24	10.18	0.38	10.43	0.41	8.50	0.31
Tm	7.34	0.10	8.92	0.16	8.22	0.09	8.34	0.13	6.76	0.06
Yb	4.15	0.14	5.25	0.13	4.67	0.11	4.80	0.12	3.84	0.07
τ_R / ps	207		130		203		131		328	

SI-Table 16 *^{31}P relaxation rates at a range of temperature K for [Tm.L^2], (CD$_3$OD, 16.5 T, 1 mM).*

R_1 / s^{-1}	T	1 / T^2 x 10^{-3}
463	295	0.0115
446	297	0.0114
426	299	0.0112
413	301	0.0111
397	302	0.0109

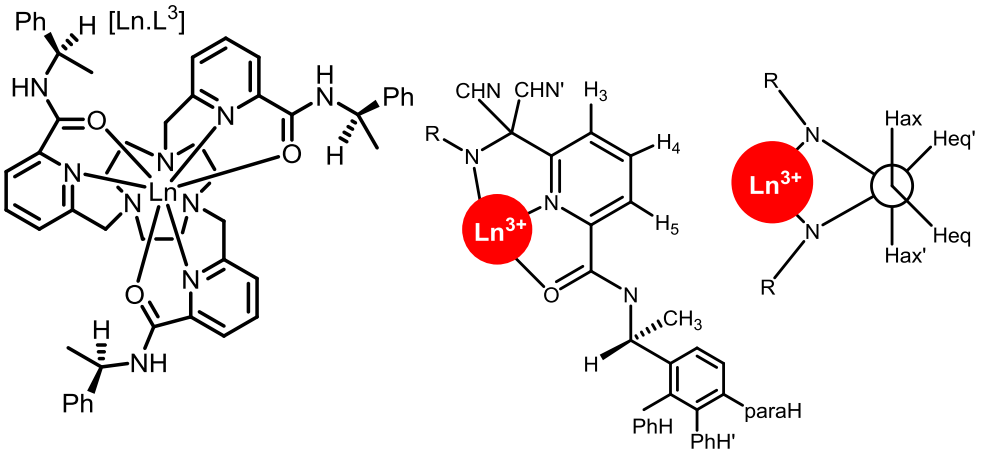

SI-Table 17 : *^{1}H nuclear relaxation rates,R_1, and single fitting values (μ_{eff} = 9.8 BM) for [Tb.L^3]$^{3+}$ (295 K, CD_3OD).*

^{1}H	R_1/ s^{-1}					Fitting values		
	4.7 T	9.4 T	11.7 T	14.1 T	16.5 T	*r* / Å	τ_R / ps	T_{1e} / ps
Hax'	793 ±45	1471 ±41	1828 ±25	2230 ±31	2574 ±58	4.18	198.1	0.35
Heq	336 ±7	668 ±28	880 ±20	999 ±36	1204 ±33	4.75	214.2	0.28
CH_3	53 ±1	96 ±1	122 ±1	147 ±1	170 ±1	6.57	196.2	0.36
H	95 ±2	169 ±2	210 ±1	262 ±3	305 ±4	5.93	169.2	0.37
PhH	23 ±1	40 ±1	50 ±1	59 ±1	67 ±2	7.70	221.6	0.41
pyH^4	46 ±3	93 ±1	122 ±1	148 ±2	168 ±3	6.56	220.0	0.24
pyH^5	115 ±2	216 ±6	294 ±4	361 ±6	400 ±16	5.67	210.4	0.27
pyH^3	122 ±3	226 ±4	305 ±7	365 ±8	433 ±10	5.59	174.4	0.30

SI-Table 18 : *^{1}H nuclear relaxation rates,R_1, and single fitting values (μ_{eff} = 10.3 BM) for [Dy.L^3]$^{3+}$ (295 K, CD_3OD).*

^{1}H	R_1/ s^{-1}					Fitting values		
	4.7 T	9.4 T	11.7 T	14.1 T	16.5 T	*r* / Å	τ_R / ps	T_{1e} / ps
PhH	23 ±1	40 ±3	49 ±1	61 ±2	69 ±3	7.89	195.5	0.45
PhH'	29 ±1	53 ±2	70 ±1	84 ±1	99 ±2	7.40	180.5	0.36
pyH^4	59 ±3	114 ±5	141 ±6	176 ±5	212 ±5	6.49	158.2	0.35
pyH^3	94 ±3	187 ±5	249 ±15	315 ±10	385 ±22	5.79	133.5	0.26

SI-Table 19 : *^{1}H nuclear relaxation rates,R_1, and single fitting values (μ_{eff} = 10.4 BM) for [Ho.L^3]$^{3+}$ (295 K, CD_3OD).*

^{1}H	R_1/ s^{-1}					Fitting values		
	4.7 T	9.4 T	11.7 T	14.1 T	16.5 T	*r* / Å	τ_R / ps	T_{1e} / ps
Hax'	721 ±51	1544 ±24	2299 ±123	2494 ±116	3252 ±93	4.15	173.6	0.21
Heq	328 ±7	830 ±37	1026 ±19	1216 ±31	1647 ±99	4.59	135.2	0.22
Heq'	448 ±13	1044 ±47	1359 ±30	1531 ±66	1864 ±150	4.56	248.5	0.18
CH_3	50 ±1	113 ±2	145 ±1	178 ±2	226 ±10	6.41	145.5	0.24
H	81 ±1	184 ±2	240 ±4	296 ±2	362 ±19	5.97	163.6	0.24
PhH'	20 ±1	47 ±1	63 ±1	72 ±1	95 ±6	7.45	159.8	0.22
pyH^3	112 ±4	262 ±10	378 ±6	405 ±9	475 ±46	5.67	238.5	0.15

SI-Table 20 : *^{1}H nuclear relaxation rates,R_1, and single fitting values (μ_{eff} = 9.4 BM) for $[Er.L^3]^{3+}$ (295 K, CD_3OD).*

^{1}H	R_1/ s^{-1}					Fitting values		
	4.7 T	9.4 T	11.7 T	14.1 T	16.5 T	*r* / Å	τ_R / ps	T_{1e} / ps
pyH^4	36 ±2	61 ±3	93 ±7	108 ±7	122 ±7	6.65	144.1	0.29
PhH	18 ±1	30 ±1	40 ±1	46 ±1	54 ±1	7.75	189.8	0.38
CH_3	52 ±1	85 ±1	107 ±1	132 ±2	153 ±2	6.47	160.2	0.40

SI-Table 21 : *^{1}H nuclear relaxation rates,R_1, and single fitting values (μ_{eff} = 7.6 BM) for $[Tm.L^3]^{3+}$ (295 K, CD_3OD).*

^{1}H	R_1/ s^{-1}					Fitting values		
	4.7 T	9.4 T	11.7 T	14.1 T	16.5 T	*r* / Å	τ_R / ps	T_{1e} / ps
CHN'	566±20	1413±97	1718±20	2088±43	2482±76	3.53	239.3	0.09
pyH^3	31±0.3	75±2	105±1	125±2	149±2	5.62	213.9	0.07
pyH^4	18±0.4	40±2	53±1	63±1	73±1	6.36	234.4	0.11
PhH'	6±0.1	13±0.1	16±0.1	20±0.1	24±0.2	7.68	179.4	0.15
PhH	4±0.1	8±0.1	10±0.1	12±0.2	15±0.2	8.27	150.7	0.19
H	22±0.1	50±0.4	65±0.3	82±1	97±1	6.71	186.5	0.15
CH_3	14±0.1	29±0.1	37±0.1	46±0.2	54±0.1	6.05	185.6	0.11
CHN	80±1	202±6	256±3	314±4	363±3	4.84	246.4	0.07
Heq	118±3	283±5	366±4	443±4	512±8	4.58	242.7	0.08
Heq'	130±24	327±10	411±9	501±6	580±9	4.48	251.8	0.07
Hax	158±2	377±9	479±5	589±4	699±5	4.36	212.6	0.10

SI-Table 22 : *^{1}H nuclear relaxation rates,R_1, and single fitting values (μ_{eff} = 4.5 BM) for $[Yb.L^3]^{3+}$ (295 K, CD_3OD).*

^{1}H	R_1/ s^{-1}					Fitting values		
	4.7 T	9.4 T	11.7 T	14.1 T	16.5 T	*r* / Å	τ_R / ps	T_{1e} / ps
pyH^3	7.4 ±1	12.0 ±1	15.3 ±1	17.4 ±1	20.6 ±1	5.47	160.6	0.09
pyH^5	7.9 ±1	12.3 ±1	15.8 ±1	17.8 ±1	21.2 ±1	5.51	170.8	0.11
pyH^4	5.0 ±1	7.3 ±1	8.6 ±1	10.1 ±1	10.7 ±1	6.23	211.2	0.15
CHN	19 ±1	29 ±1	39 ±1	46 ±1	53 ±1	4.67	156.0	0.10
Heq	30 ±1	43 ±1	56 ±1	65 ±1	74 ±1	4.46	157.2	0.12
Heq'	34 ±1	48 ±1	63 ±1	73 ±1	83 ±1	4.38	153.7	0.12
Hax	43 ±1	62 ±1	78 ±1	89 ±1	102 ±1	4.26	166.3	0.14

SI-Table 23 : *Individual estimated values of the effective magnetic moment, μ_{eff}, the electronic relaxation time, T_{1e} and the rotational correlation time, τ_R, using global fitting procedures for the quoted resonances of $[Ln.L^3]^{3+}$ (295 K, CD_3OD).*

Ln^{3+}	pyH^3		pyH^4	
	μ_{eff} / BM	T_{1e} / ps	μ_{eff} / BM	T_{1e} / ps
Tb	10.03	0.32	9.59	0.27
Dy	9.76	0.20	10.09	0.29
Ho	10.32	0.25	10.31	0.21
Er	8.95	0.30	8.80	0.22
Tm	7.76	0.11	7.77	0.15
Yb	4.53	0.10	4.56	0.17
τ_R / ps	173.0		196.0	

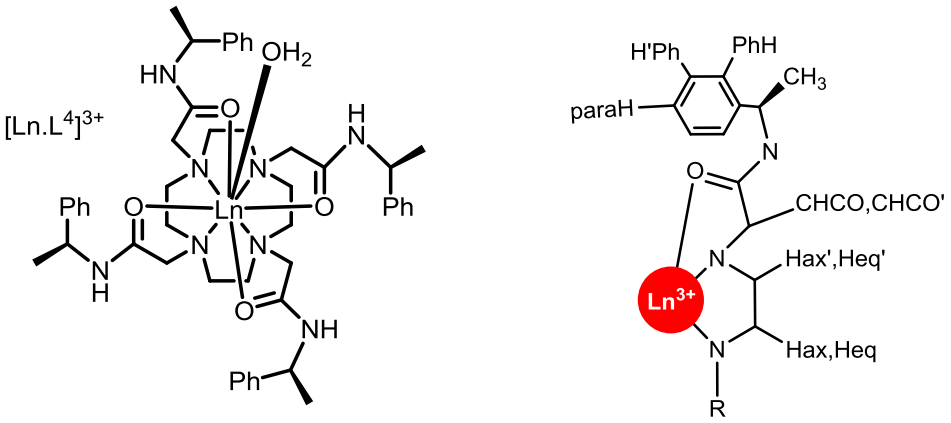

SI-Table 24 : *^1H nuclear relaxation rates,R_1, and single fitting values (μ_{eff} = 9.8 BM) for $[Tb.L^4]^{3+}$ (295 K, D_2O).*

^1H	R_1/ s^{-1}					Fitting values		
	4.7 T	9.4 T	11.7 T	14.1 T	16.5 T	r / Å	τ_R / ps	T_{1e} / ps
Hax'	3020 ±82	379 ±172	5527 ±41	6050 ±168	6693 ±398	3.58	268.9	0.63
CHCO'	2699 ±83	4088 ±339	4588 ±23	4940 ±116	5263 ±186	3.66	289.4	0.55
paraH	48 ±1	75 ±1	85 ±1	92 ±1	101 ±2	7.13	350.3	0.55
PhH'	76 ±1	121 ±1	135 ±1	148 ±1	161 ±2	6.58	358.4	0.52
PhH	224 ±1	363 ±1	407 ±1	429 ±3	477 ±15	5.47	386.6	0.46
CH_3	66 ±1	101 ±1	114 ±1	125 ±1	131 ±1	6.77	382.2	0.53
Heq'	708 ±12	1111 ±7	1275 ±5	1405 ±6	1554 ±33	4.55	316.9	0.56
Hax	1453 ±12	2205 ±145	2840 ±8	3136 ±23	3420 ±58	3.99	272.3	0.53

SI-Table 25 : *^1H nuclear relaxation rates,R_1, and single fitting values (μ_{eff} = 10.3 BM) for $[Dy.L^4]^{3+}$ (295 K, D_2O).*

^1H	R_1/ s^{-1}					Fitting values		
	4.7 T	9.4 T	11.7 T	14.1 T	16.5 T	r / Å	τ_R / ps	T_{1e} / ps
Hax'	3117 ±98	6114 ±128	6916 ±171	7722 ±268	9381 ±827	3.50	266.7	0.41
paraH	53 ±1	92 ±1	103 ±1	115 ±1	125 ±1	7.07	360.2	0.43
PhH'	83 ±1	146 ±1	166 ±1	184 1±	198 ±2	6.51	376.0	0.38
CH_3	76 ±1	126 ±1	144 ±1	160 2±	171 ±2	6.70	360.1	0.47
Heq'	785 ±11	1374 ±10	1600 ±8	1799 17±	2016 ±85	4.49	301.8	0.46
Heq	762 ±10	1379 ±13	1602 ±12	1784 ±20	1981 ±66	4.48	329.5	0.39
Hax	1769 ±52	3038 ±71	3633 ±47	3959 ±51	4448 ±57	3.93	314.6	0.46

SI-Table 26 : *^{1}H nuclear relaxation rates,R_1, and single fitting values (μ_{eff} = 10.4 BM) for $[Ho.L^4]^{3+}$ (295 K, D_2O).*

^{1}H	R_1/ s^{-1}					Fitting values		
	4.7 T	9.4 T	11.7 T	14.1 T	16.5 T	*r* / Å	τ_R / ps	T_{1e} / ps
CHCO'	1955 ±321	3715 ±121	4590 ±53	5214 ±241	6231 ±319	3.76	230.2	0.39
paraH	37 ±1	71 ±1	72 ±1	93 ±1	98 ±1	7.45	307.0	0.43
PHH'	189 ±8	356 ±3	388 ±3	443 ±3	461 ±6	6.85	305.4	0.41
CH_3	52 ±1	97 ±1	115 ±1	130 ±1	137 ±1	6.94	369.2	0.29
Heq'	613 ±9	1185 ±12	1406 ±11	1595 ±12	1707 ±46	4.57	358.3	0.27
Heq	612 ±9	1185 ±6	1410 ±14	1590 ±12	1708 ±47	4.57	360.6	0.26

SI-Table 27 : *^{1}H nuclear relaxation rates,R_1, and single fitting values (μ_{eff} = 9.4 BM) for $[Er.L^4]^{3+}$ (295 K, D_2O).*

^{1}H	R_1/ s^{-1}					Fitting values		
	4.7 T	9.4 T	11.7 T	14.1 T	16.5 T	*r* / Å	τ_R / ps	T_{1e} / ps
PhH	33 ±1	60 ±3	77 ±1	88 ±1	97 ±2	7.01	270.8	0.30
paraH	20 ±1	35 ±2	45 ±1	51 ±1	57 ±1	7.68	256.9	0.34
CH_3	30 ±1	56 ±1	69 ±1	78 ±1	85 ±1	7.12	312.3	0.27

SI-Table 28 : *^{1}H nuclear relaxation rates,R_1, and single fitting values (μ_{eff} = 7.6 BM) for $[Tm.L^4]^{3+}$ (295 K, D_2O).*

^{1}H	R_1/ s^{-1}					Fitting values		
	4.7 T	9.4 T	11.7 T	14.1 T	16.5 T	*r* / Å	τ_R / ps	T_{1e} / ps
Heq'	253 ±1	468 ±8	521 ±1	584 ±3	617 ±2	4.35	439.0	0.14
Heq	248 ±1	453 ±7	506 ±1	566 ±3	601 ±1	4.39	421.5	0.16
CH_3	18 ±1	28 ±1	33 ±1	36 ±1	38 ±1	7.14	341.1	0.33
CHCO	201 ±1	364 ±2	421 ±1	472 ±1	518 ±7	4.60	334.1	0.22
CHCO'	597 ±12	1052 ±14	1186 ±1	1354 ±4	1426 ±6	3.86	365.9	0.22
Hax	536 ±2	999 ±15	1187 ±7	1316 ±2	1412 ±7	3.84	376.6	0.16

SI-Table 29 : *^{1}H nuclear relaxation rates,R_1, and single fitting values (μ_{eff} = 4.5 BM) for $[Yb.L^4]^{3+}$ (295 K, D_2O).*

^{1}H	R_1/ s^{-1}					Fitting values		
	4.7 T	9.4 T	11.7 T	14.1 T	16.5 T	*r* / Å	τ_R / ps	T_{1e} / ps
Hax'	163 ±1	242 ±1	271 ±1	298 ±1	312 ±1	3.53	353.6	0.15
Heq'	51 ±1	69 ±1	77 ±1	84 ±1	87 ±1	4.45	312.1	0.21
Heq	50 ±1	67 ±1	75 ±1	82 ±1	85 ±1	4.48	299.3	0.22
PhH''	11 ±1	15 ±1	18 ±1	19 ±1	20 ±1	5.65	310.2	0.18
CHCO	41 ±1	56 ±1	62 ±1	68 ±1	69 ±1	4.59	346.5	0.20
CHCO'	106 ±1	157 ±1	173 ±1	190 ±1	196 ±1	3.78	393.8	0.14
Hax	98 ±1	148 ±1	169 ±1	186 ±1	192 ±1	3.79	372.8	0.13

SI-Table 30 : *Nuclear relaxation rates, R_1, and single fitted values (μ_{eff} = 9.8 BM) for $[Tb.L^4]^{3+}$ (295 K, CD_3OD).*

^{1}H	R_1 / sec^{-1}					Fitted values		
	4.7	9.4	11.7	14.1	16.5	*r* / Å	τ_R / ps	T_{1e} / ps
CHCO	860 ±48	1371 ±55	1728 ±24	1979 ±41	2040 ±48	4.32	303.66	0.44
CHCO'	2283 ±159	3480 ±318	4604 ±217	5071 ±112	5970 ±376	3.65	208.2	0.53
CH_3	60 ±0.3	98 ±2	114 ±0.3	135 ±0.1	145 ±0.1	6.76	275.5	0.51
Heq'	634 ±32	1028 ±28	1227 ±11	1414 ±4	1594 ±9	4.55	248.4	0.52

SI-Table 31: *Nuclear relaxation rates, R_1, and single fitted values (μ_{eff} = 9.8 BM) for $[Tb.L^4]^{3+}$ (295 K, ACN).*

^{1}H	R_1 / sec^{-1}					Fitted values		
	4.7	9.4	11.7	14.1	16.5	*r* / Å	τ_R / ps	T_{1e} / ps
CH_3	58 ±0.2	89 ±0.5	109 ±0.1	129 ±0.5	149 ±0.3	6.74	192.7	0.57
Heq	483 ±11	869 ±50	926 ±14	1026 ±8	1335 ±156	4.72	214.4	0.56
Heq'	539 ±7	878 ±44	1089 ±14	1313 ±13	1587 ±53	4.87	145.0	0.45

SI-Table 32 : *Individual estimated values of the effective magnetic moment, μ_{eff}, the electronic relaxation time, T_{1e} and the rotational correlation time, τ_R, using global fitting procedures for the quoted resonances of $[Ln.L^4]$ (295 K, D_2O).*

Ln^{3+}	Heq		Heq'	
	μ_{eff} / BM	T_{1e} / ps	μ_{eff} / BM	T_{1e} / ps
Tb	9.55	0.57	8.91	0.56
Dy	10.27	0.46	10.32	0.38
Ho	9.87	0.34	9.95	0.28
Tm	7.57	0.30	7.58	0.26
Yb	4.33	0.22	4.34	0.20
τ_R / ps	301		335	

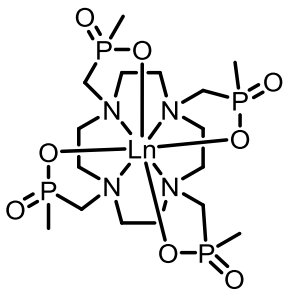

$[Ln.L^5]^-$

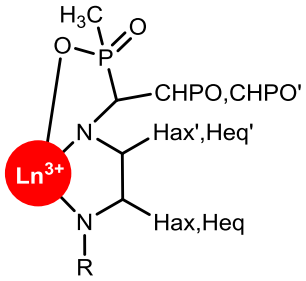

SI-Table 33 : *^{1}H nuclear relaxation rates,R_1, and single fitting values (μ_{eff} = 9.8 BM) for $[Tb.L^5]^-$ (295 K, D_2O).*

^{1}H	R_1/ s^{-1}					Fitting values		
	4.7 T	9.4 T	11.7 T	14.1 T	16.5 T	*r* / Å	τ_R / ps	T_{1e} / ps
CHPO	609 ±9	1296 ±22	1577 ±20	1833 ±15	2205 ±55	4.29	230.4	0.27
CH_3	413 ±5	791 ±5	991 ±4	1156 ±15	1304 ±14	4.68	253.5	0.31
Heq	496 ±8	992 ±19	1210 ±12	1431 ±21	1620 ±37	4.51	256.2	0.29
Heq'	491 ±6	977 ±19	1171 ±12	1366 ±12	1609 ±38	4.53	236.5	0.32

SI-Table 34 : *^{1}H nuclear relaxation rates,R_1, and single fitting values (μ_{eff} = 10.3 BM) for $[Dy.L^5]^-$ (295 K, D_2O).*

^{1}H	R_1/ s^{-1}					Fitting values		
	4.7 T	9.4 T	11.7 T	14.1 T	16.5 T	*r* / Å	τ_R / ps	T_{1e} / ps
CHPO	1021 ±42	1907 ±34	2158 ±53	2551 ±63	2903 ±99	4.24	265.3	0.44
CH_3	639 ±17	116 ±12	1377 ±8	1658 ±35	1797 ±43	4.58	249.8	0.43
Heq	736 ±23	1364 ±56	1734 ±33	1976 ±43	2375 ±190	4.39	210.8	0.39
Heq’	707 ±23	1359 ±30	1638 ±28	1950 ±48	2388 ±152	4.37	182.1	0.40

SI-Table 35 : *^{1}H nuclear relaxation rates,R_1, and single fitting values (μ_{eff} = 10.4 BM) for $[Ho.L^5]^-$ (295 K, D_2O).*

^{1}H	R_1/ s^{-1}					Fitting values		
	4.7 T	9.4 T	11.7 T	14.1 T	16.5 T	*r* / Å	τ_R / ps	T_{1e} / ps
CH_3	519 ±18	921 ±17	1124 ±21	1446 ±62	1685 ±52	4.62	154.8	0.41
Heq	606 ±28	1176 ±25	1503 ±27	1820 ±88	2108 ±88	4.48	204.4	0.33
Heq’	598 ±34	1203 ±27	1533 ±33	1841 ±74	2098 ±78	4.49	230.4	0.30

SI-Table 36 : *^{1}H nuclear relaxation rates,R_1, and single fitting values (μ_{eff} = 9.4 BM) for $[Er.L^5]^-$ (295 K, D_2O).*

^{1}H	R_1/ s^{-1}					Fitting values		
	4.7 T	9.4 T	11.7 T	14.1 T	16.5 T	*r* / Å	τ_R / ps	T_{1e} / ps
Heq’	720 ±21	1080 ±7	1303 ±11	1519 ±6	1733 ±34	4.38	210.3	0.58
Heq	700 ±26	1051 ±13	1295 ±20	1546 ±9	1735 ±52	4.36	199.7	0.54
CH_3	488 ±17	694 ±7	850 ±3	985 ±3	1106 ±5	4.72	215.7	0.64
CHPO	581 ±14	942 ±13	1130 9±	1290 ±6	1474 ±20	4.49	239.1	0.49

SI-Table 37 : *^{1}H nuclear relaxation rates,R_1, and single fitting values (μ_{eff} = 7.6 BM) for $[Tm.L^5]^-$ (295 K, D_2O).*

^{1}H	R_1/ s^{-1}					Fitting values		
	4.7 T	9.4 T	11.7 T	14.1 T	16.5 T	*r* / Å	τ_R / ps	T_{1e} / ps
Heq’	751±38	1143±12	1260±15	1388±10	1483±25	3.90	344.4	0.39
Heq	739±21	1116±16	1248±19	1365±12	1450±32	3.91	349.4	0.39
CH_3	446±40	665±2	745±3	831±5	894±5	4.27	302.3	0.43
CHPO	394±9	632±6	732±7	808±3	900±6	4.26	288.8	0.35

SI-Table 38 : *^{1}H nuclear relaxation rates,R_1, and single fitting values (μ_{eff} = 4.5 BM) for $[Yb.L^5]^-$ (295 K, D_2O).*

^{1}H	R_1/ s^{-1}					Fitting values		
	4.7 T	9.4 T	11.7 T	14.1 T	16.5 T	*r* / Å	τ_R / ps	T_{1e} / ps
CHPO'	202 ±2	249 ±1	278 ±1	311 ±1	339 ±2	3.58	162.5	0.25
Heq'	59 ±1	73 ±1	83 ±1	91 ±1	98 ±1	4.42	196.4	0.26
Heq	57 ±1	72 ±1	82 ±	90 ±1	97 ±1	4.43	206.3	0.25
CH_3	37 ±1	47 ±1	53 ±1	58 ±1	63 ±1	4.76	204.8	0.25
CHPO	41 ±1	55 ±1	62 ±1	69 ±1	75 ±1	4.60	206.1	0.22
Hax	127 ±1	174 ±1	198 ±1	219 ±1	240 ±1	3.78	226.2	0.21
Hax'	136 ±1	190 ±1	217 ±1	245 ±1	271 ±1	3.69	205.8	0.19

SI-Table 39 : *Individual estimated values of the effective magnetic moment, μ_{eff}, the electronic relaxation time, T_{1e} and the rotational correlation time, τ_R, using global fitting procedures for the quoted resonances of $[Ln.L^5]$ (295 K, D_2O).*

Ln^{3+}	CH_3		Heq		Heq'	
	μ_{eff} / BM	T_{1e} / ps	μ_{eff} / BM	T_{1e} / ps	μ_{eff} / BM	T_{1e} / ps
Tb	10.43	0.34	9.29	0.29	9.20	0.29
Dy	11.34	0.58	10.18	0.35	10.14	0.32
Ho	11.06	0.37	9.91	0.29	9.92	0.27
Er	9.85	0.70	9.31	0.48	9.28	0.53
Tm	9.30	0.98	8.93	0.74	8.97	0.75
Yb	4.46	0.26	4.18	0.23	4.17	0.24
τ_R / ps	232		233			231

$[Ln.L^6]$

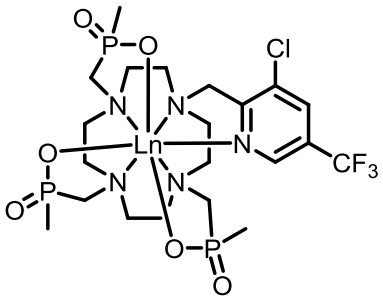

SI-Table 40 : *^{1}H nuclear relaxation rates,R_1, and single fitting values (μ_{eff} = 9.8 BM) for $[Tb.L^6]$ (295 K, D_2O).*

^{1}H	R_1/ s^{-1}					Fitting values		
	4.7 T	9.4 T	11.7 T	14.1 T	16.5 T	*r* / Å	τ_R / ps	T_{1e} / ps
CH_3'	440 ±29	727 ±31	864 ±31	945 ±32	1078 ±21	4.85	288.4	0.49
CH_3	600 ±25	1015 ±54	1163 ±30	1279 ±124	1448 ±44	4.60	311.6	0.47

SI-Table 41 : *^{1}H nuclear relaxation rates,R_1, and single fitting values (μ_{eff} = 10.3 BM) for $[Dy.L^6]$ (295 K, D_2O).*

^{1}H	R_1/ s^{-1}					Fitting values		
	4.7 T	9.4 T	11.7 T	14.1 T	16.5 T	*r* / Å	τ_R / ps	T_{1e} / ps
CH_3''	750 ±37	1403 ±98	1606 ±50	1899 ±188	2105 ±78	4.46	284.3	0.40
CH_3'	493 ±20	943 ±17	1061 ±20	1216 ±14	1395 ±10	4.78	294.1	0.40
CH_3	638 ±49	1205 ±53	1410 ±23	1659 ±21	1863 ±43	4.55	270.6	0.39

SI-Table 42 : *^{1}H nuclear relaxation rates,R_1, and single fitting values (μ_{eff} = 10.4 BM) for [Ho.L^6] (295 K, D_2O).*

^{1}H	R_1/ s^{-1}					Fitting values		
	4.7 T	9.4 T	11.7 T	14.1 T	16.5 T	*r* / Å	τ_R / ps	T_{1e} / ps
CH_3'	380 ±8	734 ±11	826 ±8	986 ±195	1111 ±12	5.00	274.4	0.41

SI-Table 43 : *^{1}H nuclear relaxation rates,R_1, and single fitting values (μ_{eff} = 9.4 BM) for [Er.L^6] (295 K, D_2O).*

^{1}H	R_1/ s^{-1}					Fitting values		
	4.7 T	9.4 T	11.7 T	14.1 T	16.5 T	*r* / Å	τ_R / ps	T_{1e} / ps
CH_3'	470 ±22	696 ±16	872 ±31	932 ±46	1027 ±55	4.75	294.2	0.54
CH_3	481 ±18	694 ±15	874 ±33	963 ±48	1042 ±56	4.75	276.3	0.58

SI-Table 44 : *^{1}H nuclear relaxation rates,R_1, and single fitting values (μ_{eff} = 7.6 BM) for [Tm.L^6] (295 K, D_2O).*

^{1}H	R_1/ s^{-1}					Fitting values		
	4.7 T	9.4 T	11.7 T	14.1 T	16.5 T	*r* / Å	τ_R / ps	T_{1e} / ps
CH_3'	169±9.0	284±9.0	375±3.8	419±6.0	459±6.4	4.73	264.9	0.24
CH_3	253±11.3	447±10.8	520±11.8	578±6.2	646±10.1	4.47	309.2	0.26

SI-Table 45 : *^{1}H nuclear relaxation rates,R_1, and single fitting values (μ_{eff} = 4.5 BM) for [Yb.L^6] (295 K, D_2O).*

^{1}H	R_1/ s^{-1}					Fitting values		
	4.7 T	9.4 T	11.7 T	14.1 T	16.5 T	*r* / Å	τ_R / ps	T_{1e} / ps
CH_3''	32 ±2	36 ±2	38 ±1	39 ±1	40 ±1	5.21	284.9	0.40
CH_3'	40 ±2	49 ±2	53 ±1	58 ±1	61 ±1	4.83	192.9	0.34
CH_3	40 ±2	45 ±2	47 ±1	48 ±1	51 ±1	5.01	271.2	0.39

SI-Table 46 : *^{19}F nuclear relaxation rates of the CF_3 resonance for [Ln.L^6] used in global fitting (295 K, D_2O)*

Ln^{3+}	δ_H / ppm	R_1/ s^{-1}				
		4.7 T	9.4 T	11.7 T	14.1 T	16.5 T
Tb	-158.4	56±1	89±1	117±3	133±1	150±4
Dy	-162.4	64±2	114±1	142±1	166±1	192±1
Ho	-107.8	67±1	129±1	154±2	189±1	218±1
Er	-16.9	94±1	136±1	175±1	188±1	219±3
Tm	17.1	59±1	107±1	132±2	152±1	173±1
Yb	-41.5	14.2±0.5	15.1±0.1	17.3±1.1	18.0±0.1	19.4±0.3

SI-Table 47 : *Individual estimated values of the effective magnetic moment, μ_{eff}, the electronic relaxation time, T_{1e} and the rotational correlation time, τ_R, using global fitting procedures for the quoted resonances of [Ln.L^6] (295 K, D_2O).*

Ln^{3+}	CF_3		CH_3	
	μ_{eff} / BM	T_{1e} / ps	μ_{eff} / BM	T_{1e} / ps
Tb	8.57	0.38	9.88	0.50
Dy	9.15	0.36	10.60	0.43
Ho	9.48	0.32	10.00	0.35
Er	9.39	0.65	9.77	0.60
Tm	8.92	0.36	7.99	0.23
Yb	4.69	0.43	4.41	0.28
τ_R / ps	240		280	

SI-Table 48 : *^{19}F nuclear relaxation rates of the CF_3 resonance of the carboxylate analogue [Ln.L^{6C}] used in single fitting (295 K, D_2O)*

Ln^{3+}	R_1 / s^{-1}					Fitting values		
	4.7 T	9.4 T	11.7 T	14.1 T	16.5 T	*r* / Å	τ_R / ps	T_{1e} / ps
Dy	70 ±1	132 ±1	158 ±2	197 ±1	233 ±2	6.36	189.9	0.42
Tm	27 ±1	54 ±2	71 ±1	90 ±2	113 ±3	5.65	112.1	0.14

[Ln.L^7]

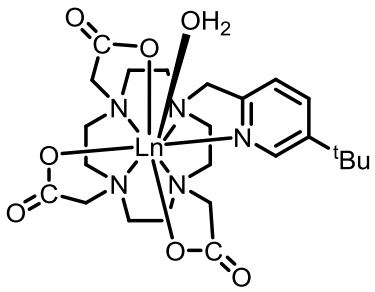

SI-Table 49 : *^{1}H nuclear relaxation rates of the ^{t}Bu resonance for [Ln.L^7] used in global fitting (295 K, D_2O).*

Ln^{3+}	δ_H / ppm	R_1/ s^{-1}				
		4.7 T	9.4 T	11.7 T	14.1 T	16.5 T
Tb	-11.6	72±1	104±2	128±1	146±1	169±1
Dy	-20.5	73±1	124±1	149±1	170±1	210±2
Ho	-7.4	45±1	89±1	118±1	144±1	169±1
Er	7.0	29±1	59±1	80±1	97±1	120±1
Tm	10.8	31±1	54±1	64±1	71±1	82±1
Yb	6.3	6.4±0.1	7.6±0.3	8.6±0.1	9.5±0.1	10.7±0.1

[Ln.L^8]

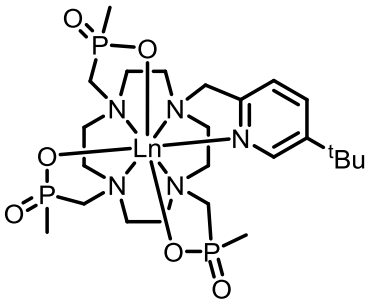

SI-Table 50 : *^{1}H nuclear relaxation rates of the ^{t}Bu resonance for [Ln.L^8] used in global fitting (295 K, D_2O).*

Ln^{3+}	δ_H / ppm	R_1/ s^{-1}				
		4.7 T	9.4 T	11.7 T	14.1 T	16.5 T
Tb	-75.9	53±2	81±2	91±1	102±1	113±1
Dy	-75.0	59±1	96±1	114±1	132±1	150±1
Ho	-31.8	61±2	100±1	127±1	147±1	166±1
Er	38.2	88±2	120±2	135±1	152±1	169±1
Tm	67.0	55±1	97±1	115±1	129±1	142±1
Yb	16.3	10.7±0.1	11.4±0.7	11.6±0.6	12.0±0.1	12.4±0.3

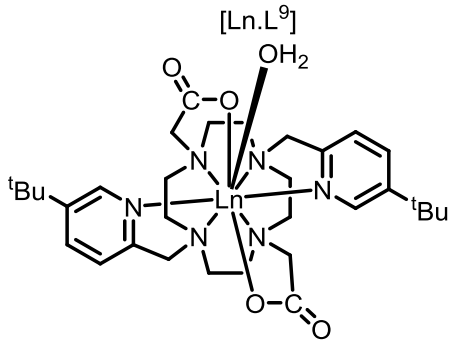

SI-Table 51 : *^{1}H nuclear relaxation rates of the ^{t}Bu resonance for [Ln.L^9]$^+$ used in global fitting (295 K, D_2O).*

Ln^{3+}	δ_H / ppm	R_1/ s^{-1}				
		4.7 T	9.4 T	11.7 T	14.1 T	16.5 T
Tb	-7.2	103±1	151±1	169±1	188±1	207±2
Dy	-17.8	119±1	174±1	203±1	230±1	256±1
Ho	-7.0	56±1	102±2	138±2	156±1	177±4
Er	3.4	19±1	41±5	53±7	71±9	81±12
Tm	6.2	21±1	40±1	51±1	59±1	68±1
Yb	9.1	4.7±0.2	7.1±0.1	8.3±0.2	9.6±0.3	10.5±0.2

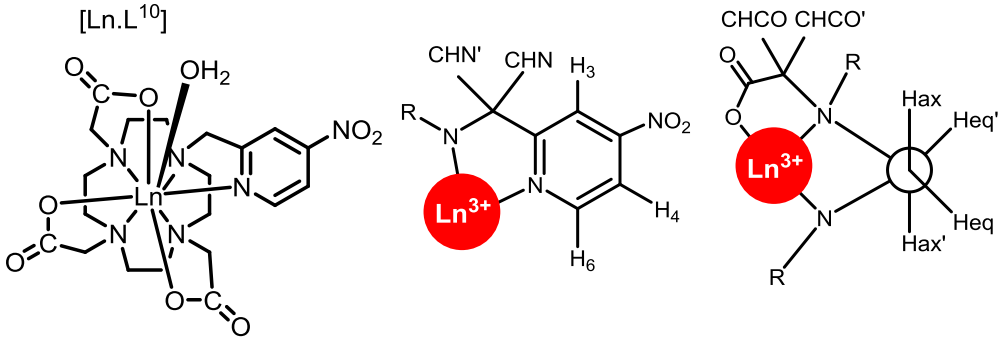

SI-Table 52 : *^{1}H nuclear relaxation rates,R_1, and single fitting values (μ_{eff} = 9.8 BM) for [Tb.L^{10}] (295 K, D_2O).*

^{1}H	R_1/ s^{-1}					Fitting values		
	4.7 T	9.4 T	11.7 T	14.1 T	16.5 T	*r* / Å	τ_R / ps	T_{1e} / ps
pyH^5	165 ±18	258 ±6	317 ±2	378 ±9	410 ±21	5.69	240.0	0.53
pyH^6	175 ±6	281 ±6	334 ±7	370 ±5	428 ±8	5.67	260.2	0.55
Heq1	756 ±39	1201 ±49	1452 ±32	1682 ±32	1889 ±41	4.42	238.8	0.54
CHCO1	746 ±35	1179 ±37	1463 ±31	1647 ±22	1826 ±23	4.44	262.9	0.52
Heq2	577 ±27	894 ±17	1079 ±14	1293 ±9	1518 ±8	4.57	175.1	0.56
Heq3	675 ±39	1037 ±47	1256 ±13	1476 ±13	1693 ±12	4.51	207.0	0.59
Heq4	541 ±28	834 ±9	1060 ±13	1196 ±16	1375 ±16	4.67	221.6	0.55

SI-Table 53 : *^{1}H nuclear relaxation rates,R_1, and single fitting values (μ_{eff} = 10.3 BM) for [Dy.L^{10}] (295 K, D_2O).*

^{1}H	R_1/ s^{-1}					Fitting values		
	4.7 T	9.4 T	11.7 T	14.1 T	16.5 T	*r* / Å	τ_R / ps	T_{1e} / ps
pyH^5	182 ±9	329 ±12	384 ±3	459 ±4	531 ±8	5.64	226.2	0.47
pyH^6	169 ±7	311 ±8	374 ±2	444 ±4	530 ±6	5.63	119.5	0.44
Heq1	841 ±17	1512 ±36	1883 ±73	2230 ±39	2690 ±152	4.28	180.1	0.43
Heq2	595 ±11	974 ±13	1232 ±10	1476 ±13	1800 ±28	4.53	143.2	0.47
Heq3	707 ±15	1247 ±31	1485 ±14	1777 ±8	2086 ±25	4.49	203.8	0.48
Heq4	552 ±23	928 ±8	1232 ±7	1449 ±24	1714 ±12	4.61	176.6	0.43

SI-Table 54 : *^{1}H nuclear relaxation rates,R_1, and single fitting values (μ_{eff} = 10.4 BM) for [Ho.L^{10}] (295 K, D_2O).*

^{1}H	R_1/ s^{-1}					Fitting values		
	4.7 T	9.4 T	11.7 T	14.1 T	16.5 T	*r* / Å	τ_R / ps	T_{1e} / ps
pyH^5	110 ±3	242 ±2	318 ±3	400 ±9	431 ±12	5.79	250.1	0.18
pyH^6	102 ±3	239 ±3	317 ±8	385 ±6	464 ±6	5.74	196.4	0.18
Heq1	410 ±7	992 ±24	1178 ±28	1649 ±62	1852 ±85	4.54	186.8	0.19
Heq2	353 ±9	837 ±22	1079 ±15	1284 ±29	1625 ±58	4.66	176.7	0.22
Heq3	400 ±7	955 ±14	1194 ±12	1507 ±128	1823 ±25	4.57	181.9	021

SI-Table 55 : *^{1}H nuclear relaxation rates,R_1, and single fitting values (μ_{eff} = 9.4 BM) for [Er.L^{10}] (295 K, D_2O).*

^{1}H	R_1/ s^{-1}					Fitting values		
	4.7 T	9.4 T	11.7 T	14.1 T	16.5 T	*r* / Å	τ_R / ps	T_{1e} / ps
Hax1	711 ±30	1861 ±47	2184 ±64	2857 ±96	3736 ±97	3.68	113.2	0.15
Hax2	835 ±29	1731 ±41	2464 ±57	3282 ±126	3902 ±120	3.67	126.6	0.15
Hax3	829 ±34	1915 ±105	2570 ±60	3278 ±137	3722 ±292	3.78	26.8	0.14
Heq1	277 ±7	645 ±75	894 ±23	1037 ±16	1359 ±51	4.45	149.0	0.16
Heq2	284 ±4	677 ±51	891 ±24	1062 ±15	1387 ±82	4.43	145.7	0.17
pyH^6	65 ±1	139 ±16	209 ±4	256 ±6	313 ±8	5.66	150.2	0.14
Heq’	253 ±12	535 ±11	806 ±11	963 ±44	1142 ±101	4.60	189.6	0.13
CHCO	243 ±3	573 ±10	780 ±16	1000 ±18	1265 ±35	4.42	121.7	0.13
CHCO2	306 ±9	739 ±32	1013 ±28	1263 ±41	1482 ±66	4.41	199.7	0.12

SI-Table 56 : *^{1}H nuclear relaxation rates,R_1, and single fitting values (μ_{eff} = 7.6 BM) for [Tm.L^{10}] (295 K, D_2O).*

^{1}H	R_1 / s^{-1}					Fitting values		
	4.7 T	9.4 T	11.7 T	14.1 T	16.5 T	*r* / Å	τ_R / ps	T_{1e} / ps
Heq1	265 ±+	474 ±23	559 ±6	679 ±13	825 ±55	4.26	148.2	0.26
Heq2	270 ±5	425 ±17	582 ±23	680 ±26	773 ±30	4.33	181.6	0.26
Heq3	277 ±4	438 ±12	597 ±20	695 ±23	768 ±4	4.35	207.2	0.27
Heq4	230 ±5	366 ±13	513 ±17	574 ±34	699 ±46	4.38	153.0	0.25
Heq'1	255 ±6	449 ±28	548 ±20	644 ±42	794 ±56	4.29	149.1	0.26
pyH^6	79 ±4	141 ±3	185 ±7	245 ±14	265 ±11	5.13	177.9	0.19
Heq'2	238 ±9	389 ±27	493 ±4	572 ±30	646 ±32	4.49	211.8	0.29
pyH^4	37 ±1	71 ±1	91 ±4	118 ±	140 ±1	5.62	129.8	0.17
CHCO1	168 ±5	322 ±3	368 ±4	447 ±13	558 ±27	4.54	142.7	0.24
CHCO2	184 ±2	315 ±7	421 ±14	505 ±8	570 ±9	4.55	192.9	0.22
CHCO3	181 ±2	311 ±9	405 ±9	485 ±14	541 ±10	4.60	207.6	0.24
CHCO'1	546 ±12	894 ±67	1080±86	1340±91	1528±85	3.87	165.5	0.29
Hax'1	457 ±9	909 ±13	1059±66	1378±42	1702±57	3.72	129.2	0.18
Hax'2	454 ±10	778 ±77	1061±61	1355±59	1545±76	3.80	147.3	0.19
CHCO'2	321 ±4	655 ±45	836 ±24	969 ±17	1095±43	4.06	267.2	0.15
Hax'3	409 ±7	738 ±39	1062±29	1258±24	1439±53	3.88	192.9	0.17

SI-Table 57 : *^{1}H nuclear relaxation rates,R_1, and single fitting values (μ_{eff} = 4.5 BM) for [Yb.L^{10}] (295 K, D_2O).*

^{1}H	R_1/ s^{-1}					Fitting values		
	4.7 T	9.4 T	11.7 T	14.1 T	16.5 T	*r* / Å	τ_R / ps	T_{1e} / ps
Hax1	115 ±8	195 ±7	256 ±7	293 ±5	335 ±2	3.45	216.0	0.08
Hax2	133 ±7	222 ±9	284 ±7	333 ±6	482 ±7	3.38	194.7	0.09
CHCO'	151 ±14	236 ±7	305 ±7	341 ±5	386 ±6	3.41	220.3	0.11
Hax3	109 ±8	183 ±6	248 ±7	277 ±4	329 ±1	3.46	193.0	0.08
Hax4	201 ±6	284 ±9	366 ±6	406 ±16	492 ±14	3.21	119.6	0.12
Heq1	67 ±2	96 ±3	111 ±2	124 ±1	137 ±1	4.13	228.3	0.18
Heq2	70 ±2	92 ±1	130 ±1	142 ±1	153 ±2	3.96	161.3	0.13
pyH^6	9.7 ±1	14.0 ±1	19.1 ±1	21.7 ±1	24.6 ±1	5.32	151.2	0.12
Heq4	69 ±3	99 ±3	128 ±2	136 ±3	155 ±2	4.01	223.1	0.15
Heq'1	52 ±4	71 ±4	96 ±2	110 ±3	123 ±1	4.11	163.0	0.13
Heq'2	58 ±4	69 ±5	96 ±4	112 ±6	125 ±1	4.16	171.9	0.16
Heq'3	45 ±8	53 ±4	75 ±11	83 ±9	96 ±5	4.23	113.8	0.14
Heq'4	47 ±9	75 ±2	87 ±10	109 ±2	134 ±2	3.95	127.6	0.09
pyCHN	63 ±4	80 ±1	97 ±4	115 ±1	125 ±2	4.13	141.5	0.18
CHCO1	46 ±2	65 ±1	87 ±12	97 ±4	110 ±1	4.21	181.4	0.13
CHCO2	45 ±6	59 ±2	73 ±2	83 ±2	91 ±3	4.39	171.8	0.18
CHCO3	48 ±4	61 ±2	78 ±2	85 ±2	93 ±2	4.40	189.6	0.19
Hax'2	80 ±5	157 ±7	207 ±5	244 ±3	271 ±7	3.52	253.4	0.05
Hax'3	71 ±3	123 ±3	156 ±7	175 ±5	207 ±9	3.76	213.4	0.09

SI-Table 58 : *Individual estimated values of the effective magnetic moment, μ_{eff}, the electronic relaxation time, T_{1e} and the rotational correlation time, τ_R / ps using global fitting procedures for the quoted resonances of [Ln.L[10]] (295 K, D_2O).*

Ln^{3+}	pyH^6		H_{eq}		$H_{eq}2$	
	μ_{eff} / BM	T_{1e} / ps	μ_{eff} / BM	T_{1e} / ps	μ_{eff} / BM	T_{1e} / ps
Tb	9.64	0.61	9.64	0.54	9.12	02.50
Dy	10.23	0.48	10.02	0.41	9.75	0.41
Ho	10.03	0.15	9.95	0.20	9.94	0.21
Er	9.14	0.06	9.52	0.14	9.25	0.15
Tm	8.66	0.20	7.75	0.32	7.64	0.25
Yb	4.59	0.12	4.59	0.17	4.78	0.17
τ_R / ps	215		172		167	

[Ln.L[11]]

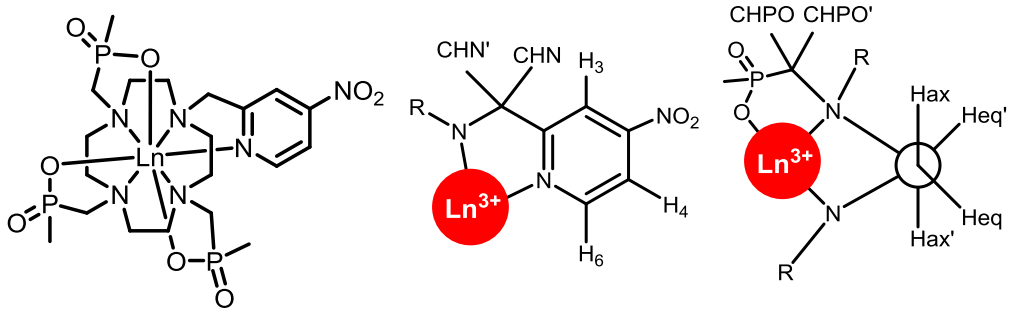

SI-Table 59 : *[1]H nuclear relaxation rates,R_1, and single fitting values (μ_{eff} = 9.8 BM) for [Tb.L[11]] (295 K, D_2O).*

^1H	R_1/ s^{-1}					Fitting values		
	4.7 T	9.4 T	11.7 T	14.1 T	16.5 T	*r* / Å	τ_R / ps	T_{1e} / ps
CH_3-1	712 ±25	1169 ±34	1367 ±46	1621 ±47	1986 ±35	4.36	161.9	0.52
CH_3-2	486 ±9	736 ±12	842 ±28	998 ±84	1082 ±73	4.86	263.1	0.65
pyH^5	231 ±5	362 ±12	427 ±23	510 ±12	562 ±7	5.41	237.1	0.57
CH_3-3	685 ±13	1079 ±32	1134 ±43	1425 ±53	1486 34±	4.59	286.7	0.64

SI-Table 60 : *[1]H nuclear relaxation rates,R_1, and single fitting values (μ_{eff} = 10.3 BM) for [Dy. L[11]] (295 K, D_2O).*

^1H	R_1/ s^{-1}					Fitting values		
	4.7 T	9.4 T	11.7 T	14.1 T	16.5 T	*r* / Å	τ_R / ps	T_{1e} / ps
CH_3-1	603 ±63	1032 ±115	1284 ±78	1636 ±86	1932 ±54	4.46	139.4	0.41
CH_3-2	447 ±23	676 ±125	812 ±56	1013 ±46	1198 ±79	4.85	140.8	0.58

SI-Table 61 : *[1]H nuclear relaxation rates,R_1, and single fitting values (μ_{eff} = 10.4 BM) for [Ho. L[11]] (295 K, D_2O).*

^1H	R_1/ s^{-1}					Fitting values		
	4.7 T	9.4 T	11.7 T	14.1 T	16.5 T	*r* / Å	τ_R / ps	T_{1e} / ps
CH_3-1	533 ±49	953 ±162	1209 ±34	1415 ±58	1540 ±68	67.7	4.72	0.39
CH_3-2	286 ±10	586 ±33	751 ±52	874 ±60	1015 ±43	36.2	5.06	0.27

SI-Table 62 : *^{1}H nuclear relaxation rates,R_1, and single fitting values (μ_{eff} = 9.4 BM) for [Er. L^{11}] (295 K, D_2O).*

^{1}H	R_1/ s^{-1}					Fitting values		
	4.7 T	9.4 T	11.7 T	14.1 T	16.5 T	*r* / Å	τ_R / ps	T_{1e} / ps
CH_3-2	404 ±16	584 ±31	671 ±25	806 ±22	865 ±25	4.92	247.3	0.67
CH_3-1	450 ±17	634 ±47	793 ±49	886 ±19	1044 ±45	4.77	197.2	0.67

SI-Table 63 : *^{1}H nuclear relaxation rates,R_1, and single fitting values (μ_{eff} = 7.6 BM) for [Tm.L^{11}] (295 K, D_2O).*

^{1}H	R_1/ s^{-1}					Fitting values		
	4.7 T	9.4 T	11.7 T	14.1 T	16.5 T	*r* / Å	τ_R / ps	T_{1e} / ps
Heq	260 ±4	476 ±8	569 ±11	619 ±26	757 ±32	4.39	235.7	0.27
CH_3-1	157 ±2	276 ±4	335 ±5	368 ±8	411 ±8	4.81	303.3	0.24
CHCO	336 ±13	606 ±35	716 ±21	810 ±60	957 ±12	4.22	233.6	0.27
CH_3-2	239 ±2	426 ±4	502 ±5	545 ±10	620 ±6	4.49	314.4	0.24
Heq	230 ±4	413 ±14	515 ±5	595 ±13	682 ±17	4.44	229.8	0.24

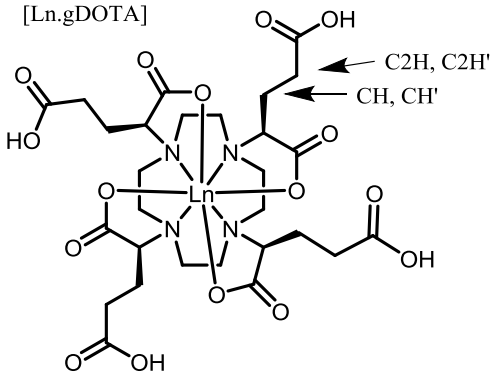

SI-Table 64 : *^{1}H nuclear relaxation rates,R_1, and single fitting values (μ_{eff} = 9.4 BM) for [Er.gDOTA]$^{5-}$ (295 K, D_2O).*

$^1H^+$	R_1/ s^{-1}					Fitting values		
	4.7 T	9.4 T	11.7 T	14.1 T	16.5 T	*r* / Å	τ_R / ps	T_{1e} / ps
C2H	76 ±2	121 ±3	140 ±2	155 ±1	174 ±4	6.40	292.4	0.52
C2H’	116 ±4	188 ±3	229 ±9	251 ±3	269 ±5	5.89	326.4	0.41
CH	198 ±5	352 ±13	393 ±16	468 ±7	539 ±8	5.31	213.2	0.46

SI-Table 65 : *^{1}H nuclear relaxation rates,R_1, and single fitting values (μ_{eff} = 7.6 BM) for [Tm.gDOTA]$^{5-}$ (295 K, D_2O).*

$^1H^+$	R_1/ s^{-1}					Fitting values		
	4.7 T	9.4 T	11.7 T	14.1 T	16.5 T	*r* / Å	τ_R / ps	T_{1e} / ps
CH’	288 ±20	432 ±15	487 ±16	533 ±4	560 ±24	4.56	352.4	0.38
C2H’	54 ±2	85 ±1	94 ±3	105 ±1	1131 ±	5.99	327.1	0.36
C2H	81 ±2	133 ±24	158 ±1	168 ±1	184 ±2	5.48	349.0	0.28
CH	189 ±3	298 ±4	333 ±4	364 ±3	382 ±4	4.85	349.8	0.34

SI-Table 66 : *^{1}H nuclear relaxation rates,R_1, and single fitting values (μ_{eff} = 4.5 BM) for [Yb.gDOTA]$^{5-}$ (295 K, D_2O).*

$^1H^+$	R_1/ s^{-1}					Fitting values		
	4.7 T	9.4 T	11.7 T	14.1 T	16.5 T	*r* / Å	τ_R / ps	T_{1e} / ps
Heq’	84 ±10	98 ±4	106 ±3	109 ±1	114 ±3	4.38	241.5	0.38
Heq	82 ±10	95 ±3	102 ±3	108 ±1	112 ±3	4.37	254.2	0.35

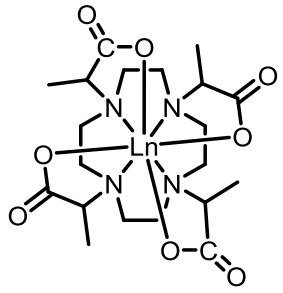

SI-Table 67 : *^{1}H nuclear relaxation rates, R_1, and single fitting values (μ_{eff} = 7.6) for [Tm.DOTMA]$^-$ (295 K, D_2O).*

^{1}H	R_1 / s^{-1}					Fitting values		
	4.7 T	9.4 T	11.7 T	14.1 T	16.5 T	*r* / Å	τ_R / ps	T_{1e} / ps
CH_3 major	143 ±2	243 ±3	275 ±2	306 ±1	342 ±1	4.98	305	0.30
CH_3 minor	114 ±4	191 ±7	235 ±5	260 ±6	284 ±5	5.14	272	0.30

SI-Table 68 : *Comparison of the Tm(III) observable shift range $\Delta\delta_H$, the crystal field splitting parameters, B_0^2, and the electronic relaxation times, T_{1e} (single fitting), ordered by increasing shift range, 295 K, D_2O ([Ln.L$^{2\text{-}3}$] in CD_3OD).*

[Ln.L^x]	Tm^{3+}		
	$\Delta\delta_H$ / ppm	B_0^2 / cm^{-1}	T_{1e} / ps
1	70	75	0.08
2	112	110	0.09
3	150	228	0.10
11	355	x	0.25
9	380	-355	0.20
DOTMA	423	-700	0.30
8[a]	>427	-570	0.31
4	454	-470	0.21
7	480	-455	0.29
gDOTA	499	-700	0.31
10	507	x	0.23
6	545	-550	0.25
5	681	-700	0.39

[a]The full spectral range was not observable for [Tm.L^8]

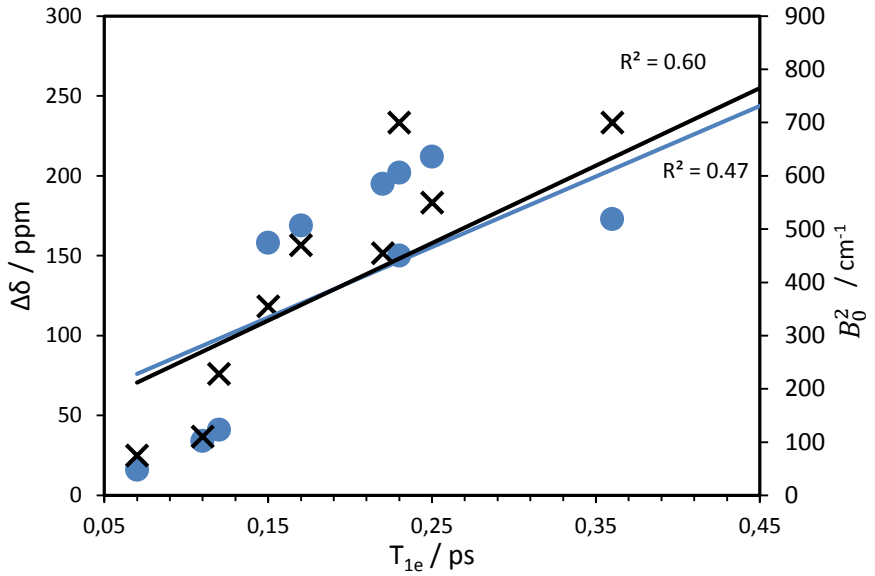

SI-Figure 2 : *The correlation between the estimated T_{1e} values with the shift range (●) and the second order crystal field splitting parameter (**x**) for the Yb(III) complexes, with the highly symmetrical systems highlighted*

SI-Table 69 : *Comparison of the Yb(III) observable shift range $\Delta\delta_H$, the crystal field splitting parameters, B_0^2, and the electronic relaxation times, T_{1e} (single fitting), ordered by increasing shift rang (295 K, D_2O ,[Ln.L^{2-3}] in CD_3OD).*

		Yb^{3+}	
[Ln.L^x]	$\Delta\delta_H$ / ppm	B_0^2 / cm^{-1}	T_{1e} / ps
1	16	75	0.07
2	34	110	0.11
3	41	228	0.12
5	150	-700	0.23
9	158	-355	0.15
4	169	-470	0.17
gDOTA	173	-700	0.36
8	192	-570	0.46
7	195	-455	0.22
10	202	x	0.23
6	212	-550	0.25

The fitting algorithm for a single fit all vary is shown on the following pages, a modified version was used for fixing individual values and for global fitting:

```
function fitter_r1

data=[x x x x];
fields=[4.7 9.4 11.7 14.1 16.5];
guess=[x1 x2 x3 x4];
ls_err(guess,fields,data)
options=optimset('Display','iter');
answer=fminsearch(@(x)ls_err(x,fields,data),guess,options)
hold on
```

```
plot(fields,data,'ro');
field_grid=linspace(4.7,16.5,100);
rates=zeros(size(field_grid));
for n=1:numel(field_grid)
rates(n)=R1(answer(1),answer(2),field_grid(n),answer(3),answer(4))
end
plot(field_grid,rates,'r-');
end

function err=ls_err(guess,fields,data)
err=0;
for n=1:numel(fields)
err=err+(data(n)-R1(guess(1),guess(2),fields(n),guess(3),guess(4)))^2;
end
end

function R1=R1(mu_eff,r,B,tau_r,tau_e)
mu0=4*pi*1e-7;
r=r*1e-10;
mu_eff=mu_eff*9.274e-24;
tau_r=tau_r*1e-12;
tau_e=tau_e*1e-12;
gamma_F=2.5181e8;
gamma_e=1.760860e11;
k=1.3806503e-23;
T=295;
omega_F=gamma_F*B;
omega_e=gamma_e*B;
tau_rpe=1/(1/tau_r+1/tau_e);
R1=(2/15)*((mu0/(4*pi))^2)*((gamma_F^2)*(mu_eff^2)/(r^6))*(7*tau_rpe/(1+(omega_e^2)*(
tau_rpe^2))+3*tau_rpe/(1+(omega_F^2)*(tau_rpe^2)))+(2/5)*((mu0/(4*pi))^2)*((omega_F^2)
*(mu_eff^4)/(((3*k*T)^2)*(r^6)))*(3*tau_r/(1+(omega_F^2)*(tau_r^2)));
end;
```

Appendix 3 : The discrepancies in Bleaney's theory of magnetic anisotropy

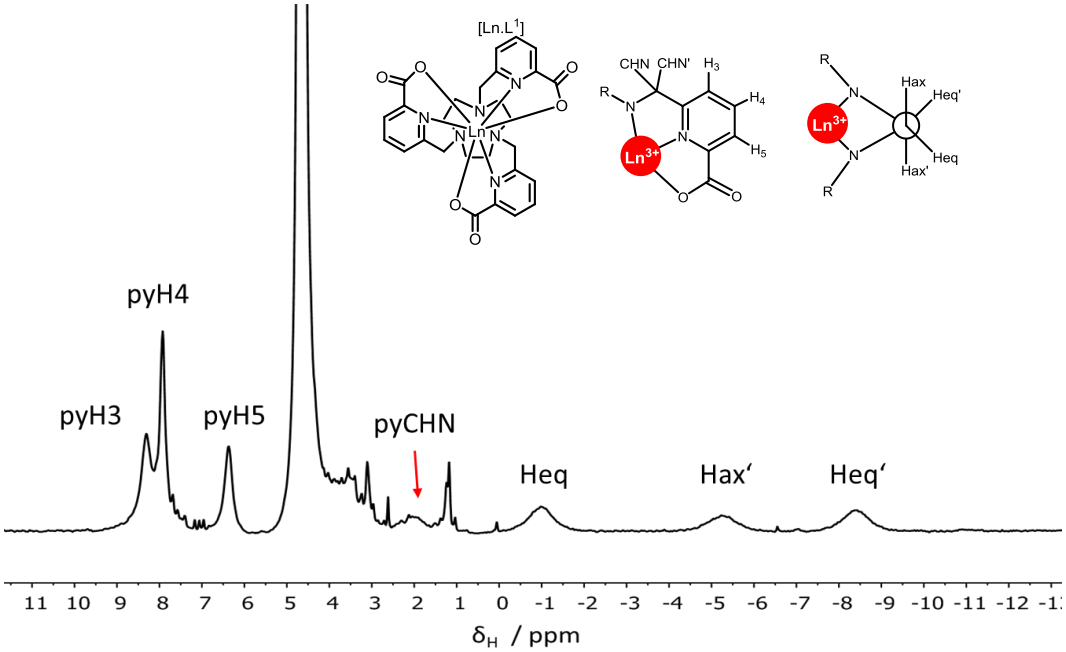

SI-Figure 3 : *^{1}H NMR spectrum of [Er.L^1] (295 K, D_2O).*

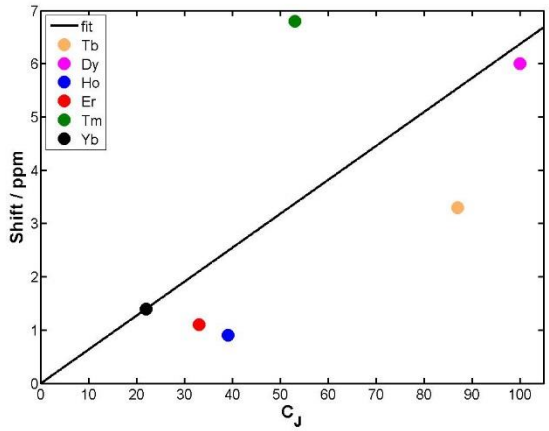

SI-Figure 4 : *Correlation of the pseudocontact shift data of the pyH^4 resonance for [Ln.L^1] with the Bleaney constant, C_J (295 K, 9.4 T, D_2O).*

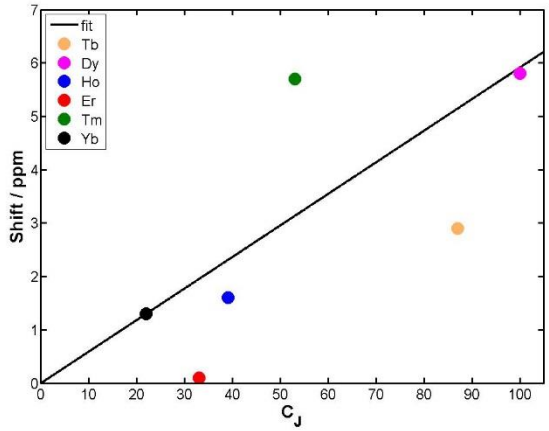

SI-Figure 5: *Correlation of the pseudocontact shift data of the pyH^5 resonance for [Ln.L^1] with the Bleaney constant, C_J (295 K, 9.4 T, D_2O).*

SI-Table 70 : ^{1}H NMR *chemical shift data for the resonances of [Ln.L^{1}] (295 K, 9.4 T, D_2O)*

Ln^{3+}	Δδ / ppm								
	Hax	Hax'	Heq	Heq'	CHN	CHN'	H^3	H^4	H^5
Tb	-5.2	x	x	x	x	x	0.1	4.9	4.1
Dy	-13.6	26.5	x	-4.9	-24.0	-29.4	9.4	10.6	11.0
Ho	x	x	x	x	2.0	-9.0	3.9	6.2	6.5
Er	x	-5.6	-1.2	-8.6	1.9	12.4	8.3	7.9	6.3
Tm	11.5	-35.9	-13.1	-15.2	5.6	34.7	14.2	13.5	14.2
Yb	5.8	-4.8	0.6	-1.8	4.2	11.1	9.5	9.1	8.8

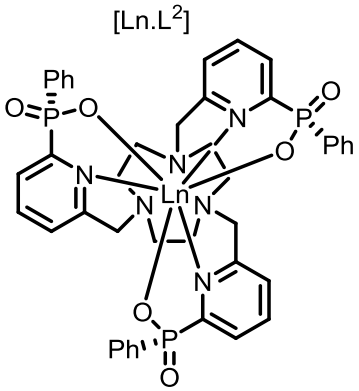

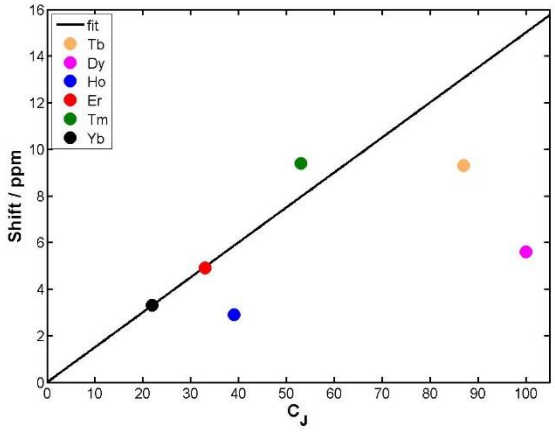

SI-Figure 6 : *Correlation of the pseudocontact shift data of the pyH^{4} resonance for [Ln.L^{2}] with the Bleaney constant, C_J (295 K, 9.4 T, CD_3OD).*

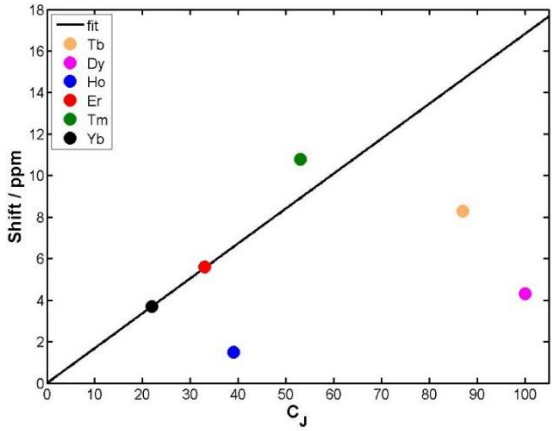

SI-Figure 7 : *Correlation of the pseudocontact shift data of the pyH[5] resonance for [Ln.L[2]] with the Bleaney constant, C_J (295 K, 9.4 T, CD_3OD).*

SI-Table 71 : ^{1}H NMR *chemical shift data for the resonances of [Ln.L[2]] (295 K, 9.4 T, CD_3OD)*

Ln^{3+}	δ_H / ppm											
	Hax	Hax'	Heq	Heq'	CHN	CHN'	H3	H4	H5	ph	ph'	^{31}P
Tb	30.9	47.7	-11.6	x	19.2	-38.1	-7.1	-2.3	-1.3	13.2	14.7	-35.7
Dy	29.5	20.1	-6.2	x	x	-23.8	-1.4	1.4	2.7	10.8	x	-15.9
Ho	15.4	13.8	-2.4	-2.7	6.6	-8.4	2.3	4.1	5.5	9.0	x	-24.6
Er	35.8	-32.2	-13.5	x	-17.7	35.8	13.6	11.9	12.6	3.2	1.0	-10.5
Tm	11.4	-56.9	-22.7	-23.0	-21.7	54.6	18.6	16.4	17.8	6.5	1.0	8.4
Yb	6.6	-13.7	-3.4	5.2	-0.6	20.7	10.7	10.3	10.7	5.2	3.8	17.7

SI-Table 72 : *Variation of the chemical shift of the ^{31}P resonance of [Tm.L[2]] with temperature over the given range (16.5 T, CD_3OD).*

T / K	δ_H / ppm
295	7.4
297	7.5
299	7.6
301	7.7
303	7.8
ppm / K	0.1

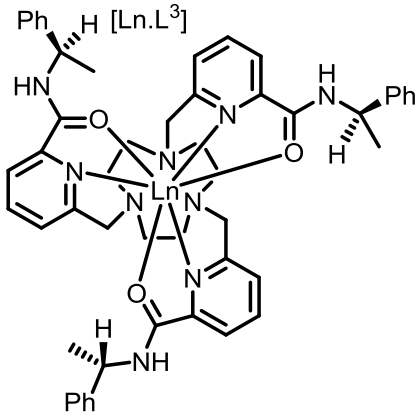

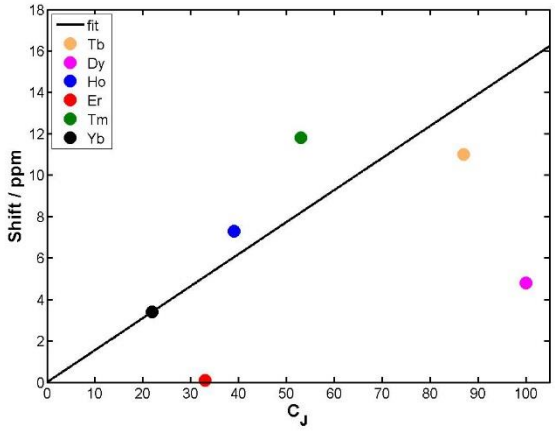

SI-Figure 8 : *Correlation of the pseudocontact shift data of the pyH[4] resonance for $[Ln.L^3]^{3+}$ with the Bleaney constant, C_J (295 K, 9.4 T, CD_3OD).*

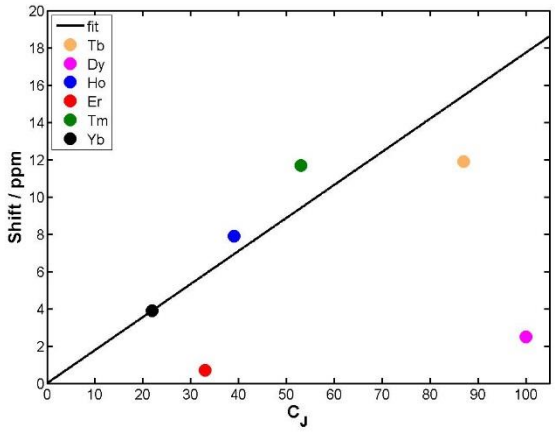

SI-Figure 9 : *Correlation of the pseudocontact shift data of the pyH[5] resonance for $[Ln.L^3]^{3+}$ with the Bleaney constant, C_J (295 K, 9.4 T, CD_3OD).*

SI-Table 73 : ^{1}H NMR c*hemical shift data for the resonances for [Ln.L^3]$^{3+}$ (295 K, 9.4 T, CD$_3$OD)*

Ln^{3+}	Δδ / ppm												
	H_{ax}	H_{ax}'	H_{eq}	H_{eq}'	CHN	CHN'	pyH^3	pyH^4	pyH^5	PhH	PhH'	CH_3	H
Tb	x	57.5	29.9	23.9	x	-45.5	-11.0	-3.2	-4.4	4.5	2.0	8.6	5.8
Dy	22.5	x	18.2	11.1	x	x	1.9	5.0	3.0	6.5	6.2	x	-1.5
Ho	-3.7	47.3	23.3	22.6	x	-32.0	-5.5	-0.4	0.5	5.5	5.1	7.2	5.8
Er	3.6	-5.1	-8.8	x	1.8	12.8	8.2	7.9	8.2	x	x	0.9	x
Tm	11.3	-79.8	-29.0	-30.5	-22.0	70.4	23.0	19.6	19.2	10.4	10.8	-7.5	9.3
Yb	8.9	-18.8	-4.2	-6.7	-2.8	22.3	11.6	11.2	11.4	7.6	8.2	-1.1	x

SI-Table 74 : *Variation of the chemical shift of the quoted resonance for [Yb.L^3]$^{3+}$ with temperature over the given range (16.5 T, D$_2$O).*

T / K	δ_H / ppm			
	pyH^3	pyH^4	pyH^5	H_{ax}
298	12.3	12.0	11.7	-23.6
313	12.0	11.8	11.5	-20.8
323	11.8	11.7	11.4	-19.2
3333	11.6	11.6	11.3	-17.8
343	11.5	11.5	11.3	-16.5
353	11.4	11.5	11.2	-15.3
ppm / K	n.d.	n.d.	n.d.	-0.2

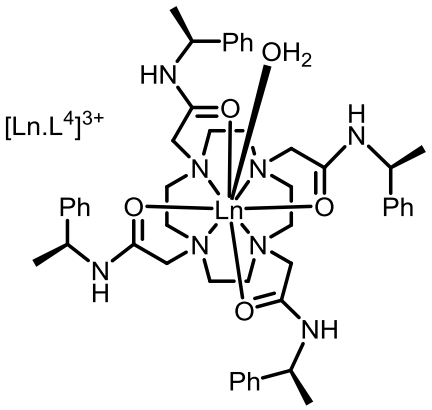

SI-Table 75 : ^{1}H NMR c*hemical shift data for the resonances for [Ln.L^4]$^{3+}$ (295 K, 9.4 T, D$_2$O).*

Ln^{3+}	Δδ / ppm									
	Hax	Hax'	Heq	Heq'	CHCO	CHCO'	paraH	PhH'	PhH	CH_3
Tb	-341.7	223.9	x	-88.5	61.8	112.3	34.9	32.5	31.1	20.8
Dy	-400.4	270.8	-91.0	-95.0	87.5	137.8	40.4	37.6	35.6	24.4
Ho	-202.4	137.5	-49.8	-51.2	39.7	70.8	24.0	22.7	15.1	12.9
Er	89.5	-73.5	15.0	x	-39.2	-42.0	-0.2	-0.8	-1.6	-4.5
Tm	225.5	-182.6	34.9	45.9	-82.7	-95.7	-14.8	x	-11.4	-13.1
Yb	103.3	-66.2	15.7	19.0	-28.4	-34.5	-0.8	0.1	2.7	-3.9

SI-Table 76 : *Variation of the chemical shift of the quoted resonance for $[Tm.L^4]^{3+}$ with temperature over the given range (16.5 T, D_2O).*

T / K	δ_H / ppm						
	Heq'	Heq	paraH	PhH''	CHCO	CHCO'	Hax
298	45.3	34.5	-12.2	-12.0	-80.0	-92.4	-176.9
303	44.0	33.5	-11.7	-11.3	-77.6	-89.8	-171.6
308	42.8	32.6	-11.3	-10.7	-75.4	-87.3	-166.5
313	41.6	31.6	-10.8	-10.1	-73.3	-84.7	-161.6
318	10.5	30.8	-10.4	-9.4	-71.2	-82.3	-156.7
323	39.5	30.0	-9.9	-8.8	-69.1	-79.9	-152.1
ppm / K	-0.2	-0.2	0.1	0.1	0.4	0.5	1.0

SI-Table 77 : *Variation of the chemical shift of the quoted resonance for $[Tm.L^4]^{3+}$ with temperature over the given range (11.7, CD_3OD).*

T / K	δ_H / ppm								
	Heq'	Heq	PhH	PhH2	paraH	CH3	CHCO	CHCO'	Hax
241	69.7	54.1	-22.2	-21.7	-23.7	-18.7	-118.7	-137.9	-269.1
251	64.4	49.9	-19.9	-19.6	-21.2	-17.1	-110.0	-127.9	-249.1
261	59.8	46.3	-17.8	-17.8	-19.0	-15.4	-102.2	-118.5	-230.9
273	55.6	43.0	-15.9	-15.9	-17.0	-14.3	-95.1	-110.2	-214.5
283	51.8	40.0	-14.2	-14.5	-15.2	-13.2	-88.7	-102.7	-199.6
298	46.9	36.1	-12.0	-12.5	-12.8	-11.6	-80.3	-92.7	-180.0
308	44.0	33.8	-10.7	-11.4	-11.4	-10.7	-75.4	-87.1	-168.7
319	41.4	31.8	-9.5	-10.3	-10.2	-9.8	-70.9	-81.7	-158.3
ppm / K	-0.4	-0.3	0.2	0.2	0.2	0.1	0.6	0.7	1.4

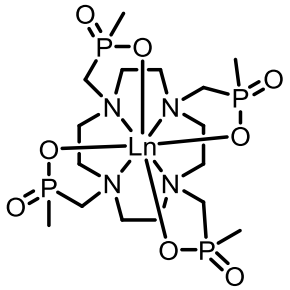

$[Ln.L^5]^-$

SI-Table 78 : ^{1}H NMR *chemical shift data for the resonances for $[Ln.L^5]^-$ (295 K, 9.4 T, D_2O).*

Ln^{3+}	Δδ / ppm						
	Hax	Hax'	Heq	Heq'	CHPO	CHPO'	CH_3
Tb	190.2	380.0	-105.8	-166.1	135.1	-450.0	42.1
Dy	320.3	163.0	-87.6	-93.5	115.2	-428.7	35.0
Ho	151.4	79.1	-42.7	-44.5	52.0	-198.7	15.7
Er	-93.8	-185.2	26.7	43.4	-79.2	260.0	-14.4
Tm	-193.7	-374.9	71.0	91.3	-154.7	305.6	-27.2
Yb	-30.9	-59.3	17.7	13.2	-24.7	90.9	-3.4

SI-Table 79 : *Variation of the chemical shift of the quoted resonance for $[Tm.L^5]^-$ with temperature over the given range (16.5 T, D_2O).*

T / K	δ_H / ppm				
	Hax	CHPO	CH3	Heq'	Heq
298	-189.9	-151.9	-26.8	89.8	69.7
301	-186.4	-149.1	-26.4	88.2	68.5
304	-182.8	-146.3	-25.9	86.7	67.3
307	-179.3	-143.5	-25.4	85.2	66.1
310	-175.8	-140.8	-25.0	83.7	65.0
313	-172.5	-138.2	-24.5	82.3	63.9
316	-169.2	-135.6	-24.1	80.9	62.8
319	-165.8	-133.1	-23.7	79.5	61.7
321	-162.9	-130.8	-23.3	78.1	60.6
ppm / K	1.2	0.9	0.2	-0.5	-0.4

$[Ln.L^6]$

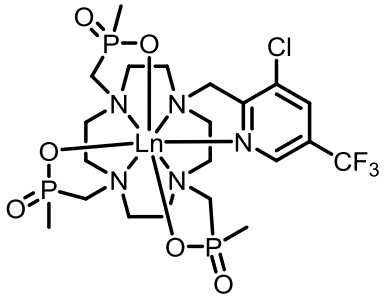

SI-Table 80 : ^{1}H NMR c*hemical shift data for the resonances of $[Ln.L^6]^-$ (295 K, 9.4 T, D_2O).*

Ln^{3+}	Δδ / ppm			
	CH_3	CH_3'	CH_3''	^{19}F
Tb	26.0	58.1	124.6	-158.4
Dy	71.4	89.9	113.5	-162.4
Ho	15.3	45.2		-107.8
Er	-37.2	-40.1		-16.9
Tm	-36.7	-37.1	-84.5	17.1
Yb	-6.9	-15.3	-29.8	-41.5

SI-Table 81 : *Variation of the chemical shift of the quoted resonance of $[Dy.L^6]$ with temperature over the given range (16.5 T, D_2O).*

T / K	δF / ppm		
	major	minor	difference
298	-160.8	-167.3	6.5
303	-158.3	-164.7	6.4
308	-155.7	-161.9	6.2
310	-154.7	-160.9	6.2
313	-153.4	-159.6	6.2
318	-151.1	-157.2	6.1
323	-148.8	-154.7	5.9
ppm / K	0.5	0.5	n.d.

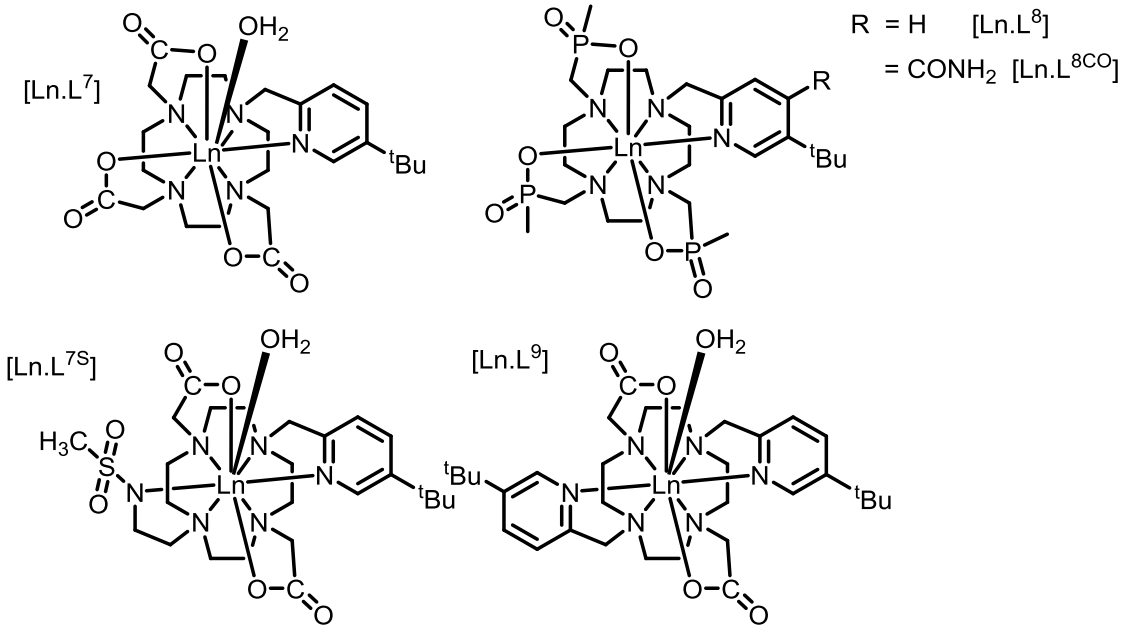

SI-Table 82 : *Overview of the chemical shift data of the major and minor isomer of the ^{t}Bu receptor group in different complex series (295 K, D_2O).*

	δ_H / ppm									
Ln^{3+}	[Ln.L^7]		[Ln.L^{7S}]		[Ln.L^8]		[Ln.L^{8CO}]		[Ln.L^8]	
	major	minor	major	minor	major	minor	major	minor	major	minor
Tb	-11.6	-22.5	-75.9	-76.9	-75.9	-76.9	-55.8	58.3	-7.2	x
Dy	-20.5	x	-75.0	-78.7	-75.0	-78.7	-58.9	-35.3	-17.8	x
Hp	-7.4	-14.8c	-31.8	-33.7	-31.8	-33.7	-26.3	-20.3	-7.0	-11.7
Er	7.0	20.0	38.2	40.1	38.2	40.1	x	x	3.4	3.8
Tm	10.8	52.3	67.0	68.3	67.0	68.3	44.3	51.3	6.2	15.5
Yb	6.3	x	16.3	18.1	16.3	18.1	x	x	9.1	13.4

SI-Table 83 : *Variation of the chemical shift of the ^{t}Bu resonance of [Dy.L$^{7-9}$] with temperature over the given range (16.5 T, D_2O).*

T / K	δ_H / ppm				
	[Dy.L^7]	[Dy.L^{7S}]	[Dy.L^8]	[Dy.L^{8CO}]	[Dy.L^9]
298	-20.2	-57.6	-73.1	n.d.	-17.3
303	-19.6	-56.2	-71.2	-75.7	-16.8
308	-19.0	-54.8	-69.4	-74.1	-16.2
313	-18.5	-53.5	-67.6	-71.9	-15.7
318	-18.0	-52.2	-65.9	-70.5	-15.3
323	-17.5	-50.9	-64.3	n.d.	-14.8
ppm / K	0.1	0.3	0.4	0.4	0.1

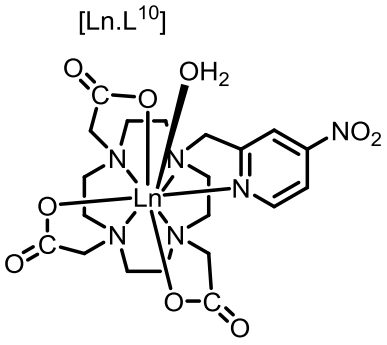

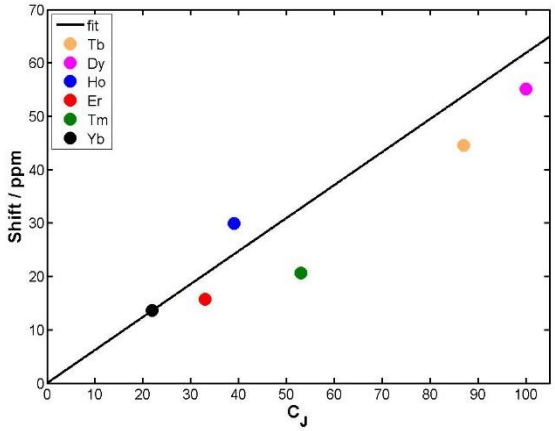

SI-Figure 10 : *Correlation of the pseudocontact shift data of the pyH^6 resonance for [Ln.L^{10}] with the Bleaney constant, C_J (295 K, 9.4 T, D_2O).*

SI-Table 84 : ^{1}H NMR c*hemical shift data for the quoted resonances of [Ln.L^{10}] (295 K, 9.4 T, D_2O).*

Ln^{3+}	Δδ / ppm								
	Hax	Hax'	Heq	Heq'	CHCO	CHCO'	H^4	H^5	H^6
Tb	-348.3	230.9	-134.4	-38.1	x	179.0	17.0	-0.7	-36.9
Dy	-424.2	380.4	-188.7	-57.6	x	19.3	x	-47.4	-70.5
Ho	-209.2	161.3	-84.2	-29.8	x	142.2	8.2	-3.5	-22.2
Er	123.6	-62.1	25.9	-7.3	x	-57.1	x	8.3	23.4
Tm	254.5	-177.5	62.6	14.3	x	-127.2	-17.4	x	28.3
Yb	93.1	-66.2	30.8	9.35	x	-61.7	x	6.1	21.3

[Ln.L^{11}]

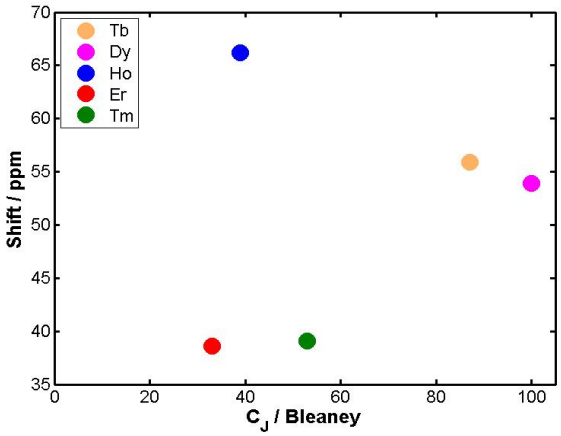

SI-Figure 11 : *Correlation of the pseudocontact shift data of the CH_3 resonance for [Ln.L^{11}] with the Bleaney constant, C_J (295 K, 9.4 T, D_2O).*

SI-Table 85 : ^{1}H NMR *chemical shift data for the quoted resonances of [Ln.L^{11}] (295 K, 9.4 T, D_2O).*

Ln^{3+}	Δδ / ppm		
	CH_3	CH_3'	CH_3''
Tb	117.2	57.9	45.8
Dy	71.1	55.4	46.3
Ho	67.2	36.2	
Er		-37.1	-35.1
Tm	-77.5	-51.6	-37.6
Yb			

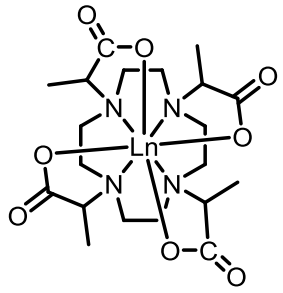

[Ln.DOTMA]$^-$

SI-Table 86 : *Chemical shift data for the CH_3 resonances of [Ln.DOTMA]$^-$ (295 K, 9.4 T, D_2O).*

Ln^{3+}	δ_H / ppm	
	major	minor
Tb	61.6	67.8
Ho	35.8	42.5
Er	-43.7	-28.0
Tm	-104.0	-67.0
Yb	-14.7	x

SI-Table 87 : *Variation of the chemical shift of the CH_3 resonances of [Tm.DOTMA]$^-$ with the temperature over the given range (16.5 T, D_2O).*

T / K	δH / ppm		ΔCH_3
	CH_3 major[a]	CH_3 minor	
298	-104.3	-65.8	38.5
303	-101.0	-64.6	36.3
308	-97.7	-63.5	34.2
313	-94.6	-62.5	32.2
318	-91.7	-61.5	30.2
323	-88.9	-60.7	28.2
ppm / K	0.6	0.2	0.4

[a]The major isomer is an 8-coordinate complex, whilst the minor isomer is 9-coordinate (q=1)

Appendix 4 : The effect of *J*-mixing on the magnetic susceptibility

The data used for the global fitting procedure can be found in Appendix 1. The SQUID measurements were performed by Dr. Johan Buurma at Durham University.

[Ln.L^2]

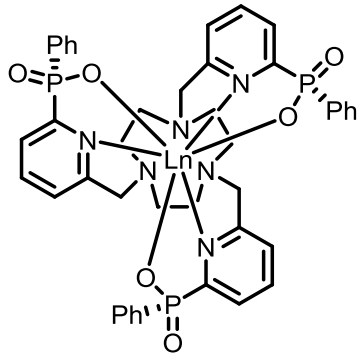

SI-Table 88 : *Concentration (highest dilution factor) and bulk magnetic susceptibility data (CD_3OD, 11.4 T) of [Ln.L^2].*

		295 K			300 K			305 K		
Ln^{3+}	C / µM	Δδ / ppm	X_M^{para} / $m^3\ mol^{-1}$	μ_{eff} / BM	Δδ / ppm	X_M^{para} / $m^3\ mol^{-1}$	μ_{eff} / BM	Δδ / ppm	X_M^{para} / $m^3\ mol^{-1}$	μ_{eff} / BM
Gd	1407.4	0.14	3.86	8.6	0.14	3.76	8.5	0.14	3.67	8.5
Dy	1323.4	0.18	6.77	11.3	0.17	6.58	11.3	0.17	6.47	11.3
Ho	584.8	0.13	6.57	11.2	0.13	6.41	11.1	0.12	6.31	11.1
Er	1040.3	0.17	4.76	9.5	0.16	4.67	9.5	0.16	4.56	9.5
Tm	647.8	0.07	3.02	7.6	0.07	2.93	7.5	0.07	2.89	7.5
Yb	1357.5	0.04	0.88	4.1	0.04	0.86	4.1	0.04	0.84	4.1
Gd	1407.4	0.14	3.86	8.6	0.14	3.76	8.5	0.14	3.67	8.5

SI-Table 89 : *Concentration (medium dilution factor) and bulk magnetic susceptibility data (CD_3OD, 11.4 T) of [Ln.L^2].*

		295 K			300 K			305 K		
Ln^{3+}	C / µM	Δδ / ppm	X_M^{para} / $m^3\ mol^{-1}$	μ_{eff} / BM	Δδ / ppm	X_M^{para} / $m^3\ mol^{-1}$	μ_{eff} / BM	Δδ / ppm	X_M^{para} / $m^3\ mol^{-1}$	μ_{eff} / BM
Gd	1474.7	0.18	3.60	8.3	0.17	3.50	8.2	0.17	3.42	8.2
Dy	1001.8	0.22	6.44	11.1	0.21	6.29	10.9	0.21	6.14	11.0
Ho	779.7	0.16	6.00	10.7	0.15	5.89	10.6	0.15	5.73	10.6
Er	1254.3	0.21	4.93	9.7	0.20	4.81	9.6	0.20	4.71	9.6
Tm	886.2	0.10	3.22	7.8	0.09	3.15	7.7	0.09	3.08	7.8
Yb	1810.0	0.05	0.83	4.0	0.05	0.80	3.9	0.05	0.78	3.9
Gd	1474.7	0.18	3.60	8.3	0.17	3.50	8.2	0.17	3.42	8.2

SI-Table 90 : *Concentration (lowest dilution factor) and bulk magnetic susceptibility data (CD_3OD, 11.4 T) of [Ln.L^2].*

		295 K			300 K			305 K		
Ln^{3+}	C / µM	Δδ / ppm	X_M^{para} / $m^3\ mol^{-1}$	μ_{eff} / BM	Δδ / ppm	X_M^{para} / $m^3\ mol^{-1}$	μ_{eff} / BM	Δδ / ppm	X_M^{para} / $m^3\ mol^{-1}$	μ_{eff} / BM
Gd	9166.2	0.53	3.59	8.3	0.52	3.51	701	0.54	3.68	8.5
Dy	6301.5	0.67	6.69	11.3	0.66	6.54	11.1	0.64	6.38	11.2
Ho	4644.4	0.49	6.32	11.0	0.48	6.18	10.8	0.47	6.04	10.9
Er	4001.0	0.63	5.05	9.8	0.63	5.05	9.8	0.61	4.82	9.7
Tm	4562.2	0.30	3.43	8.1	0.30	3.35	8.0	0.29	3.28	8.0
Yb	3710.1	0.15	0.84	4.0	0.15	0.82	4.0	0.15	0.82	4.0
Gd	9166.2	0.53	3.59	8.3	0.52	3.51	701	0.54	3.68	8.5

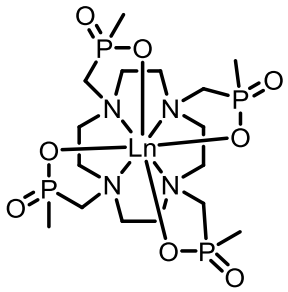

$[Ln.L^5]^-$

SI-Table 91 : *Concentration (highest dilution factor) and bulk magnetic susceptibility data (D_2O, 11.4 T) of $[Ln.L^5]^-$.*

Ln^{3+}	C / µM	295 K			300 K			305 K		
		Δδ / ppm	X_M^{para} / m^3 mol^{-1}	μ_{eff} / BM	Δδ / ppm	X_M^{para} / m^3 mol^{-1}	μ_{eff} / BM	Δδ / ppm	X_M^{para} / m^3 mol^{-1}	μ_{eff} / BM
Gd	562.8	0.06	3.36	8.0	0.06	3.30	8.0	0.06	3.30	8.1
Tb	326.0	0.04	4.45	9.2	0.03	4.32	9.1	0.03	4.20	9.1
Dy	240.0	0.05	5.75	10.4	0.05	5.75	10.5	0.04	5.50	10.4
Ho	218.3	0.05	7.28	11.8	0.05	7.15	11.7	0.05	7.15	11.8
Er	529.1	0.08	4.76	9.5	0.08	4.71	9.5	0.08	4.65	9.6
Tm	541.6	0.06	3.21	7.8	0.06	3.16	7.8	0.06	3.16	7.9
Yb	520.1	0.02	1.21	4.8	0.02	1.21	4.8	0.02	1.15	4.8

SI-Table 92 : *Concentration (medium dilution factor) and bulk magnetic susceptibility data (D_2O, 11.4 T) of $[Ln.L^5]^-$.*

Ln^{3+}	C / µM	295 K			300 K			305 K		
		Δδ / ppm	X_M^{para} / m^3 mol^{-1}	μ_{eff} / BM	Δδ / ppm	X_M^{para} / m^3 mol^{-1}	μ_{eff} / BM	Δδ / ppm	X_M^{para} / m^3 mol^{-1}	μ_{eff} / BM
Gd	756.8	0.08	3.33	8.0	0.08	3.29	8.0	0.08	3.21	7.9
Tb	311.5	0.05	4.82	9.6	0.05	5.11	9.9	0.05	4.72	9.6
Dy	313.8	0.06	5.64	10.4	0.06	5.54	10.3	0.06	5.45	10.3
Ho	281.9	0.07	7.66	12.1	0.07	7.55	12.1	0.07	7.45	12.1
Er	645.7	0.11	5.30	10.0	0.11	5.20	10.0	0.11	5.06	9.7
Tm	701.5	0.07	3.04	7.6	0.08	3.34	8.0	0.08	3.29	8.0
Yb	693.5	0.03	1.17	4.7	0.03	1.17	4.75	0.03	1.17	4.8

SI-Table 93 : *Concentration (lowest dilution factor) and bulk magnetic susceptibility data (D_2O, 11.4 T) of $[Ln.L^5]^-$.*

Ln^{3+}	C / µM	295 K			300 K			305 K		
		Δδ / ppm	X_M^{para} / m^3 mol^{-1}	μ_{eff} / BM	Δδ / ppm	X_M^{para} / m^3 mol^{-1}	μ_{eff} / BM	Δδ / ppm	X_M^{para} / m^3 mol^{-1}	μ_{eff} / BM
Gd	2270.3	n.d.	n.d.	n.d.	n.d.	n.d.	n.d.	n.d.	n.d.	n.d.
Tb	943.8	0.14	4.51	9.3	0.14	4.42	9.2	0.14	4.42	9.3
Dy	987.7	0.18	5.41	10.1	0.17	5.29	10.1	0.17	5.16	10.0
Ho	864.0	0.22	7.57	12.0	0.21	7.43	12.0	0.21	7.33	12.0
Er	2179.2	0.35	4.87	9.5	0.34	4.69	9.5	0.33	4.58	9.5
Tm	2290.9	0.23	3.03	7.6	0.22	3.00	7.6	0.23	2.96	7.6
Yb	2141.1	0.09	1.22	4.8	0.09	1.2	4.8	0.09	1.20	4.9

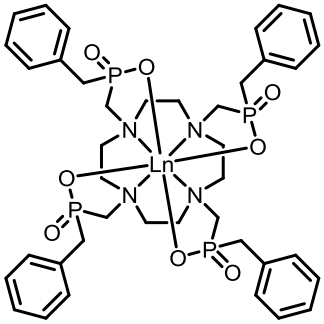

SI-Table 94 : *Concentration and bulk magnetic susceptibility data (D_2O, 11.4 T) of [Ln.L^{5Bz}]$^-$.*

Ln^{3+}	C / µM	295 K Δδ / ppm	295 K X_M^{para} / m^3 mol^{-1}	295 K μ_{eff} / BM	300 K Δδ / ppm	300 K X_M^{para} / m^3 mol^{-1}	300 K μ_{eff} / BM	305 K Δδ / ppm	305 K X_M^{para} / m^3 mol^{-1}	305 K μ_{eff} / BM
Gd	401.3	0.15	3.64	8.30	0.14	3.56	8.29	0.14	3.49	8.27
	325.0	0.16	3.04	7.60	0.16	2.97	7.57	0.16	2.91	7.56
	1451.2	0.56	3.46	8.10	0.54	3.38	8.07	0.53	3.30	8.04

[Ln.L^{10}]

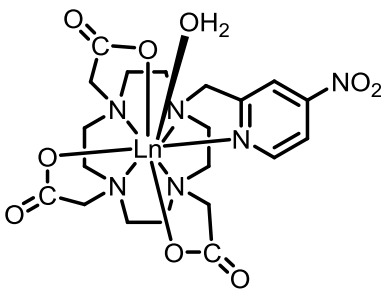

SI-Table 95 : *Concentration (highest dilution factor) and bulk magnetic susceptibility data (D_2O, 11.4 T) of [Ln.L^{10}].*

Ln^{3+}	C / µM	295 K Δδ / ppm	295 K X_M^{para} / m^3 mol^{-1}	295 K μ_{eff} / BM	300 K Δδ / ppm	300 K X_M^{para} / m^3 mol^{-1}	300 K μ_{eff} / BM	305 K Δδ / ppm	305 K X_M^{para} / m^3 mol^{-1}	305 K μ_{eff} / BM
Tb	728.0	0.09	3.75	8.43	0.09	3.71	8.46	0.09	3.63	8.43
Dy	877.1	0.13	4.31	9.04	0.12	4.24	9.04	0.12	4.14	9.01
Ho	1003.3	0.15	4.52	9.25	0.15	4.43	9.24	0.15	4.34	9.22
Er	683.3	0.08	3.56	8.21	0.08	3.51	8.23	0.08	3.42	8.19
Yb	586.7	0.01	0.51	3.11	0.01	0.51	3.14	0.01	0.51	3.17

SI-Table 96 : *Concentration (medium dilution factor) and bulk magnetic susceptibility data (D_2O, 11.4 T) of [Ln.L^{10}].*

Ln^{3+}	C / µM	295 K Δδ / ppm	295 K X_M^{para} / m^3 mol^{-1}	295 K μ_{eff} / BM	300 K Δδ / ppm	300 K X_M^{para} / m^3 mol^{-1}	300 K μ_{eff} / BM	305 K Δδ / ppm	305 K X_M^{para} / m^3 mol^{-1}	305 K μ_{eff} / BM
Tb	1116.5	0.14	3.84	8.54	0.14	3.76	8.52	0.14	3.68	8.49
Dy	1202.8	0.20	4.86	9.60	0.19	4.69	9.51	0.19	4.61	9.51
Ho	1530.0	0.23	4.53	9.27	0.23	4.43	9.24	0.22	4.35	9.24
Er	1036.3	0.12	3.59	8.25	0.12	3.53	8.25	0.12	3.47	8.25
Yb	399.9	0.02	1.13	4.62	0.02	1.13	4.66	0.01	1.05	4.54

SI-Table 97 : *Concentration (lowest dilution factor) and bulk magnetic susceptibility data (D_2O, 11.4 T) of [Ln.L[10]].*

Ln^{3+}	C / µM	295 K Δδ / ppm	295 K X_M^{para} / m^3 mol^{-1}	295 K μ_{eff} / BM	300 K Δδ / ppm	300 K X_M^{para} / m^3 mol^{-1}	300 K μ_{eff} / BM	305 K Δδ / ppm	305 K X_M^{para} / m^3 mol^{-1}	305 K μ_{eff} / BM
Tb	2308.0	0.29	3.80	8.48	0.29	3.72	8.47	0.28	3.64	8.45
Dy	2668.1	0.40	4.45	9.19	0.39	4.36	9.17	0.38	4.28	9.16
Ho	3762.0	0.49	3.88	8.57	0.46	3.66	8.40	0.45	3.60	8.40
Er	2466.7	0.26	3.14	7.71	0.25	3.08	7.70	0.25	3.02	7.69
Yb	1521.0	0.04	0.73	3.72	0.04	0.71	3.70	0.04	0.69	3.68

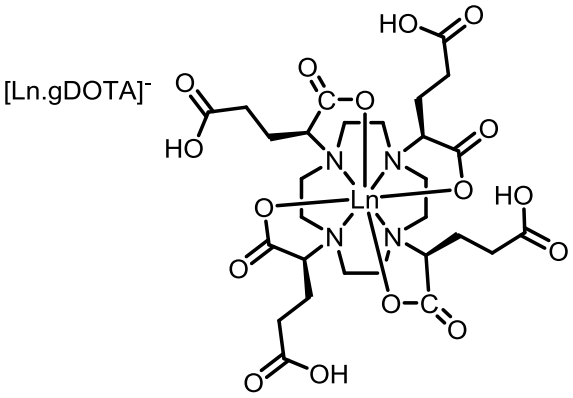

SI-Table 98 : *Concentration (highest dilution factor) and bulk magnetic susceptibility data (D_2O, 11.4 T) of [Ln.gDOTA][5-].*

Ln^{3+}	C / µM	295 K Δδ / ppm	295 K X_M^{para} / m^3 mol^{-1}	295 K μ_{eff} / BM	300 K Δδ / ppm	300 K X_M^{para} / m^3 mol^{-1}	300 K μ_{eff} / BM	305 K Δδ / ppm	305 K X_M^{para} / m^3 mol^{-1}	305 K μ_{eff} / BM
Gd	541.8	n.d.	n.d.	n.d.	n.d.	n.d.	n.d.	n.d.	n.d.	n.d.
Er	119.6	0.02	3.76	8.45	0.02	3.76	8.52	0.01	3.51	8.30
Tm	139.3	0.01	2.80	7.29	0.01	2.80	7.35	0.01	2.80	7.41
Yb	113.9	0.01	1.32	5.00	0.01	1.32	5.04	0.01	1.32	5.08

SI-Table 99 : *Concentration (medium dilution factor) and bulk magnetic susceptibility data (D_2O, 11.4 T) of [Ln.gDOTA] [5-].*

Ln^{3+}	C / µM	295 K Δδ / ppm	295 K X_M^{para} / m^3 mol^{-1}	295 K μ_{eff} / BM	300 K Δδ / ppm	300 K X_M^{para} / m^3 mol^{-1}	300 K μ_{eff} / BM	305 K Δδ / ppm	305 K X_M^{para} / m^3 mol^{-1}	305 K μ_{eff} / BM
Gd	628.6	n.d.	n.d.	n.d.	n.d.	n.d.	n.d.	n.d.	n.d.	n.d.
Er	172.5	0.02	4.17	8.90	0.02	4.00	8.78	0.02	3.83	8.66
Tm	213.1	0.02	2.39	6.74	0.02	2.39	6.79	0.02	2.225	6.64
Yb	185.4	0.01	1.29	4.95	0.01	1.13	4.67	0.01	1.13	4.71

SI-Table 100 : *Concentration (highest dilution factor) and bulk magnetic susceptibility data (D_2O, 11.4 T) of [Ln.gDOTA]$^{5-}$.*

Ln^{3+}	C / µM	Δδ / ppm	295 K X_M^{para} / m^3 mol^{-1}	μ_{eff} / BM	Δδ / ppm	300 K X_M^{para} / m^3 mol^{-1}	μ_{eff} / BM	Δδ / ppm	305 K X_M^{para} / m^3 mol^{-1}	μ_{eff} / BM
Gd	4536.7	0.47	3.07	7.64	0.45	3.17	7.82	0.49	3.25	7.98
Er	374.0	0.05	4.09	8.81	0.05	4.01	8.7	0.05	4.01	8.87
Tm	434.1	0.04	2.56	6.96	0.04	2.49	6.93	0.03	2.35	6.79
Yb	423.9	0.02	1.06	4.49	0.02	1.6	4.52	0.02	1.06	4.56

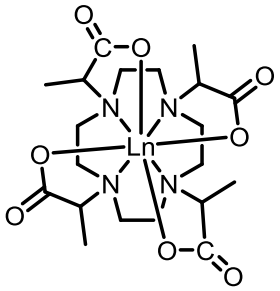

[Ln.DOTMA]$^-$

SI-Table 101 : *Concentration and bulk magnetic susceptibility data (D_2O, 11.4 T) of [Ln.DOTMA]$^-$.*

Ln^{3+}	C / µM	Δδ / ppm	295 K X_M^{para} / m^3 mol^{-1}	μ_{eff} / BM	Δδ / ppm	300 K X_M^{para} / m^3 mol^{-1}	μ_{eff} / BM	Δδ / ppm	305 K X_M^{para} / m^3 mol^{-1}	μ_{eff} / BM
Tm	4226.6	0.38	2.6	7.10	0.39	3.28	7.95	0.41	3.46	8.23

Appendix 5 : List of publications

Funk A.M., Harvey P., Kenwright A. M., Parker D.,Lanthanide paramagnetism may be dependent on coordination environment: erbium and thulium complexes that show NMR relaxation rates faster than dysprosium and terbium analogues, *Chem. Comm.*, **2015**, submitted.

Funk A. M., Finney K. N. A., Harvey P, Kenwright A. M., Rogers N. J., Senanayake P. K., Parker D., Critical analysis of the limitations of Bleaney's theory of magnetic anisotropy in paramagnetic lanthanide coordination complexes, *Chem. Sci.*, **2015**, submitted.

Neil E. R.; Funk A. M.; Yufit D. S.; Parker D. Synthesis, Stereocontrol and structural studies of highly luminescent chiral tris-amide-pyridyltriazacyclononane lanthanide complexes, *Dalton. Trans.*, **2014**, *43*, 5490-5504.

Gempf K. L; Butler S. J; Funk A. M.; Parker D., Direct and selective tagging of cysteine residues in peptides and proteins with 4-nitropyridyl lanthanide complexes, *Chem. Comm*., **2013**, *49*, 9104-9106.

Harvey P.; Blamire A. M.; Wilson J. I.; Finney K. N. A.; Funk A. M.; Senanayake P. K; Parker D., Moving the goal posts: enhancing the sensitivity of PARASHIFT proton magnetic resonance imaging and spectroscopy, *Chem. Sci*., **2013**, *4*, 4251-4258.

Funk A. M.; Fries P. H; Harvey P.; Kenwright A. M.; Parker D., Experimental Measurement and Theoretical Assessment of Fast Lanthanide Electronic Relaxation in Solution with Four Series of Isostructural Complexes, *J. Phys. Chem. A*, **2013**, *117*, 905-917.

Walton J. W.; Carr R.; Evans N. H.; Funk A. M.; Kenwright A. M.; Parker D.; Yufit. D. S; Botta M.; De Pinto S.; Wong K-L., Isostructural Series of Nine-Coordinate Chiral Lanthanide Complexes Based on Triazacyclononane, *Inorg. Chem.*, 2012, *51*, 8042-8056.